A study of the suitability of metakaolin–based geopolymers for the immobilisation of problematic intermediate level waste

by

Daniel A. Geddes

Academic Supervisors:

John L. Provis, Susan A. Bernal

Industrial Supervisor:

Martin Hayes (National Nuclear Laboratory)

A thesis submitted in fulfilment of the requirements for the degree of

Doctor of Philosophy

Department of Materials Science and Engineering

University of Sheffield

November 2020

"What you know can fill a book and what you don't will fill a library"

T. C. W. Booth (Grandad)

Abstract

Intermediate level waste (ILW) is generated as a by-product from the extraction, processing and usage of radioactive materials. ILW encompasses a wide range of materials including uranium based species, metals, sludges and organics/oil wastes. The incorporation of these species into cements can be problematic at high waste loadings, across a range of cementitious systems including alternative calcium based cements, magnesium cements and alkali activated materials. This work will focus on a sub-section of alkali activated materials, metakaolin based geopolymers which have been activated using potassium silicate solutions. It has been shown within the literature that geopolymers have the potential to encapsulate problematic wastes such as reactive metals and organics/oils.

Initially studies have been performed on the fresh and hardened state properties, and a range of formulations were postulated and the stability of these materials was tested. It has been found that $H_2O/K_2O = 11 - 13$, $SiO_2/K_2O = 0.5 - 1.5$ and $Al_2O_3/K_2O = 1.0$ is a formulation envelope that meets the UK standard performance requirements, in the most part, for cementitious materials within the nuclear industry. In-depth analysis of the rheological properties of these materials has been undertaken, and it has been shown that increasing the alkalinity of the activating solution causes a decrease in the flow of MK-based geopolymers, except when highly reactive MKs are used. This is due to rapid setting occurring within the higher alkalinity system. Detailed rheological analysis has been performed on the flow curves and it has been shown, for the first time in cementitious materials, that changes in the rheological properties occur at finite points on the flow curves. Investigation of these shear rate steps, and then analysis of the flow curves fitted to each segment of the data, has shown that differences can occur in terms of the rheological properties based around the degree of shear imparted on the paste.

Gamma irradiation has been performed on formulations with $SiO_2/K_2O = 1.0$ and $H_2O/K_2O = 11$ and 13, to show the effects of irradiation on the free and bound water, and also the degree of carbonation induced via irradiation. It has been shown, for the first time, that the irradiation of metakaolin geopolymers can lead to carbonation. The mechanism by which this is undertaken is not yet understood and will be an area for future study. It is believed that there is an increase in porosity upon irradiation, which includes the introduction of cracks. These cracks have formed due to the radiolysis of water within the pore and gel phase, and the rapid removal of this water. This increase in cracking and empty pores, is expected to cause the increase in carbonation that is witnessed and also could potentially affect the immobilisation of radionuclides.

Studies of the incorporation of organics/oils within these systems has led to the discovery that metakaolin based geopolymers, are very susceptible to the incorporation of this form of waste. Increasing or decreasing the modulus (SiO_2/K_2O) of the activating solution from unity leads to the sample "lacking structural integrity", or can lead to a "gel like bleed" on the surface of the sample. It has been show that altering the H_2O/K_2O between 11 and 13 does not, in the most part, alter the visual/structural properties of these pastes. However, when it comes to the rheological properties the higher water content systems have allowed for the immobilisation of both viscous and thin silicone oils. The incorporation of silicone oil has been shown to be stabilised by a mechanism of hydrolysis and then radiolysis. This has shown chemical changes to the oil after geopolymerisation, that have then been reversed, to some degree, using gamma radiation. The chemical stability of these materials has been shown but further studies are needed on the structure of these materials.

Therefore, it has been concluded that MK-based geopolymer cements, produced using potassium silicate activating solution, are an attractive alternative to blended Portland cements for the disposal of specific, problematic nuclear wastes.

Acknowledgments

Table of Contents

Table of Figures

Table of Tables

Chapter 1: Synopsis

The main goal for any government radioactive waste management policy is to control radioactive waste in order to protect human life and the environment, for many generations to come. Intermediate level waste (ILW) is a sub-class of waste that exceeds the acceptable radioactivity levels for low level waste, but does not generate significant heat, such that heating is not considered in the design of storage or disposal facilities [1]. This waste tends to be disposed of using cementitious materials, such as Portland cement (PC) blended with blast furnace slag (BFS). This system is incredibly robust and offers the ability to dispose of large volumes of nuclear waste. However, ILW can vary dramatically in composition, chemical and physical form which means that the treatment of some of these materials within a standard PC formulation can be problematic, unless waste loadings are significantly reduced or alternative cementitious systems can be considered.

Geopolymers are produced from the activation of aluminosilicate precursors, such as metakaolin, by an alkali silicate/hydroxide solution [2]. This produces a highly amorphous system, with a low porosity and tailorable chemistry; which makes these systems perfect for the immobilisation of problematic wastes [3]. It has been shown by studies funded by the EU (Predis) [4] and the USA (Hanford Site) [5], that geopolymers are currently receiving a large international funding drive for the use in the disposal of problematic nuclear wastes.

This thesis will study the effectiveness of metakaolin-based geopolymers as a potential replacement for Portland cement in the disposal of specific, so called problematic wastes. This will be achieved through the assessment of the fresh state properties, the structural stability, the resistance to gamma irradiation and the waste loading of surrogate oil-based problematic wastes. Overall, this study will provide an outline of these materials with the aim to help develop a safety case for the implementation of these materials within the UK nuclear industry.

Chapter 2 will outline the current UK approach to waste management of problematic wastes and the potential alternative cements that can be used for the disposal of these wastes. Geopolymers will be explained in detail, with a specific interest drawn to their chemistry and how the adaptation of this chemistry will lead to the successful incorporation of different nuclear wastes, including oils.

Chapter 3 discusses the materials that have been used to produce the geopolymer cements, whilst also explaining the experimental parameters used for the production and characterisation of the MK-based geopolymers. This includes an introduction to the analytical techniques applied, and how they can be used to analyse the low range order of the geopolymer gel network.

Chapter 4 will discuss the fresh state properties of MK-based geopolymers. This will include an understanding of the rheological properties and how the use of multiple MKs and activating solution compositions can adapt the yield stress and plastic viscosity of these pastes. An understanding will be drawn of the early stage formation of the geopolymer gel structure, and how the reaction kinetics can change the formation of certain bonds within the gel network.

Chapter 5 will examine the effects of shear on the fresh state properties of MK-based geopolymers. The effects of shear regime are of particular interest to the UK nuclear industry due to their unique requirements for pastes that can be used as pumped grouts and that can also be mixed in-drum with the waste. In order to prevent blockages and predict satisfactory infill of solid wastes or ability to mix sludges/slurries etc., an understanding of the effect of shear rates on rheology is important. A detailed explanation of the steps found within the flow curves are also examined.

Chapter 6 will provide a baseline study of the hardened state properties of the formulations that have been examined in chapter 4. This will show the stability of these materials up to 360 days. Long term structural stability is a highly desirable and important characteristic within the UK nuclear industry. Minimal changes can be seen within the microstructure up to 360 days of curing.

Chapter 7 will assess the irradiation resistance of these MK based geopolymers, and will show that they are resistant to the changes that can be caused in the structure by significant doses of gamma radiation. This chapter will assess the pre-curing of a sample prior to irradiation and the effects of this on the changes induced in the structure. Overall, this chapter shows the lack of damage that is caused within these materials (both structurally and chemically), whilst also providing a methodology for examination of the materials that have been irradiated using a ^{60}Co gamma irradiator.

Chapter 8 will develop a formulation envelope for the encapsulation of oils within these materials. Most waste oils within the nuclear industry tend to come from the operation of pumps and hydraulic systems that require oil as a lubricant, and so various oils will need to be tested. Silicone oils of two different viscosities, and a petroleum jelly, have been tested in a range of geopolymer formulations. A candidate formulation was selected and then irradiated to 1 MGy with 20 wt.% silicone oil incorporated within it. The chemical stability of this system was then tested.

Chapter 9 contains a series of concluding remarks, a formulation envelope for further testing within the nuclear setting, and also a candidate formulation for the incorporation of oil at 20 wt.% loading.

Chapter 2: Introduction and Literature Review

2.1. Nuclear Waste Management

The development of nuclear power within the UK began after the second world war, with the race to produce a nuclear arsenal. This led to the production of the Windscale and Harwell Piles in the late 1940s, which were designed for the production of enriched plutonium for the use in the nuclear weapons programme. The nuclear weapons programme led to the formation of the UK Atomic Energy Agency (UKAEA) in 1954, which was tasked with the development of our understanding of nuclear energy for use in both the civil energy sector and defence. The development of these nuclear weapons and the generation of nuclear power has led to the production of a significant amount of waste.

2.1.1. Nuclear Waste Types

The UK has produced approx. 133,000 m^3 of waste, as of 2019, and is expected to produce a further 4,500,000 m^3 of conditioned waste, over the lifetime of the current operation [1]. Management of radioactive waste requires the containment of radionuclides for time periods in excess of 100,000 years [6]. This requires stringent product quality and safety testing to be undertaken on any waste product that is stabilised. Waste can be categorised into the following three categories [1, 7]:

- Low Level Waste (LLW) contains a low level of radioactivity. This waste does not generate in excess of 4 GBq per tonne of alpha activity and/or 12 GBq per tonne of beta/gamma activity. This waste is generated during the operation and decommissioning of nuclear sites. This usually includes scrap metal, waste plastics and contaminated clothing. This waste can be disposed of relatively safely through cementation and storage in containers at the Low-Level Waste Repository situated at Drigg in West Cumbria, or by, incineration and metal recycling. Supercompaction processes may be applied to waste containers before cementation and storage [8].
    - Very Low-Level Waste (VLLW) is a sub-category of LLW, and is waste that has a sufficiently low activity that it can be disposed of at municipal landfill sites. This waste must be below 4 MBq per tonne of activity.
- Intermediate Level Waste (ILW) generates an activity in excess of those described for LLW waste, but does not generate significant heat. This waste category is the most diverse and contains not only products from the decommissioning of nuclear sites, but also wastes generated from the long-term storage of fuels. This leads to the production of a large

array of chemical mixtures, containing a diverse range of elements. Some of the wastes within this section are designated "problematic" as they are difficult to treat in high quantities using conventional blended Portland cement formulations [9].

- High Level Waste (HLW) not only passes the threshold of activity for LLW, but also produces significant quantities of radiogenic heat. This waste typically consists of spent nuclear fuel [9].

Of the more than 4,500,000 m^3 of nuclear waste that will be produced over the lifetime of the UK nuclear estate, the majority will be designated as LLW (or VLLW). The disposal routes of LLW is well understood and the majority of the waste streams are disposed of without any issues. HLW makes up less than 1 % of the waste that currently requires disposal, but is responsible for 95.2 % of the total radioactivity from UK nuclear wastes [7]. HLW is currently produced as a by-product of fuel reprocessing, this waste is incorporated into a glass matrix, which immobilises the radionuclides and can lead to a volume reduction in the waste. This is then stored in stainless steel drums, and is planned for disposal within a geological disposal facility [6]. This waste corresponds to 0.9 % of the current volume of waste and has mostly been completely treated. This is represented in Figure 2-1.
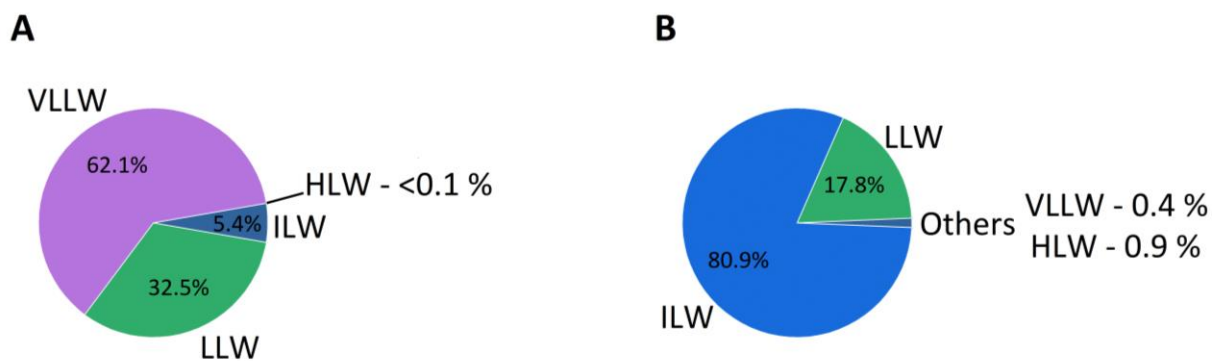
Figure 2-1 - An overview of the volumes of each waste category that are expected over the lifetime of the Sellafield site (A) and the current waste that needs to be addressed (B). Reproduced from the 2019 UK Nuclear Waste Inventory [1].

ILW currently makes up 80.9 vol.% of the overall waste that needs to be addressed. Many of these waste streams still need an optimised disposal route to be developed. The main components of this waste stream are Magnox alloy, plutonium contaminated materials (PCMs), ion exchange media (such as clinoptilolite) and other radioactive wastes, which may be designated as problematic. The most common disposal route for ILW waste is in Portland cement (PC) based matrices that are blended with high volumes of blast furnace slag (BFS) or pulverised fuel ash (PFA)/fly ash (FA) [10]. These

formulations have been in use for many years and have been optimised to satisfactorily treat the majority of intermediate level wastes.

2.1.1.1. Problematic Wastes

The designated problematic wastes make up approx. 400 m^3 ($\approx$ 1000 tonnes) of UK wastes, which is less than 0.1 % of the overall total waste that is to be disposed of [11]. Waste that is problematic for the UK nuclear industry is defined as having no defined waste treatment or disposal route available due to its diverse chemistry. A full list can be found in the Problematic Waste IPT Summary [11]; however, some key constituents are:

- Oil and oily wastes
- Aqueous liquids and solvents
- Heavy metals and mercury
- Ion exchange materials such as zeolites and organic resins
- Sludges
- Uranics
- Reactive metals

2.1.1.1.1. Oil and other Organic Wastes

Radioactive oil waste found within the nuclear industry is mainly derived from the lubrication of mechanical parts used in various stages of the nuclear fuel cycle. This waste is classified as a secondary waste due to it not being developed from the direct production of nuclear power, but from a process associated with this production [12, 13]. This lubricating oil/grease can be problematic to conventional cement formation, as it can prevent the hydration of cementitious phases through the production of an oil based layer surrounding the cement particle [14]. It has been shown that geopolymer cements can offer an alternative method of disposal for these oil products [15, 16]. A full discussion of this is provided in section 2.2.4.4.4.

The disposal of organic solvents and sludges is also problematic when considering the incorporation of these materials within cementitious systems. Solvents are used prominently within cementitious materials as a method of stopping the hydration of cementitious phases [17, 18]. A large component of these wastes tend to be halogenated solvents, which have negative effects on cement hydration, but also the added environmental concerns should these samples potentially leach and contamination

of groundwater supplies [19]. This is an additional risk in comparison to the leaching of radioisotopes. Therefore, the development of a stable wasteform, with a high waste loading and minimal leaching, is essential.

2.1.1.1.2. Sludges

During the legacy storage of materials such as Magnox, which is the cladding used to encase the fuel pins for the reactor of the same name, the disposal of this material was considered to be too dangerous at the time [20]. Due to their high level of radioactivity and the associated radiogenic heat that this produces, these materials were stored in large ponds at Sellafield, or at the reactor site, in order to allow them to cool down and also allow time for a treatment route to be identified [20]. The main components of pond sludges therefore arose from the oxidation and decomposition of Magnox, a magnesium-aluminium alloy used as fuel cladding, in the aqueous pond environment to form a white paste like material. Figure 2-2 shows these ponds at Sellafield (A), and the Magnox sludge (B) content within them. The disposal of this waste is difficult as the water content of these sludges can vary from quite low to extremely high. This leads to an incredibly diverse waste stream that is difficult to immobilise in a cementitious matrix, due to the variability in water contents which can lead to a significant rheological challenge during mixing or retarded set in cement systems with significant bleed production [21]. It has been shown that when magnesium-rich sludges are cemented very little changes can be seen in the chemistry of the cement product formed, and this is also consistent with literature showing that the magnesium does not bind into the C-S-H [22]. Therefore, the waste is encapsulated but not bound into the cementitious system, and devising an alternative method of encapsulation will allow for higher waste loadings to be attained [23]. Radiolysis of this excess water can also lead to further cracking and changes to the pore structure of these cementitious materials, and this will be discussed further in section 2.2.4.4.2.
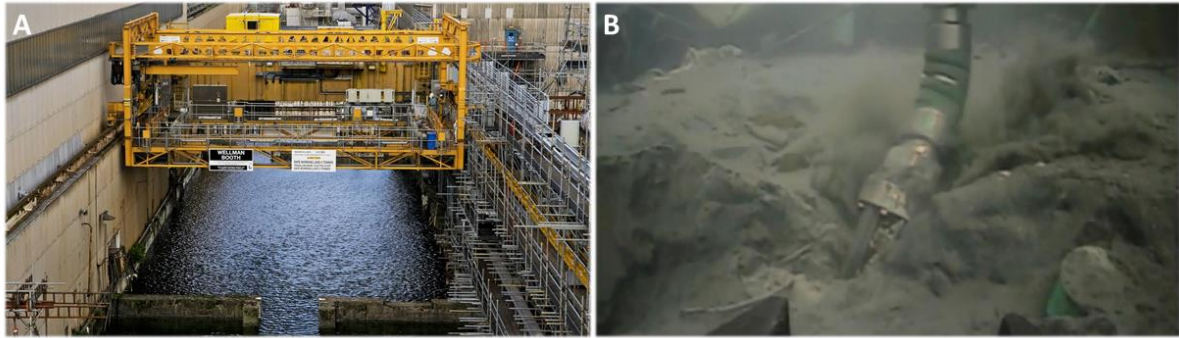
Figure 2-2 – Magnox alloy, produced from the de-cladding of uranium fuel, was stored in the ponds shown in A [24]. Magnox has corroded into oxide products and produces the sludge shown in B [25].

2.1.1.1.3. Reactive Metals

A significant proportion of the metals that are present within the nuclear industry are reactive within cementitious systems. These include, but are not limited to, aluminium and magnesium from cladding materials and associated uranium fuel arising from the de-cladding process. The highly alkaline environment of Portland cement blends also causes the aluminium to corrode, which can lead to the production of large volumes of hydrogen gas in the acute corrosion phase which will require management during the encapsulation process and causes the production of the less dense $Al(OH)_3$, which may lead to expansion [26]. This gas production can be a significant risk within a nuclear waste treatment facility as the gas can be explosive/flammable in the worst case, which will require management in an encapsulation process and may impact on waste loadings and plant throughputs as gas generation rate must fall to an acceptably low level prior to a final cementitious cap being applied could lead to damage of the container or cracking of the cement [27]. Reducing this level of corrosion, through rigorous formulation design [26, 27], or the development of alternative cements using corrosion inhibiting materials [28], may therefore yield significant improvements in plant throughput and waste loadings that may be achieved.

2.2. Cementitious Materials and the Nuclear Industry

2.2.1. Blended Portland cements

The cements currently used within the UK nuclear industry are blends of Portland cement and supplementary cementitious materials (SCMs). The inclusions of SCMs, such as BFS and FA, has for many years been a valid solution that has increased the setting time, reduced the thermal output and reduced the pH of the paste. This has allowed for standard formulations to be made that allow for the

incorporation of the majority of wastes. These usually fall in the envelope of 3/1 to 9/1 BFS/Portland cement, with a water/solids mass ratio (w/s) of around 0.35 [23, 29]. The adaptable Portland cement chemistry makes it an ideal material for the incorporation of variable waste streams. However, the hydration chemistry and available free water content of these systems may serve to restrict waste loadings for wastes such as oils, sludges and reactive metals and hence for these types of waste blended PC systems may be considered sub-optimal. As a result, a range of alternative cement matrices have been studied [30]. The powders used within the UK nuclear industry have also historically had to meet additional levels of quality over and above those used within the construction industry to guarantee process or product quality of resultant waste forms produced in encapsulation plants in a radioactive environment, in which responses to powder variability cannot be readily accommodated [31]. Although these cements still comply with BS EN 197-1 [32], historically 5 wt.% of "minor additional constituents" (MAC) were not included in the Sellafield Ltd powder specification as this could, lead to small variations in the quality/properties of the product used, and also will introduce an associated organic content (if limestone is used as the MAC). Specific parameters have been presented by Angus et al. [31], and show that the inclusion of any additional minor constituents may not affect the waste product but this would need to be tested for every minor constituent product. The UK nuclear industry purchase higher or equivalent quality Portland cement, BFS and FA than is used for standard construction applications. Due to the closure of UK coal fired power stations and the shrinking of the UK steel industry, the required high grade UK based SCMs have become difficult to source [33]. In order to ensure that work is ongoing at Sellafield and that the best cementitious material is used for the treatment of the relevant wastes, alternative cements are now being considered as one of the approaches to mitigate future supply concerns [34]. Some of these alternatives are discussed in the following sections.

2.2.2. Alternative Calcium based Cements

Calcium sulphoaluminate (CSA) cements have been shown to be an attractive alternative to Portland cement within many industries, as they react at a lower pH than standard Portland cements , and hence may be chemically more compatible with amphoteric metal wastes e.g. aluminium, whilst also lowering the CO_2 emission footprint [35]. These materials are based around ye'elimite ($4CaO \cdot 3Al_2O_3 \cdot SO_3$), which is activated through mixing with water and a source of $CaSO_4$ (gypsum or anhydrite, usually inter-ground into the cement) [26]. This reaction leads to the formation of ettringite as the principle hydration product. This is a major cement component found within Portland cement and is responsible for the expansive nature of some Portland cements [36, 37]. As ettringite is the

major cementing component of CSA, it means that dimensional stability is an important consideration for CSA cements and would need to be satisfactorily demonstrated for the treatment of ILW [31].

It has been shown that the pore solution of CSAs can changes from pH = 10 during early age to pH = 13 upon the depletion of all sulphates after a day or so [35]. This initial delay in pH rise has been given as reasoning for the use of CSA cements for disposal of reactive metals, such as Al, where the passivation point is approx. pH 9. However, the increasing pore solution pH could potentially lead to later corrosion of the Al. A significant reduction in the level of corrosion of Al when compared to Portland cement has been shown by Zhou et al. [38]. This research has shown that CSA cements have the potential to be used for nuclear waste disposal. However, the long-term corrosion of reactive metals has not yet been fully understood in CSA cements.

Supersulphated cements are produced using a small quantity of Portland cement clinker, BFS and anhydrite [39]. The reaction leads to the formation of C-S-H and ettringite [39, 40]. The raw materials all tend to have a high specific surface area and therefore require more water to produce a viable and flowable mix [40]. However, this high water content does mean that these pastes could be suitable for the immobilisation of nuclear sludges, as has been shown to work for Fe and Al rich sludges [41]. Supersulphated cements have also been shown to contain a significantly lower pH than standard Portland cements, with a pH of approx. 12 [42]. This lower pH and the formation of ettringite is a benefit to CSA and supersulphated cements, as it has been shown that heavy metals can be incorporated within the ettringite structure [40, 43, 44], and the lower pH will lead to a reduced level of corrosion of amphoteric metals [40]. The immobilisation of heavy radioactive metals has not yet been shown; the incorporation of Pb and I has been shown but elements such as U, Tc and Th (and many others) also have the potential to be immobilised [45].

Calcium aluminate cements are a cementing system that have similar pore solution pH to CSA cements, which means that these materials have the potential to be used for the same type of metallic wastes as CSA cements [46]. However, the hydrate products of calcium aluminate cements are known to be unstable over time, undergoing a reaction process called "conversion", which leads to an increase in porosity and loss of strength. This is undesirable and needs to be carefully controlled if these cements are to be used for waste immobilisation [47, 48].

2.2.3. Magnesium-based Cements

Magnesia (MgO) has been used for hundreds of years as a cementitious material. However, in recent years the drive to be carbon neutral has led to much investment in these materials. MgO can absorb

CO_2 and form a cementitious material, and combining this with the low firing temperature of MgO leads to claims of "carbon-neutral" status that are sometimes applied to carbonating magnesia cements [49].

Two other major types of MgO-based cements are magnesium (potassium) phosphate cements and magnesium silicate hydrate cements. Magnesium phosphate cements are produced from the reaction between an ammonium or potassium phosphate and magnesia, which leads to the formation of a hardened binder similar to the materials used for denture cements (zinc based phosphate cements [50]). Magnesium phosphate cements can be designed to set rapidly and have been used in the rapid repair of cracked, damaged and pot-holed road surfaces [51, 52]. Wagh et al. have produced "ceramicrete" which is essentially Magnesium potassium phosphate and has been patented as a method for the stabilisation of U and Pu-bearing materials [53], and also the immobilisation of caesium within the struvite structures [54]. It has been shown by Covill et al. [55] that magnesium phosphate cements have a suitable pore solution pH and sufficient workability in order to produce cements that meet the Nuclear Decommissioning Authority (NDA) requirements. This requires the inclusion of large quantities of water which has been shown to lead to the production of radiolytic hydrogen and oxygen, as it can lead to pressurisation and cracking of the cements and damage to the containers [27, 56]. Therefore, the work of Covill et al. and Cartier et al. [27] has shown that inclusion of large volumes of water within cementitious systems can help meet the rheological requirements but this can also lead to large percentages of free water losses from these samples upon evaporation and also radiolysis. Further research into magnesium phosphate cements has shown that with some further understanding of the water binding chemistry will help with the disposal of uranium and other reactive metals. It has been described as a good encapsulation matrix for general waste streams and could have applications within non-problematic wastes [57, 58].

MSH cements are based around the formation of a magnesium silicate hydrate phase that is formed from the reaction of MgO or $Mg(OH)_2$ with a reactive source of silica, such as silica fume. These materials can have a very slow setting time at room temperature, which would not meet standards for construction applications. However, this is desirable for nuclear applications, provided this is under 48 hours [49]. As $Mg(OH)_2$ is a major component of Magnox sludge waste, it has been proposed that the waste can be used as the major cementitious component, which will significantly increase the waste loading [59]. The chemistry of C-S-H and magnesium silicate hydrate have been studied in detail and it has been shown that these gels are incompatible [60] when the pH is held below 10 [61]. Magnesium silicate hydrate cement has been considered for the direct immobilisation of wastes, such as Cs^+/Sr^{2+} [62, 63] and aluminium [64]. The leaching of Cs^+ from magnesium silicate hydrate cements has been shown to be below the standards set in China and it has been shown that caesium can be

directly encapsulated within magnesium silicate hydrate [62]. The low pH of this cement facilitates Aluminium being in the passive state, and so this does not corrode to the same degree as it would in traditional Portland cement systems [64, 65]. It has also been shown that the Al^{3+} can be incorporated into the magnesium silicate hydrate gel structure, onto the octahedral and tetrahedral binding sites but not on the surface exchanging cations [66]. Aluminium is successfully incorporated into the structure and also has a very slow corrosion rate. Further investigation into the long term chemical stability of magnesium silicate hydrate cements is needed in order to assess their potential as a waste encapsulation matrix.

2.2.4. Alkali-activated materials (AAM)

AAMs have been shown to offer a viable alternative to Portland cement for nuclear applications [67]. This thesis will focus on the chemistry of these materials and will therefore explain in greater detail than has been done for PC, CSA and magnesium cements, the history, chemistry and applicability of these materials to waste disposal and also construction applications.

With the current need to reduce global emissions of CO_2 and other greenhouse gases, environmentally friendly alternatives to Portland cement, which as an industry produces approximately 8 % of the world's CO_2 emissions [68], have been considered. Therefore, significant research has been put into many different alternative cements. These alternative cements are compared to Portland cement throughout section 2.2, and these have been described in greater detail in sections 2.2.2 and 2.2.3. As the alkali activated materials (AAMs) cover such a wide range of Al, Ca and alkali contents, they have the potential to be tailored to meet the demands of many different applications. AAMs are produced from the chemical reaction between an alkali based 'activating solution', which is usually but not always an alkali hydroxide or silicate, with a precursor that contains relatively high molar contents of reactive SiO_2 (S) and Al_2O_3 (A). The precursors used can be industrial by-products such as BFS and FA, and also can be produced by calcining naturally occurring pozzolans to produce reactive powders such as metakaolin (MK). The most important factor regarding the precursors are the availability of S and A which are used to form the gel network [2].
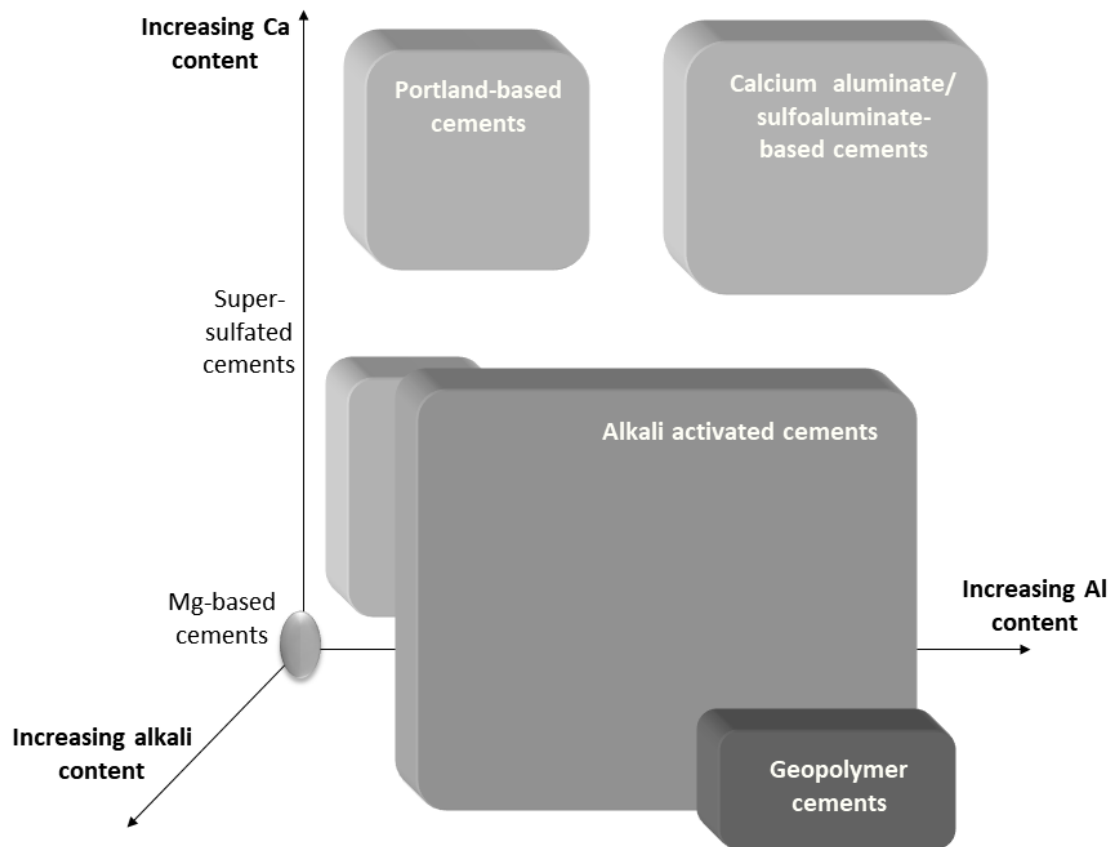
Figure 2-3 – A schematic summary of the alkali, aluminium and silicon content of different cementitious materials. Reproduced from Provis and van Deventer [2].

2.2.4.1. History of AAMs

AAMs are a relatively new technology to be implemented on a bulk scale, with a full building being produced from precast geopolymer concrete and erected to form the Global Change Institute, at the University of Queensland, Brisbane in 2010 [69]. However, the first use of AAMs was the patenting of "cement" manufacture using caustic activated slag, undertaken by Whiting in 1895 [70], followed by the work of Kühl in 1908 [71]. A full history of AAMs is given by Provis and van Deventer, in the RILEM TC 224-AAM State of the Art Report [2], but a short summary will follow to highlight some areas of interest. Following the work of Kühl, Purdon investigated the effects of different activators and their interactions with slags [72]. Glukhovsky was empowered by the Soviet Union to investigate alternatives to Portland cement. Glukhovsky was the first to discover that the alkali activation of low or calcium-free aluminosilicates can lead to a successful cementation matrix [73]. Glukhovsky is famed for using this pioneering research into AAM technology and its applications into many different applications such as construction and the transport infrastructure network [74, 75]. The work at the Kiev Research Institute (now named after Glukhovsky) has continued with Krivenko, who has been

instrumental in the implementation of AAMs for construction and nuclear applications [75-77]. This work overlapped with that of Davidovits, who is renowned for coining the term *'geopolymer'* and is responsible for the significant publicity received for these systems in the 1990s and early 2000s.

Major scientific contributions have been undertaken during the 1990s at the Eduardo Torroja Institute for Construction Science in Madrid, by Palomo and Puertas. This has led to a significant improvement in the scientific understanding of AAMs, with a specific focus surrounding how and why these systems form. They were the first research group to characterise and postulate the structure of the N-A-S-H gels [78], along with doing research into the practical applications of these materials [79, 80]. From the late 1990s onwards, developments have been made in the chemical structure of the materials through the work of the group led by van Deventer at the University of Melbourne [2, 81-87]; this research will be explained in greater detail in the following sections. Provis carried on this research at the University of Sheffield, creating an understanding of the in-depth gel chemistry [88-94] of these materials and also developments in understanding the structural changes of these materials when undergoing environmental attack [88, 95-97]. The French Alternative Energies and Atomic Energies Commission (CEA) has been responsible for a large amount of research into geopolymer cements as a useful grouting matrix within the EU nuclear industry, and work has also been performed in this area at Imperial College London [98-101]. Illikainen et al. at the University of Oulu have recently begun to show the possibility for commercial applications of geopolymer cements in the harsh Finnish weather, from materials produced from industrial waste streams [43, 102, 103].

2.2.4.2. Gel Chemistry of AAMs

The gel chemistry of AAMs is first of all described in terms of the calcium oxide (C) content of the initial precursor used. A low Ca (geopolymer) system forms a gel rich in silicon dioxide (S) and aluminium oxide (A) that is charge balanced by the reactive alkali cation (M) provided by the activating solution, which tends to be Na or K. The need for this charge balancing arises from the tetrahedral co-ordination of the Si and Al that are present in the gel, giving rise to a negative charge due to Al^{3+} in tetrahedral (four-fold) coordination. These systems can be based on precursors such as metakaolin and fly ash/pulverised fuel ash [2, 3, 104], but other novel wastes such as glass wool can also be used [103]. High Ca systems will not be focused on in this thesis. However, for completeness a brief summary of the structural chemistry is given here. A high Ca AAM system forms a Ca-rich gel similar to the tobermorite-like structure of calcium silicate hydrate (C-S-H) that is present in Portland cement-based systems. However, with inclusion of Al^{3+} in the precursors, this replaces some of the Si^{4+} sites in the C-S-H structure and leads to the development of an Al-substituted tobermorite based structure, known

as C-A-S-H. It has been shown by Myers et al. [92] that Ca^{2+} ions are selectively replaced by M^+, which charge balances the negative charge arising from Al^{3+} in tetrahedral sites in the aluminosilicate chains, shown in Figure 2-4. This leads to the formation of a C-(M)-A-S-H gel phase. Similar structures have been shown in very high replacement BFS-PC systems, that are used in the UK nuclear industry [29]. The work by Prentice et al. [29] has shown, amongst other comments, the effects of heating on the formation of C-A-S-H systems and the ability to thermodynamically model the formation of this and other cement based phases. The understanding of how C-(M)-A-S-H develops is important for the prediction of the long-term stability of these materials.
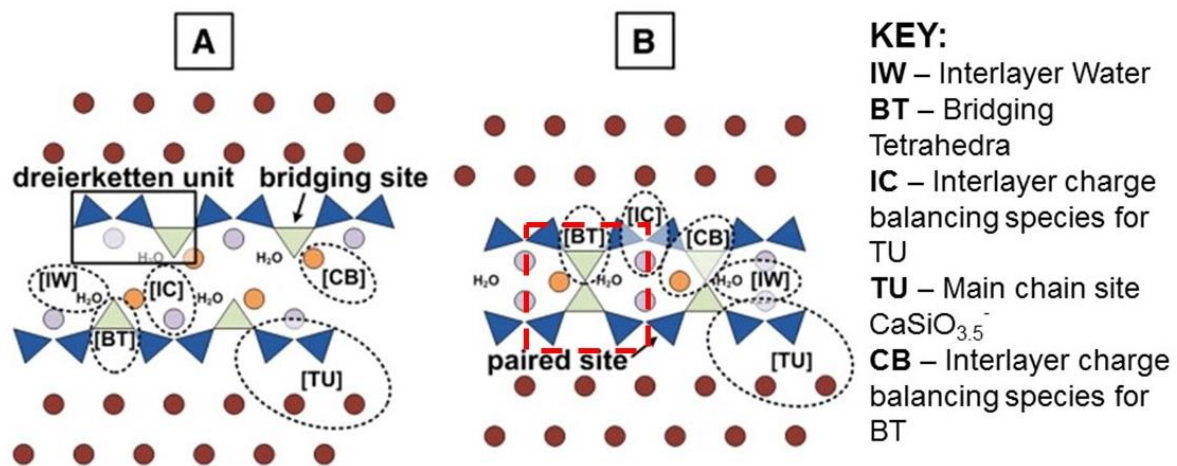
Figure 2-4 - This schematic shows the different C-(M)-A-S-H structures for non-crosslinked (A) and crosslinked (B) gels at pseudo-infinite chain length. Triangles represent paired and bridging tetrahedral sites (blue and green, respectively). Red circles represent Ca sites in the Ca – O sheets, and the orange and purple circles represent positively charged species (M+ (Na+/K+), Ca+, H+). These species charge balance the aluminosilicate tetrahedra in BT and TU, respectively. The red-dashed box indicates the 11 Å normal tobermorite structure. Adapted from Myers et al. [92]

2.2.4.2.1. Low Ca Based Binders

When Ca is not present, the layered tobermorite-like gel structure shown in Figure 2-4 cannot form. Instead, a highly disordered, highly cross linked 3-dimensional structure containing high levels of Al and Si is formed. The M-A-S-H gel has been studied in detail in order to understand the effects of long-term evolution on these materials, whether in the construction or waste disposal industry. The main method applied by many researchers for analysing the gel structure is Magic Angle Spinning Nuclear Magnetic Resonance (MAS NMR) spectroscopy, for both [29]Si and [27]Al [81, 88, 90, 105-107]. Early studies were undertaken using Fourier Transform Infrared (FTIR) spectroscopy, however this has been mostly surpassed by MAS NMR [90]. The formation of this gel structure is closely related to the Si/Al

ratio of the aluminosilicate precursor [90, 106]. In order to account for variations between different mined and/or produced precursors that occur globally, the use of synthetic precursors has been considered [90]. However, most of the analysis in this field is performed on extensively characterised raw materials and activating solutions [86, 108].

The study of geopolymerisation leading to gel formation, which is produced using the same methods as slag based AAMs just with a low Ca content, shows that the overall chemistry of these binders has mainly been performed on systems activated with sodium (Na)-based activators, mainly sodium silicate and sodium hydroxide. Na-based activators are cheaper and easier to purchase when compared to potassium-based activating solutions [84]. A major conclusion of research is that the $SiO_2/(Na,K)_2O$ ratio plays an important role in defining the degree of polymerisation [105], and therefore the chemistry of the final cementitious material, but there is still a significant degree of missing information, particularly regarding K-activated binders. Therefore, the development of a testing matrix that involves a range of SiO_2/K_2O ratios will be examined in this thesis and the results for the fresh state and hardened state properties are shown in Chapter 4 and Chapter 6, respectively.

An M-A-S-H gel is formed of Al and Si atoms in tetrahedral co-ordination bridged by oxygen (Si-O-Al) [28], with the alkali cations balancing the negative charge arising from Al^{3+} in tetrahedral coordination. The microstructure will be formed within a few hours, however it can take up to 28 days to fully develop the microstructure [90, 106], which is usually represented through changes in strength [109]. The development of at least an initial microstructure and setting of the material within 48 hours is essential when considering nuclear waste grouts [31]. Fourier Transfer Infrared (FTIR) analysis of the gel chemistry of FA-based AAMs led to the proposal of the production of a two stage gel evolution process, named Gel 1 and Gel 2 [110, 111]. This is where a high proportion of Si-O-Al formation (gel 1) is formed in the initial stage, which is then substituted with Si to lead to a higher proportion Si-O-Si formed (gel 2) later in the reaction. Gel 1 forms as the presence of non-bridging oxygen sites on Si are preferred over Al incorporation. Al may or may not be chemically bound into the gel, however there is a relatively high concentration of Si-O-Al bonds [110, 111]. The cross-linking of the structure advances through the condensation of Si-OH groups, as the Al is released progressively from the precursor and the gel and Si appears to integrate into the Q^4 gel structure [112, 113].

Figure 2-5 demonstrates a conceptual model for the formation of gel chemistry within a FA based system. This gel has been found to have short-ranged order and with the silicon having a variety of $Q^4(nAl)$ (where n = 0 – 4) environments [111]. The reduction of silica within the solution, i.e. a high alkali system, leads to the production of Al-rich zeolites and similar crystalline phases [105]. The production of zeolites, which contain crystalline aluminosilicate porous networks which has given

them the name 'molecular sieves' [114], is common within sodium activated geopolymers [115-117]. This leads to the formation of a more porous and crystalline internal network, which can in turn be used for the absorption of radionuclides such as Cs^+ [105, 115, 118, 119].
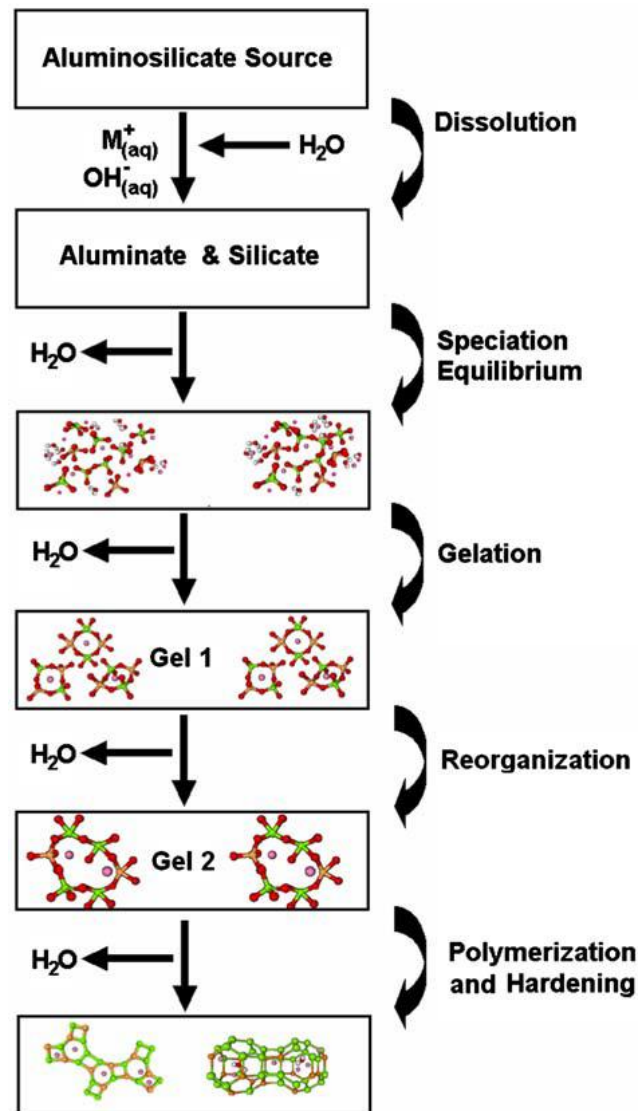
Figure 2-5 - A conceptual model for the alkali hydroxide activation of a fly ash source, including the multi-step gel formation reactions. Reproduced from Duxson et al. [120].

The initial studies describing the gel structure shown above have been extended recently by the work of Walkley [89, 90, 94, 107], Although most charge balancing is attributed to alkali cations, with a sufficiently high Al concentration, Al^{VI} can also contribute as a charge balancing ion for AlO_4^- tetrahedra in the M-A-S-H gel phase [94]. This work has been conducted heavily on Na^+ systems and there have been limited studies on the gel structure of K^+ based structures. The work of Duxson et al. [121] has

shown that K+ ions are preferentially incorporated into the gel network, when compared to Na. The K is less able than Na to remain free within the pore solution of the geopolymer gel. NMR studies have also been performed by Walkley et al. [122] which has shown a slight shielding of the ^{27}Al nuclei as the Na$^+$ ion is smaller than the K$^+$ ion. K$^+$ has been shown to displace Na$^+$ within the gel structure, when a combination of Na and K ions are used, and independently charge balances the Q^4 Al sites.

2.2.4.2.2. Reaction Kinetics

The use of isothermal conduction calorimetry (ICC) and rheology experiments can provide some interesting results when discussing the activation of geopolymers. Rahier et al. [123] produced some initial studies of the reaction kinetics using an isothermal set-up on a differential scanning calorimeter, these experiments produced many interesting results including a reduction in the rate of reaction for MK with a particle size as low as 2 μm and made the initial discovery that the reaction begins with the dissolution of the MK grains. An important study in hydroxide activation by ICC on activation of MK-geopolymers has been performed by Zhang et al. [124]. This paper used a model presented by Provis and Van Deventer [113, 125] that suggested the dissolution and rearrangement reactions are the driving force for the production of MK-based geopolymers, similar to that shown in Figure 2-5. This model is shown below schematically in Figure 2-6. The initial rate increase is accredited to the dissolution of the SiO$_2$ and Al$_2$O$_3$ in the MK (denoted by I). The modelled species G and Z are used to define the thermodynamics of the polymerisation reaction and are defined as a highly disordered amorphous Q^4 structure and a nanostructurally ordered Q^4 structure, respectively [124, 125]. This work produced promising results for calculating the thermodynamics of a Na silicate activated system, which has then led to the gel structure formation that has been shown in Figure 2-5. The final stage is the formation of a more ordered, crystalline phase that has the potential to be analysed using X-ray diffraction (XRD) experiments. This overall re-arrangement reaction has the potential for the production of zeolites [115], which is likely to be beneficial for the incorporation of different nuclear waste streams [124].
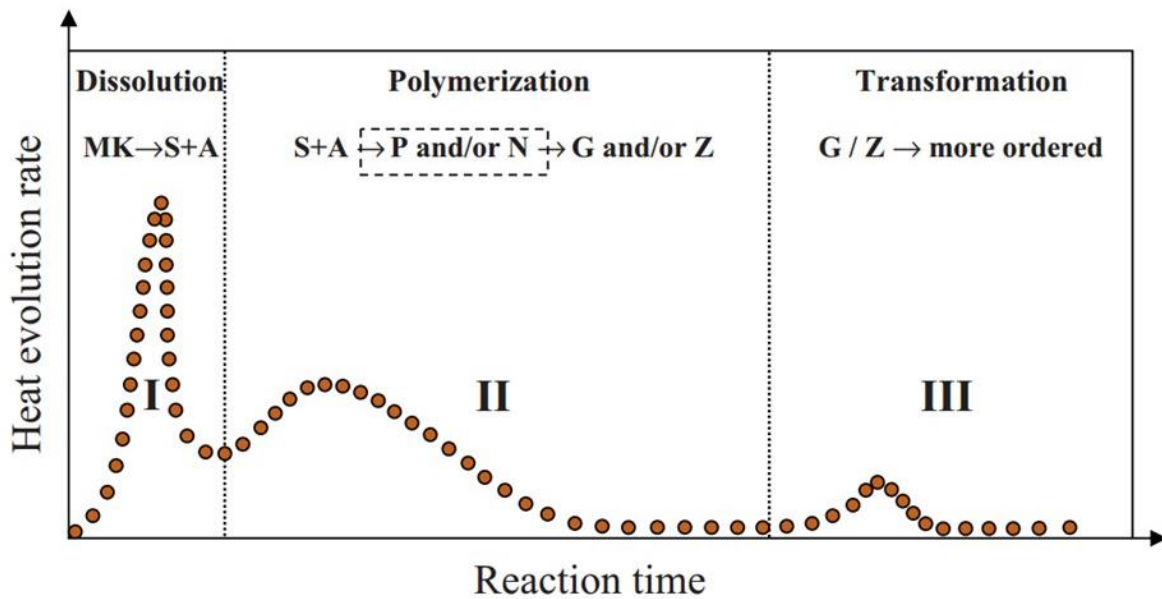
Figure 2-6 - Schematic showing the reaction mechanism for the formation of a hydroxide activated metakaolin (MK) geopolymer. S and A represent the silicate and aluminate monomers with the reaction mixture. Small fragments or proto-zeolitic nuclei, P or N, respectively. These are the intermediate, thermodynamically metastable phases that convert to G and Z, which represent the thermodynamically stable species associated with geopolymerisation. Reproduced from Zhang et al. [124].

Poulesquen et al. [126] have analysed NaOH when compared to KOH activated systems. It has been shown that the NaOH system sets faster than the KOH activated system, when the concentration of the activating solution is kept constant. It has also been shown, and as is expected, that a higher curing temperature causes faster setting. The reaction kinetics of a K-based geopolymer are slower than that of a Na activated system which leads to a greater extent of reaction for a K-based geopolymer. This paper also describes a greater activation energy required for a Na system compared to a K system, 74.5 to 64.8 kJmol^{-1}, respectively. However, when these values are compared to the literature they are approximately double the values provide by other authors; Provis and van Deventer [127] produced a value of 31.5 ($\pm$ 6.0) kJmol^{-1}. Both of these models used a first order rate reaction, which is an over-simplification of the complex processes occurring within the geopolymerisation reaction. However, the work by Provis and van Deventer shows close comparison to that in the literature [128]. Further study needs to be performed in order to distinguish between these results. This will allow a model involving the reaction kinetics of the system to be produced and increase the overall understanding how the geopolymerisation reaction progresses.

Activation using silicate solutions offers an increased microstructural stability when compared to hydroxide activation whilst also having increased Si/Al ratios within the gel structure [2]. The reaction

of sodium silicate is renowned for its own problems. As the activating solution has been shown to form sodium metasilicate crystals at low solution modulus ($SiO_2/Na_2O < 1$), this leads to the solidification of the activating solution and can also represent flash setting within sodium activated MK based geopolymers [129]. Technology regarding one-part systems and the activation of metakaolin using a "just add water" process are often designed around powdered silicate based activators [130]. However, these systems have been responsible for slow strength development which would suggest that the formation of the gel structure is slow, due to the time required for complete dissolution of the activator within the cement mix [131]. ICC results has been shown up to 98 hours shows a fairly standard heat evolution curve [102]. However, further and more in-depth studies are needed in order to show the potential applications of these easier to prepare systems.

Zhang et al. [132] have followed the model shown in Figure 2-6 and produced an extensive study based on silicate activated metakaolin systems. This report found, amongst other things, that the presence of extra silicate molecules hinders the activation and re-organisation of the gel structure and therefore supresses the formation of zeolites. By controlling the alkali silicate concentration and the temperature of curing then the production of zeolites can be controlled [133], which allows for microstructural control at later ages. By controlling the formation of zeolites it is possible to control the internal porosity formed at later ages, which will help with the immobilisation of different wastes [134]. It has been shown by van Jaarsveld [135], that potassium silicate based activators lead to the production of less zeolites than the sodium silicate activators.

2.2.4.2.3. Rheology

2.2.4.2.3.1.The Basics of Rheology
When considering cementitious systems, rheology is related to the yield stress and flow properties of the material being considered. These flow properties and yield stress can also be considered as the workability of the paste and this is usually used to describe the transportation, pumping, compaction and pouring properties of cementitious systems [136]. The rheology of cement paste can be used to order to develop an understanding of the performance and structural properties of cement [137]. The rheology of geopolymer cements, can be affected by the water content, activator composition and also the type of precursor used [126, 138-140].

In order to understand the rheology of cement pastes, then multiple rheological models will need to be considered. In order to understand the rheological properties of cementitious pastes, then an understanding of the Newtonian and non-Newtonian behaviour needs to be assessed. Figure 3-2 is a

standard representation of the rheological properties that can occur within different fluid materials. Newtonian fluids are defined as those where shear rate is proportional to shear stress. Pastes where shear rate is not directly proportional to shear stress are described as non-Newtonian. Cement pastes are classified as yield stress pastes [141], and they can be explained using Eqn. 2.2.1 and Eqn 2.2.2. [142], which represent tend to follow a Bingham (linear) or Herschel-Bulkley (power law) model, respectively. These equations show the relationship between the shear stress (τ) and the shear rate (γ̇), is dependent on the gradient of the curve (given by μ for the plastic viscosity of a linear curve and K for the derivative power law gradient or *consistency factor*) and to the power of the flow index (n) [137].

$$\tau = \tau_0 + \mu\dot{\gamma}$$
Eqn.2.2.1.

$$\tau = \tau_0 + K\dot{\gamma}^n$$
Eqn. 2.2.2.

The standard methodology for measuring the rheology of cement paste is to use vane rheometery. This involves, submerging a 5 blade head into the paste and shearing the paste at a known shear rate. This allows for the torque of the blade to be measured and a plastic viscosity, or flow curve to be calculated. This flow curve, can be used to determine the rheological parameters explained in Eqn. 2.2.1. and Eqn. 2.2.2., which in turn allow for a judgement to be made on the suitability of the cement paste. This methodology can also be used to determine the agglomeration and flocculation of precursor particles within the reaction mixture [143]. Breaking down agglomerations or flocculations using high shear, can have cause a decrease in the apparent viscosity of the cement paste [144].

2.2.4.2.3.2.Rheological Properties

There are limited studies on the rheological properties of alkali activated MK [2]. A major study has been carried out by Poulesquen et al. [126], in the same study that has been detailed in section 2.2.4.2.2. This work has shown that the nature of the charge balancing cation used has a strong influence on the viscoelastic properties of the cement paste. It was shown that when NaOH and KOH are used to produce a geopolymer system, then the structure becomes more rigid with the K^+ ions, due to its ability to form larger oligomers that can lead to the formation of a much greater 3-dimensional structure. Na^+ has a weaker interaction within the gel network and therefore leads to faster setting times and reduced gel structure propagation [126].

Some work has also been carried out by Favier et al. [138, 139] who have begun to isolate the Newtonian behaviour of geopolymer species. It has been shown that the rheology is nearly Newtonian in nature, with a low active yield stress [138]. However other researchers have also shown that these

pastes can undergo non-Newtonian behaviour [145, 146]. This contradiction demonstrates that there is a lack of knowledge on the rheology of geopolymer systems and further study needs to be performed to analyse this system in detail. The colloidal behaviour of the MK has been shown to not be a dominant factor when compared to the composition of the silicate solution, but the true understanding of the clay effects does need to be understood. With changing precursors and activators having such a large effect on the rheological properties [2] then the need for a new and divisive rheological model is evident.

In order to understand some of the effects of MK on the rheological properties of geopolymer cements, some of the information learned from MK substituted Portland cement systems can also be analysed. This has been done effectively by the RILEM TC 282 CCL [147], and is currently submitted for publication. This work has been used to show that the use of superplasticisers within calcined clay based systems is an effective method for reducing the viscosity [148]. The use of superplasticisers has historically not been endorsed within grouted wasteforms used in the UK nuclear industry, as actinides may complex with the superplasticiser in free solution, thereby increasing their mobility post closure of a geological Disposal Facility (DCF) [149]. However, more recent studies have indicated that polycarboxylate ether (PCE) superplasticisers have a low impact on actinide mobility in grouted products [150]. Hence restrictions on their incorporation in grouted ILW waste forms have largely been removed, pending a formal assessment via the RWM Disposability Assessment Process, with the endorsement subject to the provision by waste packagers to confirm the superplasticiser is of the PCE type, the brand name of the PCE product, the proposed dosage (and manufacturers recommended product dosage range), the percentage breakdown of the various chemical components within the product and any associated Material Safety Data Sheets provided by the product manufacturer [150]. Further, other countries have shown willingness to include superplasticisers [151]. Sonebi et al. [152] have examined the effect of MK on the viscosity of Portland cement pastes and has found that a small increase in the wt.% of MK from $6 - 20$ wt.% has led to a significant increase in the yield stress and plastic viscosity of the paste. It has been shown by Cassagnabere et al. [153] that the metakaolin calcination type (discussed in detail in section 2.2.4.3) is very important when considering the viscosity of cement samples. This is due not only to different sample morphology but also the reactivity of the clay type used [153].

2.2.4.3. Calcination Methodology

MK is a reactive pozzolanic material that can be used as a Supplementary Cementitious Material (SCM) or as a AAM precursor. MK has approximately $1 - 2$ % CaO [154, 155], depending on the composition

of the initially extracted kaolin, therefore AAM binders produced from MK are classed as geopolymers (Figure 2-3). This material has not been used to its full extent due to its relative expense in comparison to FA and BFS and also, its complex rheological properties that can lead to the production of very viscous pastes [152]. However, aluminosilicate industrial by-products that meet the currently accepted standards within the UK are now in dwindling supply, and MK is becoming an attractive and viable alternative [68].

MK is produced through the thermal activation of kaolin at 600 – 900 °C by a dehydroxylation mechanism. This reaction forms a highly reactive transition state, at a sufficiently low temperature to stop the formation of mullite [155, 156]. The original structure of kaolin before calcination is shown in Figure 2-7. The octahedral co-ordination of Al species in kaolinite converts largely to tetrahedral co-ordination structure upon calcination [2].
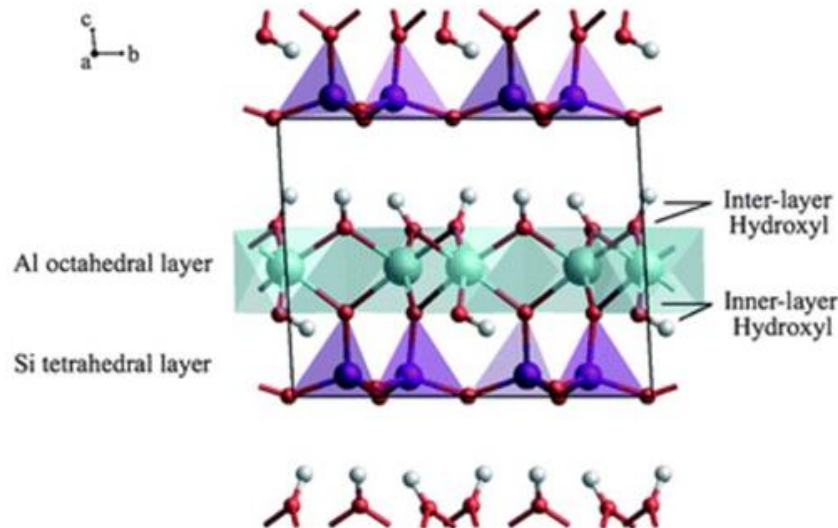
Figure 2-7 – The ideal layered structure of a kaolin unit cell. This shows the SiO_4 tetrahedra are linked to the AlO_6 octahedra by a strong ion-covalent bond. These layers are connected by hydrogen bonding [157].

The thermal treatment of the kaolin can be performed by either rotary calcination or flash calcination, and these processes lead to the formation of a species with different reactive properties [154]. This may be based on the particle shape and structure, with a flash calcined MK having a more spherical nature and a slightly larger particle size [99, 154]. The flash calcined MK appears to have a greater wettability and therefore dissolution. This leads to a more reactive clay when compared to rotary calcined MK.

Rotary calcined MK tends to be produced via the following staged process. In Stage 1, the kaolin raw clay is ground using an industrial grinding process. Stage 2 is where the calcination using in a rotary kiln for many hours between 650 - 700 °C takes place. In the final stage, the clay is then reground to produce a material with a flaky and irregular morphology, which leads to a high specific surface area [158, 159], this grinding is needed as it reduces the agglomeration of the particles.

Flash calcination has been shown to be a novel method for the production of MK [154, 160, 161]. This method is different from the 3 stage process outlined above, as the material is only ground initially and is then calcined at temperatures in excess of 1000 °C for a few tenths of a second [154, 160]. This process reduces particle agglomeration, provides a large throughput potential and is also more time/environmentally friendly due to the reduction in grinding [160]. Industrial processes using flash calcination to produce AAMs have shown real promise in recent years and the development of commercial small kilns has been undertaken in the UK [162] and in mainland Europe [154]. Figure 2-8 shows a standard pilot kiln that could be scaled up for use as a calcination method. Clay reactivity within flash calcined systems is greater than that of rotary calcined MK, understanding the effect of this increased reactivity will be key for developing these systems [163].
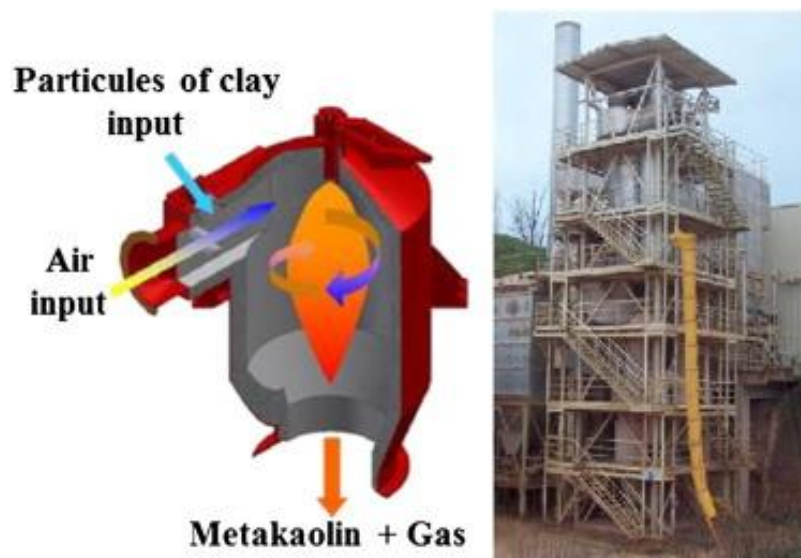
Figure 2-8 – A schematic representation of the kiln that is used by Argeco Development in order to produce Argicem. The photograph is of the calcination tower. This has been reproduced from the works of San Nicolas et al. [154] and Claverie et al. [160].

Investigation of the calcination temperature, as well as time, has allowed some interesting conclusions to be drawn in the literature. Zuhua et al. [164] presented an increase in compressive strength in rotary calcined MK that had been thermally treated between 600 – 900 °C and then a fall off at temperatures above this. This paper also presented some interesting characteristics, including the

incorporation of water within the geopolymer matrix and how geopolymers react to changes in temperature. Calcination temperatures at around 700 °C have been shown to be optimum for the production of MK for use as a precursor in the production of geopolymers. However, these MKs, when activated with sodium based activators, can produce zeolites within the geopolymer structure [165].

2.2.4.4. Uses of AAMs in the Nuclear Industry

AAMs have been shown to offer a viable alternative to Portland cement for nuclear applications [67]. From the discovery of geopolymer based technology, the nuclear industry has planned to incorporate different aluminosilicate precursors into its encapsulation methodologies. The International Atomic Energy Agency (IAEA), in 1975, performed experiments incorporating caesium (Cs) based wastes into alkali activated clay systems, including those based on kaolinite [166]. They reported permanent immobilisation within the gel network, however some of the results were inconclusive with regards to leaching. This conclusion should have promoted further study into the use of clay based immobilisation systems however this work was then relatively untouched until Khalil et al. [167] in 1994 examined the use of a trademarked geopolymer formulation called TROLIT™ (supplied by Hüls Troisdorf AG). This work revolved around leaching experiments and again entailed the use of Cs salts, along with Sr and Mo salts. This work introduced a 15 wt.% loading of the salts in a brine form, into the geopolymer matrix with varying leach rates. Overall the leaching of these materials raised rapidly over the first 120 days and then the rate slowed down. Davidovits has also produced results, regarding the structure and formation of geopolymers, in the early 1990s that state the potential of geopolymers for use in the immobilisation of various hazardous wastes [168]. Large volumes of research have been ongoing within the area of waste immobilisation in AAMs for the last 20 years, as discussed in section 2.2.4.1..

2.2.4.4.1. Encapsulation of Reactive Metals

As was described in section 2.1.1.1.3, the waste loadings of reactive metals may be restricted within Portland cement systems due to the high pH in the pore solution of these systems or the availability of free water to support on-going corrosion reactions. The potential to incorporate different reactive metals offers an interesting area of study. Geopolymers based on MK have been shown to be receptive to the incorporation of NaF, which has been used as a corrosion inhibitor, for aluminium and magnesium alloys [100]. The work of Kuenzel et al. [100] has involved the incorporation of Al metal within geopolymers using different Si/Na molar ratio sodium silicate activating solutions. Changing the

Si/Na ratio also changed the pH of the activating solution, which has shown the effect of pore solution pH on the corrosion of Al. This study found that a lower pH geopolymer (around pH 11) allowed for the incorporation and limited corrosion of the Al. The corrosion reaction of Al did not completely stop but was inhibited as $Al(OH)_3$ was formed on the surface, and acted as a passive layer (or corrosion inhibitor) in preventing further corrosion of the metal. The lower pH activating solution did affect the structural properties of the geopolymer somewhat, and will inhibit the dissolution of the MK which is needed in order to produce a stable geopolymer gel structure. The use of corrosion inhibiting compounds, such as NaF, could help to prevent this loss of physical characteristics whilst still incorporating Al successfully within the geopolymer matrix [100].

The ability to react geopolymers with corrosion inhibitors is of interest to nuclear industries around the world, as there are many types of metals that currently need a disposal plan. For the Uranium Naturel Graphite Gaz (UNGG) reactors, based in France, the fuel cladding was based on a Mg and Zr alloy. The work of Rooses et al. [28] presents the problems and a possible solution to the encapsulation issues of these highly corrosive alloys, with potential increases in waste loadings above those achieved in typical blended Portland cement systems. This MK is activated using an alkali hydroxide, which is then reacted with NaF to prevent to the corrosion of the Mg alloy. Corrosion of these reactive metals leads to the production of hydrogen gas, and also radiolytic hydrogen from the irradiation of the pore water, which can lead to flammable gas production. A complete assessment of the chemical and physical properties of the system has been performed. The rheology of this system with the addition of NaF has shown no difference in the development of the yield stress over time, which is an indication that the setting time does not change with the addition of NaF. The use of ^{19}F NMR data, which targets the nuclei related to NaF incorporation, has demonstrated that the fluorine species has had no direct effect on the geopolymer formed. This experiment also included an examination of properties formed from gamma irradiation. This is examined in further detail in section 2.2.4.4.2. When Mg-Zr alloy is encapsulated into OPC-based systems the corrosion is found to be an order of magnitude greater than Na-based geopolymer systems [169].

2.2.4.4.2. Gamma Irradiation

The gamma irradiation of geopolymer systems has also received great interest in recent years. In order to develop a safety case for the use of these materials within the nuclear industry, the resistance of these materials to irradiation is a key parameter when considering these types of applications. It has been shown that the gel structure is highly dependent on the bound water within the system, and that the drying of these materials is related to the alkali cation used. As has been shown in section

2.2.4.2.1, the alkali cation is important to charge balance and provide a gel structure that can immobilise waste. The use of K^+ as opposed to Na^+ has been shown to require less structural water to be bound within the gel structure [98]. This will be advantageous in terms of rheological properties and also allow for the use of less water, which can undergo radiolysis and lead to large structural changes within the geopolymer/waste matrix [170].

Studies have been varied between slow low dose rates that have produced large total doses in excess of 0.5 MGy [170-172] and a more rapid, high dose rate over a very short period of time giving a total dose in the range of 100 kGy [173-175]. However, all of these studies have demonstrated that the position of the pore size distribution curve has increased, showing that larger pores have been produced. Chupin et al. [170] has confirmed that the gamma irradiation of geopolymer systems causes the radiolysis of the water within this structure which, as this water is released, it can account for the large changes in the pore size distribution that is seen in most sources. It has been demonstrated that small relaxations within the tetrahedral structure (T-O-T, where T represents the tetrahedral co-ordinated Si and Al species) have occurred via irradiation and this has led to a densification of the cementitious system [172]. This densification could also have been due to the amount of pre-curing that the samples have undergone before irradiation. It has however been shown that the inclusion of corrosion inhibitors within these systems can lead to a reduction in the level of radiolytic hydrogen produced under irradiation [28].

2.2.4.4.3. Encapsulation of Caesium, Strontium and Ion Exchange Resins

Clinoptilolite is used within the nuclear industry as an effective barrier to prevent problematic radionuclide movement [176]. Clinoptilolite has been shown to be an effective substrate for the sorption of Cs and Sr [177], whilst also reducing the leaching of these materials [176]. Kuenzel et al. [101] have demonstrated a method for the incorporation of clinoptilolite that is contaminated with the radioactive decay products Cs and Sr. These materials have a half-life of 30.17 and 28.5 years for ^{137}Cs and ^{90}Sr, respectively [6]. Therefore, the immobilisation of Cs and Sr is not an issue that requires 100,000 years of stability, but requires short term high durability immobilisation. This reaction involved the use of a high pH geopolymer formulation, which caused rapid dissolution of the clinoptilolite and therefore released Cs and Sr ions into the geopolymer matrix. This paper used the hard and soft acids and bases (HSAB) theory to describe the reactions present and concluded that there was less leaching of Cs because it replaces the charge balancing alkali cation in the geopolymer matrix and balances against the aluminate species. The HSAB principle states that the larger K ion is displaced to a smaller degree than the Na species and therefore more Cs is incorporated into the Na

based geopolymer [101]. The activation of geopolymer systems using Cs has been reported in the literature [156, 178, 179] and could be an interesting method for a direct disposal of Cs waste as an activating solution [179].

Sr uptake within the geopolymer was limited to 0.4 mol per mol of Al, and any excess was found to be immobilised by the system through precipitation as a hydroxide/carbonate species [101]. Provis et al. analysed the effect of Cs and Sr salts on the gel structure and has shown that inclusion of these elements as hydroxides can accelerate gel formation, whilst the nitrate and sulphate forms lead to a slight retardation of the gelation process followed by a significant disruption in the gel formation processes. This study also backs up the work of Kuenzel et al. and shows the formation of a dynamic pore network and also carbonation of some of the Sr salts [180]. Walkley et al. has also shown that Sr can be substituted into the zeolite A, that has been shown to form in geopolymers at extended curing ages. They have also shown that the gel structure is changed slightly by the incorporation of Sr, but this is only with a small change to the Si/Al ratio within the M-A-S-H structure [122].

It has been shown that the incorporation of Cs is effective in a geopolymer matrix, and as is expected the diffusivity of the Cs and Sr is based on the critical pore diameter [181]. The Cs-based MK geopolymers appear to set at a much slower rate, whilst incorporating more raw MK, than K or Na activated systems [179]. The use of Cs as an activating solution cation has also reduced the mechanical properties of geopolymer systems, but due to the low levels of strength required for grouted waste products, this does not necessarily affect the use of these materials in the nuclear industry. The size of the Cs ion compared to ions such as K and Na is responsible for the gel structure formed. This research does show that the incorporation of caesium within the gel structure is a viable option and therefore potentially offers additional levels of immobilisation capacity. Analysis of this binding capacity using various leach testing methodologies has shown that the binding within a Na-based system is increased compared to a K-based system [101]. The use of radiotracing [134]Cs has shown that when leaching in water and concentrated sulphuric acid solution, no Cs species were detected in the leachate solutions [182]. When fly ash based geopolymers have been examined minimal Cs has been leached when this system is compared to a Portland cement formulation [183].

2.2.4.4.4. Encapsulation of Oils in Geopolymers

The encapsulation of oils within Portland cement systems has been a problem for the nuclear industry as oils tend not to bind with the gel structure due to the fundamental effects of hydration [14]. If these oils are in a sufficiently high concentration, then cement hydration can be inhibited. This is due to the

formation of a hydrophobic coating around the cement grains [14]. Therefore, the development of an alternative encapsulation system was necessary. Cantarel et al. [15] presented a limited study of emulsification of a Na silicate solution with a waste lubricating (motor) oil for use in geopolymers. This paper developed a novel method for the encapsulation of oil within a geopolymer system, shown in Figure 2-9. This involved the formation of an oil in alkali silicate emulsion, which was then used to activate the MK upon mixing. The geopolymer retained some of its physical properties, while the oil remaining within the geopolymer matrix in the form of 50 μm droplets. This produces a very low porosity foamed cement. Waste loadings of up to 20 vol.% were reported with a very limited amount of leaching. This was a preliminary study that has a large scope for further investigation and is currently ongoing in the Predis project [4].

Oils have been shown to be used as a method for developing porosity in geopolymer cements using an oil stabilisation method [184]. Low viscosity K geopolymer systems have been shown to be effective in the immobilisation of 70 – 75 wt.% mineral oil, as this produced an emulsion within the geopolymer network that has led to the development of a porous network [185]. As this network is highly porous, the encapsulation of radioactive waste will potentially lead to significant leachability but it does show that this method can be used as a method to produce porous cementitious materials. Davy et al. produced a 3D X-ray tomographic study of geopolymer/oil matrices, which has shown that the incorporation of more than 27 vol.% oil leads to a percolation that causes connectivity within the macroporous structure [186]. Therefore, in order to limit the leachability of the oil then a waste loading less than 27 vol.% will be analysed in further studies within this thesis.
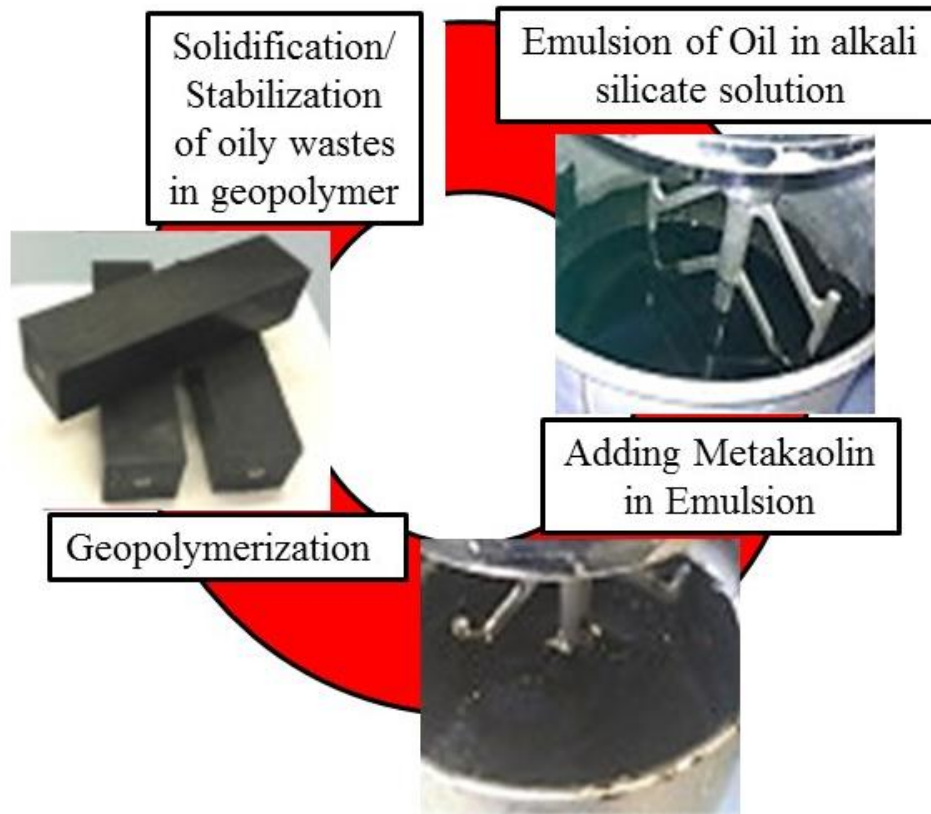
Figure 2-9 – The methodology for the stabilisation of oil within a geopolymer matrix. Reproduced from Cantarel el al. [15]

2.3. Conclusions

Nuclear waste management within the UK has found methods of disposal for the majority of the waste streams that have been created from the production of nuclear power. However, certain wastes have been classified as problematic and current disposal routes using Portland cement based matrices for significant volumes of waste within this category may be sub-optimal. These wastes include, but are not limited to, oils and organics, uranics, reactive metals and ion-exchange media. The incorporation of these wastes into various cementitious systems has been discussed and potential disposal routes have been presented.

A suggested method for incorporation of some of these problematic wastes is geopolymers based on metakaolin (MK), which has been selected for its availability in the UK in comparison to blast furnace slag or fly ash. The chemistry surrounding the structure of these systems has been analysed in detail and potassium silicate based activation has been seen as the best potential methodology for nuclear waste disposal. This is due to its preferential positioning on the charge balancing site within the alkali metal aluminosilicate hydrate gel network, when compared to sodium activated systems and also its

superior rheological properties. By using potassium silicate as activating solution, a reduction in the production of zeolitic structures at long term curing ages has been demonstrated for MK-based geopolymers. Different methods of calcination of MK have been analysed and recent advances in flash calcination have shown that this could be a promising material for investigation. There has been very little study on the use of flash calcined MK based geopolymers for nuclear applications.

The overall stability of MK-based geopolymers under gamma irradiation has been examined and this has, on the most part, shown that these materials are resistant to changes both chemically and physically from gamma rays. Studies including the incorporation of oils, reactive metals and Cs/Sr based wastes have been examined, and overall the literature indicates that these materials appear to remain stable and allow for the successful incorporation of these wastes. Further studies into the fresh and hardened state properties of these materials, the stability of these materials under gamma irradiation and also the incorporation of oil will be examined in greater detail throughout this thesis.

In order to develop the understanding of MK-based geopolymers for applications within the UK nuclear industry, some key research questions will need to be answered:

- How do the fresh and hardened state properties of MK-based geopolymers change with different curing times? What are the changes that are caused within these systems?
- What are the effects of gamma irradiation on the reaction mechanism leading to the formation of the aluminosilicate gel network? What effects does the loss of water have on the structural stability of the MK-based geopolymers?
- How does the incorporation of Oily-waste effect the rheology, long term structural stability and the resistance to gamma irradiation? What quantities of oily-waste can be incorporated into MK-based geopolymers?

Chapter 3: Materials and Methods

3.1. Materials

3.1.1. Metakaolins

The metakaolins (MK) used within this research all comply with the pozzolan definition described within BS EN 197-1 (2011) [187]. In order to analyse the effects of clay purity and calcination methods three commercially available MKs have been studied; the chemical compositions are presented in Table 3-1, and the physical properties are shown in Table 3-2. The MetaMax product was obtained from BASF (Germany) and Lawrence Industries (UK), the Argicem from Argeco Development (France), and Argical M1200 was obtained from Imerys (UK).

Table 3-1 – Chemical composition, in wt.%, obtained by X-ray fluorescence (XRF) of the three commercial MKs. LOI is loss on ignition.

MK Type	Calcination Method	SiO_2	Al_2O_3	TiO_2	Fe_2O_3	CaO	K_2O	Na_2O	LOI	Others
MetaMax	Rotary	52.54	44.54	1.31	0.36	trace	0.15	0.21	0.63	0.20
Argicem	Flash	70.37	23.36	1.14	2.91	0.74	0.25	0.08	0.38	0.77
M1200	Flash	52.18	42.40	1.74	1.90	0.11	1.07	0.09	trace	0.51

Table 3-2 – Particle size distribution parameters obtained by laser scattering for the 3 MKs.

MK Type	Particle Size / µm		
	d_{10}	d_{50}	d_{90}
MetaMax	1.45	4.49	13.8
Argicem	3.64	25.0	69.6
M1200	1.52	5.22	21.8

The crystallinity, or lack thereof, of these MKs is an important characteristic when formulating a geopolymer cement. Therefore, X-ray diffraction patterns have been analysed and the results are shown in Figure 3-1. The data below shows that the calcination method has minimal effects on the crystallinity of the clay. MKs with very low contents of secondary mineral phases (MetaMax and M1200) are both fundamentally amorphous aluminosilicates, with only a small crystalline signal arising from these secondary minerals (i.e. quartz, anatase, etc.). This is in contrast to the flash

calcined (Argicem) product that contains 48 wt.% crystalline quartz, determined by San Nicolas et al. [154] via the Rietveld method.
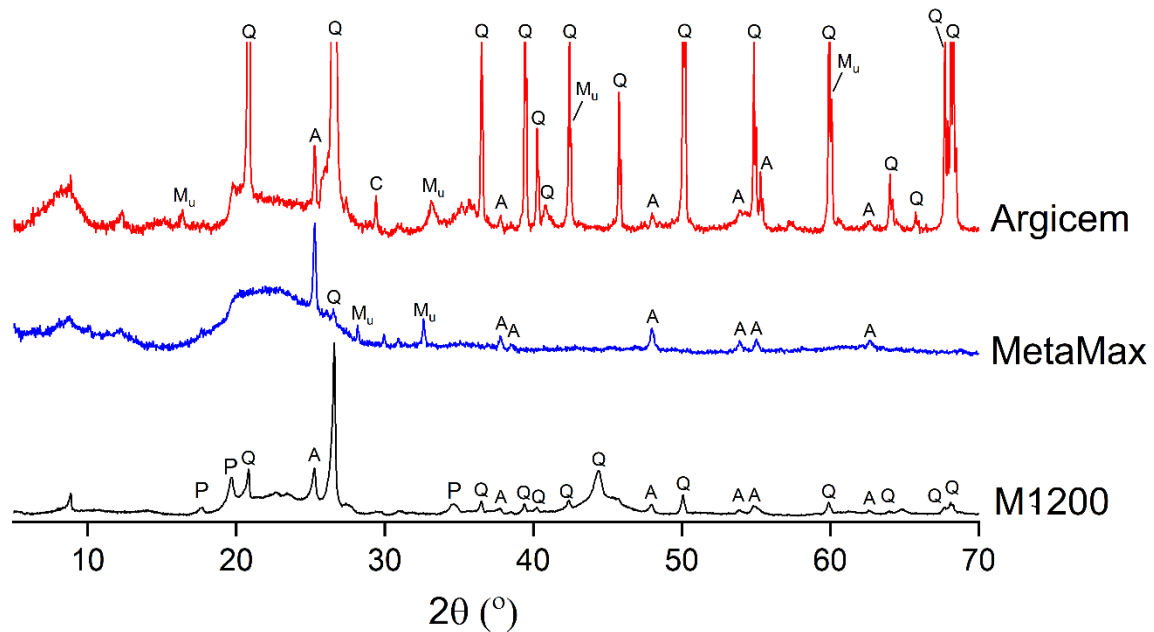
Figure 3-1 - X-ray diffraction patterns for the raw MK products. Identified phases include, Q – quartz (Powder diffraction file (PDF) – 01-078-1252), A – anatase (PDF – 01-071-1166), M_u – mullite (PDF – 04-012-0161), C – calcite (PDF – 04-008-0198), and P – pseudowollastonite (PDF – 04-011-3072).

3.1.2. Potassium Silicate Activating Solutions

The activating solutions for this experiment were devised based on the work of Duxson et al. [82, 83]. The activating solutions were formulated using a potassium silicate stock solution, K120 provided by PQ Silicates (UK), whose composition is shown in Table 3-3. The alkalinity of this system, which will be expressed as the $SiO_2/(Na,K)_2O$ molar ratio, is adjusted by blending the stock solution with analytical reagent grade (Na,K)OH purchased from Fisher Scientific (UK). The water content of the activating solution is adjusted using distilled water, which contains less than 0.3 mgL^{-1} total of contaminant ions such as Ca and Si. The compositions of the activating solutions used will stay within the following ranges: $H_2O/(Na,K)_2O = 11 - 13$, $SiO_2/(Na,K)_2O = 0.5 - 1.5$. The $Al_2O_3/(Na,K)_2O$ ratio of the overall geopolymer mix was set to 1.0 for all formulations tested within this thesis.

Table 3-3 – Compositions of the potassium and sodium silicate stock solutions used.

wt.%	SiO₂	(Na,K)₂O	H₂O
Potassium Silicate Stock	30.2	21.4	48.4
Sodium Silicate Stock	29.4	14.7	55.9

3.2. Methods

In order to understand and allow for comparison to be drawn in the future, the majority of these tests have been undertaken using the recommendations of PAS 8820:2016 [188]. This publicly available specification is the first UK attempt to provide standardisation to AAMs, and the tests described therein have in the most part been adapted from BS EN 196:2016 [189].

3.2.1. Geopolymer Preparation

The metakaolin and potassium silicate activating solutions are blended with metakaolin at a ratio designed so that the molar ratio of $K_2O/Al_2O_3 = 1.0$. This is standard within most of the key geopolymer literature and is shown to produce a charge-balance that is key for the structural development of the cementitious material [190]. Raw MK powder is added to the required amount of activating solution and mixed by hand until a homogenous paste is formed. This paste is then sheared using either a Kenwood Master Planetary Mixer or a Heidolph Overhead Stirrer; both of these have programmable speeds. All samples are mixed for 10 minutes at 900 or 2000 RPM with the planetary mixer or overhead stirrer, respectively; unless otherwise stated within the specific Chapter. The samples are cured at constant temperatures using LTE environmental control chambers set to 20, 40 and 50 °C.

3.2.2. Gamma Irradiation

Gamma irradiation was undertaken at the University of Manchester's Dalton Cumbrian Facility, using a Foss Therapy Services Inc. model 812 ^{60}Co gamma irradiator [191]. Due to the large dose to be accumulated by these samples, a non-continuous irradiation of up to 10 days was undertaken in order to reach the required dose. The samples were exposed at a dose rate of approximately 12 kGy·hr^{-1} to produce a total dose of 1.0 or 3.0 MGy. Control samples were heated to 50 °C for a duration similar to the period of irradiation to represent and to deconvolute the conditions within the irradiator, and comparisons were also drawn to samples that were cured at room temperature (20 °C). Pre- and post-irradiation curing of all samples was performed at a controlled room temperature of 20 °C.

3.2.3. Simulant Oil Waste Incorporation

Silicone oil was purchased from Sigma Aldrich, at kinematic viscosities of 350 cSt (3.5×10^{-4} m²s^{-1}) and 60000 cSt (6.0×10^{-2} m²s^{-1}). Petroleum Jelly (Branded as Skincare) was purchased from a local shop. These were incorporated into the activating solution for samples studied for oil encapsulation purposes, using the Heidolph high shear stirrer, at 20 wt.% of the overall paste. The MK was then added and the pastes were sheared for 10 minutes at 2000 RPM.

3.2.4. Fresh Paste Analysis Methods

3.2.4.1. Rheological measurements

The flow of cementitious pastes can be examined using vane rheometry. In terms of rheological geometry complexity, this is a fairly simple design as it requires placing the vane blade into an infinite volume of paste and stirring [192]. This allows for the production of a shear rate vs shear stress curve, which can be used to show whether the paste undergoes Newtonian or non-Newtonian behaviour. Cementitious pastes have also been shown to undergo shear thinning and shear thickening, whilst also offering the properties of a yield stress paste. These are all demonstrated in Figure 3-2.
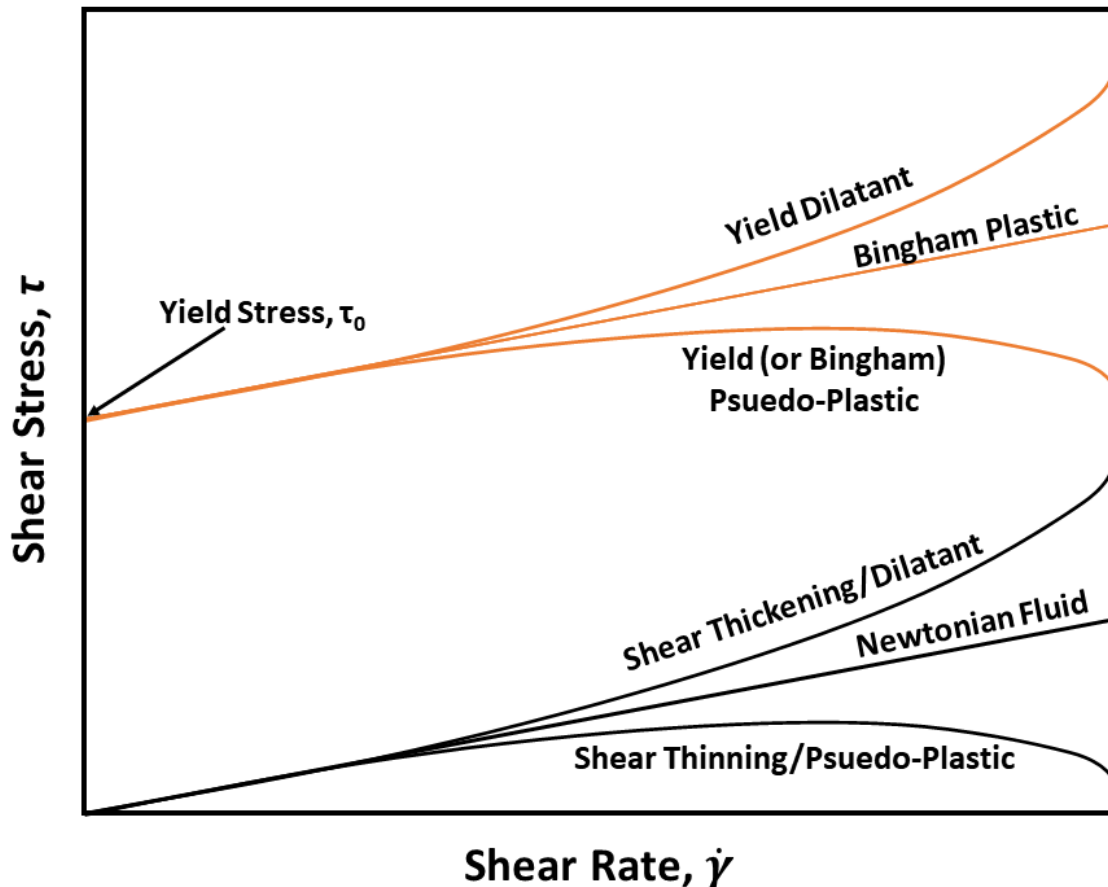
Figure 3-2 - Standard shear stress vs shear strain curves showing ideal pastes. Pastes that pass through the origin are represented by the black lines. Bingham or yield stress pastes are represented by the orange lines. This is reproduced in part from Walters and Jones [193].

Vane rheometry has been used to analyse the bulk flow properties of the paste. A 6-blade vane is coupled to a Thermo Scientific HAAKE Viscotester 550, to undertake plastic viscosity analysis. A schematic of how shear is applied to the cement paste using both the high shear mixer and also the viscometer is shown in Figure 3-3. The data is collected from the decreasing oscillating frequency curve, from 100 s^{-1} over a 60 s time period. Working on the decreasing shear rate of the flow curve allows for the removal of any errors that can be seen within the data. If working with an increasing frequency from a stationary elastic fluid, then as the strain is applied to the paste the inertia is high and the measurement also includes the force required to overcome this inertia, as opposed to simply maintaining the flow of the paste. Measuring on a downward shear rate ramp allows this to be overcome and the measurement to be taken quickly, as the viscosity of this paste will change with time [142].
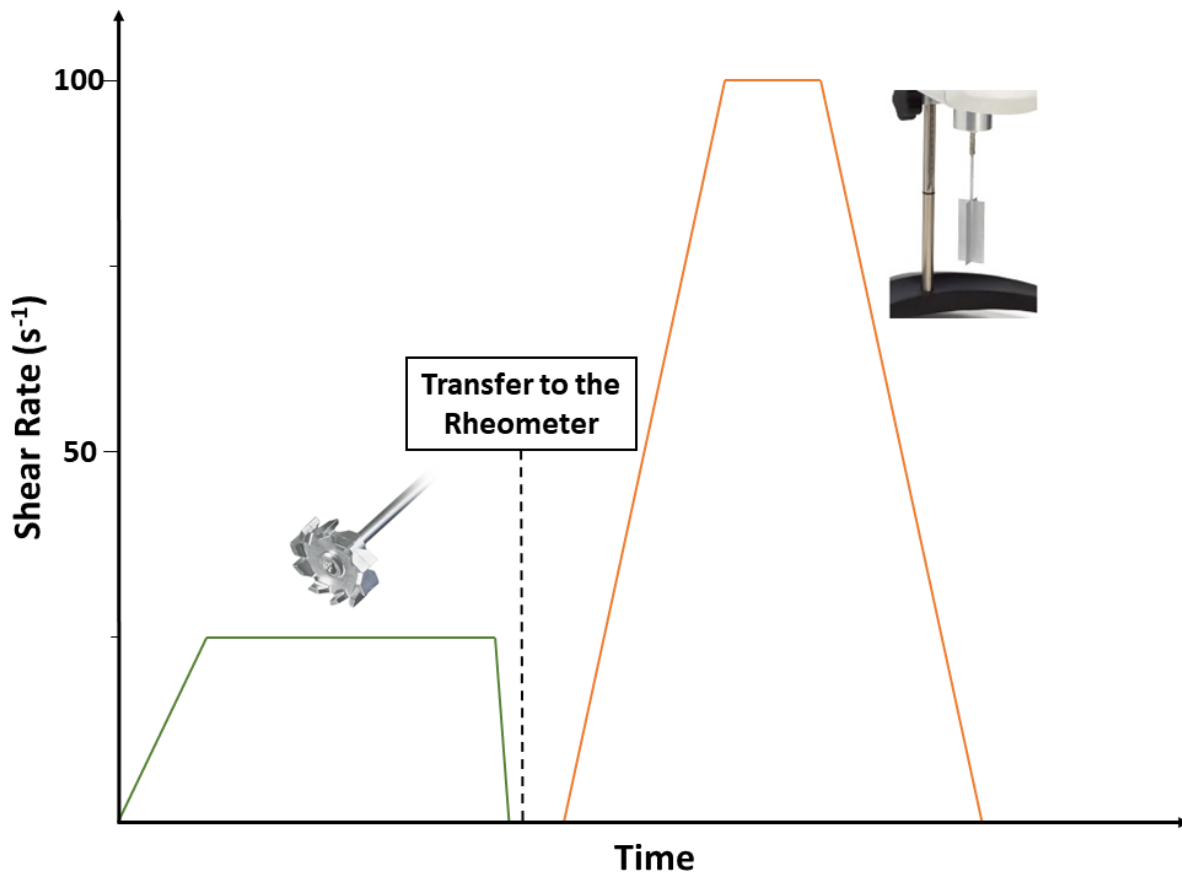
Figure 3-3 – A schematic representation of the mixing speed and rheometry measurements that are undertaken on these pastes. The green regime represents the shear applied during mixing and the orange lines represent the shear applied during rheometry measurements.

In order to fit the linear and power law relationships (**Error! Reference source not found.**and **Error! Reference source not found.**, respectively) to the descending shear rate curve. In order to fit this data, the models described above are applied to expected data. Then the error of least squared is calculated, totalled and then minimised by adjusting the applied modelled data. When this data is adjusted slightly the error in least squares is calculated again and should this be minimised changes are made to the positions of the changes in model. When steps, vertical changes in the shear stress, are seen within the data a new rheological model is counted from this point. An r^2 value has been calculated for each line. The modelled data is then presented as an overlay to the calculated data.

3.2.4.2. Setting time measurements

The Vicat technique has been used to understand the setting times of the different formulations used during this project. This has been performed using an automatic and a manual device, both of which are consistent with BS EN 196-3:2005 (which is superseded but has been used in PAS 8820). Initial set is defined as when the separation of the needle and the base plate is 6 (±3) mm and the final set is

defined as when the sample is not penetrated by more than 0.5 mm. The sample is not inverted as described in the standard, as the paste would not remain within the mould. Automatic measurements were taken using a Matest VICATRONIC with a 1.13 mm needle, which was used to penetrate a 400 mm deep sample, at 10 minute intervals, until final set conditions have been achieved for 1 hour.

Carbonation of MK-based geopolymer samples has been shown to be rapid, when compared to other AAM systems [194]. This can be seen in the setting time measurements, when a solid layer forms on the surface of the sample. This produces a false result, as the sample appears to be set but remains fluid underneath this layer. Therefore, in order to protect against this carbonation/drying layer, a surface layer of agar was added. A 2 wt% agar (Fisher Scientific, UK) plate was produced, at approximately 5 mm in depth. This was added to the surface of the sample. However, due to the hydrogel properties of the agar, it did not add any resistance to the measurement and provided a good surface protection.

3.2.4.3. Reaction Kinetics

All of the reaction kinetic experiments are performed on a TAMAir Isothermal Conduction Calorimeter, from TA Instruments. The instrument compares the thermal output generated within the sample at a level of µ/mW and it is then compared to the thermal output of a reference sample held at the same temperature. 20 (±1) g of sample is added to a 20 mL glass scintillation vial. The mass of water present within the mass of paste added to the calorimeter is used as a reference sample. The data has been collected at 20 and 40 °C, with the data sampled at 10 s increments, for time periods in excess of 7 days.

3.2.5. Hardened State Chemical Analysis Methods

3.2.5.1. Solvent Exchange Methodology

Unless otherwise stated during the experimental methodology, any experiment that required a powder or solid section of a sample has been solvent exchanged using the following methodology. A section of the sample, no larger than 10 x 5 x 5 mm, was placed in approx. 60 mL of isopropanol. This was replaced at 6, 30 and 78 hours after addition. The powder samples are then crushed using a pestle and mortar and dried using vacuum desiccation. The solid samples are dried using a vacuum desiccator for 7 days. This method is based on, but has been adapted from, the work of Scrivener et al. [195].

3.2.5.2. Thermogravimetric Analysis coupled with Mass Spectrometry (TG-MS)

TG-MS can be used effectively to determine the amount of free water and carbonation within a geopolymer system, through the decomposition of the characteristic carbonates and the evaporation of the water at characteristic temperatures [88]. Combination with mass spectrometry allows a distinction to be drawn between overlapping peaks on the thermogravimetric plot. This can be done by calculating the percentage contribution of each phase, based on the mass spectrometry data, and then calculating the percentage of an equivalent mass change that is related to the CO_2. Comparisons can then be drawn between the carbonation trends, whilst also taking into account any bound water within the formulations.

TG-MS experiments were performed on a Perkin Elmer TGA 4000, coupled with a Hiden Analytical Mass Spectrometer. 40 ± 4 mg of sample is loaded into an alumina crucible, which is top-loaded into the machine under a N_2 purge gas at 40 mL·min^{-1} and a pressure of 1 bar. The sample is heated between 30 and 950 °C at a heating rate of 10 °C·min^{-1}. At elemental specific temperatures parts of the samples are vaporised and are passed into the MS using the N_2 as a carrier gas. These vaporised compounds are analysed using a time of flight detector.

3.2.5.3. X-ray diffraction (XRD)

XRD can be a very powerful tool for the examination of crystalline phases, and can also produce information for poorly crystalline materials such as geopolymers. Geopolymers have a distinctive X-ray amorphous, diffuse scattering feature between 20 and 40 ° 2θ that is characteristic of the gel structure that is formed within these products. The presence of this diffuse scatter shows that the main binding phase within the geopolymer gel network has formed [196].

Powder XRD diffractograms have been produced for the geopolymer specimens using a Panalytical X'pert[3], using CuKα radiation generated at 45 kV and 40 mA, which has been shown in the literature to be appropriate parameters to use when examining cementitious materials [197]. A scan from 5 – 70° 2θ was used, with the scan being undertaken in increments of 0.02° 2θ and a relative time per step of 0.02° this equates to 2.2 s per step. Metakaolins, or more specifically clay powders, are prone to preferred orientation and this can be overcome by the use of a backfill sample holder.

A sample changer has been used during this project; this was suspected to be a potential problem for geopolymer samples and this was expected to cause carbonation of the ground powder. A high water content system has been tested at 0 and 72 hours after production of the XRD sample, left under the conditions within the spectrometer and then tested (shown in Figure 3-4). A small quantity of calcite

can be seen within the XRD patterns for the raw Argicem MK shown in Figure 3-1. Other than these, no other carbonation products can be seen in the raw materials. When examining the results shown in Figure 3-4, then no additional carbonation can be seen and using the sample changer should not cause any measurement-induced carbonates to be detected. Should these be collected with any of the diffraction patterns then further analysis may be needed.
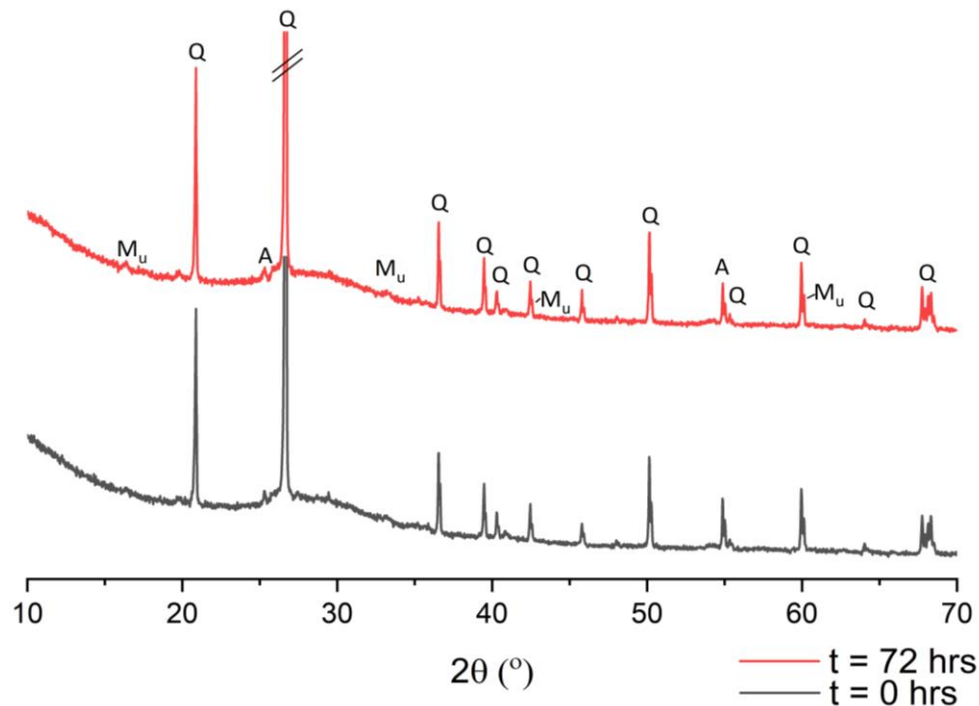
Figure 3-4 - X-ray diffraction patterns for the Argicem MK geopolymer cured for 360 days with a $H_2O/K_2O = 13$ and $SiO_2/K_2O = 1.0$. The grey line represents a sample that had been tested at t = 0 hrs after production of the sample and the red line represents a sample held in the XRD holder for 72 hrs prior to testing. The black peak markers represent Q – quartz (PDF - 01-078-1252), A – anatase (PDF – 01-071-1166), M_u – mullite (PDF – 04-012-0161), which were shown in the raw metakaolin in Figure 3-1.

3.2.5.4. Nuclear Magnetic Resonance (NMR)

Solid state magic angle spinning nuclear magnetic resonance (MAS-NMR) spectroscopy has been used to probe the local environment of aluminium based species contained within the gel network. As geopolymers are poorly crystalline, low-ordered materials, NMR can be used to probe the local environment of many of the complex gel phases present within these materials [198]. NMR relies on inducing an intrinsic magnetic moment within the specific nuclei that is being probed. Therefore, in order to probe aluminium then the ^{27}Al nuclei will be examined as the odd number of protons and neutrons leads to a magnetic moment that when exposed to a strong magnetic field, will become polarised. The addition of radiofrequency radiation induces a spin with the polarised nuclei, as these

samples undergo relaxation, then an electromagnetic signal is processed and converted using a Fourier transform. NMR spectra contain useful information regarding nuclei surrounding the ones that have been probed [198, 199]. Geopolymers produced from potassium silicates contain a highly disordered K-A-S-H gel structure. The environments of the potassium, aluminium and silicon species can be probed using MAS NMR [81, 90, 121].

MAS NMR has been conducted, in the Department of Chemistry at the University of Sheffield, using a Bruker Avance III HD 500 spectrometer at 11.7 T with a 4.0 mm dual resonance CP/MAS probe producing a Larmor frequency of 130.32 MHz for ^{27}Al nuclei. ^{27}Al spectra were collected at a spinning speed of 12.5 kHz, with a minimum of 512 scans, a pulse width of 1.7 us and a relaxation delay of 5s. The chemical shifts are compared to an external standard of 1.0 M Al(NO$_3$)$_3$. All analysis has been performed using Bruker Top Spin 4.0.6.

3.2.5.5. Fourier Transform Infrared (FTIR) Spectroscopy

When infrared radiation is passed through a sample, some of the radiation is absorbed by the sample and the remainder is transmitted through and can be collected in a detector. The infrared radiation is generated with at wavenumbers between 4000 – 400 cm^{-1}, and is fired at the sample through a series of complex optics that lead to a single beam interferogram produced from the constructive and destructive wave inferences. This single beam is passed through the material and is absorbed by the covalent bonds within the sample, causing them to vibrate. These vibrations, causing the stretching and bending of different bonds, occur at characteristic wavenumbers and can be used to show the environment in which a specific bond type exists [200]. As FTIR provides information about the surrounding atoms to a specific point, it does not require long range order and is therefore an ideal technique for understanding the amorphous gel structure of geopolymer cements [201, 202].

A Perkin Elmer Frontier FTIR spectrometer coupled with a triglycine sulphate detector and KBr beam splitter optics was used. 2 mg of geopolymer was mixed with 200 mg of anhydrous KBr, which is then pressed into a pellet at 10 tonnes of force. 16 scan iterations were taken at a resolution of 2 cm^{-1} between 4000 – 400 cm^{-1}. In order to perform the in-situ, wet paste analysis, the FTIR spectrometer was fitted with an attenuated total reflection (ATR) crystal set-up. This crystal was covered by 1.8 μm thick, Mylar film to protect the crystal. A background was taken to take account for the Mylar and a spectrum was run with the same parameters as for the KBr method.

3.2.5.6. Mercury Intrusion Porosimetry (MIP)

Analysis of the pore structure of cement materials can be a difficult process and MIP has been used extensively within the literature. The technique does have drawbacks, including the renowned "ink-bottle effect" which leads to an underestimation of the pore volume, inability to access all the closed pores and also varying contact angles of mercury per material tested [203]. However, the technique has been shown to be effective at measuring an estimated percentage porosity within the materials, and also at offering an idea of the pore size distribution. The calculation of the pore radius and pore pressure is calculated by the Washburn equation [204], which is the base calculation surrounding the instrument:

$$P = -\frac{2\gamma \cos(\theta)}{r}$$
$\qquad$ Eqn. 3.1

Where,

P = pore pressure

r = meniscus curvature radius (pore entry radius)

γ = surface tension of mercury

θ = contact angle of mercury/cement interface

Samples for MIP consisted of solid cylindrical samples that had been cast to an approximate diameter of 10 mm and a height of approx. 5 mm. These samples were then cut into approximate quarters to make a total mass of 2.20 ± 0.2 g. Analysis was completed using a Micrometrics Autopore V instrument. A contact angle of 130°, which is the closest available contact angle for geopolymers as this is the value used for blended cements [205], studies calculating the contact angle of mercury on MK-based geopolymers need to be developed but will not be investigated here. A surface tension of 0.485 Nm^{-1} were used in calculations [195, 204]. Samples were collected in triplicate to create a statistical average and a standard deviation is then calculated.

3.2.5.7. Compressive Strength

The ASTM C109 standard test for compressive strength of hydraulic cement mortar cubes at 50 mm size [206] has been adapted to analyse the strength of geopolymer cements. Slight deviation from this standard was undertaken, as paste samples were used that did not contain sand. Each cube was placed between the parallel plates with the top-cast or *"trowelled"* surface facing to the right hand side of

the instrument. This allowed for the same orientation of each cube during testing and also for the top-cast surface to not meet the parallel plate, as it is not perfectly flat. A Controls Automax 5.0 machine was used with a loading rate of 0.25 MPas^{-1}. The results were collected in triplicate and a standard deviation was calculated.

3.2.5.8. Imaging Techniques

3.2.5.8.1. Vacuum Impregnation

Fluorescence dyed epoxy resin was prepared at 40 °C in a 22:3 ratio of epoxy to hardener, the samples are then encased on all sides other than the side to be analysed. This side was then impregnated at 2.5 bar, using a 22:3 epoxy resin that contains 5 % toluene, for 3 – 4 hours. Compressed air, at 0.25 MPag, was then applied to allow the resin to impregnate. These samples are then ground and polished using silicon carbide paper and diamond suspension, down to 0.25 μm grit size.

3.2.5.8.2. Optical Microscopy

An Olympus SZX10 stereo microscope was used in conjunction with UV light, at an exposure time of 3 – 5 ms. A magnification of 6.3× and a resolution of 2560 × 1920 px was used to obtain the images.

3.2.5.8.3. Scanning Electron Microscopy

Back scattered electron scanning electron microscopy (BSE-SEM) was conducted, at Imperial College, London, using a Hitachi TM4000Plus at a magnification of 400× and an accelerating voltage of 15 kV. All images that are collected are then balanced upon the histogram for brightness and contrast. 20 images are taken of each sample in order to produce a statistical analysis of crack widths. The cracks that have been impregnated with epoxy resin, and show a dark band, are then analysed using ImageJ analysis software. A screenshot of this technique is given in Figure 3-5. This multi-position crack width analysis is performed on different positions, along each crack over the all the images. This produces a statistical average with a reliable standard deviation.
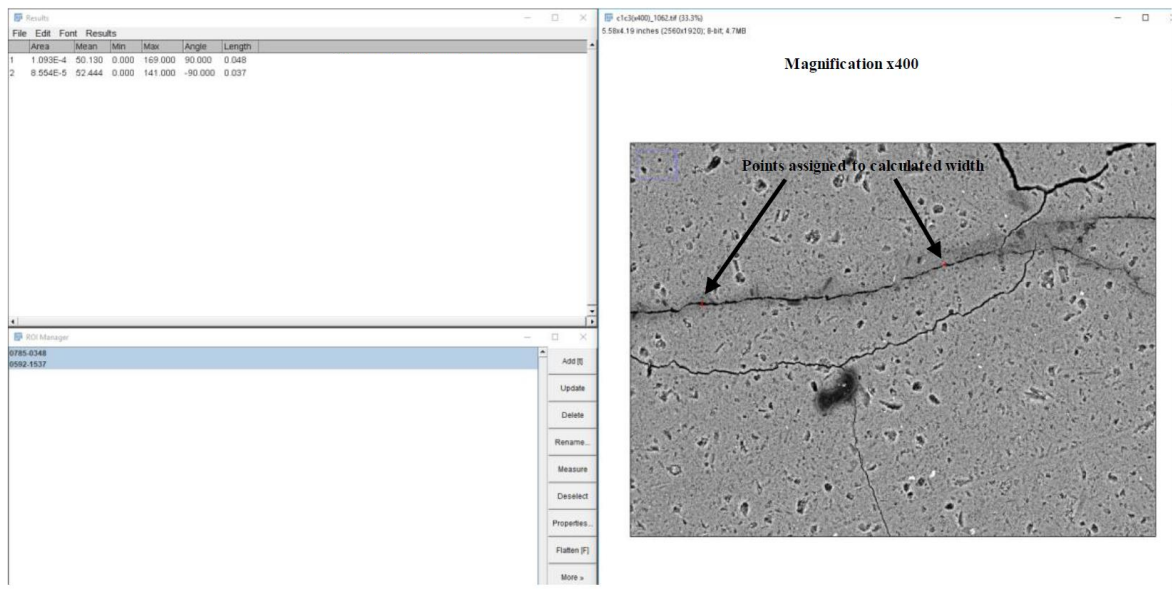
Figure 3-5 – A screenshot collected by Awni Abdullah (Imperial College, London), to explain the image analysis of cracks that have been impregnated with epoxy resin (dark banding).

Environmental SEM images were collected for a range of samples that had been cast, set and polished in epoxy resin as has been described in 3.2.5.8.1, but without the vacuum impregnation of the epoxy resin. The low vacuum conditions and high humidity present in an environment SEM, could potentially limit the drying cracks that can occur when undergoing conventional SEM of geopolymer samples [98]. These samples were collected using a FEI Quanta 250 field emission gun environmental SEM. An accelerating voltage of 10 kV was used with a dwell of 45 μs in a high humidity atmosphere.

3.3. Concluding Remarks.

This chapter outlines the key experimental parameters that have been used to describe the structural stability of different geopolymer formulations throughout this thesis. Deviations from any of the methodologies outlined above, within any given chapter or section in the remainder of this thesis, have been explained in detail as part of the discussion surrounding that section.

Chapter 4: The Development of a Solid Geopolymer Cement – Fresh State Properties

4.1. Introduction

Understanding the development of the reaction between the MK precursor and a potassium silicate activating solution, that leads to the production of a highly cross-linked aluminosilicate gel network, is incredibly important in understanding whether these materials are acceptable for use within the nuclear industry. This understanding will help to decide the compatibility of certain nuclear waste streams with geopolymer cements. In conjunction with this understanding, the UK nuclear industry has specific requirements that a grout must pass in order to meet the implementation requirements for use on plant [31, 207]. These requirements pertain to more specific processing properties of Portland cement blended pastes, and producing a product that meets a series of set values. The UK nuclear industry has the following parameters for a cement grout in order to be accepted [207]:

- The paste must remain workable to allow satisfactory infill of wastes for up to 150 min mixing i.e. does not undergo any rapid setting processes.
- Flows that exceed 200 mm on the bespoke Colflow channel designed for the UK nuclear industry are acceptable.
- Not have a high thermal output. All grouts should not exceed a thermal output of 180 kJ/kg, after 24 hours at 35 °C.
- Bleed volume should be <2 vol% on a 100 mL sample at 24 hours curing after mixing for 150 min.
- An initial setting time greater than 4 hours and a final set that is greater than 24 hours.

Sanderson has recently performed extensive studies to correlate the Colflow and Vane rheological measurements. One of the outcomes of this work was empirical determination of values for the shear stress that must be applied to the paste to reach a shear rate of 100 s^{-1}, which produced data between 100 – 400 Pa. Using 400 Pa as a maximum shear stress, on a flow curve, within these experiments, will allow comparison to Portland cement blends and therefore show consistency to the UK nuclear industry [31, 33].

There has been much cited literature that has examined the rheological properties of geopolymers and AAMs [126, 135, 139, 146, 208-212], and this has been analysed in detail in section **Error! Reference source not found.**. However, discussions surrounding the use of potassium silicate over sodium silicate based around the rheological need, are required to be analysed in detail. It has been

shown that alkali activation of MK using potassium based silicate solution provides a much more controllable rheology and also a 5-fold reduction in the viscosity of the final paste [138, 146]. The thermal evolution is also significantly reduced for certain formulations, as spontaneous crystallisation of sodium silicate solution can occur in low modulus systems, which has been shown to produce significant thermal energy [129]. Due to the increased safety procedures within a waste encapsulation plant and also the expense related to shutting down a nuclear waste encapsulation plant, the most stable paste would need to be used. Therefore, the use of potassium silicate appears to produce not only the more rheologically viable option, that is not prone to rapid crystallisation [129] and also the most microstructurally stable mixture [82, 83, 213].

Duxson et al. [82-84, 213] has shown that the concentration and species of the alkali cation can play a dramatic role in the chemistry of geopolymers. Isothermal conduction calorimetry (ICC) is a common method for attaining an understanding in the early age structural development of cementitious systems. Whilst Zhang et al. [124, 132], has shown that the thermal output of sodium silicate activated systems undergo an initial MK dissolution peak, followed by gel propagation (or (geo)polymerisation), and then a gel formation stage. This has been shown and extensively studied for sodium based geopolymers, however understanding the effects of potassium based activators using ICC data has not been studied.

The yield stress (τ_0) values of geopolymer cements based around fly ash have been stated to be 1 to 2 orders of magnitude lower than that of standard Portland cement [126, 138]. The τ_0 of MK based geopolymers has been shown to fluctuate a lot more [138]. It has been stated that the activating solution is responsible for the changes in viscosity within the final paste, and that the colloidal interactions between MK grains suspended in alkaline solutions do not affect the rheology of the paste [138, 139]. However, this explanation does not satisfactorily describe the vast differences in the viscosity of pastes produced from different clays with different reactivity's [126, 138, 139].

In order to explain the differences in rheology present within geopolymer pastes produced from different MK sources and activating solutions, the following study has analysed 3 different MKs, using 4 different activating solutions ($H_2O/K_2O = 11$ and $SiO_2/K_2O = 0.5, 1.0, 1.5$; $H_2O/K_2O = 13$ and $SiO_2/K_2O = 1.0$) and compared the results obtained by ICC, in situ ATR-FTIR, and vane rheometry. This is intended to bring understanding of the early age gel structure development within MK-based geopolymers.

4.2. Results and Discussion

4.2.1. Effect of Alkali Cation

Although literature has shown that the use of a potassium-based alkali cation over sodium is more beneficial for lower viscosity pastes [126, 138, 139], a study has been undertaken in order to demonstrate the rheological difference whilst using the Argicem MK (defined and described in section 3.1.1). This is shown in Figure 4-1. Each potassium system has a 4-fold smaller viscosity at 100 s^{-1} the comparable sodium systems. The curves appear to undergo different rheological trends depending on the composition of the activating solution. This will be investigated further in section 4.2.2.1.

Due to the complex infill systems used within the encapsulation plants of the UK nuclear sector, and the need to produce a grout that will infill into many different complex waste shapes, highly viscous formulations will not be studied further in this thesis. When combining this with the risk of spontaneous crystallisation of the activating solution and the formation of zeolitic species it has been determined that a sodium based system will not pass the rigorous safety tests required to be used within the UK nuclear industry. Therefore, this thesis will focus purely on the use of potassium silicate activated geopolymers.
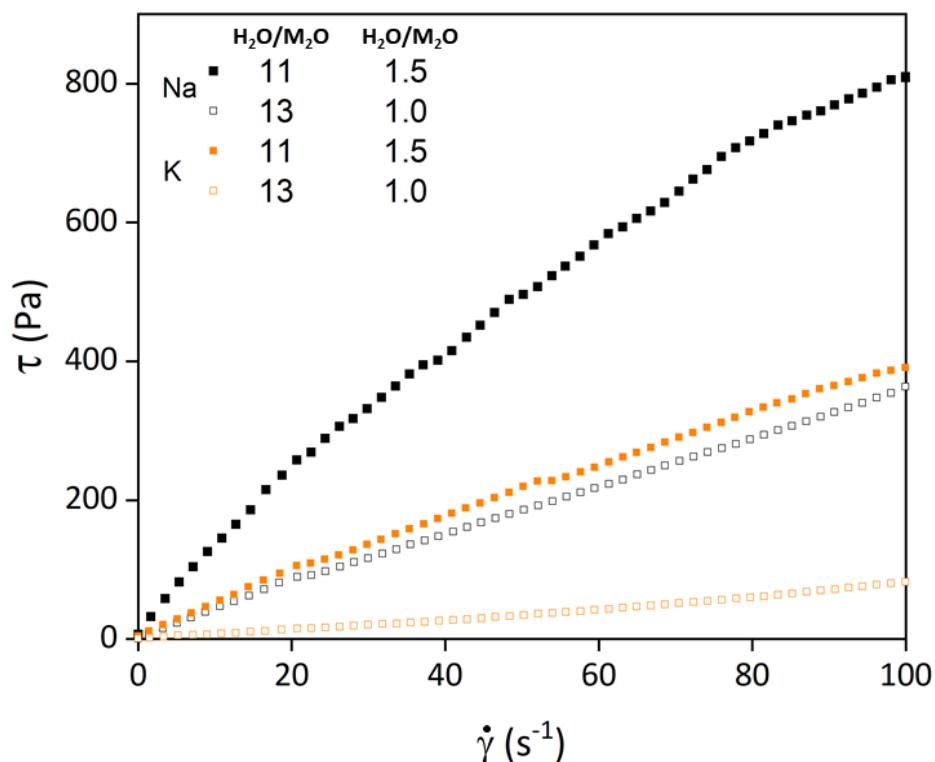
Figure 4-1 – The effect of alkali cation type on the rheology of different metakaolin geopolymer paste formulations, formulated as indicated in the legend.

4.2.2. Fresh State Properties of Potassium Silicate Activated Metakaolin

In order to understand the potential differences in potassium based geopolymer formulations, systematic changes to the activating solutions have been made. The modulus of SiO_2/K_2O in the activator has been varied between 0.5 and 1.5, along with a change of H_2O/K_2O to be 11 or 13 (for a modulus of 1.0). This is intended to lead to the development of a formulation envelope that shows how these materials can be used for a wide variety of nuclear wastes.

4.2.2.1. Rheological Properties

The work of Sanderson [33] has shown that standard pastes used within the UK nuclear sector, which can broadly be approximated by a 3:1 blend of BFS:PC with w/s of 0.35, have a shear stress at a shear rate of 100 s^{-1} between 100 and 450 Pa, depending on the inclusion of different types of BFS. This has been shown in Figure 4-2. It should be noted that this data was fitted using a Bingham model for the data, which assumes that the pastes do not exhibit any thixotropic properties, although this is not the case for geopolymer cements [209]. Following literature surveys, the initial thought for this work was to apply a Herschel-Bulkley model [138]. However, when the data has been investigated further it appeared that the data features some evidence of steps (which will be explored in more detail below). Which demonstrate that the data set is more complicated than a standard Herschel-Bulkley model and therefore, a simplified Bingham and power law model (**Error! Reference source not found.** and **Error! Reference source not found.**, respectively) need to be applied in order to allow for data accurate interpretation. These steps show distinctive changes in the rheological models of geopolymer cements along the decreasing shear rate of a flow curve. This work will show the details of the models applied to each section of the flow curve and how these change with decreasing shear rate of the flow curve, activating solution and MK precursor.
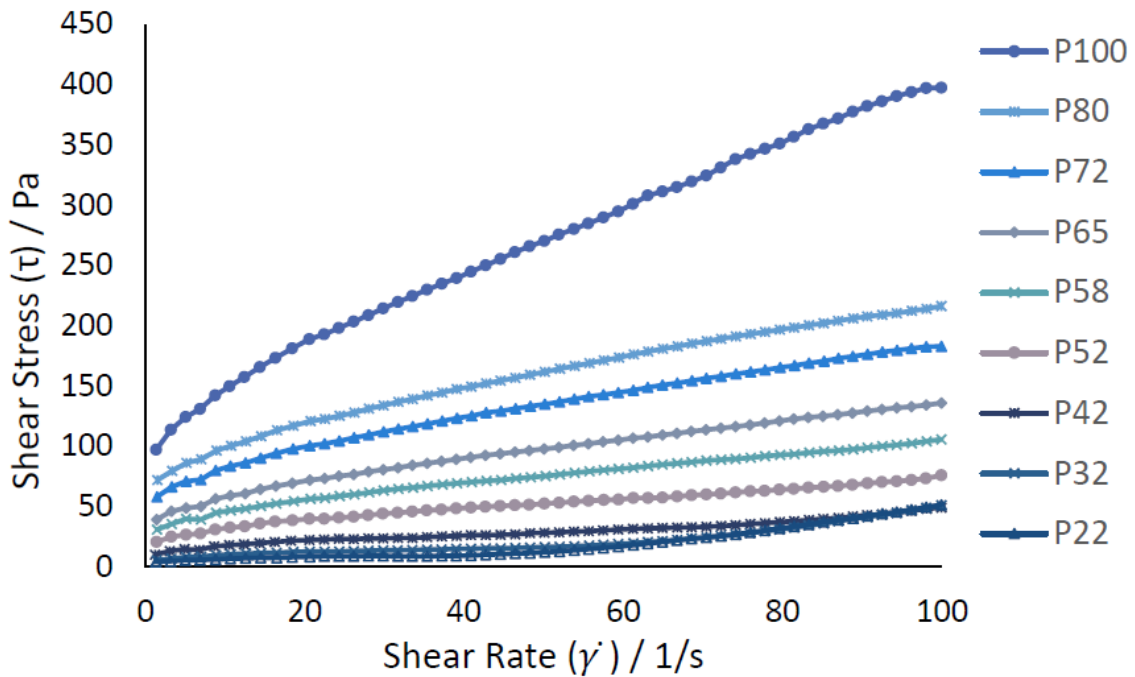
Figure 4-2 – Viscometry data showing the effects of BFS:calumite blends on a 3:1 BFS:PC ratio formulation. The legend represents the BFS:calumite ratio, with P80 representing 80 wt.% BFS and 20wt.% calumite. This has been reproduced from the thesis of Sanderson [33].

4.2.2.1.1. Rotary Calcined MK (RC MK)

The effect of formulation design on RC MK formulations produced from MetaMax is shown in Figure 4-3. It can be seen that the paste viscosity can vary dramatically with changes in the activating solution (both the alkalinity or water content) and the composition/calcination of the raw MK. This experimentally collected data points are shown for a decreasing shear rate of the flow curve, which minimises any artefacts of blade jamming from particle interactions with the blade [214]. This can be a cause of 'steps' within data sets, as the jammed particle is ejected from the blade. It has also been shown by Sanderson et al. [33], who used the same instrument and experimental parameters, that has been used to produce a flow curve for Portland cement/BFS blends and these do not contain the steps that have been shown within the curves presented throughout this thesis. When the curves that are shown in Figure 4-2 are compared to those collected throughout this chapter, the clear and distinct steps that are present in the geopolymer formulations are not shown for these, nuclear specific, Portland cement blends. Therefore, it can be concluded that these steps are due to the paste that is being tested.
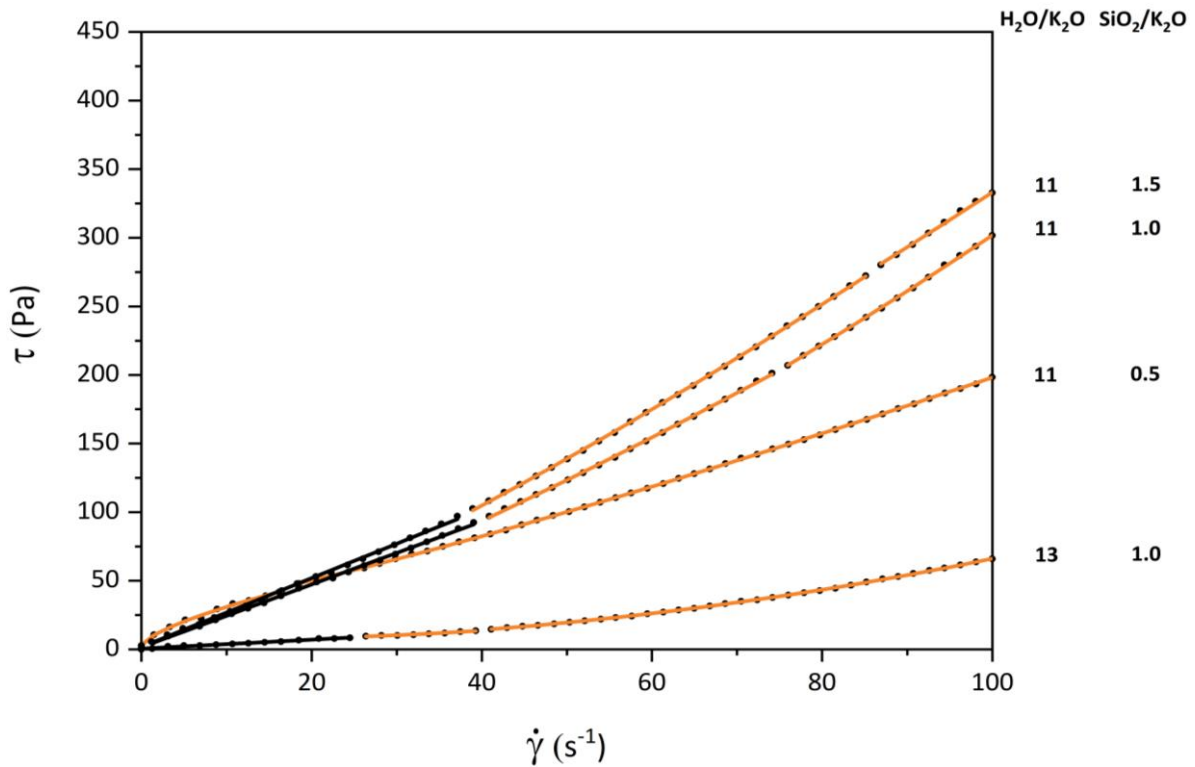
Figure 4-3 – The viscosity of different rotary calcined MK geopolymer formulations, produced from MetaMax. The activating solution compositions are varied and given on the right-hand side. The orange lines are a power law fit and the black lines are a linear fit.

Steps in rheology curves, for the purposes of this thesis, are defined as where the viscosity of the paste appears to decrease and then increase again over a 3-point range. This work will describe these transitions between different viscoelastic behaviours and also give an element in predictability of the data, as appose to being artefacts of the testing method. Jamming or particle ejection can lead to similar steps as is shown in these samples. However, this data is collected on a downward ramp, so particle jamming and material ejection from within the blade is minimised [142, 215]. The work of Phan et al. [216] has shown that when superplasticisers are added to cementitious formulations then it can undergo a shear thinning – Newtonian – shear thickening transition when water content is increased. This is the only reported existence of changes between rheological models during a shear ramping regime. The work will be based around a simple linear (black) and power law (orange) relationship, **Error! Reference source not found.** and **Error! Reference source not found.**, respectively. Transitions between Newtonian and non-Newtonian behaviour have been observed, with a full list of the rheological parameters given in Table 4-1. In order to allow a clear distinction between linear and power-law data, when the exponent, n, falls in the range of $0.85 \leq n \leq 1.15$, then the value is set to 1.0 and a linear equation is assumed. In order to fully distinguish between Newtonian and yield stress

fluids, when $\tau_0 \leq 0.01$ Pa, then it is set to 0 and it is defined that no yield stress behaviour is observed. Setting these ranges allows for any experimental/instrument errors to be overcome and a comprehensive study of the data to be made. The error in the flow curve has been calculated using an r^2 method and these values have been presented in the table. Combining this with the parameters set for the exponent of the power, n, then providing a high r^2 is seen the results can be vindicated, and the methodology selected has been shown to be feasible for MK-based geopolymers. Over the course of this thesis, this method has been used in Chapters 4, 5 and 8 and the closeness of fit has been shown to be close to be within 0.05 in most cases and the lowest presented value of r^2 is 0.969 (section 8.2.1.2).

When the SiO_2/K_2O ratio is increased from 0.5 to 1.5 for the RC MK based geopolymer, Figure 4-3, the initial flow segment (between 0 and approx. 20 s^{-1}) at a low shear rate, the paste moves from a shear thinning paste with n = 0.69, through to a Bingham plastic paste. This initial segment has a low τ_0, between 1.5 – 3 Pa, which makes the pastes with an $SiO_2/K_2O \geq 1.0$ virtually Newtonian in nature. At the intermediate and higher shear rates, all pastes become shear thickening in nature. Changes in the alkalinity has induced a small change of n by ± 0.2, and so altering the SiO_2/K_2O modulus has a minimal effect on the degree of shear thickening behaviour of these pastes at higher shear rates. However, it has not been ruled out that changing the alkalinity of these pastes could be a useful tool in controlling the rheology of these pastes in localised positions. The Newtonian or yield stress behaviour is clearly affected by the alkalinity. At higher shear rates the τ_0 for SiO_2/K_2O = 0.5 is 25.8 Pa, whereas when the SiO_2/K_2O modulus is increased above 0.5, then the pastes have τ_0 = 0 Pa. When th e is $SiO_2/K_2O \leq 1.0$, and the alkalinity is increased, then a Bingham fluid is observed at low shear rates, which then moves onto a shear thickening fluid at higher shear rates. The SiO_2/K_2O = 0.5 formulation contains a greater concentration of alkali cations (K^+) and is therefore expected to have a higher pH. This drives a faster dissolution of the clay particles and leads to the faster formation of the gel phase. This is shown physically by a faster setting time, which is shown in Figure 4-7. This is more evident at the faster shear rates as the paste becomes a shear thickening fluid, and there is an increase in the yield stress (τ_0), which shows that the paste is acting more solid-like under a greater degree of shear. This can lead to the tacky or sticky properties that have been noticed during the preparation of MK based geopolymers. The gradient of the curves (K) decreases when the shear rate is increased for all curves, which allows for the shear thinning conclusion that is usually drawn in the literature for AAMs.
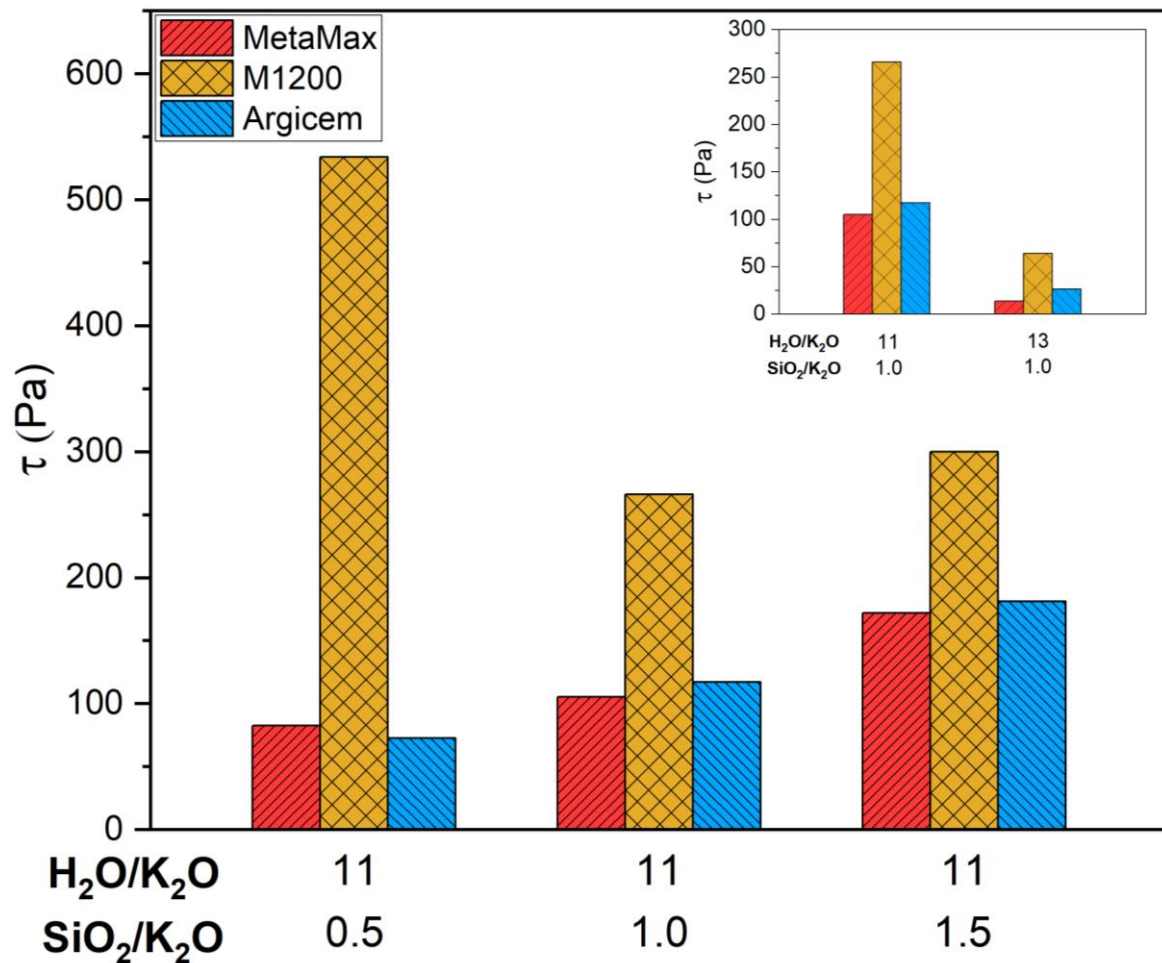
Figure 4-4 – Measured shear stress (τ) 40 s^{-1} comparing the effect of activating solution and clay type on the shear stress of geopolymer pastes. This is taken after zero hold-up time.

Increasing the H_2O/K_2O ratio from 11 to 13 at SiO_2/K_2O = 1.0 causes a dramatic decrease in the viscosity of the paste, which is to be expected [138] and is shown as an inset on Figure 4-4. Over the initial segment both pastes are virtually Newtonian in nature, with τ_0 = 1.57 and 0.53 Pa for the H_2O/K_2O = 11 and 13, respectively. Shear thickening behaviour is observed in both pastes at higher shear rates. However, the higher water paste becomes a yield stress fluid with the value of τ_0 = 7.00 and 5.01 Pa for the intermediate and high shear segments. The value of n for the higher water content system is n > 2.0, with a gradient to the line of less than 0.05 Pa s^n and therefore, cannot be reported accurately due to the limitations of the equipment used. This value is not zero as this would lead to a removal of the power-law term, leading to the production of a horizontal line, and therefore these values have been shown to be low but when multiplied by the value of n for a specific paste can still lead to a slope. This shows that the higher water content paste is significantly lower in viscosity, but the effect of adding water has caused the pastes to become shear thickening in nature. The yield stress of the paste

has also undergone a 3-fold increase with a decreasing water content over the initial period. The Newtonian behaviour of the $H_2O/K_2O = 11$ formulation then proceeds to a fluid that undergoes shear thickening when the rate of shear is increased. At higher water contents the pastes have shown to follow significantly different rheological parameters when compared to lower water content systems with the same modulus; however, the higher water content formulations have a significantly lower viscosity at 100 s^{-1}. The higher water content systems have an increasing shear thickening behaviour and yield stress. The dilution of the activating solution is causing changes in the reaction mechanisms that are leading to the formation of the early age gel structure. This will be analysed further in section 4.2.2.2.

4.2.2.1.2. Flash Calcined MK (FC MK)

The FC MK, shown in Figure 4-5, gives pastes with completely different rheological properties to those produced from the RC MK. Comparisons of the flow properties between different calcination mechanisms have been studied for PC blends [153] and has shown effectively that the pre calcination properties of the kaolinite, such as high quartz contents and spherical particles are present post calcination and maintains flow properties in these blended cements. The chemical and physical make-up of the clay appear to affect the rheological behaviour that is undergone upon mixing with the activating solution. The number of steps on each curve has been affected. Similarities can be seen with the RC MK, as an initial step at approx. 20 s^{-1} is present in each paste. However, the position of this peak does change slightly and is therefore dependent on the MK properties. Considering the Argicem MK (Figure 4-5 (a)), the value of τ_0 increases after each step whilst the paste remains a Bingham plastic fluid overall. However, when the water content of the activating solution is increased then the paste follows a more standard power law relationship over the whole curve. The presence of steps has led to the conclusion that applying one model to a curve will lead to inaccurate results.
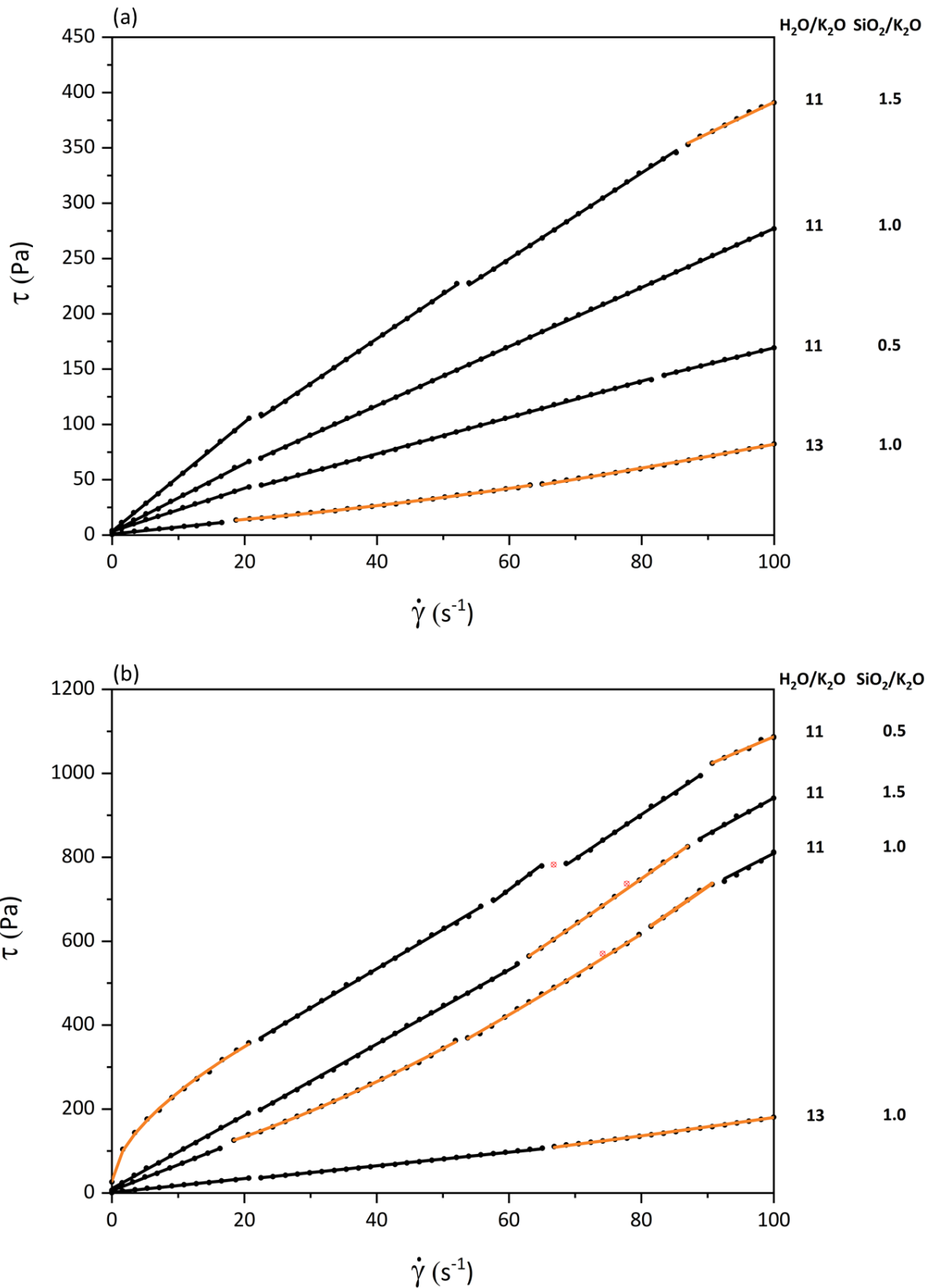
Figure 4-5 – Flow curves of different flash calcined (FC) MK geopolymer formulations. The activating solution compositions are varied and given on the right-hand side. Different MK powders are shown in (a) = Argicem and (b) = M1200. The orange lines are power law fits and the black lines are linear fits. The red crossed-through circles indicate anomalous data points.

For the Argicem MK, when H_2O/K_2O is fixed at 11, and the alkalinity of the activating solution is changed by adjusting the SiO_2/K_2O ratio; then the τ_0 for the flow curve to 20 s^{-1} is approximately 3 Pa. However, as the modulus (SiO_2/K_2O) is increased, then the τ_0 from this second, intermediate curve increases which gives the curves their characteristic Bingham nature. This increase in yield stress midway through the decreasing shear ramp has led to some pastes being generally classified as shear thinning pastes [211], and when considering the higher modulus systems, some literature has stated that these pastes are shear thickening [126, 138]. This is shown schematically in Figure 4-6. The overall viscosity of the pastes is dependent not only on the water content but also the modulus. This concept was proposed and explained by Favier et al. [138], along with the work of Palomo et al. [208] showing that the rate in the rise of viscosity is dependent on the silica content of the system. This is particularly evident in this system; effects like this correlate in the work here, and appear to state that the driving factor within these systems is the SiO_2 content, rather than the alkalinity of the system. Overall when comparing the Argicem, M1200 and MetaMax MKs then the linear (Bingham) regions of this line occur over larger regions (a minimum of 15 s^{-1}) when compared to the power law relationships which occur over a minimum of 10 s^{-1}. Therefore, the regions of shear thinning occur over shorter shear ranges and therefore can be more difficult to control by controlling the shear of the paste. Further investigations into this shear control are given in Chapter 5, as analysis of the types of mixing available within the nuclear industry will allow for effective selection and control of the viscosity of the paste to be analysed. For broader applications outside the nuclear industry, producing a cementitious system that has shear controllable rheology will be very important for producing construction materials that can be used in specialist situations [137].
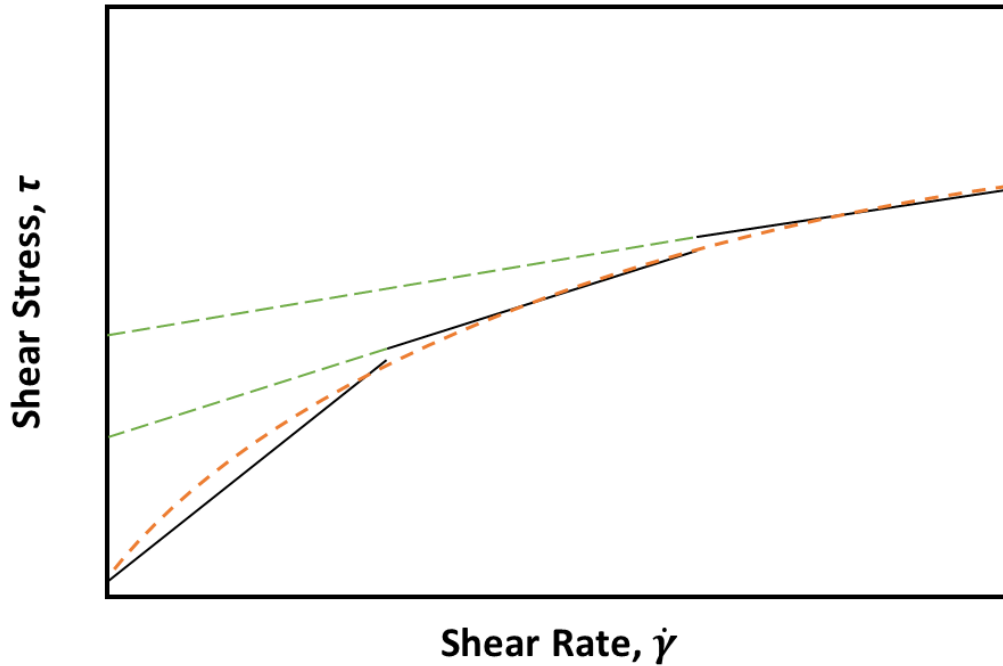
Figure 4-6 – A schematic explanation showing how a paste with a changing Bingham rheology (black lines) with an increasing τ_0 (shown by the extrapolated green dashed line) can be mistaken as a paste following a Herschel-Bulkley (power law), shear thinning regime (orange dashed line).

The shear stress vs shear rate curve for the M1200 clay is shown in Figure 4-5B. At first glance it appears that the $SiO_2/K_2O = 0.5$ has a higher viscosity than the pastes of lower alkalinity ($SiO_2/K_2O >$ 0.5). However, it should be considered that the τ_0 values determined for the first 2 steps are 28.5 and 160 Pa, which are 3 times higher than that of any other M1200 paste at the same step point. This is very similar in curve structure to the high sodium content slag systems shown by Puertas et al. [210]. This work shows that increasing the mixing time and decreasing the modulus of sodium silicate activated slags can lead to a reduction of the yield stress of these pastes. However, the trend in the higher modulus M1200 pastes appears to follow the trends shown in the Argicem and MetaMax MKs. The higher viscosity MK-geopolymers contain the higher viscosity activating solutions, which contain significantly more SiO_2 [138, 210]. Another process must therefore be in play. Struble and Leit [217] have shown that yield stress increases dramatically upon the setting of a Portland cement paste. This is the basis of the Vicat test. Therefore, as the Vicat experiment (shown in section 3.2.4.2) shows that initial setting of this paste is within 60 mins of mixing, it can be assumed that the paste is beginning to set during the testing procedure (approximately 11 mins after initial mixing), which has led to a dramatically more viscous paste. The setting process of pastes based on this MK has not been analysed using the ATR-FTIR test method shown in section 4.2.2.2, as the process is too fast and reactive to be analysed using the Mylar film method. Therefore, further work will need to be undertaken to assess

the early age gel chemistry for these materials. However, the high pH of the activating solutions [138, 139], small particle size [154] and also the high reactivity of the different clays [99, 154, 218] it can be suggested that the particle dissolution and gel propagation stages of the structural development. Further examination of the reactivity of different clays needs to be undertaken. However, examinations of the kinetic properties and setting times using isothermal calorimetry and a modified VICAT method have been shown in section 3.2.4. This data offers an insight into the reactivity of the MK used. Use of the R^3 test could provide useful insight into the reactivity of these materials [219].

Once the silica content of the activating solution is increased ($SiO_2/K_2O \geq 1.0$) for the M1200 formulations, then similar trends are followed when compared to the MetaMax and Argicem MKs. The overall viscosity at 100 s^{-1} is 3-fold greater for $SiO_2/K_2O \geq 1.0$ than that of the Argicem material. The inert quartz that is in the Argicem product leads to a dilution of the reactive component of the MK, acting in a similar manner to sand in mortars. This shows a potential to control the rheology and reactivity of the precursor using a dilution with an inert filler. When the Argicem and M1200 MKs are compared further, it is clear that the presence of the inert filler reduces the shear thickening properties of the MK-GP. As the ratios for the activating solution are related to the molar ratio of Al_2O_3 of the MK to the K_2O of the activating solution, the presence of the unreactive fine SiO_2 particles leads to a reduction in the overall activator to binder ratio. This reduces the volume of activating solution per gram of reactive material in the MK, so can also pose a safer alternative to other AAMs, as less activating solution needs to be transported which reduces the risks associated with the transportation and handling a highly caustic solution, which includes the use of unskilled workers using solutions in excess of pH 14 [104]. This shows that the rheological behaviour of the MK-GPs is based not only around the SiO_2 content, but also around the alkalinity of the activator.

The rheological data for the M1200 MK-GP contain significantly more steps than the MetaMax and Argicem MKs: in most cases these contained 2 – 3 steps, with an initial phase up to approx. 20 Pa and then beyond this an intermediate and possibly a final stage (between 70 – 85 Pa) was seen. However, for the M1200 pastes with $H_2O/K_2O = 11$, these contain 4 or 5 steps. The initial phase still remains around 20 Pa but the intermediate and final phases become distorted. The data for the lower modulus paste appears erroneous, as rapid setting which generates a high yield stress by definition and therefore produces a larger overall viscous paste. The effect of setting on the rheology has been demonstrated here. However, as the modulus is increased to 1.0 and 1.5, similar trends to the Argicem appear for the τ_0 and K values. τ_0 and K both increase as the modulus increases; this increasing yield stress shows that the higher modulus system resists the applied stress to a greater extent. Combining this with the higher gradient of the curve, this gives rise to the stickier nature of this high SiO_2 content paste. These pastes show Bingham rheology for the initial curve. As the curves move beyond the initial

stage and onto this intermediate stage the $SiO_2/K_2O = 1.0$ system moves away from the linear trend and becomes a shear thickening fluid (n = 1.45) with τ_0 = 58.5 Pa. At the next 3 stages the yield stress moves to 0 Pa, but the exponent increases to n = 1.3 – 1.4 and a steeper gradient is seen. Therefore, at this higher speed point of the shear regime, shear thickening behaviour is still observed. However, when the shear rate exceeds 90 s^{-1} then the data becomes linear and no shear thickening behaviour is observed.

When working with these pastes it is physically observed that shear thickening is present in the $SiO_2/K_2O = 1.0$ formulation. When trying to transfer these pastes to moulds or for long term storage, the pastes become thicker and more difficult to work with when shear forces are applied. Increasing the modulus of the activating solution for this paste to 1.5 causes an increase in the gradient of the line at all points and also contains one less step in the intermediate stage of the shear curve. This paste has an overall higher viscosity than that of the lower modulus system. However, the difference between these pastes comes from the shear thickening behaviour. The paste follows more of a Bingham fluid trend at low shear and then it moves to apparent Newtonian behaviour that was not evident in the lower modulus system. The shear thickening behaviour resurfaces at the 2nd intermediate stage. The real difference in this paste is in the final stage, where the linear Bingham behaviour returns with τ_0 = 75.60 Pa. This shows that the paste is much stiffer when shear is applied, which makes the loading of this sample into moulds difficult. The M1200 pastes are difficult to work with on the whole, and the stiffness and/or stickiness of the pastes with a $H_2O/K_2O = 11$ means that these are likely to be unsuitable for nuclear waste disposal applications. Increasing H_2O/K_2O to 13 should allow for control of some of these rheological properties. This increase has caused the τ_0 to decrease to 1.32 Pa (from 5.65 Pa for $H_2O/K_2O = 11$) and then decreasing down to 0 Pa over the intermediate and final steps. The paste does undergo a change in rheological properties: the paste initially shows a Bingham rheology, this then becomes apparently Newtonian in the intermediate stage, and this is followed by shear thickening behaviour that is symbolic of these potassium silicate activated M1200 geopolymers. The low gradient and also the significantly reduced yield stress of these pastes shows that increasing the H_2O/K_2O to 13 is a good way of controlling the harsh rheological properties seen with these pastes. Further research into the higher modulus, high water content formulations is needed.

The shear thickening nature of all the pastes described above has not previously been shown for any geopolymer formulations and is very rare in cementitious systems. However, it has been shown in high water content self-compacting concretes presented by Feys et al. [220]. That work explains that the intensity of shear thickening increases as the water to powder ratio decreases, but this is in contradiction to what is seen in this data seen for geopolymer cements. The work of Cyr et al. [221]

has shown that increasing the water content of a MK-blended Portland cement system, then the paste has a greater shear thinning behaviour which does appear to be the case in these materials (as a reduction in the shear thickening is seen). The addition of a superplasticiser causes the pastes to become shear thickening through electrostatic interactions. But, as with the self-compacting concrete, this decreases in magnitude with water content. Therefore, the literature for cementitious systems appears to contradict that what is shown here, but those systems are based around Portland cement, which can offer significantly different rheology compared to MK-GPs.

Table 4-1 – The rheological parameters for the lines fitted to the data in Figure 4-5. If the value of n was calculated to be between 0.85 – 1.15, then this was fixed at 1.0 and a linear model was applied.

MK Type		Argicem				Argical M1200				MetaMax			
H_2O/K_2O		11			13	11			13	11			13
SiO_2/K_2O		0.5	1	1.5	1	0.5	1	1.5	1	0.5	1	1.5	1
Model 1	n	1.00	1.00	1.00	1.00	0.60	1.00	1.00	1.00	0.69	1.00	1.00	1.00
	τ_0 (Pa)	3.31	2.69	3.37	1.02	28.5	5.65	10.4	1.32	2.97	1.57	1.76	0.53
	K (Pa s^n)	1.95	3.09	4.93	0.62	53.3	6.16	8.73	1.65	5.69	2.29	2.51	0.33
	r^2	0.998	0.999	0.999	0.987	0.997	0.998	0.998	0.998	0.995	0.999	0.998	0.981
Model 2	n	1.00	1.00	1.00	1.43	1.00	1.45	1.00	1.00	1.20	1.24	1.26	2.39
	τ_0 (Pa)	7.68	10.1	15.6	6.80	160	58.5	0.0	0.00	25.8	0.00	0.00	7.0
	K (Pa s^n)	1.64	2.67	4.05	0.10	9.36	0.99	8.87	1.62	0.64	0.98	1.00	<0.05
	r^2	1.000	1.000	0.995	0.999	0.999	0.999	0.999	0.999	0.999	1.000	1.000	0.976
Model 3	n	1.00	-	1.00	1.37	1.00	1.30	1.18	1.24	-	1.37	1.21	2.07
	τ_0 (Pa)	20.60	-	16.8	0.00	0.46	0.00	0.00	0.00	-	0.00	0.00	5.01
	K (Pa s^n)	1.49	-	3.88	0.15	12.0	2.04	4.23	0.59	-	0.54	1.27	<0.05
	r^2	1.000	-	1.000	0.999	0.999	0.999	0.997	0.998	-	1.000	0.998	1.000
Model 4	n	-	-	0.71	-	1.00	1.38	1.00	-	-	-	-	-
	τ_0 (Pa)	-	-	0.00	-	58.1	0.00	75.60	-	-	-	-	-
	K (Pa s^n)	-	-	14.7	-	10.5	1.49	8.65	-	-	-	-	-
	r^2	-	-	0.997	-	0.999	0.997	0.997	-	-	-	-	-
Model 5	n	-	-	-	-	0.61	1.00	-	-	-	-	-	-
	τ_0 (Pa)	-	-	-	-	0.00	0.00	-	-	-	-	-	-
	K (Pa s^n)	-	-	-	-	66.7	8.09	-	-	-	-	-	-
	r^2	-	-	-	-	0.993	0.998	-	-	-	-	-	-

Rheological Parameters of Lines in Figure 4-3 and Figure 4-5

All formulations, beside the high alkalinity pastes for the M1200 and MetaMax MKs, exhibit an initial linear Bingham behaviour. Therefore, to compare the apparent viscosities of these pastes, interpolation of the data needed to occur before the pastes began to exhibit significant thixotropic effects. This point appeared to be approx. 40 s^{-1} for most of the formulations. This is represented in Figure 4-4. Similarities between the RC and FC MK can be seen in the higher water content formulations. All formulations have a lower overall apparent viscosity compared to the respective lower water content systems, which can be seen in the inset in Figure 4-4 and clearly shows that the MetaMax formulation has the lowest apparent viscosity. Figure 4-4 shows that when the SiO_2 content of the activating solution is decreasing, then the apparent viscosity of this activating solution decreases, which is also demonstrated by the work of Favier et al. [138]. The only exception to this is the M1200 formulation with H_2O/K_2O = 11 and SiO_2/K_2O = 0.5. This discrepancy has been put down to the reactivity of the base clay, reacting with the highly alkaline activating solution, which has caused the MK-GP to begin setting during the testing procedure. The Argicem and MetaMax viscosities at γ = 40 s^{-1} are very similar, and both well within the range expected for Portland cement. However, if the curves shown in Figure 4-3 and Figure 4-5(a) are considered, the MetaMax pastes exhibit a shear thickening behaviour, which is not seen on the Argicem pastes which exhibit a more linear Bingham plastic behaviour, and makes the rheological properties of the Argicem material much easier to predict and understand. Therefore, predicting which material should be used for the UK nuclear industry based solely on the rheometry results is impossible, and an understanding of the reaction kinetics and the hardened state properties is also important to understand the potential of these materials in a waste disposal context.

4.2.2.2. Reaction Kinetics

4.2.2.2.1. Isothermal conduction calorimetry (ICC)

The reaction kinetics of cementitious systems are usually studied using isothermal conduction calorimetry (ICC), and the chemistry of Portland cement systems has been well understood using this technique. ICC has been shown to offer some benefits for geopolymer cements, and a characteristic trend has been proposed by Zhang et al. [124]. This heat flow curve involves an induction or MK dissolution period, a gel rearrangement or structural formation section, followed finally by a gel propagation and paste hardening state. The UK nuclear industry specification states that the cumulative heat output at 35 °C should not exceed 180 Jg^{-1}, over the first 48 hours [31]. In order to

show the thermal stability of these materials and to compare to established literature, this experiment has been conducted at 40 °C.

Figure 4-7 shows the heat flow isothermal calorimetry curves, with the cumulative heat curves inset, at 20 and 40 °C for the 12 of the pastes that have been studied above. The setting time of these pastes has been analysed using a modified Vicat test, as described in section 3.2.4.2. The UK nuclear industry also has strict requirements for setting time. These are performed following the British standard for testing setting time of Portland cement, BS EN 196-3 [189]. In order to pass these tests for Portland cement, set out in the NNL specification NNL 13324 [31, 207], the material must undergo initial set within 4 hours and then final set after 24 hours. However, as is described in section 4.2.2.1, the yield stress development of these geopolymer pastes is not comparable to Portland cement. As the Vicat method is a measure of the yield stress, using this in conjunction with the ICC data will be the most accurate way to establish if these materials have met the required standards.

Overall, the reaction occurs much slower in the 20 °C samples compared to the 40 °C sample, which is to be expected [124, 132]. When the reaction is undertaken at 40 °C, similar trends are shown to the data that are collected at 20 °C. However, the reaction occurs much quicker and produces a large heat flow. Comparing the cumulative heats for each paste at 20 and 40 °C, the final output remains constant across these two temperatures, but the time taken to get to this output is much lower; i.e. the reaction comes to completion much quicker. Slight differences in the values can be associated to small differences in the temperature of the paste that is added to the calorimeter.

RC MK, MetaMax, geopolymer has been shown to have the lowest overall viscosity, even though its rheological properties are more complex than that of the FC MK, Argicem, geopolymer. This has been postulated to be due to a significantly more reactive MK, which is shown in the ICC data. Increasing the modulus of the activating solution from 0.5 to 1.5 causes a change in the intensity and peak position of the polymerisation section of this curve. The concentration of alkali cations within the activating solution has been the driving factor for the polymerisation process that is undergone in the gel network of these materials [124]. The initial dissolution peak at $t \leq 90$ mins shows that the dissolution of the clay when reacted with the higher alkalinity activating solution ($SiO_2/K_2O = 0.5$) causes a significantly greater dissolution of the MK, as the intensity of the peak is greater than those of the rest of the formulations. This is then carried on through the curve to the polymerisation stage, where the paste with $SiO_2/K_2O = 0.5$ remains the highest in terms of peak intensity. This shows that significantly greater heat is being released from this formulation, which can be seen from the cumulative heat curves.

Increasing the modulus to 1.0 and 1.5 causes a reduction in the overall intensity of the initial dissolution peak at each stage. However, these do become different when considering the polymerisation peak. Increasing the SiO_2 content of the activator to 1.5 causes a significant reduction in the intensity and also an elongation of the peak. The delay in the formation of the gel structure should allow for the propagation of a more stable gel structure [201]. A likely reason for a slower reaction is due to a slower release of aluminium from the MK [222] leading to an overall slower reorganisation of the gel structure. This slower gel formation should lead to a more organised and stable gel structure, although this has only been shown for sodium silicate activated fly ash [201]. The modified Vicat method has shown that the onset of the setting process, at 20 °C, correlates with the increase in the heat output for the polymerisation peak.

Increasing the temperature to 40 °C causes some changes in the RCMK GP thermal output. Increasing the reaction temperature causes a significant increase in the thermal output at early ages, which causes the initial dissolution and polymerisation peaks to be merged into one, in all formulations. However, the cumulative heat flow for each curve reaches a very similar maximum, with the only change being the time frame in which the gel reaches that total cumulative heat value. The high modulus (SiO_2/K_2O = 1.5) formulation falls below the 180 Jg^{-1} set out in the NNL acceptance criteria, while the cumulative heat values for the modulus values of 0.5 and 1.0 are 214 and 212 Jg^{-1} respectively, at 24 hours. It is possible that a small increase on the currently acceptable criteria may nonetheless be acceptable, due to the different reactions that are being undertaken in these systems compared to Portland cement hydration.

The FC MK geopolymer ICC curves are shown in Figure 4-7 (C-F), with the Argicem MK in Figures 6C and D, and the M1200 in Figures 6E and F. These follow the same general trends that are described above for the RCMK system. Differences are, however, present in the intensities of the heat flow curves; these are then translated into significant different intensities in the cumulative heat patterns. The cumulative heat for the Argicem is approximately 50 – 75 Jg^{-1}, which is much less than the M1200 and MetaMax formulations. The inclusion of secondary mineral phases within the Argicem product has diluted the thermal output of the reaction, when compared to M1200 and MetaMax. The cumulative thermal outputs for the M1200 and MetaMax reach a very similar value over all formulations. However, for the M1200 reaches the cumulative heat value significantly quicker than that of the MetaMax. This has shown that the calcination method used in the production of these MK based geopolymers does not change the gel structure formation. The level of reactivity of the M1200 clay in the polymerisation stage of the reaction is greater than that of any other MK tested here.

Increasing the curing temperature of the M1200 samples to 40 °C causes the same merging of the dissolution and polymerisation parts of the ICC curves that is seen in the MetaMax samples, with a significantly greater intensity compared to the other MKs. This occurs over a significantly quicker time than the MetaMax system, so the total cumulative heat remains comparable. Therefore, the driving force in the production and extent of the gel phase formed is the activating solution composition, which can be seen to have significant effects on the heat flow curves produced. The clay reactivity and the reaction temperature will play a less dominant, but still significant role on the gel structures that are formed in the MK-based geopolymer. As mentioned above, the Argicem MK does have a significantly reduced thermal output compared to the other MKs used, and this is attributable to the approx. 50 % dilution of the raw MK by the presence of inert crystalline silica. The Argicem MK does have a thermal output that passes the NNL acceptance criteria across all formulations. The setting time is where the real differences occur between the M1200 and Argicem MKs. The setting time for the Argicem is greater across all formulations when compared to the relevant M1200 formulation. Adjusting the formulation for the M1200 appears to make a minimal difference in the setting times of this material. As mentioned above in section 4.2.2.1, the setting time of the $SiO_2/K_2O = 0.5$ M1200 paste is less than 90 minutes. This is linked to the strange rheological properties that do not match the trend of the rest of the data. The kinetic data shown in Figure 4-7 demonstrate that the clay reactivity has not changed the products formed, but has mainly changed the speed at which these are formed.

Upon increasing the H_2O/K_2O from 11 to 13, which are given by the blue and red lines in the plots, respectively, there is a slight decrease in the intensity of the polymerisation peak at higher water content when compared to the equivalent lower water content formulation. The reaction kinetics follow the same pattern as the $H_2O/K_2O = 11$ formulations, just with a reduced intensity; the more dilute, $H_2O/K_2O = 13$ system reacts slower. This correlates nicely with the setting time data, which show that in all cases the higher water content formulations take longer to set. This increase in setting time shows that the setting of the cementitious system is driven by the pH of the activating solution. Changing the water content of the grout increases the setting time slightly, and this allows the setting time of the RC MK formulation to become more acceptable under the criteria set out. The FC MK setting time, however, seems to depend on the raw clays that are being tested. The M1200 MK follows that of the RC and FC MK but with a much faster reaction time, which correlates nicely to what has been shown for the M1200 heat flow curves. The Argicem MK has been shown that when increasing the water content of the activating solution, the setting time decreases slightly. Further investigation into why this has happened will be performed using in-situ ATR FTIR, in section 4.2.2.2.2. When comparing the difficult rheological properties, the stiffness and stickiness of the paste and also the

rapid setting time of all the M1200 formulations, it is looking increasingly likely that this material will not be used as a nuclear waste immobilisation grout. Therefore, combining these above properties, the quick setting time and also the difficult nature of this paste to work with, the pastes made from this MK have not been included in the ATR-FTIR study.
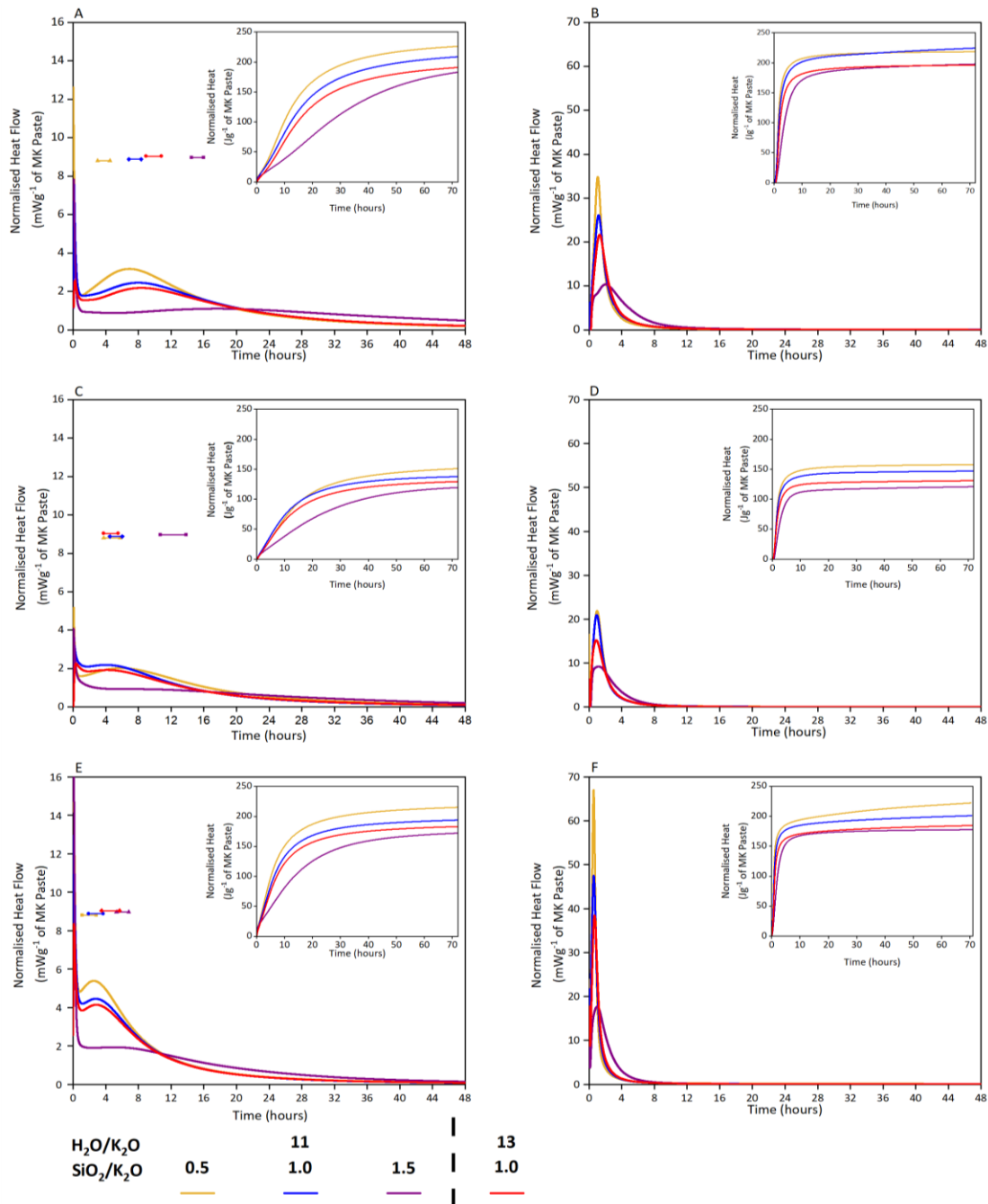
Figure 4-7 – Isothermal conduction calorimetry curves for MetaMax (A, B), Argicem (C, D) and M1200 (E, F). with the 20 °C data on the left and the 40 °C data on the right. Inset is the cumulative heat data for each formulation. Initial and final setting time at 20°C are represented by the points connected by the lines shown in figures A, C and E. The y-axis scales for the normalised heat flow for the 2 temperatures tested are different.

4.2.2.2.2. Attenuated Total Reflectance Fourier Transform Infrared Spectroscopy (ATR-FTIR)

The use of in situ FTIR has been performed in the literature for geopolymers [222-224], and this technique has been used to show the development of the gel structure within a fresh paste sample of a geopolymer or alkali-activated material. The work of Lee and van Deventer [224] and also Rees [223] has shown that the most characteristic spectral range for these materials is between 800 – 1350 cm^{-1}. FTIR measurements can be used to determine changes in the aluminosilicate gel structure, through the stretching of the T – O – T (where T = Al or Si) bond, which allows for the determination of the coordination of silicon at different times during the curing process [120]. Small peaks can be at approx. 2300 cm^{-1}, and these are likely related to HCO_3^- caused from the carbonation of the samples which have been left in open air environments during testing [225]. Over longer time frames, MAS NMR can be used to show similar results [88, 90], but it is not simple to conduct NMR experiments on a timeframe as fast as is used for in-situ FTIR. FTIR can also be useful at showing the location of bound water within the gel structure, along with finer refinements of carbonation [226]. The use of in situ FTIR should bring an understanding of how the chemistry of these species changes during the setting process. The samples have been tested over a 6-hour period, which is intended to demonstrate the changes that are taking place during this time, Figure 4-7.
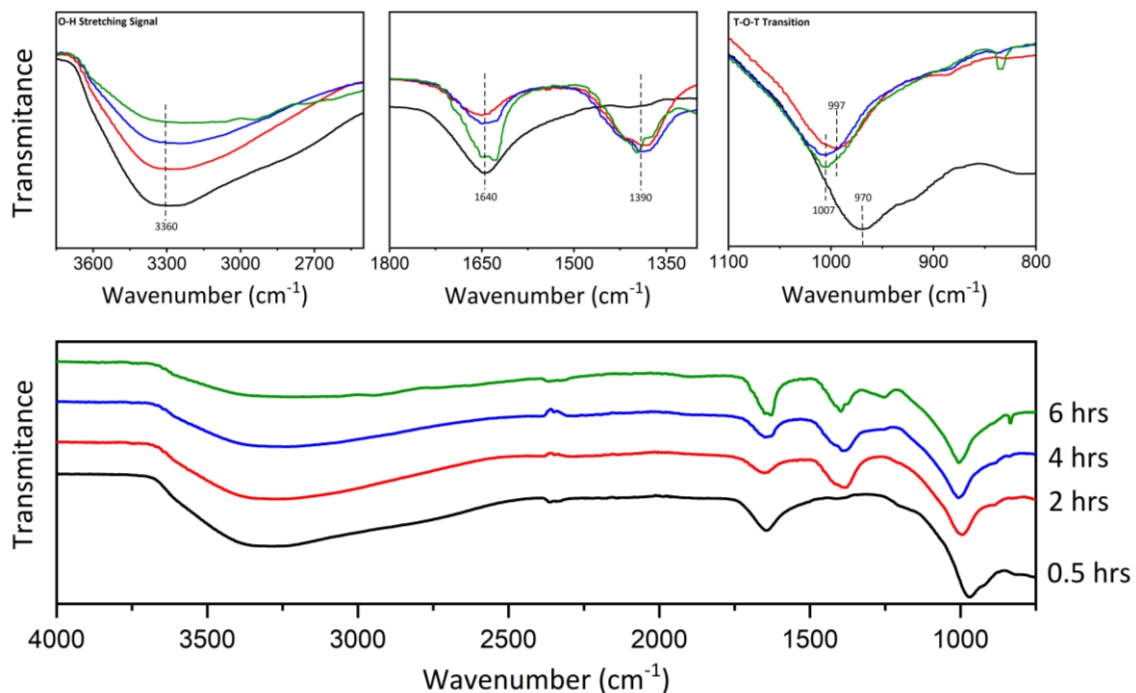
Figure 4-8 – In-situ ATR FTIR of the Argicem MK geopolymer with H_2O/K_2O = 11 and SiO_2/K_2O = 1.0. The inset regions at the top show the important stages on the FTIR curve below. The black, red, blue and green lines represent ½, 2, 4 and 6 hours after mixing, respectively.

For the Argicem MK, the sample remained stable without problematic drying during the experiment, and data have been collected periodically up to 6 hours after the initial mixing. The effect of increasing

water content has been compared in Figure 4-8 and Figure 4-9, with the H_2O/K_2O increasing from 11 to 13. The use of insets has allowed for specific analysis to be drawn on important characteristics within the ATR FTIR curves shown below. All peak assignments that have been used throughout this section to represent characteristic stretching's and vibrations will be discussed in Chapter 6 in the context of the work presented there and referenced in Table 6-2. Comparing the setting times and the reaction kinetic curves in Figure 4-7, it would be expected that increasing the water content would not affect the gel structure formation. However, that is not what has been seen here. In Figure 4-8, the Argicem formulation with $H_2O/K_2O = 11$ has been analysed, and it shows very clear differences between the intensities and the position of transmittance peaks. The first peak position, at 3360 cm^{-1}, remains constant over all curing times, as this is the O-H stretching peak for the bound water within the system. This peak shows the presence of water within the MK geopolymer, which is to be expected, and that the intensity of this peak decreases with time. However, as the sample is unsealed when this test is being performed, it can be seen that water is also lost from this sample. This has led to 6 hours being the limit of the reaction time that can be analysed here. Interestingly, a further H-OH stretching can be seen at 1640 cm^{-1}, and the intensity of this peak after the initial ½ hour decreases and then begins to increase again. This is characteristic of the bound water of these samples, and shows that as the samples begin to cure more water is being bound into the gel.

The peak at 1390 cm^{-1} has previously been attributed to carbonation in cementitious materials, with this indicating the stretching of the O-C-O bond [227]. Carbonation has occurred within 2 hours for these samples that have been cured in the open air. An important point of note is that the initial 30 mins of open air curing did not produce any carbonation products and therefore, for the formation of precast products with the need for low CO_2 inclusions, a significant 'working time' is available for these materials. The intensity of this peak remains constant after 2 hours of curing, which suggests that the limit of natural carbonation has been reached quickly within these small samples of the geopolymer materials.

The Si-O-T transition is described by the inset to the right of Figure 4-8, which has occurred between 1100 – 950 cm^{-1} [228]. This shows a development of the gel structure by a shift in the position of this peak from 970 cm^{-1}, to 997 cm^{-1} and then 1007 cm^{-1}, after 6 hours of curing. This has been described by Rees et al. [229], as at the lower wavenumbers an Si-O-Al rich gel (970 cm^{-1}) structure is formed, which is then replaced by an Si-O-Si rich gel (997 cm^{-1}) structure. This has been described in the literature as the beginning of the gel formation phase, and studies of the microstructure after 6 hours will allow for a complete understanding of the structural development of the gel structure. Gels 1 and 2, that are described in section 2.2.4.2.1, are seen to be formed here with the Gel 1 structure being formed first and this then being closely followed by the Gel 2 structure. The peak at around 1007 cm^{-1}

[1] has been attributed by Bernal et al. [230] as being characteristic of a highly cross-linked gel structure that can lead to a long term stability of these materials. As it has been shown that these samples have dried and also are fluid for a period of time during the testing, it is possible that the samples could have moved or the drying could have caused the sample to move away from the crystal, which could have led to this change as the IR radiation is not capable of probing at different depths.
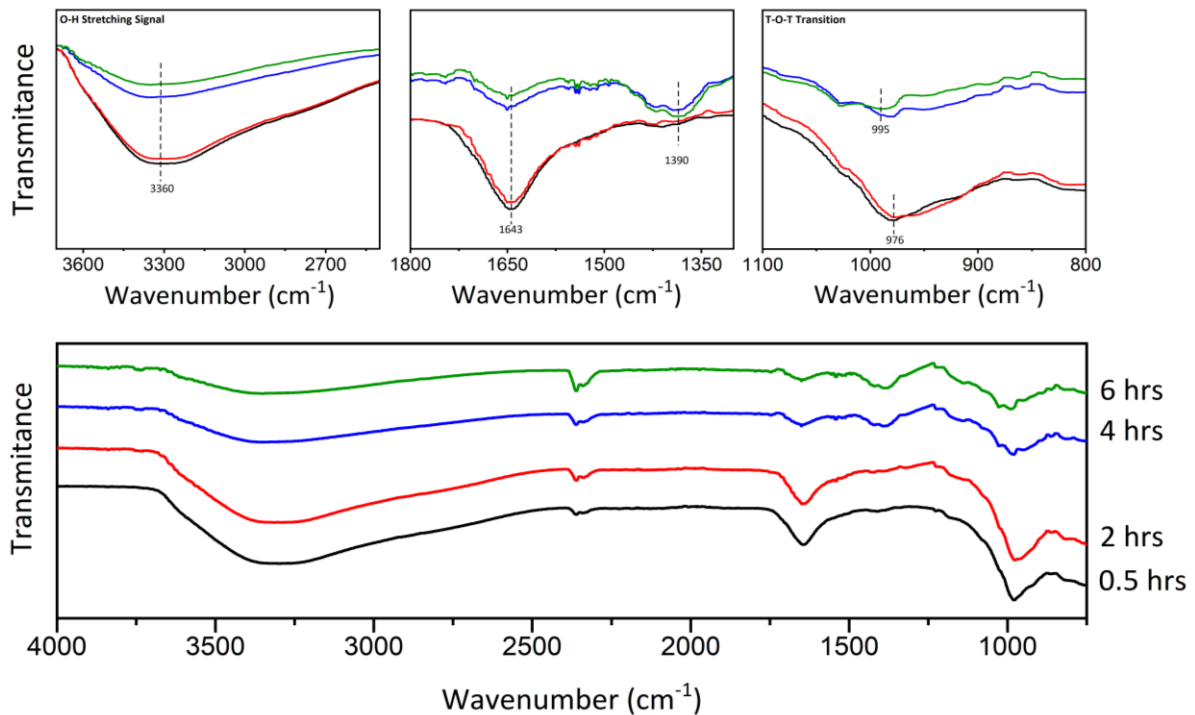
Figure 4-9 - In-situ ATR FTIR of the Argicem MK geopolymer with $H_2O/K_2O = 13$ and $SiO_2/K_2O = 1.0$. The inset regions at the top show the important stages on the FTIR curve below. The black, red, blue and green lines represent ½, 2, 4 and 6 hours after mixing, respectively.

When the H_2O/K_2O ratio is increased to 13, changes in the development of the gel structure are seen. The first point to note is that this sample undergoes drying in a significantly faster way than the $H_2O/K_2O = 11$ system. Therefore, the intensities of the peaks studied are difficult to interpret. The water position and the O-H stretching still remain in similar positions to the lower water system, 3360 and 1643 cm^{-1}. Interestingly the carbonation (O-C-O) stretch at 1390 cm^{-1} is still present but it takes longer to form in comparison to the lower water content formulation. This is unexpected as in conventional cementitious systems the higher the water content, the faster the carbonation due to an increased porosity [231]. Again, within this formulation a limit of natural carbonation is reached after 4 hours of curing. The gel structure transition is shown on the right hand inset in Figure 4-9, this shows a similar structural change to what is shown in Figure 4-8.

The development of the 1007 cm^{-1} cross-linked gel structure has not been seen at 6 hours of curing. This is demonstrating that the setting time, which is the same when H$_2$O content is changed, may not be solely due to the development and formation of a cross-linked gel structure. However, when combining the ATR-FTIR data and the ICC it can be seen that the second polymerisation peak is related to the setting time of this material. Further research needs to be undertaken in order to assess the production of specific gel products and how they relate to the setting of the different geopolymer formulations.

However, testing the MetaMax samples led to the instrument recording an absorbance greater than 100 %. This shows that light was entering the ATR crystal; this has occurred from the sample lifting from the Mylar film and the sample has moved away from the crystal. This is shown in Figure 4-10. Some of the trends within this data set can be interpreted on a broad scale, however analysis of specific peak positions will not be possible. It is clear to see that the broad scattering between 3500 – 3000 cm^{-1} is present within these samples, this is related to the O-H stretching bond stretching within water contained within the sample, and it does appear that this peak is getting shallower with time. It is believed that the sample is drying on the Mylar film, which is causing the lifting as is hypothesised above, due to shrinkage. The silicate based T-O-T band can be seen between 900 – 1000 cm^{-1} at 2 and 4 hours. Although this dataset contains some errors, which were unfortunately not able to be overcome through repeating this sample, it does show that this method can be used to elucidate key information on the gel structure, using this in-situ FTIR methodology. If the technique is adapted to remove this drying effect, then we will be able to understand the early stage development of these MK based geopolymers. This technique can experience some issues regarding the intensity of some peaks, due to the drying demonstrated in Figure 4-10, and also the intensity of the radiation that is lost within the ATR crystal when compared to a method such as KBr pellets, which is performed on powders (shown in section 6.2.2)
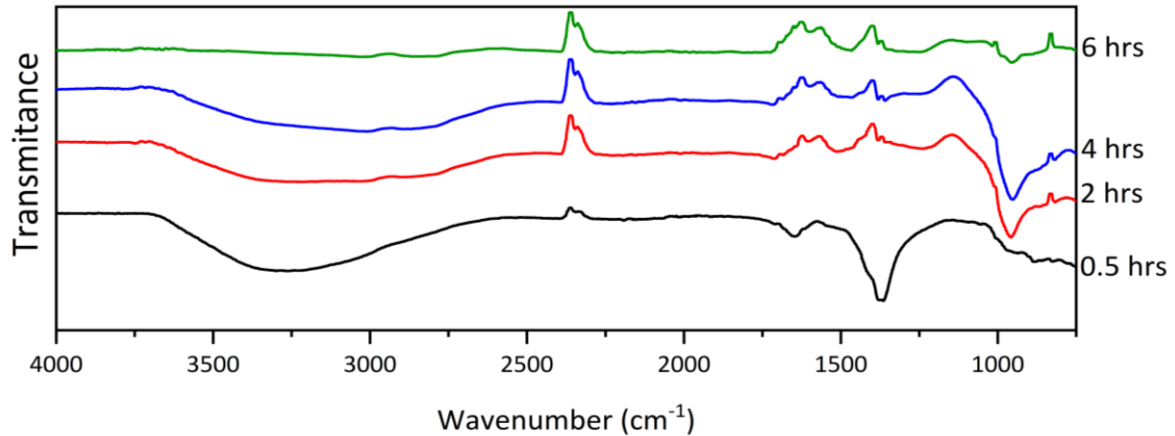
Figure 4-10 – In-situ ATR FTIR of the MetaMax MK geopolymer with a H_2O/K_2O = 11 and an SiO_2/K_2O = 1.0. The black, red, blue and green lines represent ½, 2, 4 and 6 hours after mixing, respectively.

4.3. Conclusions and Future Work

The presence of multiple rheological trends being observed within a $0 – 100$ s^{-1} shear rate curve has been observed for the first time in geopolymer cements. MK-based geopolymers activated with potassium silicate were chosen over sodium silicate, although sodium silicate is significantly cheaper, as potassium silicate offers a 5-fold reduction in the viscosity of the paste. Potassium silicate activation is seen as a more stable method of activation when compared to sodium silicate, as sodium silicate may rapidly crystallise causing a rapid solidification. This would cause severe complications to any of the waste encapsulation plants that this cement was used on, and would therefore not be an effective grout for waste immobilisation.

The rheological properties of 3 MKs have been tested, these had varied properties with 1 clay being RC MK (MetaMax) and 2 clays being FC MK. One of these FC MK was pure (M1200), and the other contained approx. 50% secondary mineral phases (Argicem). The geopolymerisation process of these clays led to vastly different rheological properties occurring across all the clays. As shear increased up to 20 s^{-1}, a step occurred which led to a change in the rheological properties. This then led to an intermediate stage, which was followed by a further step between $70 – 80$ s^{-1}. This was consistent across all pastes, apart from the M1200 which contained multiple steps in the intermediate stage. It has been shown that there is a potential to control the viscosity of MK based geopolymers by shearing the pastes at specifically predetermined speeds that will allow for the production of a paste with the viscosity that is required. It has been shown that the viscosity of an MK geopolymer is dependent on not only the activating solution, but also the clay type and the reactivity of this clay. The M1200 clay gave a higher apparent viscosity than that of the MetaMax or Argicem MK pastes, and when this is

combined with the rapid setting times it has been decided that this does not meet the standards set out by the UK nuclear industry. The remainder of this thesis work will focus on the MetaMax and Argicem raw materials.

The cumulative heat curves have been affected significantly and reduced by the inclusion of secondary mineral phases, which shows that the thermal output during the geopolymerisation process is less. However, the profile of the heat flow curves has remained constant and a polymerisation peak is present in all formulations tested at 20 °C. This polymerisation peak links to the setting time assessed by Vicat testing, however the direct mechanism of this cannot be concluded using the results below. ATR-FTIR has been used to try to elucidate the gel structural changes over the early ages of curing. It has shown that the gel structure does change between an aluminium rich Si-O-Al gel to form a Si-O-Si rich structure. This structure in the low water content system becomes highly cross-linked, which is linked to the stability of the geopolymer structure. Interestingly this does not occur in the higher water content system, although the higher water content system has a very similar setting time to the lower water content system. Therefore, it has been concluded that the gel structural formation is not the sole factor controlling the solidification of the geopolymer cementitious product. Further work needs to be done to understand what structural changes exist as the geopolymer paste is setting. Linking this to the overall reactivity of the clay, studied via an R^3 test (or similar) will allow for a thorough understanding of how MK reaction leads to the formation of a geopolymer gel structure.

Chapter 5: Can mixing geopolymer cements at different shear rates affect the physical and chemical properties of the paste?

5.1. Introduction

Understanding the effect of mixing on geopolymer cements will be useful for applications within the nuclear industry and also for different construction applications. This chapter will not fully assess the blade geometry. However, the work undertaken here was using an overhead stirrer with speed control up to 2000 RPM, whereas the work in Chapter 4 was undertaken using a planetary mixer with less precise speed control. Comparisons will be drawn between this work throughout this section. A full explanation of the Newtonian and non-Newtonian rheological properties is given in Figure 3-2, along with a demonstration of how the mixing and testing has been performed on these materials which is presented in Figure 3-3.

Chapter 4 has examined the overall rheology of the MetaMax and Argicem MK pastes at different composition of activating solutions. MetaMax and Argicem will be referred to as RC MK and FC MK, respectively, throughout this chapter and the remainder of this thesis. Overall it has been shown that increasing the water content is the most effective way to reduce the viscosity of these pastes. However, effective control of the rheological properties can also be achieved by adjusting the composition of the activating solution. The lower the alkalinity of the activating solution, the higher the shear stress. Tests were performed at 40 s^{-1} (Figure 4-4) and this demonstrated the above effects clearly. The MK affects the viscosity and the RC MK is overall a lower viscosity that the FC MK. However, the inclusion of secondary mineral phases, such as quartz, within the FC MK allows for more control of the rheology and appears to reduce the number of steps within the flow curve.

The steps that have been seen within section 4.2.2.1 have been analysed in great detail and transitions between different rheological models have been demonstrated. However, an understanding of how these changes have come into effect is unknown, and a study of different shear rates is presented here in order to analyse the rheological properties of pastes that have undergone different shear routines. Literature has shown that flocculation can occur within colloidal aluminosilicate systems [232]. Flocculation is the reversible process by which colloidal particles are held together by weak physical interactions that lead to the formation of a larger colloidal precipitate that can phase separate [233]. Geopolymer systems have been demonstrated to undergo colloidal reactions [139, 140] and therefore, have the potential to undergo flocculation. In the processing of Al_2O_3 flocculation has been observed, and this has led to sharp changes in shear stress at finite shear rates [234]. These sharp

71

changes show similarities to the steps that have been shown within Chapter 4. Studies of flocculation have been undertaken on kaolinite slurries, and it has been shown that the inclusion of quartz within these slurries can lead to a reduction in the overall flocculation [235]. Therefore, MKs that have a level of quartz inclusion, such as the Argicem FC MK, could potentially reduce the number of steps within the flow curve and allow for more controllable flow.

5.2. Materials and Methods

To more fully assess the rheological characteristics of the pastes, including the steps seen in the flow curves presented in Chapter 4, the geopolymer pastes (formulated in Table 5-1) have been mixed at speeds that correspond to the first stage step that has occurred in the flow curves in Figure 4-3 and Figure 4-5, for the RC and FC MK, respectively. In order to analyse this, the overhead stirrer was set to specific shear rates that occur at the step periods. These speeds are 650, 1300 and 2000 RPM, which corresponds to 11.8, 21.7 and 33.3 s^{-1}, respectively. These speeds are as close as possible to the step positions in section 4.2.2.1, as is possible with the limitations of the equipment, in order to fully assess the resilience of these pastes to the speed of mixing and also the effect of mixing time on these pastes. This will show at which point during the mixing, with a shear blade, leads to the transitions that have been shown in Chapter 4.

Table 5-1 – Geopolymer formulation that have been used throughout this chapter.

H_2O/K_2O	SiO_2/K_2O	K_2O/Al_2O_3
13	1.0	1.0

5.3. Results and Discussion

The flow curves for the FC and RC MK pastes that had been mixed at different mixer speeds are given by Figure 5-1 and Figure 5-2 , respectively. The curves are analysed following the same principles given in Chapter 4, with the linear and power law fits being given by black and orange lines, respectively. Table 5-2 shows the equations of the linear and power law lines.

5.3.1. Rheological Properties

The flow curves of the FC MK given in Figure 5-1 show that the effects of mixing are very pronounced within the FC MK geopolymers, and increasing the shear rate applied to the paste during mixing causes a systematic decrease in the shear stress at 100 s^{-1}. As this occurs at both 10 and 20 mins of mixing (Figure 5-1A and Figure 5-1B, respectively), this shows that a significant shear dependency occurs for this formulation. This shear dependency can also be a useful tool in controlling the viscosity of the paste, beyond changing the formulation. It has been described by Roussel et al. [215] that the shear properties of cement pastes can change dependent on the shear rate applied to that paste, and this has been shown for Portland cement/admixture blends [216]. However, this has not previously been seen within alkali activated materials research. Effects of mixing duration have been studied by Palacios and Puertas for alkali-activated slags [209], but this has not been studied for metakaolin-based geopolymers.

The steps within the flow curves are still present in the same locations as mixing speed is changed, and show a change between rheological parameters over all the formulations tested. This indicates, and also by comparison to other published work using the same instrument and parameters, that an instrument effect is not likely to have caused these steps. The assessment of each of these rheological parameters is given in Table 5-2.
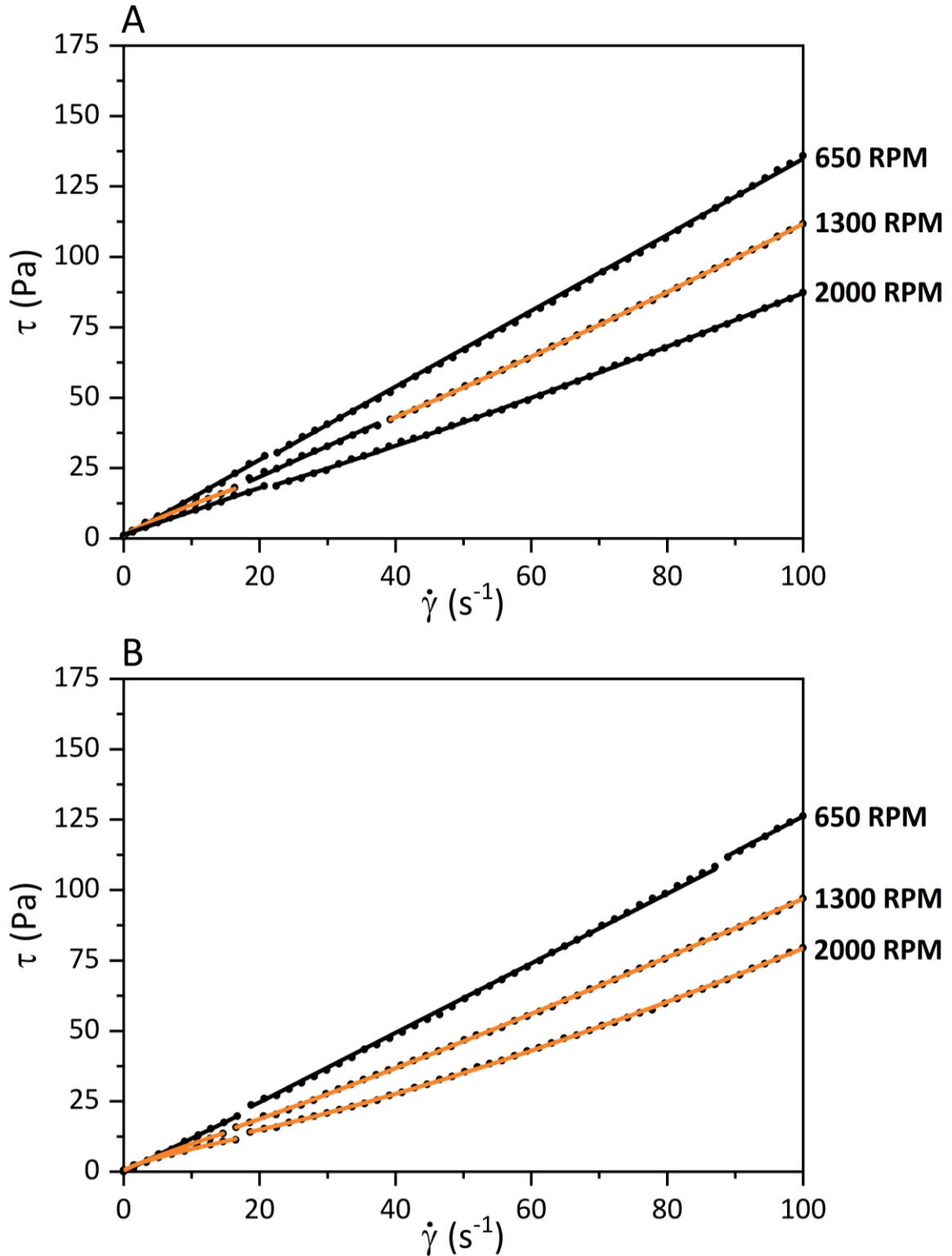
Figure 5-1 – Shear stress-shear rate curves for the FC MK paste, that has been mixed using a high shear impeller. The mixing rates marked on each curve are the implied rates given by the instrument. Mixing for 10 and 20 minutes is represented in A and B, respectively. The black lines represent a linear fit and the orange lines represent a power law fit.

The application of 10 mins of shear to the FC MK paste has led to some different rheological properties to those seen in Figure 4-5. For the FC MK paste, shear dependency surrounding these steps appears to have a significant effect on the rheological properties that are seen. A shear speed of 650 and 2000 RPM undergoes linear (Bingham) behaviour in the first, low shear rate stage, with a very small initial yield stress of 0.68 Pa. When the paste is sheared at 1300 RPM, two steps are present within the data, which have occurred at approx. 15 and 40 s^{-1}. The yield stress of these pastes starts at approx. 1.1 Pa, then decreases to 0 Pa and then increases again to 8.8 Pa. This is a fairly significant change and does show that the changes in the steps are likely due to a mechanism that is causing large amounts of resistance to the blade at finite shear rates. 1300 RPM is as close as possible, with the equipment available, to the step seen in Figure 4-5 for the H_2O/K_2O = 13 formulation. This curve at 1300 RPM has shown a very complex rheology compared to the 650 and 2000 RPM pastes tested, which is an indication that changes are occurring to the overall structure of the paste based around the shear parameters. The plastic viscosity (η), explained in (**Error! Reference source not found.** and **Error! Reference source not found.**), changes significantly between 3 steps and transitions from a shear thinning to linear to shear thickening regime, in contrast to the planetary mixed sample (Figure 4-5) which followed an initial Bingham regime and then underwent significant shear thickening (Table 4-1). This demonstrates that not only does the speed that the sample is mixed at, but also the geometry of the blade used for the mixing, provides significant changes in the rheological properties of these pastes.

Therefore, understanding the physics of the blade geometry would be a key next step for this research and how this imparts shear into the paste. The shape and geometry of the blade can lead to changes in the rheological properties of the paste, with the angle of the impeller, blade twist, diameter and the down flow of the paste induced by the blade [236]. It has been shown that a Rushton blade, which is similar to the Heidolph TR 20 used in these experiments, leads to an increase in the flocculation of particles [237]. Appropriate blade/impeller choice is needed when designing a mix set-up for geopolymer systems. It has been shown by Han and Ferron [143] that when comparing the use of high shear and planetary mixing, there is an increase in flocculation of cement pastes under high shear. This has led to an overall increase in the viscosity when compared to the planetary mixed formulations, and the flocculation has been shown to lead to shear thinning properties within cement pastes. The work of Ley-Hernandez et al. [238] has tried to eliminate the flocculation through the introduction of a "mostly de-flocculated" reference state and then begin to analyse the effects of mixing on the rheological state. However, they were not able to confirm the removal of this shear history, and therefore it is believed that an understanding of a universal test procedure is needed. This would also be a recommendation from what has been seen within this study.

Increasing the mixing time to 20 mins, Figure 5-1B, has shown that the FC MK paste rheology is not only dependent on the blade geometry and the speed of mixing, but the mixing time is also important. Increasing the mixing time has also exaggerated the properties shown for the 1300 RPM mixed sample and produced a formulation that transitions between shear thinning and shear thickening, missing out the Newtonian/Bingham stage at intermediate shear rates. This is repeated for the 2000 RPM formulation, which shows that increasing mixing time has caused a significant change in the rheological properties of these materials. These correspond more closely to the data presented in (Table 4-1), as the majority of the shear stress curve (after approx. 20 s^{-1}) is shear thickening. It is likely that the flocs that had been caused within the metakaolin/activating solution paste upon the start of high shear mixing, have been broken up using the sharp edges of the shear blade. This theory has been tested using laser diffraction of Portland cement paste in conjunction with the rheometry measurements, by Yim et al. [239]. A thorough understanding of the effects of blade geometry will not be analysed here but is definitely an area that should be investigated in significant detail.

At these higher shear rates, there is also an increase in the yield stress with increasing mixing speed. This shows that as more shear has been applied to the paste, then there is a greater resistance to further shear being imposed upon the paste. In combination with this higher yield stress, increasing the shear rate has caused a further decrease in the viscosity of the paste when it is sheared at a greater rate and for a longer period of time. The reduction in apparent viscosity from a shear rate of 650 RPM to 2000 RPM at 100 s^{-1} is 38%, for both the 10 and 20 min durations of mixing. This uniform level of reduction between the 10 and 20 mins samples shows that the shear rate prior to testing gives a uniform relationship in the overall viscosity of the pastes. For completeness, interpolation at 40 s^{-1} has been calculated at 1300 RPM, giving a shear stress of 35.4 Pa, compared to the 10 mins planetary mixed sample which has a shear stress at 40 s^{-1} of 26.2 Pa. The shear regime of the planetary mixer does reduce the apparent viscosity compared to overhead high shear mixing, when full speed and 1300 RPM are used, respectively. Full speed of the planetary mixer is in the region of 900 – 1300 RPM, but calculation is difficult due to the dual movement of the blade. The approximate blade rotation speed is 900 RPM for the planetary mixed system.
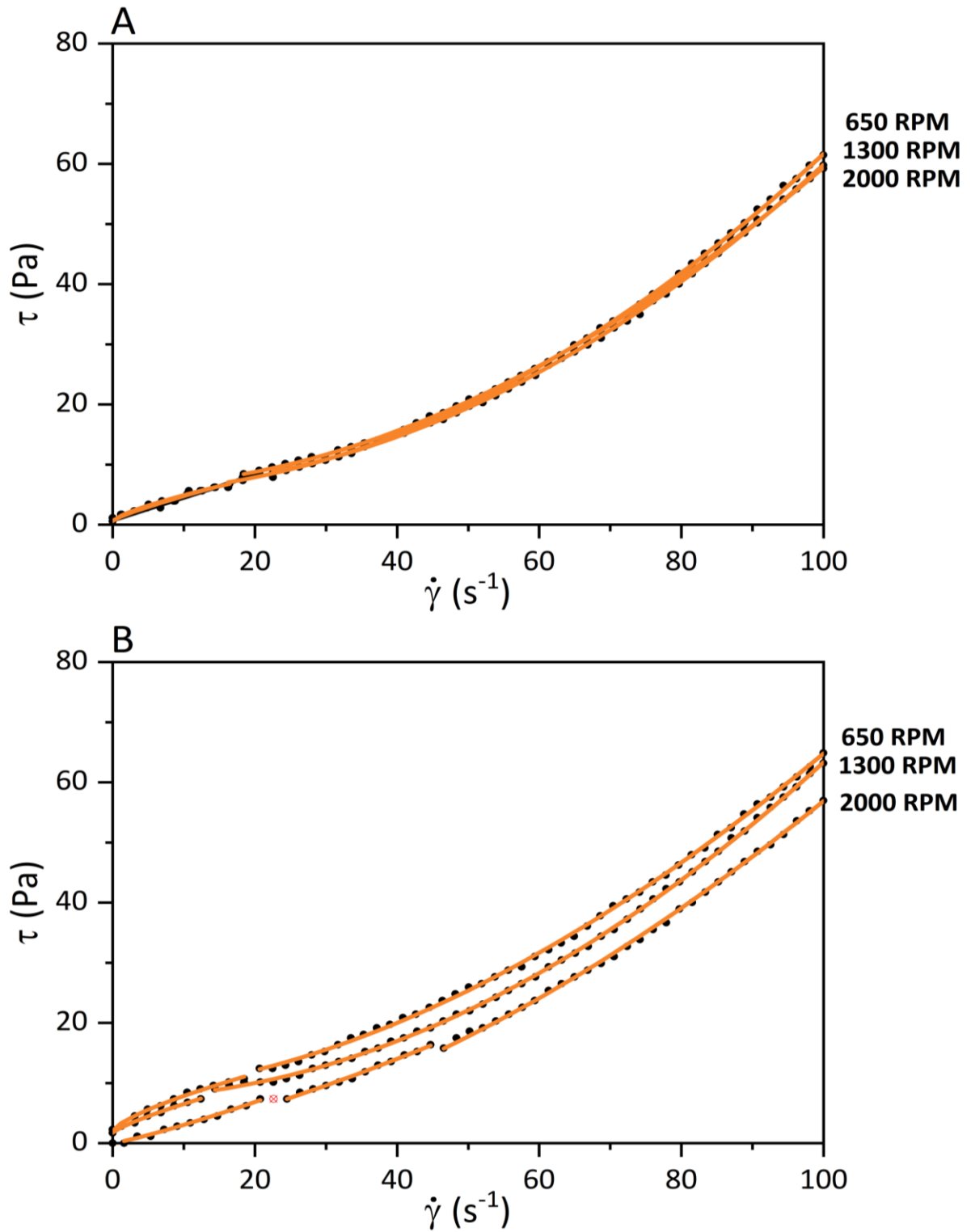
Figure 5-2 - Shear stress-shear rate curves for the RC MK paste, that has been mixed using a high shear impeller. The mixing rates marked on each curve are the implied rates given by the instrument. Mixing for 10 and 20 minutes is represented in A and B, respectively.

In comparison to the shear curves for the FC MK paste, the rheology of the RC MK (shown in Figure 5-2) pastes appears not to be related to the shear stress history of the paste. This is an interesting finding as the chemistry of the reactive component raw materials is very similar. The likelihood is that a shear rate dependent, critical transition point occurs within these formulations and this has been passed by the 650 RPM mixing speed. It has been shown that in suspensions of kaolin, with plate-like particles, the particles can align within the suspension when the shear rate passes a critical value [240]. Differences in rheological properties can be associated to particle size and shape; and potentially the inclusion of the secondary mineral phases which has been discussed in detail in section 4.2.2.1. The work of San Nicolas et al. [154] shows that the FC MK product contains around 10 % spherical particles. Spherical particles are most likely to be responsible for the shear related differences seen between each paste, as the inclusion of the unreactive quartz may lead to a small reduction in the flocculation properties of these pastes [235]. These parameters of the FC MK product could allow for significantly more rheological control of the paste when compared to the RC MK products. The shear stress at 100 s^{-1} of the RC MK product is approximately half that of the FC MK.

Comparing the behaviour of these pastes to nuclear industry standard PC pastes, that were tested on the same instrument by Sanderson [33], the RC and FC MK pastes that have $H_2O/K_2O = 13$ have a low viscosity when compared to standard PC pastes tested. The shear control that can be applied to these pastes will also be a benefit to the UK nuclear industry; due to the different methods of mixing and shear regimes that are used, pastes can be shear controlled to a precise degree [10]. Therefore, selection of a specific MK precursor cannot be solely based upon the effects of shear and should be based around considerations required for the immobilisation of specific waste streams. The adaptability of the shear rate of the FC MK paste, when working with different viscosity oils and sludges/slurries, could be a real advantage in the encapsulation of these wastes.

Understanding the shear based viscosity of the RC MK paste is still important. These pastes also show an initial step present in the data at approx. 20 s^{-1}, demonstrated in Figure 5-2. The paste is seen to follow an initial shear thinning phase followed by a drastic shear thickening process. This is independent of the shear history, as this occurs at all mixing speeds. As the mixing speed applied to the pastes is increased, there is an increase in the degree of initial shear thinning and a decrease in the degree of the secondary shear thickening process which occurs after the initial step at low shear rate, which can be seen by a decrease or an increase in the value of n, respectively. These are shown along with the values of shear stress at both 40 and 100 s^{-1}, in Table 5-2. These are very consistent even though the shear history of the paste is different at these shear stress values. Upon increasing the mixing time to 20 mins, a very similar trend to the 10 mins mixed samples occurs at 650 and 1300

RPM, with a greater increase in the shear thickening behaviour of the 650 RPM sample, but there is a minimal effect on the viscosity at 1300 RPM.

Mixing at 2000 RPM has shown significant changes when compared to the samples sheared at the slower speeds, as the pastes show quite different rheological properties. This formulation has become shear thickening over the entire shear rate-shear stress curve. This shear thickening is observed over three different steps within the shear curve. However, the overall degree of shear thickening within this formulation is lower at 100 s^{-1} than that of the pastes sheared at lower speeds. This paste appears from the rheological data to be more homogeneous and contain significantly less flocs than all other formulations, as the shear thickening nature is relatively constant over the entire run of the paste. Larger values of yield stress are recorded at 20 mins of mixing when compared to 10 minutes.

For the 650 RPM mixing speed, increases are observed from 0.7 to 2.0 Pa over the first step point and then from 6.0 to 8.8 Pa over the next point, and this increase is common across all samples tested. As increasing yield stress over time is usually attributed to the beginning of the setting process [241], the changes in yield stress do demonstrate that a hold-up process, where the paste is mixed continuously at slow speed in order to prevent setting, can potentially be used to prevent the setting of these materials. This has not previously been demonstrated for MK-based geopolymers and has applications that extend beyond the nuclear industry. Having a method of increasing the setting time for any cementitious system without the use of additives will be a benefit, particularly as MK based geopolymer cements have often been shown to have a short setting time. An extensive study of different SiO_2 and Al_2O_3 contents within MK geopolymers by De Silva et al. [242] found a maximum setting time of MK based geopolymers to be 220 mins. This has been shown within section 4.2.2.2 to not be an absolute limit, and formulations are likely to have been developed and not published by other researchers with much longer setting times. Setting times that are less than 24 hours may not be sufficient for nuclear applications and the development of a hold-up mechanism that can mechanically retard these pastes would be key. In order to test this further, the use of the adapted Vicat method, described in 3.2.4.2 can provide detailed information about this hold-up process, and results similar to those shown in section 4.2.2.2 can be interpreted.

Table 5-2 – The rheological parameters extracted from the flow curves in Figure 4-3 and Figure 4-5. When the value of n is 0.85 > n > 1.15, the value is given as n = 1.00 and fits to a Bingham model.

	MK Type	FC MK						RC MK					
	Mixing Time (mins)	10			20			10			20		
	Mixing Speed (RPM)	650	1300	2000	650	1300	2000	650	1300	2000	650	1300	2000
Model 1	n	1.00	0.85	1.00	1.00	0.85	0.77	1.00	0.84	0.73	0.71	0.80	1.16
	τ_0 (Pa)	0.68	1.07	0.68	0.00	0.26	0.50	0.73	0.69	0.58	2.00	1.74	0.00
	K (Pa s^n)	1.36	1.48	1.36	1.18	1.31	1.28	0.38	0.57	0.80	1.14	0.76	0.21
	r^2	0.999	0.998	0.998	0.999	0.999	0.996	0.981	0.986	0.976	0.991	0.994	0.998
Model 2	n	1.00	1.00	1.00	1.00	1.15	1.38	2.04	1.94	1.89	1.75	1.96	1.33
	τ_0 (Pa)	0.00	0.00	0.00	0.00	3.34	6.75	6.04	5.39	6.26	8.74	7.51	0.14
	K (Pa s^n)	1.36	1.09	1.34	1.23	0.53	0.14	<0.05	<0.05	<0.05	<0.05	<0.05	<0.05
	r^2	1.00	0.999	1.00	0.996	1.00	1.00	0.999	0.999	1.00	1.00	1.00	0.999
Model 3	n	-	1.20	-	1.00	-	-	-	-	-	-	-	1.68
	τ_0 (Pa)	-	8.79	-	0.00	-	-	-	-	-	-	-	0.01
	K (Pa s^n)	-	0.41	-	1.26	-	-	-	-	-	-	-	<0.5
	r^2	-	1.00	-	0.998	-	-	-	-	-	-	-	0.999
τ @ 100 s^{-1} (Pa)		134.8	111.6	87.2	126.2	96.8	79.3	59.8	61.6	59.4	64.8	63.3	56.9
τ @ 40 s^{-1} (Pa)		53.1	43.0	33.6	48.2	37.0	27.6	14.9	15.2	15.0	20.4	20.4	17.2

5.3.2. Reaction Kinetics

The isothermal conduction calorimetry curves below represent the same mixes that have been analysed above. Overall, the chemical reactivity of the paste does not appear to change significantly with changes in mixing speed and time. Examining the RC MK paste (Figure 5-3 A/B), a small decrease in the cumulative heat flow at 10 mins is seen when the shear rate is increased to 1300 RPM. The curve then begins to follow a similar cumulative heat curve as the 650 RPM mixed formulation for a paste that is mixed at 2000 RPM. This small decrease does occur at the rheological step point that has been explained in detail in section 5.3.1 that has been defined for this material, and also corresponds to the changes that are seen in the rheological properties summarised in Table 5-2. The smaller thermal output from the gel nucleation peak (explained in section 2.2.4.2.2) is the main contribution to the lower overall cumulative thermal output of this 1300 RPM mixed paste and has therefore shown that this paste, under these mixing conditions, has a slower rate of reaction. The reason for this currently remains unknown and further study will be undertaken in order to analyse this. This has shown that the reaction of this paste has occurred with a lower intensity than the pastes that have been sheared at 650 and 2000 RPM. This does show a significant effect of shear on the ability of the Al and Si species to polymerise and develop the aluminosilicate gel structure [232], and the fact that this small change affects the calorimetry results not only shows the sensitivity of the technique, but also the sensitivity of the cement to mixing [132]. This sensitivity could be used to develop the hold-up process described in section 5.3.1.

Increasing the mixing time to 20 mins has changed the thermal output of these pastes by a small margin. The cumulative heat curve for the 650 RPM mixed paste has a cumulative heat in excess of 200 Jg^{-1} at 48 hours. An explanation for this is that insufficient mixing has been undertaken, and led to larger particles or agglomerates of MK which require dissolution in the activating solution. This has required a greater thermal output. Hence why the onset of the cumulative heat curve, which is linked to the rapid initial dissolution, starts at approx. 25 Jg^{-1}. These agglomerates of particles are larger flocculated clusters of MK than in the higher sheared samples. It has been hypothesised that the dissolution effect has been missed in the 1300 and 2000 RPM samples, as this dissolution step has already occurred in the mixer due to the increased shear rate and extended time period. Understanding at which point these agglomerations have disintegrated has not been shown by isothermal conduction calorimetry. Further studies using advanced imaging techniques should be undertaken in order to understand the environment that is caused by mixing. Removing this starting effect of dissolution will lead to a significant reduction in the final intensity of the cumulative heat curve. However, the cumulative heat of the 1300 RPM formulation has remained consistent with that of the 10 mins mixed formulation. A reduction in the total cumulative heat has occurred in the 2000

RPM formulation. Due to the outbreak of COVID-19, I have been unable to comprehensively understand the differences in these reaction kinetics. However, running an experiment to isolate the heat of mixing from these formulations, using a clay/water slurry, will allow for a fuller understanding of the effects of particle dispersion on these MK-geopolymers.
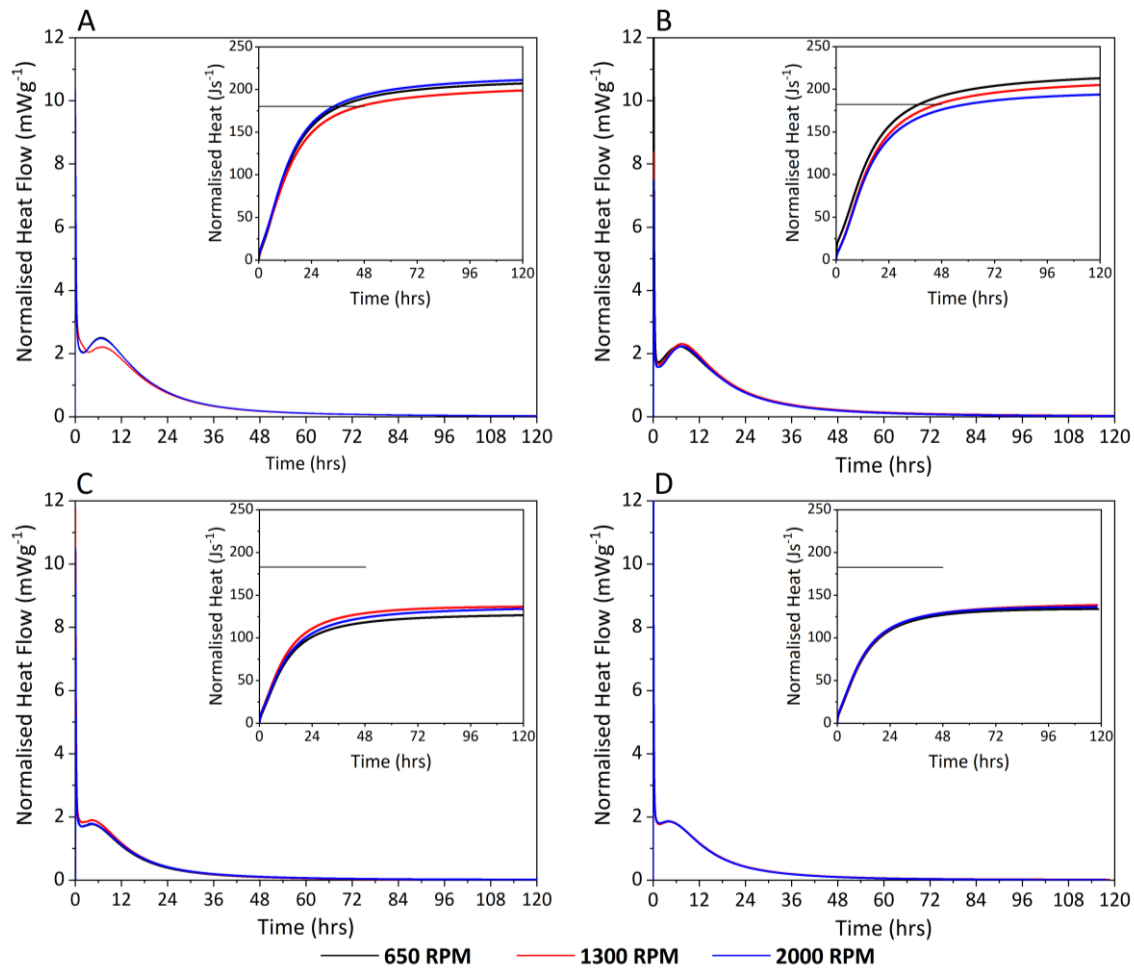
Figure 5-3 – The isothermal conduction calorimetry curves for the RC MK (A, B) and FC MK (C, D) based geopolymer formulations. A and C represent 10 mins of mixing and B and D represent 20 mins of mixing. The black line represents the nuclear industry cut-off at 180 Jg^{-1} for thermal output up to 48 hours [31].

The RC-MK formulations follow a different trend to that of the FC-MK formulations; the main difference between these formulations is the particle size and shape. The RC-MK used here has a completely plate shaped particle structure, however the FC-MK contains between 8 - 10 % of spherical particles, which will allow for a more flowable paste. It has been shown for spherical fly ash particles in cementitious pastes, that these particles improve the flowability as they reduce the friction between the angular cement (or in this case MK) particles [243]. The differences shown in the reaction

kinetics for both MK types, is likely due to the interaction of the spherical particles within the FC MK product that are not present in the RC MK product. Literature has shown that a reduction in the shear speed can lead to greater dissolution of the cement particles and therefore, produce a more stable chemical structure [238]. Increasing the shear speed of the FC MK pastes at 10 mins appears to follow this trend and a similar outcome can be seen for the RC-MK geopolymer with increasing mixing speed. However, this change is negligible at 20 mins of mixing and complete dissolution is likely to have been driven by the large shear rate.

(a) House of Cards or Card-House Structure
edge-face interactions

(b) Band-like structure
"overlapping-coin" interactions
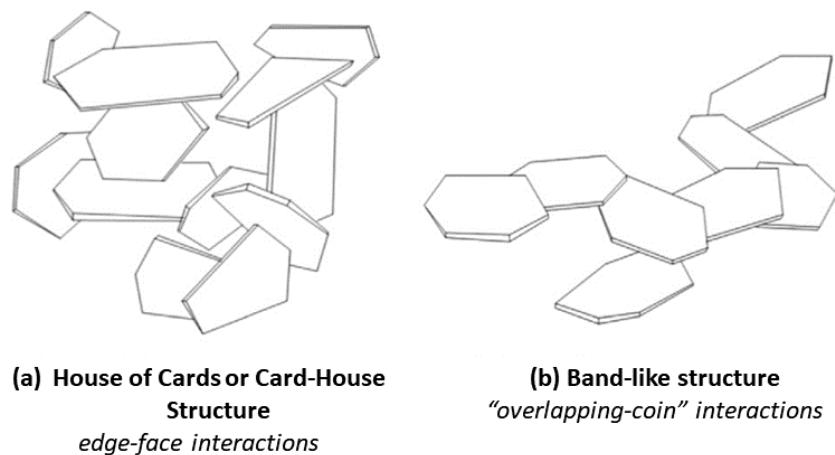
Figure 5-4 – Schematic representation of the clay microstructures. (a) represents the House of Cards structure and (b) represents the Band-like "overlapping" structure. This has been reproduced from Shankar et al. [244].

The development of the geopolymer gel structure has required analysis of the components of the activating solution and an understanding of the ionic conditions that are occurring in the gel structure. Potassium hydroxides and chlorides have been shown to adjust the isoelectric point of the clay particles at pH > 8 [245]. A lower ionic strength leads to a more agglomerated clay structure that follows a "house of cards" or face/edge interaction model for clay particle morphology. The structure of the clays is likely to follow a combination of the "house of cards" and a more planar "overlapping coin" model [244]. Schematics of these models are shown in Figure 5-4. As this planar-overlapping structure has a greater exposed surface area, the clay particles that are following this structure can be dissolved preferentially. This would leave behind these more agglomerated particles, that will require significant more time to dissolve. Dissolving these agglomerates will lead to a significantly greater thermal output. Increasing the shear from 1300 to 2000 RPM for these formulations has caused a slight decrease in the overall thermal output of these formulations. As the shear regime has been undertaken using an impeller with sharp edges, which is also designed to produce radial flow within

the paste, then agglomerations and flocs will be broken apart using these edges. This is providing that the intensity of shear and also the time is significant enough to break down all these agglomerations and flocs.

Therefore, shearing for longer periods of time at all speeds has reduced agglomeration and is likely to lead to a significantly more homogeneous paste. This influence of shear rate has been shown to delaminate clay structures within the paper industry, to develop less agglomerated/flocculated clay structures [246]. Therefore, applications of this type of technology to the UK nuclear industry will allow for the same delamination and can lead to the production of a suitable waste package.

5.4. Conclusions and Future Work

The effects of shear on the fresh state properties of rotary and flash calcined metakaolin have been studied and interesting developments in terms of the overall viscosity and the reaction kinetics studied. A formulation with a high water content (H_2O/K_2O = 13) has been studied and parallels have been drawn to the results present in Chapter 4. Distinct differences can be seen between the metakaolin types used and how they respond to different rates of shear and the time frame in which this shear is applied. A mixing speed of 1300 RPM has been selected as this matches, as closely as possible, to the step that is seen at 20 s^{-1} in section 4.2.2.1. It has been shown that when the flash calcined formulation passes this mark, then a change in the rheological properties is seen and a shear thinning, linear, shear thickening regime is demonstrated. This is explained through the production of flocculated metakaolin particles that are shear dependent due to the composition of the activating solution used. The reaction kinetics suggest the above is a possible theory and there is a need to perform further experiments using clay slurries in different solutions of different pH and composition. This will allow the detection of these flocs or agglomerations without the hindrance of a setting mechanism. Studies of these formulations may be done via direct observation using microCT imaging and also through isothermal calorimetry, which may show the effects of dissolution on the reaction kinetics of solutions with different compositions. Further understanding of how the blade geometry can be adapted in order to reduce agglomeration and also change the rheological properties that are seen within these pastes will be understood. Pastes will be subjected to not only radial flow impellers but also blade flow and propeller type geometries.

Chapter 6: The Development of a Solid Geopolymer Cement – Hardened State Properties

The SEM images shown in Figure 6-10 *have been collected at Imperial College London by Dr Hong Wong and Awni Abdullah. The author would like to thank these collaborators for their work.*

6.1. Introduction

The structural stability of MK-based geopolymers has been widely discussed, and many of the techniques that have been used within this chapter have been addressed previously in the literature [2, 82-84, 117, 190, 213, 247-249]. However, in order to show stability of these geopolymers for the specific MKs that have been reacted with a specific potassium silicate activating solution, which have been marked as potential formulations within the UK nuclear industry, then a full range of these techniques need to be undertaken on these formulations. This includes analysis of the materials at the nano, micro and macro-scales of analysis to determine the overall structural properties of these materials. The thermal stability of MK-based geopolymers has also been examined.

6.2. Results and Discussion

In order to understand the long term stability of MK-activated geopolymers a series of chemical and physical tests have been performed to determine the nano- and microstructural characteristics of these materials. Due to the Covid-19 pandemic a study showing the 2 – 3-year stability of these materials was not possible, which means that data for longer term stability cannot be shown. As all formulations underwent similar tests and to reduce repetition, Table 6-1 has been produced to show the colour scheme has been used throughout this chapter.

Table 6-1 – The colours below correlate to the curing times and the formulations of the samples examined in Figure 6-1 to Figure 6-8.

H_2O/K_2O	SiO_2/K_2O	7 Days Cured	28 Days Cured	360 Days Cured
11	0.5	——	——	——
11	1.0	——	——	——
11	1.5	——	——	——
13	1.0	——	——	——

6.2.1.X-ray Diffraction

X-ray diffraction of geopolymer samples has been shown to reveal the development of an amorphous product, and at later ages for sodium activated geopolymers, the production of zeolite species [122]. Carbonation can also be assessed using X-ray diffraction, through the formation of carbonate products such as alkali metal carbonates [250]. X-ray diffraction has been performed on the Argicem and MetaMax based geopolymers, with the results shown in Figure 6-1 and Figure 6-2, respectively. These data sets have both been normalised to the highest peak, which is quartz for the Argicem product and anatase for the MetaMax. This normalisation allowed for discrepancies in intensities associated with changing of X-ray tubes and other instrumental adaptations over time to be minimised.

The FC (Argicem) MK-based geopolymers have been studied using X-ray diffraction in order to show the stability of these materials over time, as shown in Figure 6-1. Overall the structures of these materials, as observed by XRD, fundamentally do not change over time and the production of crystalline species has not yet been experienced. Due to the large levels of quartz present within this raw material, the usual amorphous products formed within geopolymer systems are difficult to see. However, a broad feature due to diffuse scattering can still be seen between 25 and 35° 2θ, with significant amorphous character being present at low angles (<15° 2θ). Small impurities of mullite, formed from the over-calcination of kaolin particles leading to a recrystallisation [251], and forms of silicon dioxide are seen within activated geopolymer systems. The likely reasons for the silicon dioxide impurities are likely impurities found during the sample preparation stages, as quartz is used as a cleaning agent within all the grinding and sample preparation stages. It is also likely that preferred orientation, the fact that some lattice structures occur more within a structure compared to others, could have meant that one of the lower statistically likely quartz structures has enough lattices in the correct orientation to show a different peak. A small level of crystallinity within the activating solution used to make the geopolymer formulations could have also led to the formation of small crystalline impurities [252]. The samples tested in this chapter are all unique samples, and therefore differences in the small levels of impurities between formulations can be attributed to small differences in the activating solutions and/or the quartz used within the preparation stages. However, further discussion of these impurities is not needed, as the important point of note is the lack of zeolitic structures being formed at curing times up to 360 days. Therefore, these materials appear to be chemically stable over extended curing ages.
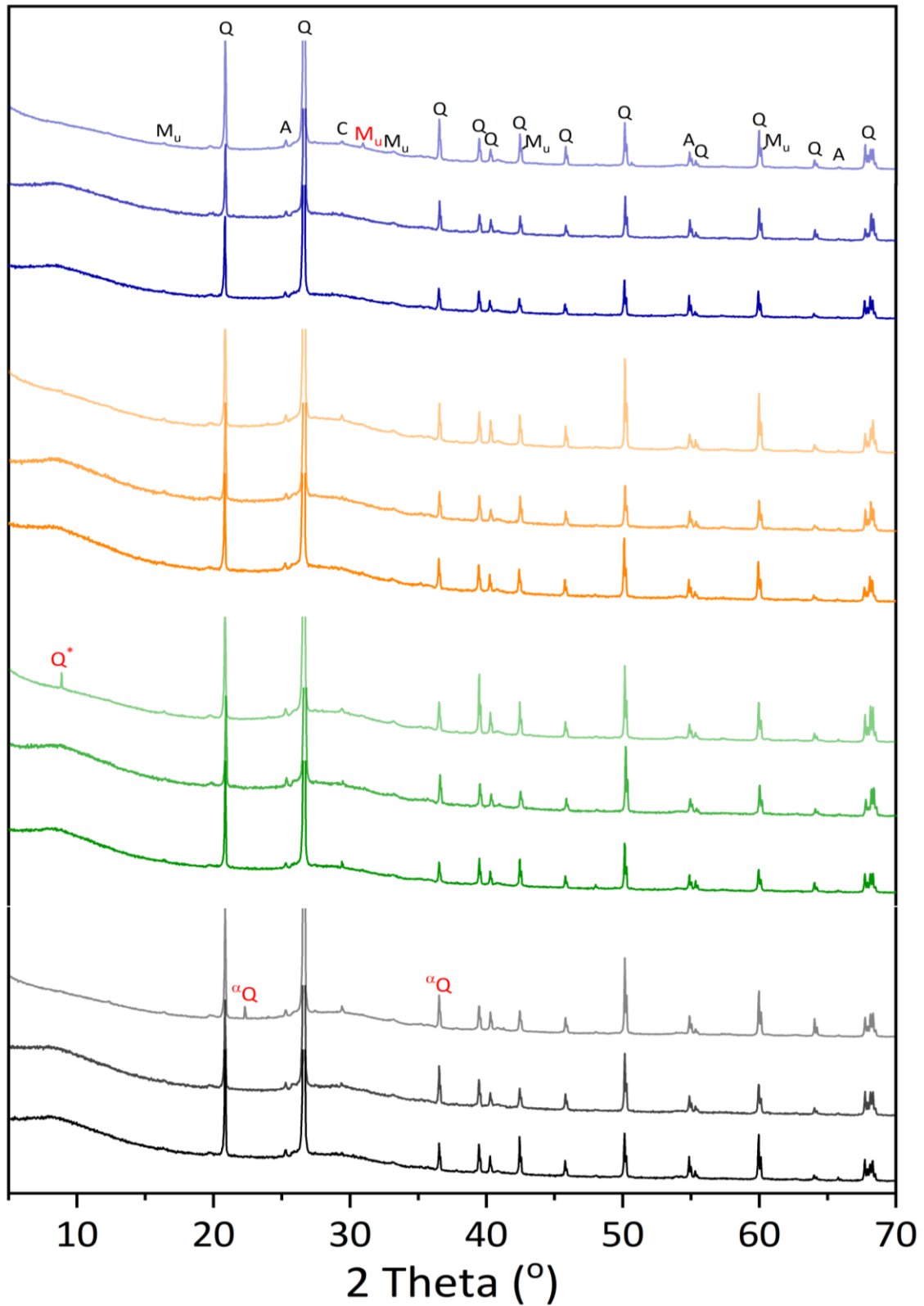
Figure 6-1 – X-ray diffraction patterns for the Argicem MK geopolymers cured for 7, 28 and 360 days. The colour scale for each sample is defined in Table 6-1. The black peak markers represent Q – quartz (PDF - 01-078-1252), A – anatase (PDF – 01-071-1166), M_u – mullite (PDF – 04-012-0161), which were shown in the raw material in Figure 3-1. The red letters represent the differences in the patterns with $^\alpha$Q – α-quartz (PDF – 04-008-7831) and Q* - SiO_2 (PDF - 04-014-7415), with the M_u being the same PDF card as above.

The largely amorphous character that can be seen in the geopolymers produced using MetaMax is very characteristic of these materials and has been shown in great detail in the literature [253]. Small impurities that are present in the raw clay (as shown in Figure 3-1), can be seen in all the XRD traces presented in Figure 6-2. Anatase and a small proportion of quartz are present in the raw material, which can then be seen in a more dilute form in the XRD pattern of the geopolymer samples. An interesting point of note is the movement of the characteristic amorphous hump of the raw clay from approx. $18 - 30°$ 2θ in the raw MK product to $25 - 36°$ 2θ after geopolymerisation. This demonstrates that rearrangements in the highly amorphous gel network have occurred [117]. To elucidate these structural changes, examination of the nanostructure using techniques capable of analysing the low range order of these materials needs to be undertaken. The development of the gel structure will be analysed using FTIR in sections 6.2.2. However, the crystal structure of these materials over time has been shown in the XRD data to remain unchanged in a very similar manner to the Argicem geopolymer formulation. This shows that the formation of zeolite species and other carbonate products has not occurred.

This structural stability shows that potassium activated MK geopolymers have been demonstrated to be resistant to changes in their crystal structure up to curing periods of 1 year. Further study of these formulations at different curing temperatures and longer curing times will allow for the full development of the structural stability of these materials and allow for a safety case to be developed for their use in the UK nuclear sector.
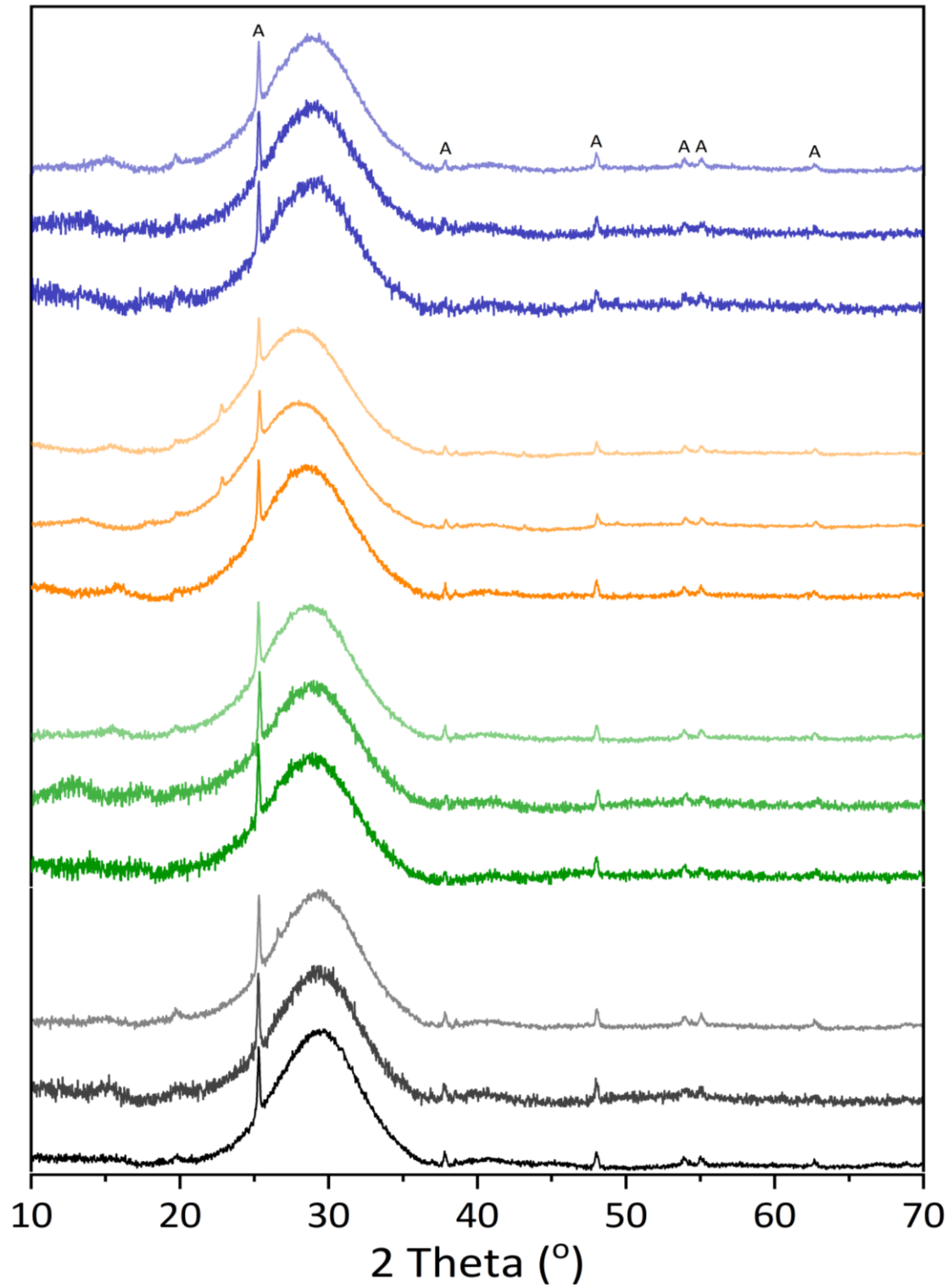
Figure 6-2 - X-ray diffraction patterns for the MetaMax MK geopolymer cured for 7, 28 and 360 days. The colour scale for each sample is defined in Table 6-1. The black peak markers represent A – Anatase (PDF – 01-071-1166) which was shown in the raw product in Figure 3-1.

6.2.2. FTIR Analysis

In order to analyse the nanostructure of these geopolymer systems, FTIR spectroscopy data are shown in Figure 6-3 and Figure 6-4 for the Argicem and MetaMax MK geopolymers, respectively. A list of the assigned bands can be seen in Table 6-2, which has been taken from mineral phase literature and also research on cement/geopolymer chemistry literature. The general chemical structure of sodium activated geopolymer systems has been examined in great detail [229, 254, 255]; however, a full understanding of the potassium based systems has not yet been examined. Small amounts of work have been presented by Lee and van Deventer [224], Duxson et al. [121] and Walkley et al. [122]. Comparison between RC and FC MK precursors has not been undertaken, and this is therefore presented in this study.
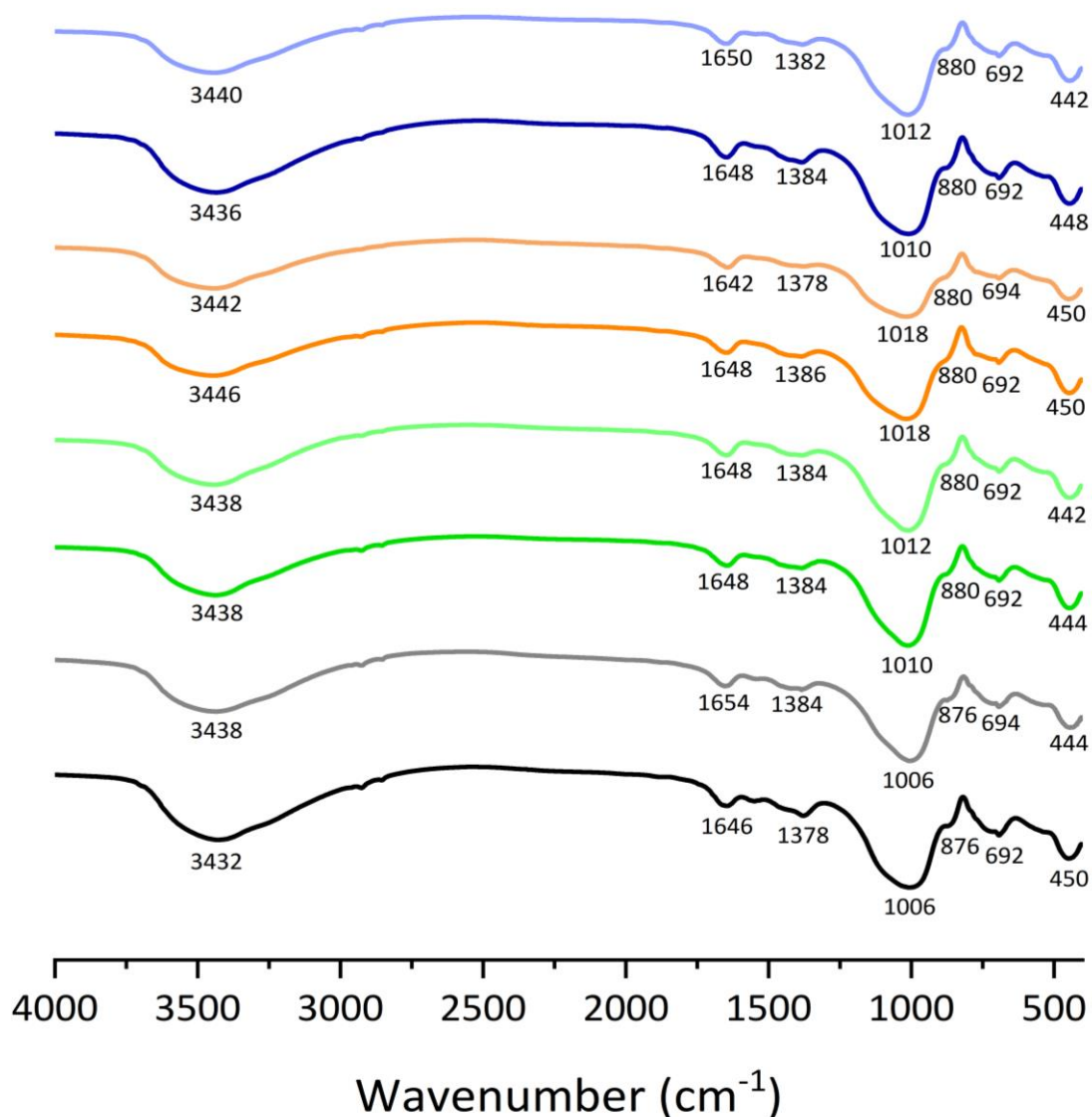
Figure 6-3 – FTIR spectra of the Argicem MK geopolymers cured for 7 and 360 days (dark and shaded, respectively). The colour scale for each sample is defined in Table 6-1.
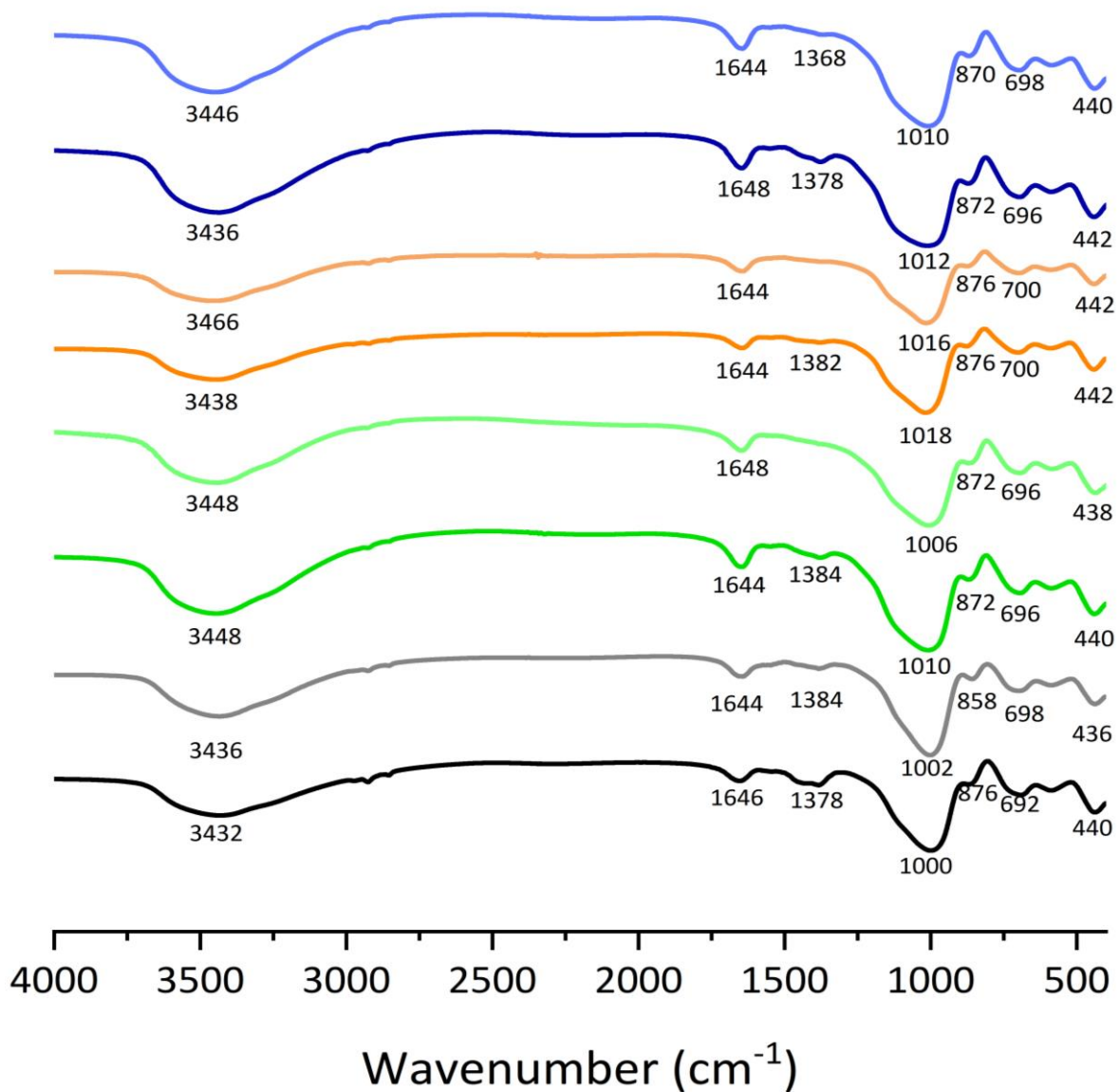
Figure 6-4 - FTIR spectra of the MetaMax MK geopolymers cured for 7 and 360 days (dark and shaded, respectively). The colour scale for each sample is defined in Table 6-1.

The asymmetric stretching of Si-O-T bonds (where T = Al or Si) presents in multiple positions within the FTIR spectra [201, 229]. This stretching is seen mainly in the region between 1150 – 980 cm^{-1}. The expansion of the band in order to produce a peak between 900 – 840 cm^{-1} shows the substitution of Al into the Si dominated tetrahedral site that is found at the higher wavenumbers [255]. The production of this structure can be used to show the production of a K-A-S-H like structure [224]. The literature has shown the presence of the sodium aluminosilicate geopolymer gel phase at approx. 940 cm^{-1} [255]. The development of the K-A-S-H gel network needs to be examined using ^{27}Al NMR but the

assignment of this peak to the formation of the gel phase seems to be consistent with the studies already performed [224, 255]. The formation of the K-A-S-H gel has been completed at 7 days, as the peak at lower wavenumbers is present in all samples and remains unchanged. The water content of the gel phase and also the remaining pore solution, that has not been extracted via solvent exchange, can be seen in the shifts that centre around $1648 - 1644$ cm^{-1} and $3466 - 3432$ cm^{-1} for the H-OH and OH$^-$ stretches, respectively. The overall production of the binding phase within these MK-based geopolymers appears to have reached its conclusion at 7 days of curing and has not changed up to 360 days of curing. The overall development of the gel phase has not been elucidated further within this work. However, stability has been shown over 360 days, which indicates that the overall stability of these materials is very consistent with the gel phase that is formed at early age. Alterations to the activating solution also do not affect the position of the wavenumber shift and therefore do not change the overall nanostructure of the material in a noticeable manner according to the FTIR data.

Table 6-2 – Stretching regions commonly seen within MK-based geopolymers.

Stretching Region	Assigned Stretch	Reference
$450 - 436$ cm^{-1}	O – Si – O amorphous stretching from the unreacted MK.	[254, 256]
$700 - 690$ cm^{-1}	Al – O – Si bending within a ring structure.	[255]
$900 - 840$ cm^{-1}	Si – O – T with Al beginning to substitute into the Si site, correlating to the K-A-S-H gel.	[201, 254]
$1150 - 980$ cm^{-1}	Si – O – T (T = Si or Al) asymmetric stretching in geopolymers.	[201, 257]
$1385 - 1378$ cm^{-1}	This peak is likely associated with the CH_3 associated to residual isopropanol from the solvent exchange procedure and also C - O stretching within an alkali carbonate species	[133, 258]
$1648 - 1644$ cm^{-1}	H – OH bond stretching	[254, 255]
$3466 - 3432$ cm^{-1}	OH$^-$ stretching vibrations	[254, 255]

6.2.3. Compressive Strength

Although the strength of these materials is not the most important parameter when understanding the long term durability of these materials for applications within the nuclear industry, it can nonetheless be used as a method of showing long term stability and also that the materials do meet the minimum standards explained in various technical specifications, which state values around 1 - 5 MPa [31]. However, pastes produced from the current UK nuclear industry standard blends of Portland cement and blast furnace slag tend to produce a strength at 28 days of approx. 50 MPa [33]. Finding a compressive strength that competes with Portland cement based formulations will allow for a safety case to be made regarding the durability of these materials.

Figure 6-5 shows the compressive strength data for the Argicem MK based geopolymer formulations. The numbers above each bar represent the number of days that each sample has been cured for prior to testing. This system shows an increase in the compressive strength of these formulations with increase in the SiO_2/K_2O ratio. At $SiO_2/K_2O = 1.5$ a maximum compressive strength of 76 MPa can be seen at 7 and 28 days; this formulation exceeds the performance of the baseline Portland cement blends described above, and does also show that these geopolymer materials have the properties that lead to high compressive strength. Increasing compressive strengths based around increasing silicate concentrations and also density of the microstructure has been shown for FA-based geopolymers [259]. It has also been shown that increasing water content leads to an increase in the porosity of alkali activated slag, which in turn leads to a decrease in the compressive strength of these materials. Therefore, an increased silicate content and a reduced water content leads to an increased strength. It can also be seen that when H_2O/K_2O is increased from 11 to 13, the 3-day compressive strength remains constant, however the development of strength from 7 to 28 days occurs at a much slower rate when the water content is at the higher level (13).

For the formulations with the lower water content, the strength begins to decrease between 28 and 360 days of curing. This decrease in strength is an interesting and potentially problematic finding for the long term stability of these materials, as a strength decrease over extended curing times does show that changes are occurring. The more alkaline ($K_2O/SiO_2 = 0.5$) and higher water content ($H_2O/K_2O = 13$) samples have not yet undergone this decrease in strength at 360 days, and may not undergo the process at all. A similar study to this has been presented by Lloyd et al. [260] and it has shown a slight but very clear decline in the strength of MK-based geopolymers that have been cured at ambient conditions for time periods in excess of 7 days. A likely explanation is the increasing coarsening of the gel structure which leads to an increasing evolution of the gel phase which leads to a slightly more ordered state at long-term curing. It is strange that the higher silicate systems, that

have actually undergone this strength regression, are the systems that have been shown to usually not undergo any strength change [260].
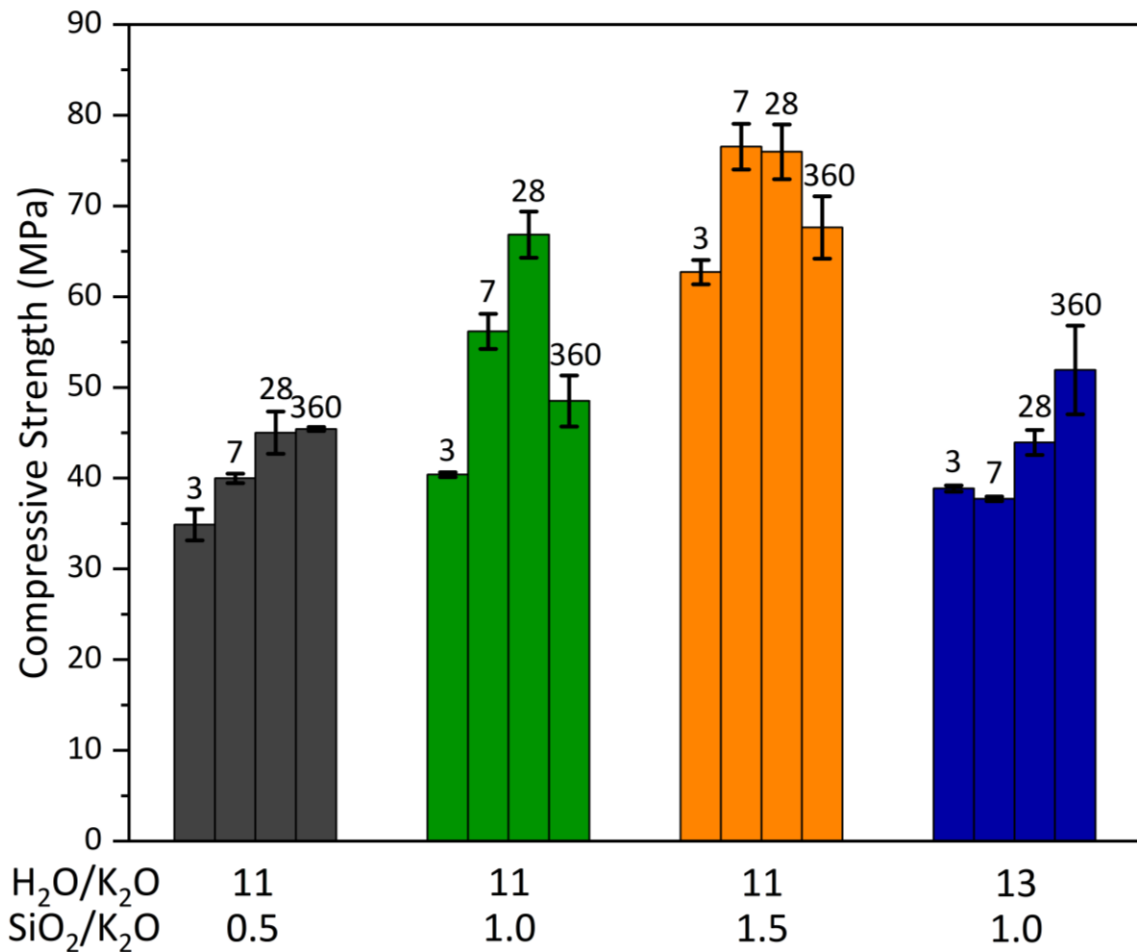
Figure 6-5 - Compressive strength measurements for the Argicem MK based geopolymers. The numbers above the bars represent the days of curing for the samples.

Figure 6-6 shows the compressive strength data for the MetaMax MK formulations. These do not follow the same dramatic strength increase seen for the Argicem MK formulations with the increasing silica content, but there is still an increase. The majority of the compressive strength of these materials appears to have been reached within 3 days, and within a small error the overall strength of these materials does not appear to change between formulations. This does show that these materials are mechanically stable at early age and that these properties remain constant over time. The overall compressive strength of these materials is less than that of the Argicem and also the Portland cement materials that have been shown in the work of Sanderson [33]. It has been mentioned that the strength of these materials is not a necessary acceptance criterion, as the reference documents state 1 MPa of strength [31, 207]. Therefore, it is reasonable to assume that the overall strength of these

materials is constant and therefore, shows that these materials are acceptable. Studies of the porosity of these samples will be useful in understanding the comparison of the porosity. The changes that occur between formulations could be due to small defects occurring within the cast cubes. The method for casting these materials is based around Portland cement and the adhesive nature of MK-based geopolymers can cause sticking within the moulds which changes the shapes of the cubes to not be exactly 50 x 50 x 50 mm in size and shape. Due to the difficulties of demoulding and sample storage related to MK-based geopolymers, it was not always possible to collect these results in triplicate. However, when duplicate was used the standard deviation was considered and had been shown to be within an acceptable range for the rest of the data.
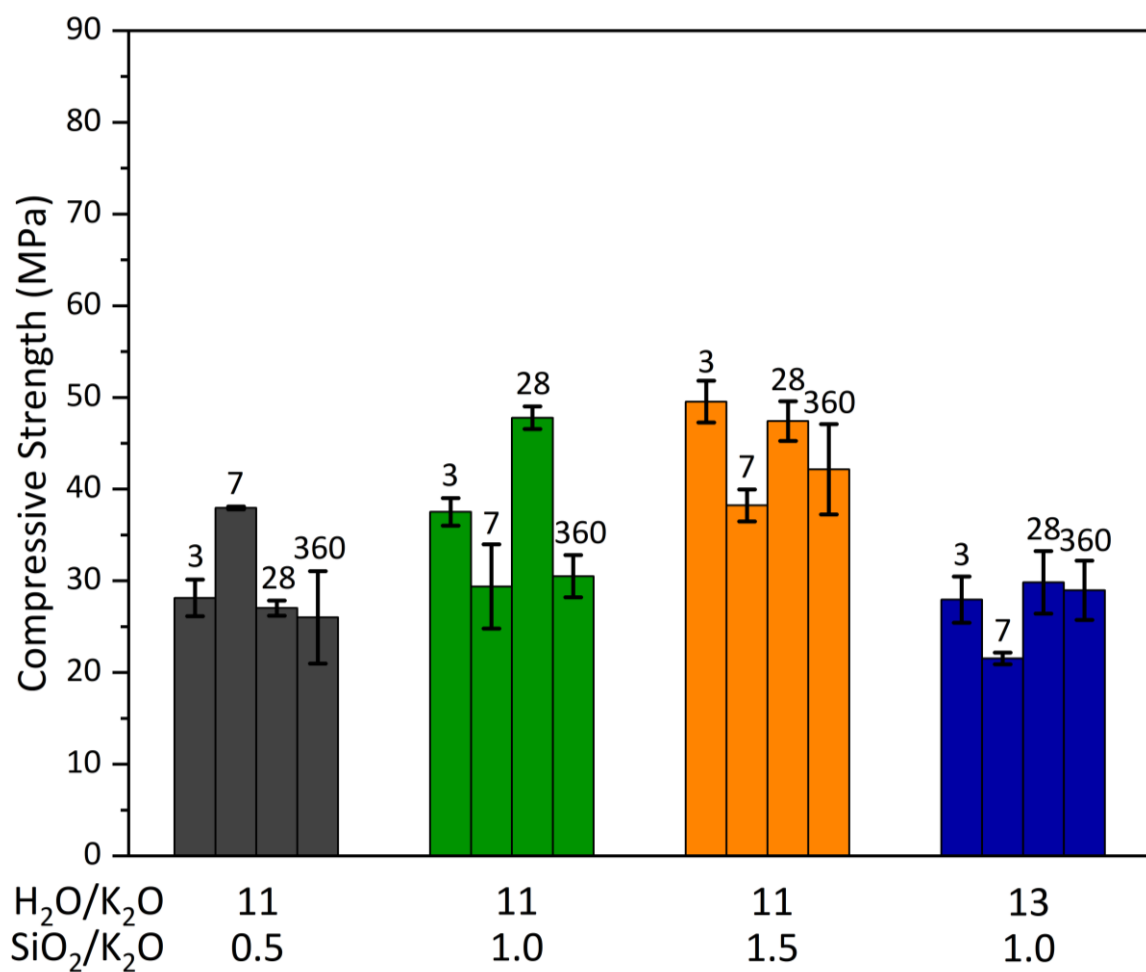
Figure 6-6 – Compressive strength measurements for the MetaMax MK based geopolymers. The numbers above the bars represent the days of curing for the samples.

6.2.4. Thermogravimetric Analysis coupled with Mass Spectrometry (TG-MS)

Discussion of the long term durability of geopolymer cements in the applications of interest here is essentially based around the free and bound water content, and also the carbonation, which can both

be examined using TG-MS. Therefore, a comparison of the 7 and 360 day thermal response is given in Figure 6-7 and Figure 6-8 for the Argicem and MetaMax products, respectively. Fundamentally the TG-MS data for all the Argicem and MetaMax formulations remains relatively unchanged when viewed as differential TG (dTG) data. As these samples have been solvent exchanged prior to examination the free water will have been removed and therefore, the water that is released from all formulations between 50 – 200 °C will be structural water that is either bound to the gel phase or held within the pore network [82, 98]. The water content of each formulation is very similar between formulations and curing times, but it is shown that upon curing for longer ages the quantity of water increases within the formulation. This shows that with time, greater zeolitic water is seen within formulations at lower silicon concentrations, indicating that the structural development is occurring over a time period greater than 7 days whilst also allowing for ordering of the gel structure. Considering the calorimetric data given in Figure 4-7, the main reaction for the $SiO_2/K_2O = 0.5$ geopolymer occurs within a few hours, compared to the $SiO_2/K_2O = 1.5$ geopolymer which occurs over 20 hours. This shows that the slow formation of the gel structure at higher silicon contents leads to a faster stabilisation of the final gel structure, whereas changes within this structure may still be occurring in the lower silicon content formulations over timeframes of months.

Comparisons between formulations have shown minimal changes in terms of water content. However, the mass spectrometry data for carbon dioxide does show small changes in the degree of carbonation of each formulation. Firstly, the important point of note is the vertical scale in Figure 6-7, which is 10 times smaller than the carbonation shown on the irradiated samples that will be given in Figure 7-11 when these are discussed in Chapter 7. This shows that carbonation within these formulations is at a very small level, which is to be expected in sealed samples. However, the samples that have been cured for 7 days have experienced a greater level of carbonation than that of the 360 day cured samples. The samples are sealed prior to solvent extraction, and therefore the small degree of carbonation likely occurs during the cutting and grinding stages of the sample preparation. The temperature at which CO_2 is released for the MetaMax formulations, shown in Figure 6-8, varies depending on the formulation and the curing time of the sample. Releases of CO_2 at low temperatures (around 150 °C) are related to the decomposition of potassium hydrogen carbonate [261].
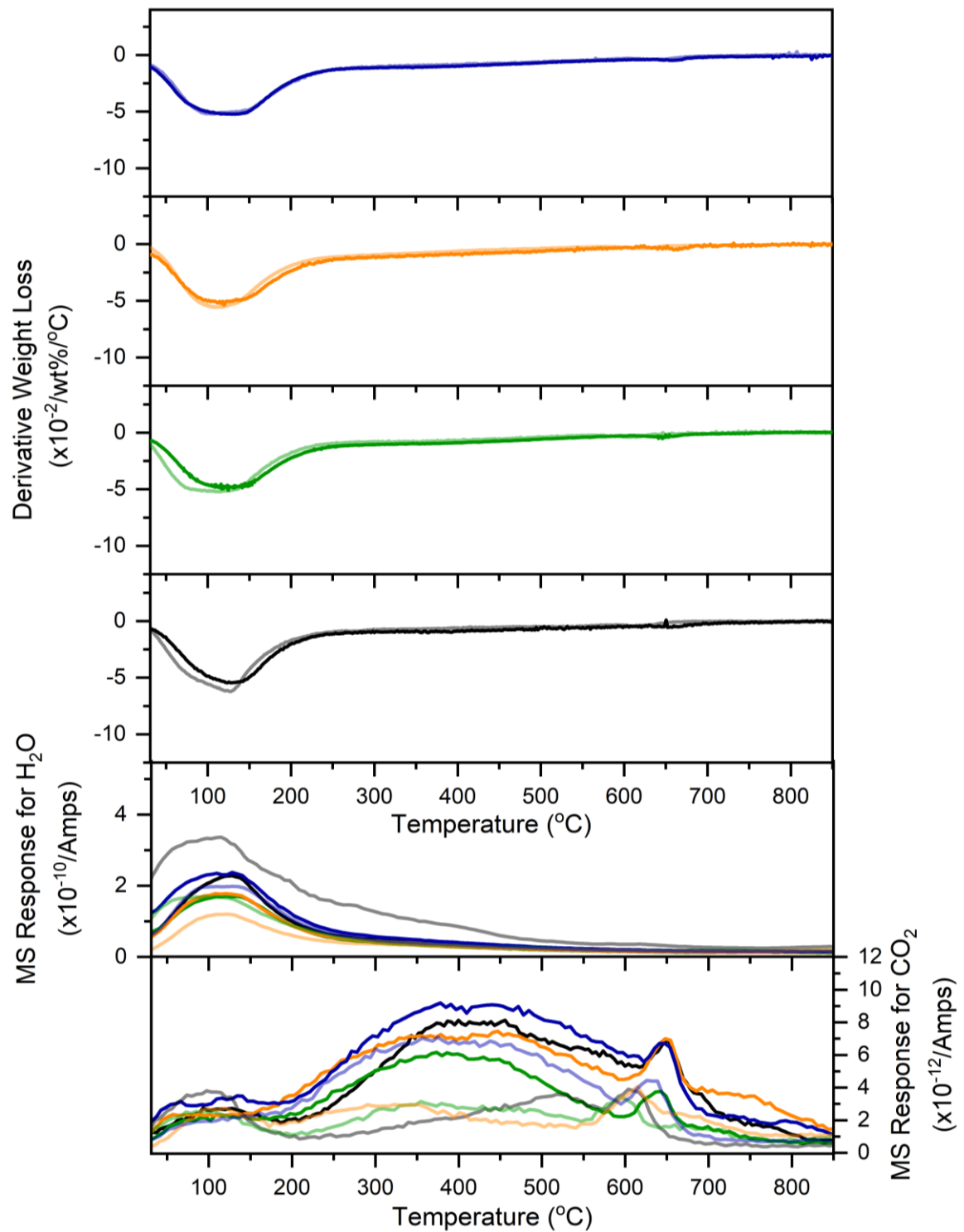
Figure 6-7 - Differential TG coupled with mass spectrometry conducted on Argicem-based MK geopolymers produced cured for 7 and 360 day cured samples. The mass spectrometry data was collected for water and carbon dioxide, which are given by the left and right axis graphs, respectively. The colour scale for each sample is defined in Table 6-1.
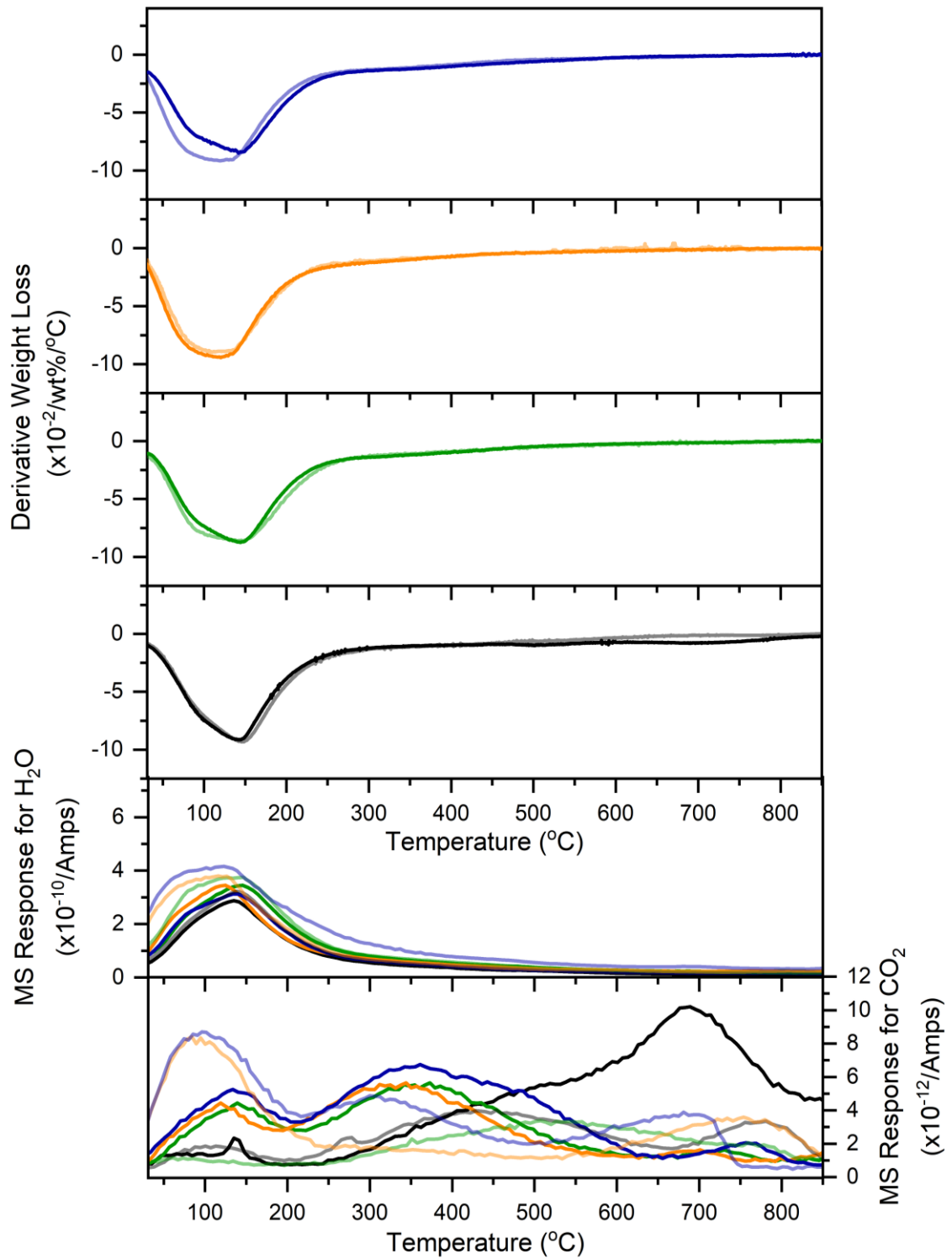
Figure 6-8 - Differential TG coupled with mass spectrometry conducted on MetaMax-based MK geopolymers produced cured for 7 and 360 day cured samples. The mass spectrometry data was collected for water and carbon dioxide, which are given by the left and right axis graphs, respectively. The colour scale for each sample is defined in Table 6-1.

6.2.5. Porosity and Microstructure

The use of environmental scanning electron microscopy imaging has been shown as a potential method for analysis of cementitious phases, as its low vacuum pressure is not expected to cause cracking within the cementitious matrix [262]. It has been shown to present a more rough surface morphology on geopolymer cements, and this rough surface was credited to surface reactions on fly ash geopolymer systems in the study of Duchesne et al. [263]. Figure 6-9 shows the formation of salt-like crystals on the surface of both the RC and FC MK products. These samples have been prepared with a high water content which has been shown in sections 4.2.2.1 and 5.3.1to have desirable flow properties for use within the nuclear industry. This salt like formation is similar to efflorescence and sub-fluorescence that has been shown for sodium activated metakaolin geopolymers [264], and which is formed from the deposition of salts on the surface of the sample from the partial drying of the vacuum followed by the humidity present within the chamber. Further study into the chemistry behind this needs to be undertaken to assess whether the formation of salt crystals under these conditions can lead to the degradation of these MK-based geopolymers. However, when considering the application of the environmental SEM to potassium activated metakaolin based geopolymers then it is clearly shown to induce cracking as is seen in Figure 6-9B, and also the production of salt demonstrates the need for a more appropriate mechanism for imaging.
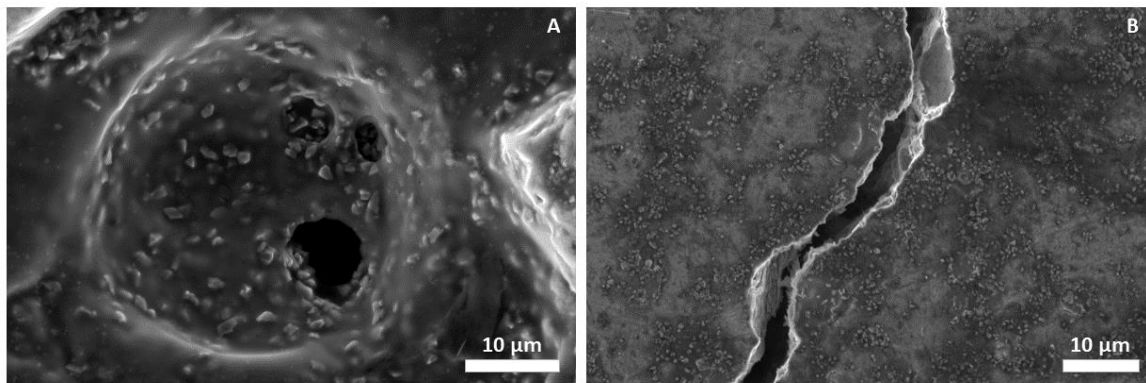
Figure 6-9 – Environmental scanning electron microscopy images of the Argeco (A) and MetaMax (B) formulations.

Novel epoxy impregnation methods have been developed at Imperial College London for examination via imaging of the microstructure [265-267]. This technique can be seen in Figure 6-10 and the epoxy resin can be be seen impregnated into the pore structure and also the crack network, with the dark banding that is very evident in Figure 6-10D. The cracks that contain this banding are produced prior to irradiation and the ones that are produced from the vacuum of the microscope would not contain

this banding. This is due to the epoxy impregnation methodolgy allowing for the resin to be pulled into the pores of the sample, at a relatively small vacuum pressure, and filling these pores. They appear as a dark band around the pore on the SEM as the backscattering coeficient of the epoxy resin is greater than that of the paste that surrounds it. However, the crack remains darker, along with the pore network, which allows for analysis of both of these parameters (shown in section 7.3.2.4 for the irradiated samples). This methodology has been trialled and offers a much better alternative to environmental SEM.
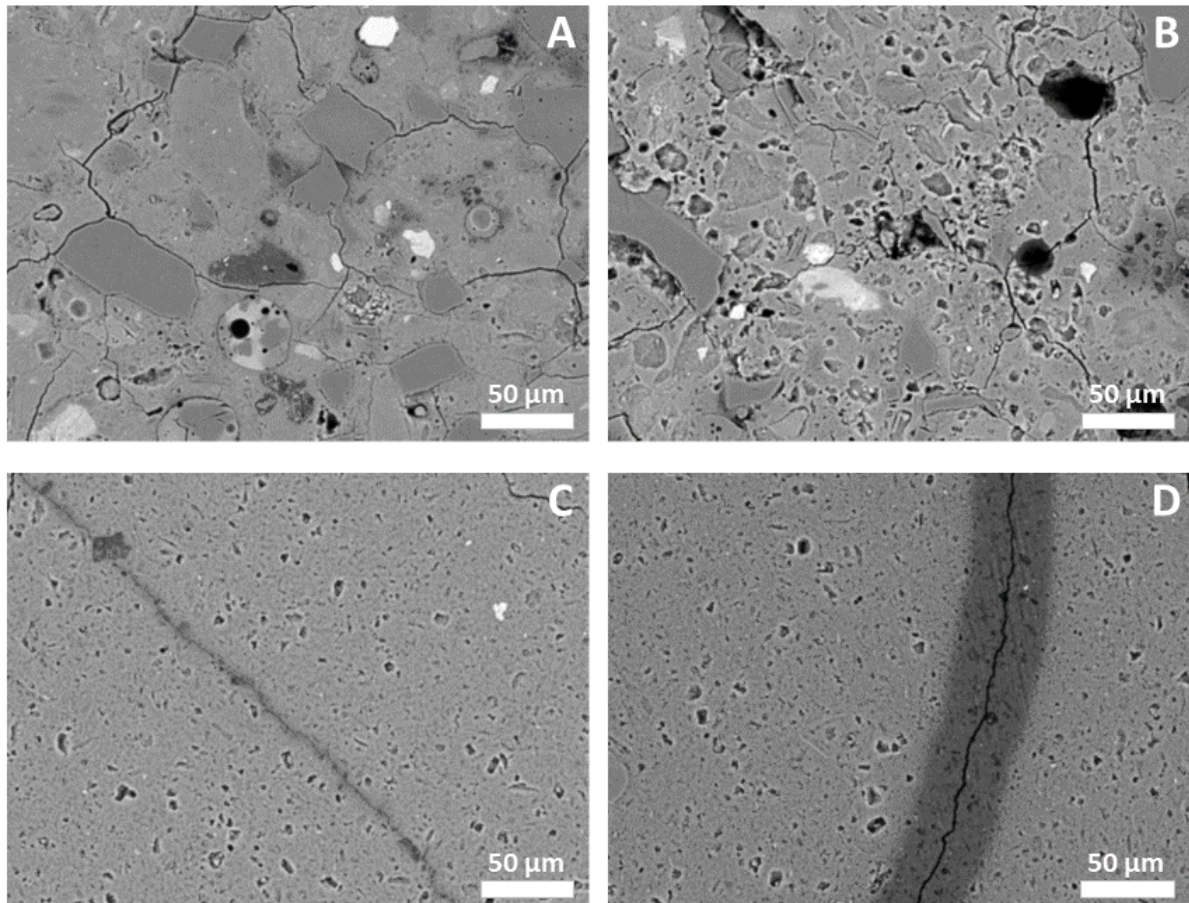
Figure 6-10 – Backscattered scanning electron microscopy images taken of epoxy impregnated geopolymer samples produced from Argcicem (A and B) and MetaMax (C and D) with $H_2O/K_2O = 11$ (A and C) and 13 (B and D). Images courtesy of Imperial College London (Hong Wong and Awni Abdullah).

The images shown in Figure 6-10 appear to show an increase in the porosity when the water content of the MK-geopolymers is increased. However, the percentage porosity has been calculated using mercury intrusion porosimetry (MIP) for the geopolymers based on Argeco MK, and it shows that a significant number of pores are below the threshold that can be seen using these SEM images. Therefore, MIP was seen as a more appropriate technique for this situation. The visual changes in the

larger pores that can be seen in Figure 6-10 agree with the MIP data shown in Table 6-3. The MIP data presented shows that there is a 10 % increase in the porosity when the H_2O/K_2O is increased from 11 to 13. Future examinations of all formulations will provide an in-depth analysis of the overall porosity of MK geopolymers as the formulation is adapted, which will be incredibly useful in predicting the service life of these materials.

Table 6-3 – Mercury Intrusion Porosimetry (MIP) results for the Argeco MK based geopolymer aged to 360 days. Standard deviations are calculated from 3 replicate samples.

H_2O/K_2O	% Porosity	Standard Deviation
11	21.3	2.9
13	31.3	2.1

6.3. Conclusions and Future Work

The work presented within this chapter was designed to show an overall physical and chemical stability of the MK-based geopolymer formulations that have been proposed in chapter 4. Overall these materials do not change on a chemical level, with the bonding shown via FTIR remaining consistent between both formulations and also curing times. The XRD patterns are also unremarkable and do not show the formation of zeolite materials that have been seen within sodium activated MK geopolymers. Overall the thermal stability of these materials does not appear to change with curing time. The zeolitic water, present within the geopolymer gel, appears to have a finite amount that does not change based on the overall formulation of the MK-based geopolymer. Structural changes within these materials are interesting and changes in the porosity are seen within an increasing water content for the Argeco MK. Changes to the overall structure of the system are seen when the compressive strength decreases between 7 days and 360 days of curing. A thorough understanding of this mechanism has not been developed and will need to be examined in the future.

Future work within this chapter will include an examination of the nano-structure of the gel network using solid state MAS-NMR to probe both the [27]Al and [29]Si nuclei. A greater understanding of the effect of MK, activator formulation and mixing conditions on the porosity of MK based geopolymers will help in the understanding of the long term durability of these materials. Extending this study to analyse samples that have been cured to ultra-long ages will allow for a thorough understanding of the long term stability of these materials, particularly with regards to the strength decreases that have been seen. These strength decreases can potentially hamper the use of these materials within both the construction and nuclear sector.

Chapter 7: Understanding the effect of gamma irradiation on the physiochemical structure of MK based geopolymers.

This chapter is based around the conference proceeding for the 15th International Congress on the Chemistry of Cement, Prague, Czech Republic, 16 – 20 September 2019 "Producing Effective Geopolymer Samples for Gamma Irradiation Studies", and the publication that is due for submission "Stability of Geopolymer Cements Under Gamma Irradiation". Both pieces of work have been authored by D. A. Geddes, B. Walkley, A. Abdullah, S.A. Bernal, M. Hayes, H. Wong and J. L. Provis. Special recognition should be given to Awni Abdullah and Hong Wong (Imperial College, London) for their collection of the SEM images used throughout this chapter.

7.1. Introduction

Cementation using a Portland cement blended with a high volume replacement of blast furnace slag and/or fly ash is currently the accepted method for the encapsulation of most ILW. However, Portland cement is not a perfect disposal method for some of these more problematic waste forms. Therefore, a few alternative cementitious systems have been suggested. Geopolymers have shown to be an alternative cementation method that can be used within the nuclear industry [67, 268] and have shown significant promise in the disposal of oil based wastes [15], reactive metals [28, 100] and wastes with varying water contents [269]. Geopolymer cements offer a viable alternative to Portland cement as they do not follow a hydration mechanism like Portland cement, which is not fully compatible with all problematic wastes that interfere with this hydration mechanism.

The geopolymer gel structure is produced from the reaction between the aluminosilicate precursor and alkali silicate activating solution. In order to produce a stable and rheologically acceptable product, potassium silicate activated MK based geopolymers have been produced, as it has been shown in sections 4.2.2.1 and 5.3.1 that these offer the most attractive properties. The gamma irradiation of cementitious systems has been shown in the literature to reduce the free water content, particularly of high slag replacement Portland cement [270, 271] and in some cases induce carbonation [272, 273]. The radiolysis of the free water, which leads to the production of hydrogen [170], causes cracks to appear within Portland cement systems [273]. As the geopolymer formulations proposed here have significantly contained more free water than Portland cement, it is expected that the cracking will be significantly greater within these cementitious systems. Further to the structural changes, it is believed that metakaolin based geopolymers show order on the nanoscale and produce nanocrystalline products similar to that of zeolites when activated with sodium based solutions [117].

For these systems to be accepted as a nuclear waste grout, the systems need to be stable under irradiation and have not shown significant changes to the gel structure and that these nano-zeolite structures have not grown within the network. As in order to pass the stringent safety parameters associated with the UK nuclear industry, long term stability to irradiation is required. It has been shown that potassium based activators do tend to resist the formation of zeolites [121].

Gamma irradiation is shown in section 2.2.4.4.2 to remove additional water from the sample when compared to heating to the same temperature. The liberation of water is seen between $50 - 150\ °C$ [173]. Gamma irradiation also induces carbonation within certain cement samples, which can be analysed using TG-MS [273]. This is believed to be due to the dehydration of the sample through radiolysis, removing the mobility of the free water, and increasing the effect of atmospheric carbonation on the sample [274].

This chapter will assess the stability of these materials under a dose of 3 MGy of gamma radiation. This will be done through assessment of the chemical structure via thermogravimetric analysis, X-ray diffraction and nuclear magnetic resonance. Mechanical stability will be assessed using novel scanning electron microscopy techniques. This will demonstrate effect of gamma irradiation on different calcined MK based geopolymers, at different water contents.

7.2. Materials and Methods

In order to understand the ability of different formulations of MK based geopolymers to be used within the UK nuclear industry, building an understanding of the effect of gamma irradiation on chemical and physical stability of these materials will be an important step in understanding and developing the safety case for their use. To develop a comprehensive study of the gamma irradiation effects, the conditions to which the samples are subjected in the irradiator is key. The irradiator used in this study is the ^{60}Co irradiator at the University of Manchester Dalton Cumbrian Facility [191]. In order to reproduce the effects of the irradiator, control samples are cured at 50 °C and sealed using Parafilm, which replicates the conditions within the irradiator at the position that was used for these samples [191]. These samples will be referred to as *heated controls*. For some of the sections of this chapter, *room temperature controls* are also used; these are samples that are cured at 20 °C and are sealed in the same way as the heated controls.

A factor that is often not sufficiently considered when cements are being examined under irradiation is the effect of pre-curing the sample before putting it into the irradiator. This is not mentioned in many of the studies of cement irradiation, and in the research that does mention this factor, the

precuring period varies drastically between years [275], months [273] and days [270]. As the cements used in wasteforms are irradiated from the inclusion of the nuclear waste, pre-curing for periods of months and years will give unrealistic results in this scenario; however, precuring may be needed for cements used in the construction of a reactor. Therefore, this study has been developed to investigate the stability of the geopolymer materials, with the formulations described in Table 7-1, over a series of pre-irradiation curing times and with a total dose of 1 MGy. 1 MGy has been selected as this is a low total dose for ILW, but is a significant dosage as to show any significant structural changes.

These controls need to simulate the thermal history to which the samples have been subjected in the irradiator, which for a dose rate of approx. 12 kGy·hr^{-1}, is a temperature of 50 °C [175]. The cementitious wasteforms produced in the UK nuclear sector are stored at the Sellafield site, and are expected to be held at 20 °C for extended periods of time before being placed into long term storage [29]. Therefore, control samples have been cured at 20 and 50 °C in this study, for comparison with the irradiated geopolymer cements. All samples were cast in prismatic moulds, then covered with Parafilm; this provides a seal to prevent large amounts of evaporative drying, which may cause drying shrinkage, but also allows for any gases produced in the irradiation process to escape. This prevents a build-up of pressure, which can lead to excess cracking, which is unrealistic for a grouted nuclear waste container, as the container is vented [276].

The carbonation has been assessed from the TG-MS data for the irradiated samples. The mass spectrometry data has been integrated to provide an area under the curve between 200 – 825°C. A ratio between the H_2O and CO_2 contributions is calculated and the mass loss between 200 – 850°C is associated solely to the loss of H_2O and CO_2. The mass of CO_2 released is then calculated and an estimated degree of carbonation can be produced.

Table 7-1 – Geopolymer formulation that have been used throughout this chapter.

H_2O/K_2O	SiO_2/K_2O	K_2O/Al_2O_3
11	1.0	1.0
13	1.0	1.0

7.3. Results and Discussion

7.3.1. Effect of precuring on the irradiation resistance properties of MK GPs

7.3.1.1. Chemical Stability of the FC MK Geopolymer

7.3.1.1.1. Changes in the free water content

The gamma irradiation of many different cements has been shown to affect the free water content and can potentially also lead to the formation of carbonates and other chemical species [172, 175, 273], and this includes geopolymer cements [169, 172]. The effects of irradiation on the chemical structure are shown in section 7.3.1.2. Very clear differences are seen in the changes in water content and also in the degree of carbonation for both MK types and the formulations tested. In order to provide a clear control, the heated control for the 20 hours pre-cured formulation has been used. This will give a comparison to the worst case scenario of water loss through heating, as heating a sample that has only been cured for a short period of time will give a greater reduction in the free water content due to the undeveloped microstructure leading to greater evaporation [277].

The geopolymer with $H_2O/K_2O = 11$ is shown in Figure 7-1, which shows that the change in the water content is affected by irradiation. Changing the curing time between 20 and 168 hours causes very minimal changes in the water content after irradiation. When comparing this to the heated control, the water that has been removed is not only the free water that is removed up to 100 °C. The water that is removed between 100 – 250 °C is seen as the bound water, and this is an important product for the development of structure of the geopolymer system [278]. This bound water has remained unaffected in the most part within these formulations. However, the free water which resides within the open accessible pore structure of these samples originates from the excess mixing water. This release of free water is not expected to cause large changes in the chemical structure of the geopolymer product, but it could cause changes in the porosity.

Figure 7-1 – Derivative thermogravimetric analysis (dTG) for the H_2O/K_2O = 11 FC-MK geopolymer. The MS data for H_2O and CO_2 is represented by the middle and bottom MS curves, respectively. The heated control samples are given by the dashed line, and the data for 20 and 168 hrs of curing is given by the black and grey lines, respectively.

When the water content is increased to H_2O/K_2O = 13, then significant differences are seen between the dTG results. This is shown in Figure 7-2. Upon increasing the water content, significant changes are seen in the free and bound water present post-irradiation when the water content is increased significantly. The high dose rate that is experienced by these samples is unrealistic when compared to the dose rate that intermediate level waste. In its lifetime an ILW container is expected to receive a total dose of 10 MGy at a dose rate of 24 Gyhr^{-1} [276]. Insufficient pre-curing has occurred in order to

resist the effect of irradiation on the free and bound water content. It is clearly shown that when the sample is cured for 168 hours, this is very similar to the irradiation characteristics of the $H_2O/K_2O = 11$ formulations. Therefore, it is shown that the effects of pre-curing are very important when assessing the effects of irradiation on MK based geopolymers. The removal of the bound water from the 20 hrs cured products is expected to cause changes in the overall gel structure of this product. Consideration of the gel structure has been undertaken by XRD, and this is shown and discussed in section 7.3.1.1.2.
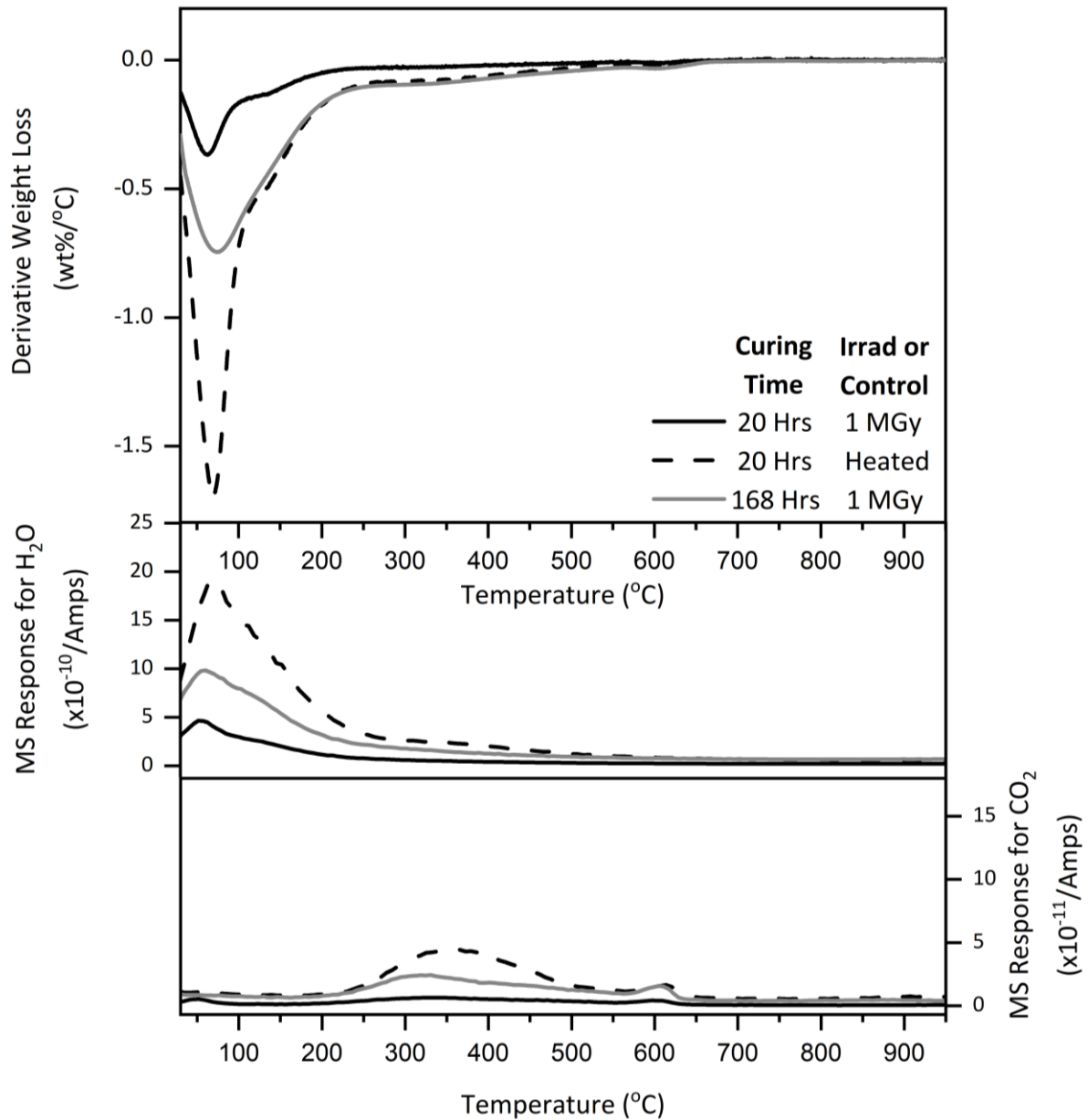
Figure 7-2 – Derivative thermogravimetric analysis (dTG) for the $H_2O/K_2O = 13$ FC-MK geopolymer. The MS data for H_2O and CO_2 is represented by the middle and bottom MS curves, respectively. The heated control samples are given by the dashed line, and the data for 20 and 168 hrs of curing is given by the black and grey lines, respectively.

7.3.1.1.2. Changes in the crystallinity

In order to assess the stability of these materials when exposed to irradiation, X-ray diffraction has been undertaken in order to show the formation of any crystalline species. Figure 7-3 shows this comparison for the 20 and 168 hrs pre-cured samples, and the 20 hrs heated control. No clear difference can be seen between any of the diffractograms shown in Figure 7-3. The FC MK contains a significant content of quartz and this leads to the highly crystalline X-ray diffraction pattern. Carbonation is seen in the TG-MS data presented in section 7.3.1.1.1 from the CO_2 MS trace, and so the formation of crystalline carbonation products is expected to be shown in the crystal structure of the MK-geopolymer. Therefore, a separate assessment of the carbonation from the TG-MS data is given in section 7.3.1.1.3. The lack of changes in the diffractogram does show that the FC MK geopolymer is resistant to irradiation doses of 1 MGy, independent of the pre-curing, in terms of any changes in crystalline ordering. This is a positive step when developing a safety case for these materials and also in the understanding of the effects of pre-curing on the chemical stability of these materials.
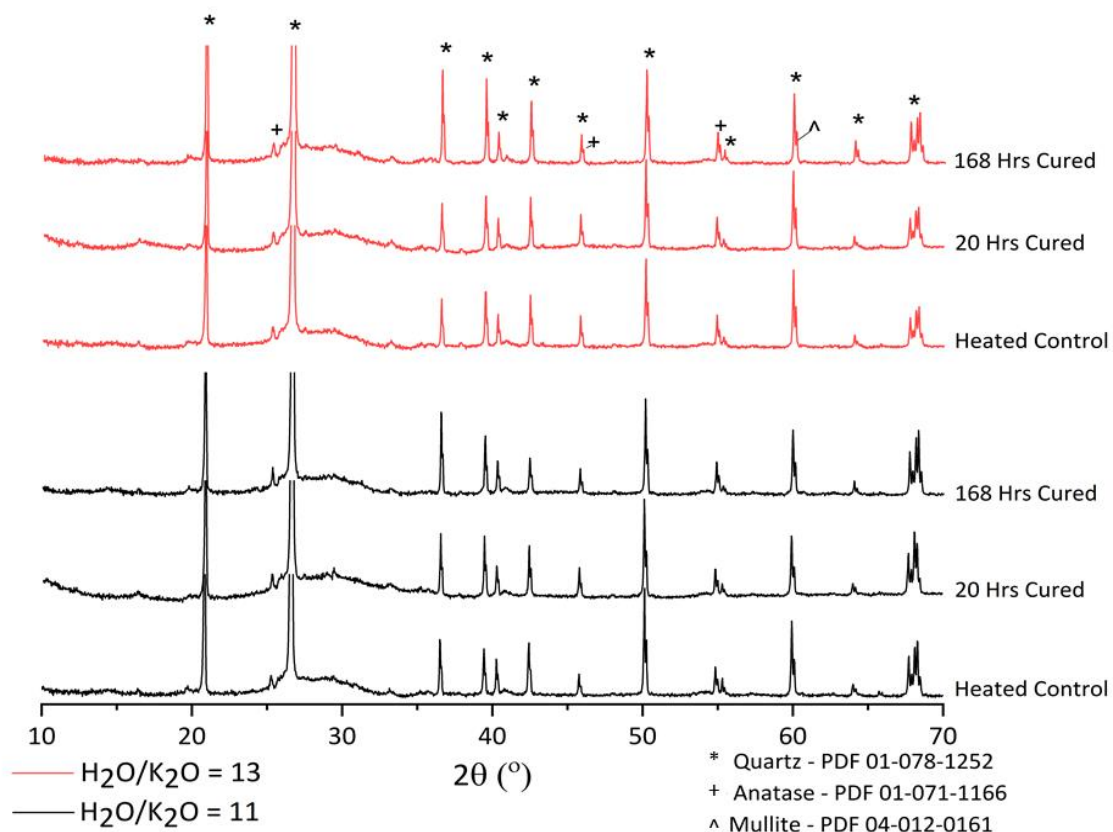
Figure 7-3 – X-ray diffractograms of the 20 hrs cured heated control sample and the 20 and 168 hours irradiated samples. Data for H_2O/K_2O = 11 and 13 are given by the black and red lines, respectively.

7.3.1.1.3. Carbonation

The carbonation within the geopolymer samples is clearly shown by the mass spectrometry data in the TG-MS data given in Figure 7-1 and Figure 7-2. Figure 7-4 shows how the TG-MS data can be integrated in order to show the degree of carbonation that has been induced as a result of the irradiated samples have shown carbonation. The driving force for the carbonation of the H_2O/K_2O = 11 samples is the irradiation which has caused the liberation of the pore water and provided a route for carbon dioxide to enter the system and carbonate different species. Pre-curing of the H_2O/K_2O = 11 geopolymers has affected the carbonation level. As this change is not consistent in the H_2O/K_2O = 13 formulation, this is not attributed to any form of curing condition, as these samples were cured in the same conditions. The carbonation of the H_2O/K_2O = 13 formulations has been greater in the heated control than in the samples that have been irradiated. These samples contain a greater volume of water in the pores when compared to the H_2O/K_2O = 11 samples. The 168 hours cured sample is more carbonated in the irradiated sample, due to the removal of free water over the preceding 168 hours. This gives more rapid access of the carbon dioxide to produce carbonate species. For the H_2O/K_2O = 13 formulation, the level of carbonation of the heated control sample is greater than that of the irradiated sample. It is unclear why this is the case.
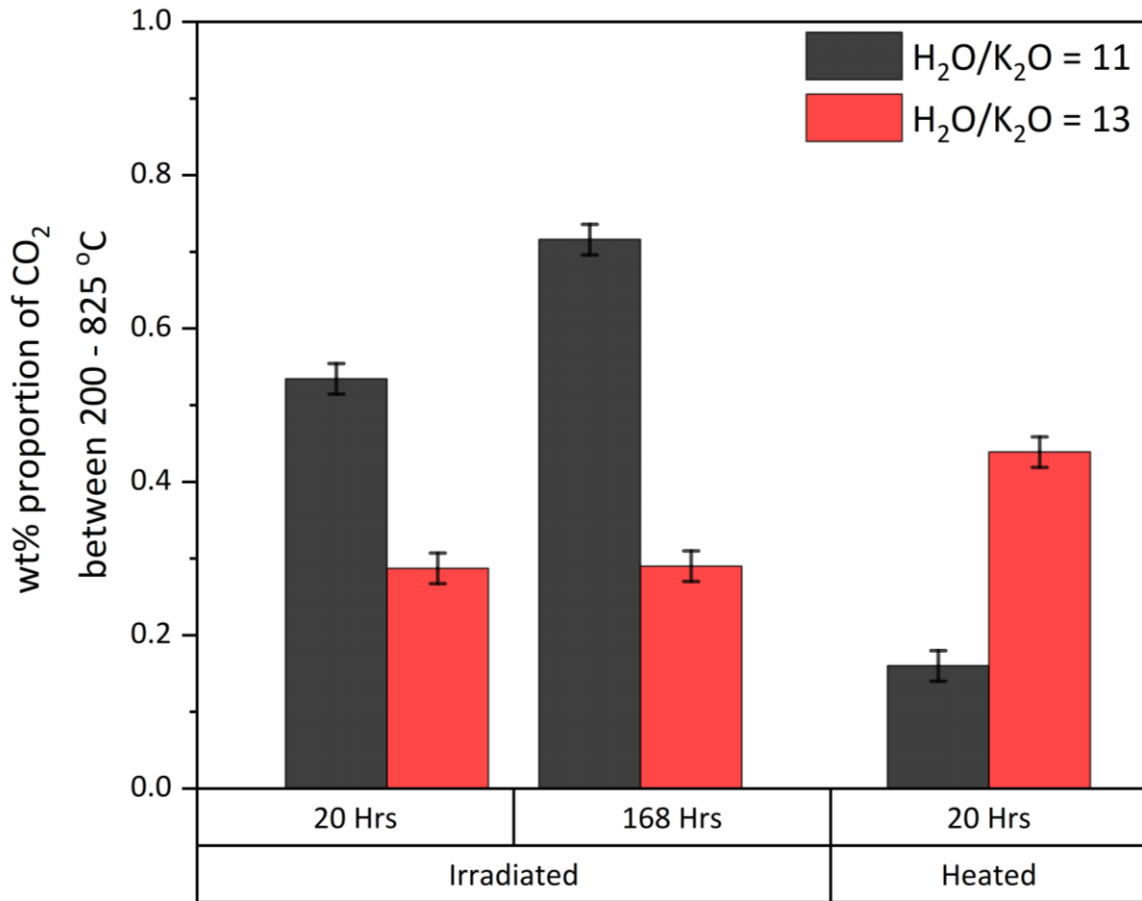
Figure 7-4 – Integrated mass spectrometry data showing the wt.% proportion of CO_2 that is present in the heated controls and the irradiated samples that were cured for 20 and 168 hrs. Data for H_2O/K_2O = 11 and 13 are represented by the black and red bars, respectively.

7.3.1.2. Chemical Stability of the RC-MK Geopolymer

7.3.1.2.1. Changes in the free water content

The RC-MK product reacts differently in comparison to the FC MK product, and the effects of curing on the free water content post-irradiation are clear. These are shown in Figure 7-5 and Figure 7-6 for H_2O/K_2O = 11 and 13, respectively. The effect of pre-curing on these formulations does appear to affect the impact that irradiation has on the bound and free water within the chemical structure of these materials. Interestingly in the sample with H_2O/K_2O = 11, when compared to the heated control, the irradiated samples do not reduce the free water content of the samples when comparing the dTG data. However, when examining the mass spectrometry data, this shows that the heated control sample has a slightly lower water content than the pre-cured samples. This is inconsistent with what is to be expected in the irradiation of cementitious materials [270]. This has shown that the differences

between these samples are not within the error of the equipment that is used for analysis. Therefore, differences in heating and irradiation cannot be elucidated from this data. However, irradiation has led to a change in the degree of carbonation, which is shown in section 7.3.1.2.2.
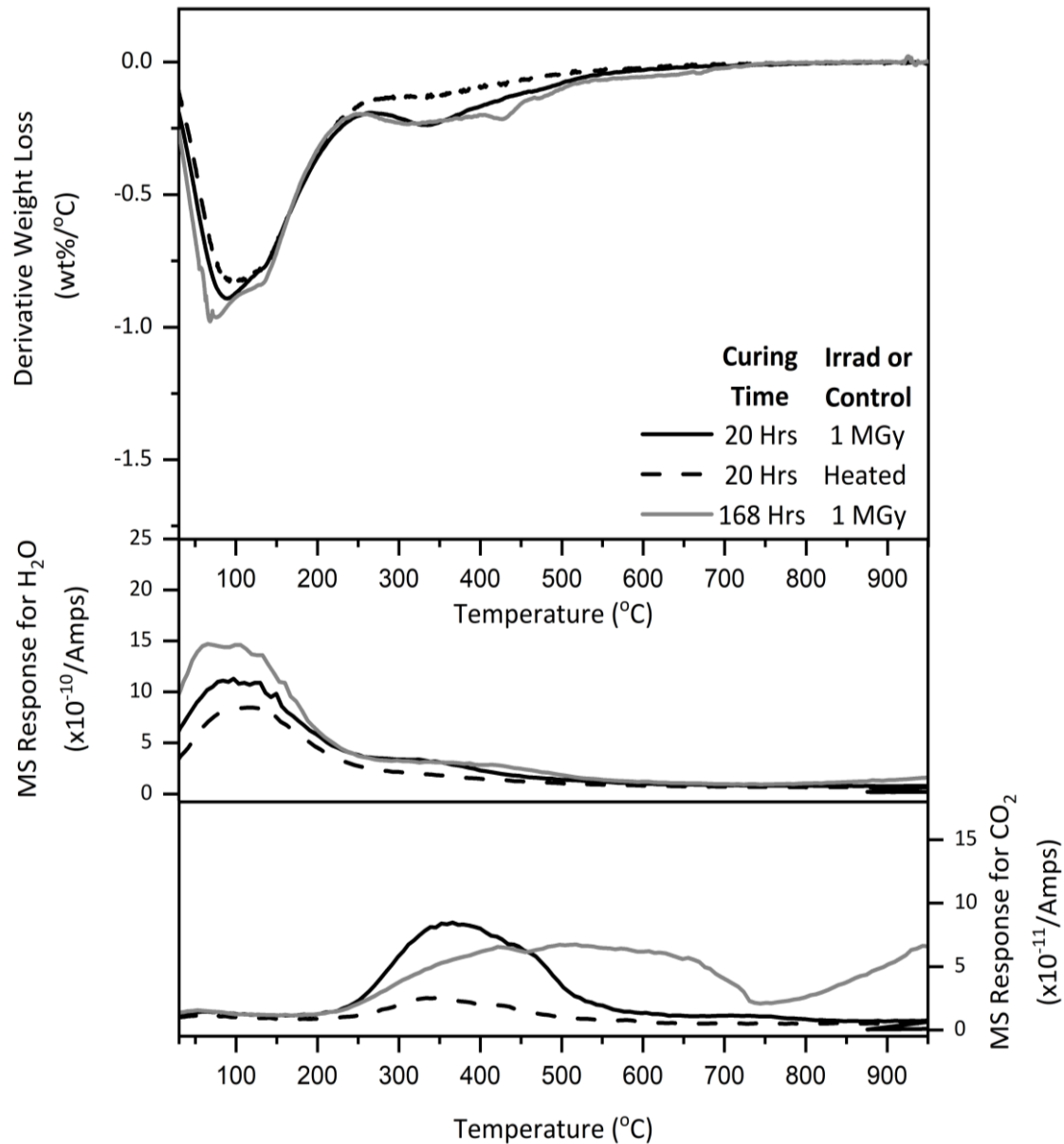
Figure 7-5 – Derivative thermogravimetric analysis (dTG) for the H_2O/K_2O = 11 RC MK geopolymer. The MS data for H_2O and CO_2 is represented by the middle and bottom MS curves, respectively. The heated control samples are given by the dashed line, and the data for 20 and 168 hrs of curing is given by the black and grey lines, respectively.

When H_2O/K_2O is increased to 13, Figure 7-6, then according to the changes in the free water content, there is a drastic change between the heated control and the two irradiated formulations. The two irradiated formulations have little difference in water content post irradiation. Comparing this to the

H_2O/K_2O = 11 system, the effect of pre-curing is minimal in terms of the effects on the free water content of this paste. This shows a more realistic effect of the irradiation on the water content of the RC MK formulations. This is explained in greater detail in section 7.3.2. However, it is clear that the 168 hrs cured sample has undergone significantly more carbonation than the 20 hrs and heated control formulations. This is likely to be because of an increase of porosity at higher water content, as shown by Duxson et al. [213] who stated that increasing the water content causes a swelling in the porosity.
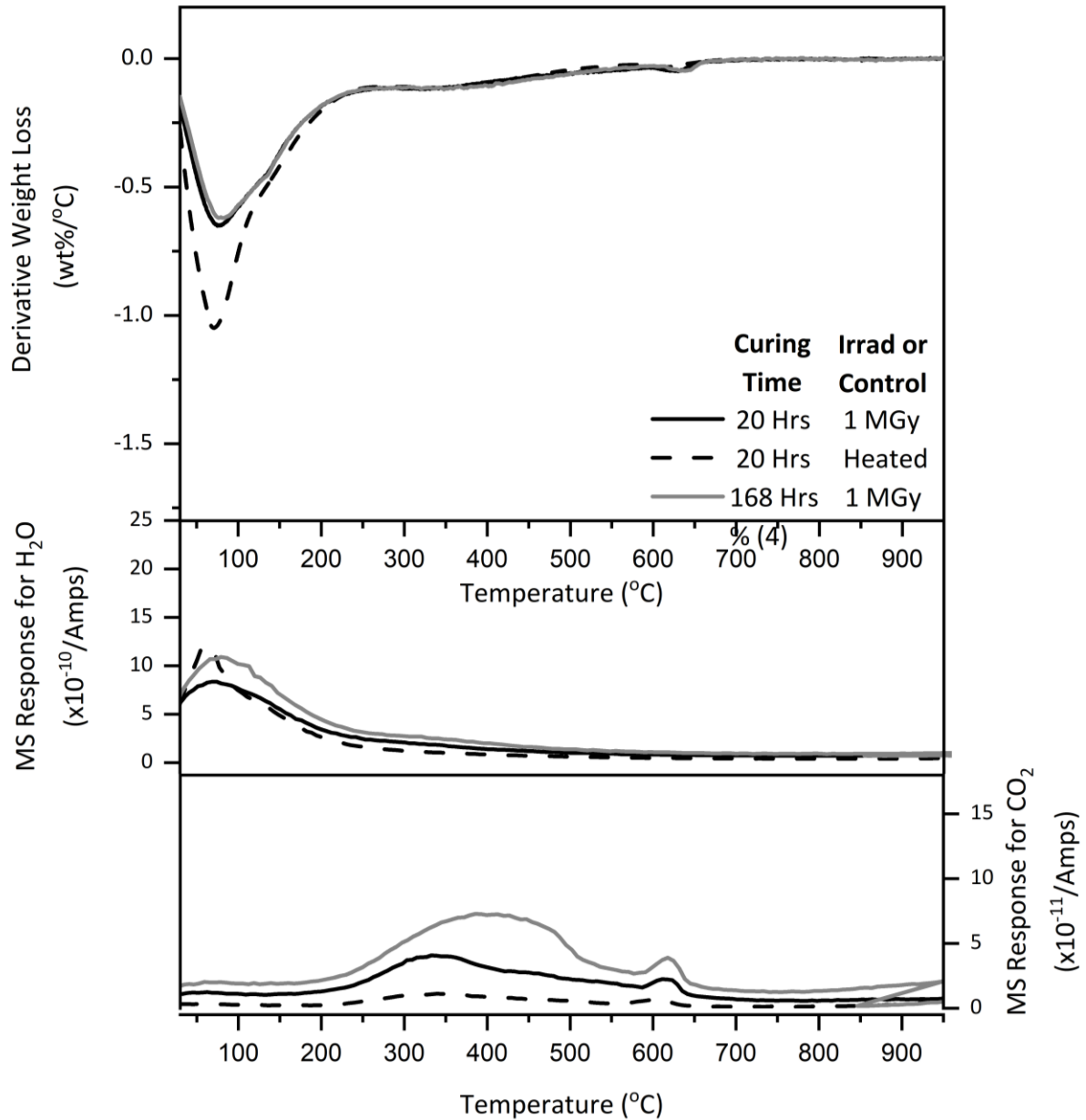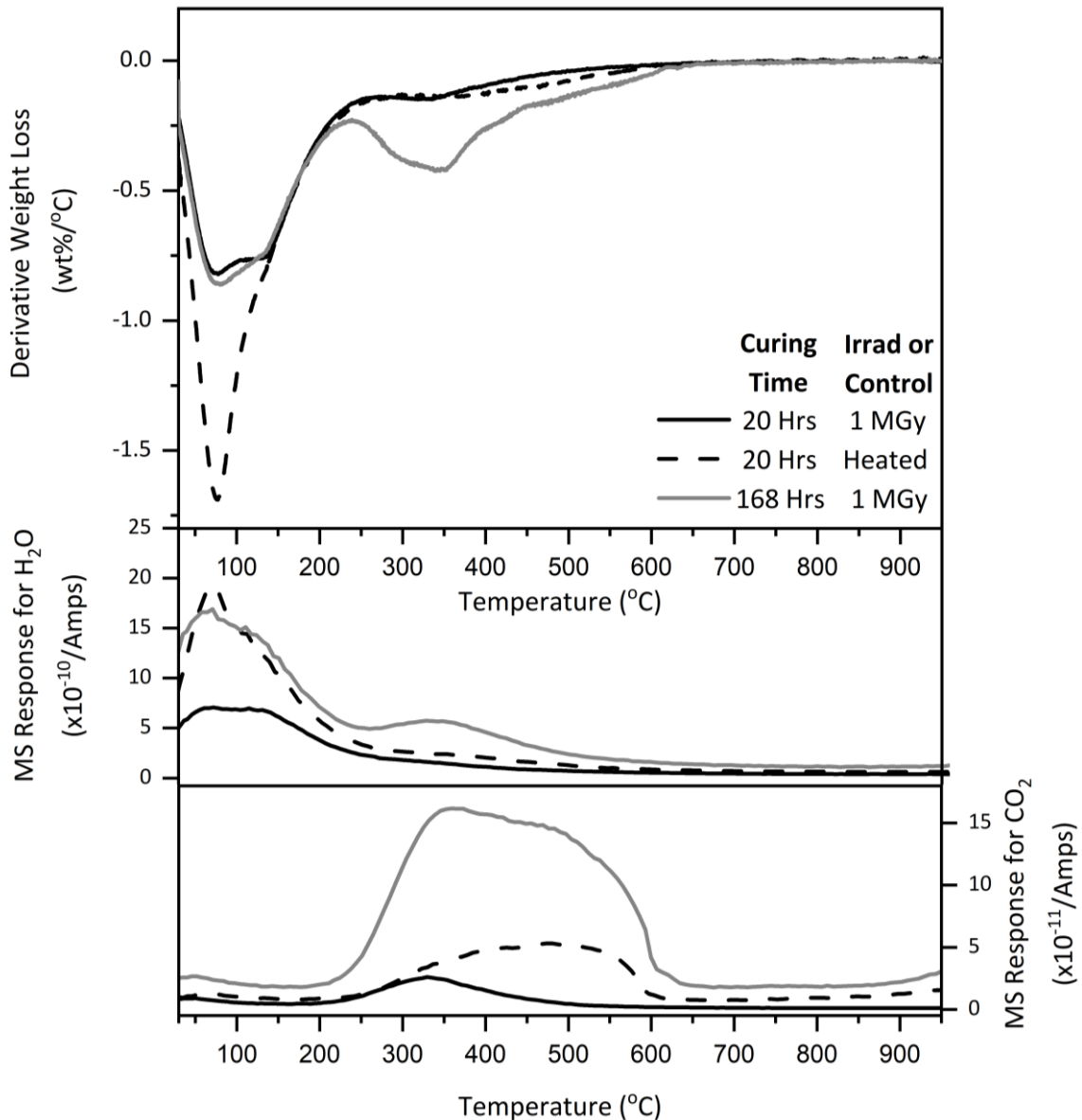

Figure 7-6 – Derivative thermogravimetric analysis (dTG) for the H_2O/K_2O = 13 RC MK geopolymer. The MS data for H_2O and CO_2 is represented by the middle and bottom MS curves, respectively. The heated control samples are given by the dashed line, and the data for 20 and 168 hrs of curing is given by the black and grey lines, respectively.

7.3.1.2.2. Carbonation

The dTG-MS data given in Figure 7-5 and Figure 7-6 shows a significant level of carbonation for the RC MK geopolymer when compared to the FC MK geopolymer. In order to analyse the degree of carbonation within the RC MK formulations an integrated mass spectrometry plot has been produced (Figure 7-7), similar to that of the FC MK formulations (Figure 7-4). When considering the effect of carbonation on the heated control sample for the $H_2O/K_2O = 11$ formulation, this is reduced when compared to both of the irradiated samples. The samples that have been irradiated have undergone a significant degree of carbonation, when compared to the heated control samples, with more carbonation occurring in the 20 hr cured sample compared to the 168 hr cured sample. This is the opposite trend to what is shown in the FC MK samples (Figure 7-4). As the pore structure of these cements will develop with time, it is expected that the 168 hr cured sample would undergo more carbonation due to a more refined pore network, which is what is seen when H_2O/K_2O is set at 13. This increase to $H_2O/K_2O = 13$ leads to a larger pore network that can lead to an increase in carbonation [84]. An explanation for the difference between the $H_2O/K_2O = 11$ and 13 systems carbonating differently under irradiation when compared to the FC MK system is that the alkaline cations within the lower-water ($H_2O/K_2O = 11$) system are more available to carbonate within the sample, but when this value is increased to 13 the larger pore distribution takes over and allows for carbonation to occur within a deeper pore structure.

Figure 7-7 – Integrated mass spectrometry data showing the wt.% proportion of CO_2 that is present in the heated controls and the irradiated samples that were cured for 20 and 168 hrs. $H_2O/K_2O = 11$ and 13 are represented by the black and red bars, respectively.

7.3.1.2.3. Changes in the crystallinity

As the degree of carbonation demonstrated in Figure 7-4 and Figure 7-7, are shown to be greater for the RC MK product, then it is expected that the XRD pattern for the RC MK product is going to be a more powerful technique for showing the carbonates when compared to the FC MK. The RC MK used here (Metamax) is a poorly crystalline, highly disordered product (as shown in section 3.1.1). Thus, small changes in the X-ray diffractogram may be lost relative to the higher background from the disordered material, and become difficult to see. The X-ray diffractograms are shown in Figure 7-8. The highly disordered structure is obvious for the RC MK product, with the only difference observable in the 168 hour irradiated, $H_2O/K_2O = 13$ sample, which has been assigned to an erroneous quartz peak which is likely due to the preferred orientation of a quartz lattice that is generally in low concentration during the system, which in this trace has become visible by statistical probability. This lack of changes in the diffractograms show that the changes in curing time and also a dose of 1 MGy have no effect on the observable crystal structure of this product.

114
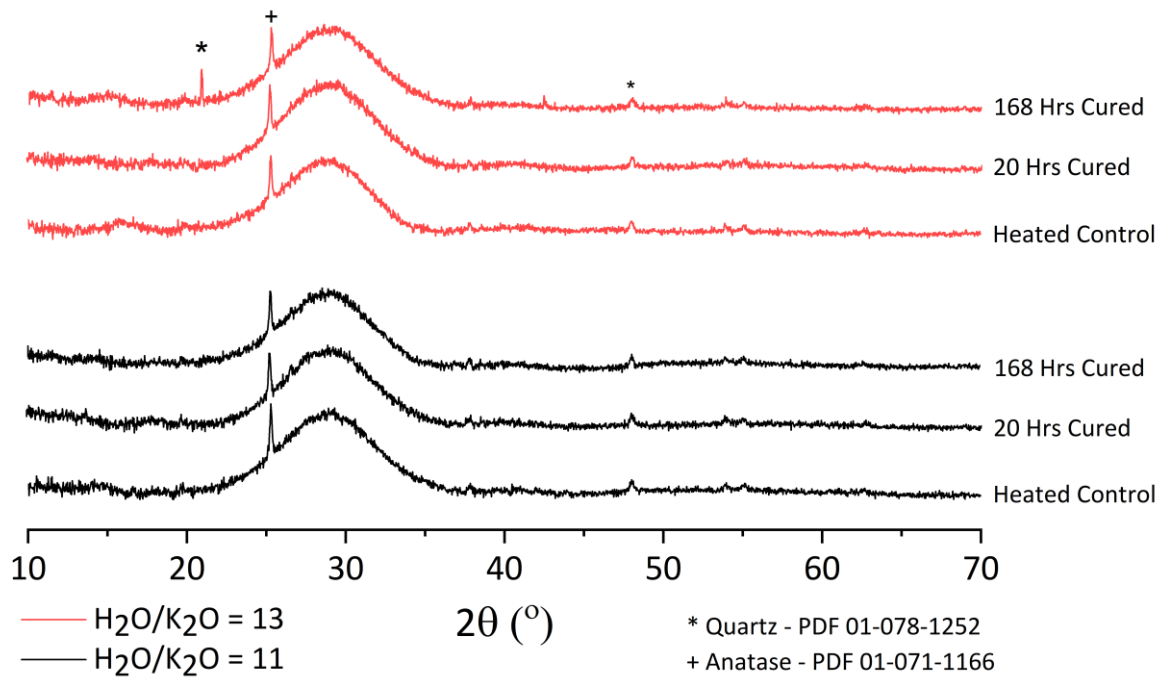
Figure 7-8 – X-ray diffractograms of the 20 hrs cured heated control sample and the 20 and 168 hours irradiated samples. H_2O/K_2O = 11 and 13 are given by the black and red lines, respectively.

7.3.1.3. Concluding and Assessing an Effective Precuring Time

The pre-curing of these systems has led to a series of very interesting changes in the carbonation and free water content, and no observable changes to the crystal or gel structure according to XRD analysis. Further analysis of the porosity, and how this affects the carbonation rate of samples that are cured for different amounts of times pre irradiation, is needed to draw valid conclusions regarding the carbonation of the MK-geopolymers. The FC and RC MK geopolymers react differently to irradiation when considering this pre-irradiation curing regime. All the remaining work within this section will be performed on samples that have been cured for 48 hours before irradiation. This allows for effective comparison between clays, whilst also providing a reasonable amount of time in order to process the samples before irradiation and deliver them to the irradiation facility, which proved to be difficult for the 20-hour pre-curing process.

7.3.2. Effect of water content on the irradiation resistance properties of MK GPs

7.3.2.1. Thermogravimetric Analysis

7.3.2.1.1. Changes in the water content

In order to analyse the chemical stability of these materials under irradiation, thermogravimetric analysis coupled with mass spectrometry (TG-MS) has been used to determine any changes in water content and also the presence of carbon dioxide within these samples (Figure 7-9 and Figure 7-10). Carbonation is seen as a deterioration mechanism in concretes produced with Portland cement and supplementary cementitious materials where significant changes in phase assemblage and mechanical properties are identified. Carbonation can have a positive or negative impact on the physiochemical properties of grouts containing fly ash and/or blast furnace slag [279]. However, a thorough understanding of the effect of carbonation on UK specification nuclear waste grouts has not been shown within the literature. There is little understanding of the carbonation mechanism in MK-geopolymer systems, but there is a consensus that sodium activated system follow a 2 stage process leading to a carbonate which is then evolved into a bicarbonate/carbonate phase evolution [280].

For comparisons between samples in the TG-MS data for the RC and FC MK, given in Figure 7-9 and Figure 7-10, respectively. The water traces from MS are normalised to the maximum of each individual signal. However, the CO_2 traces are instead normalised to the maximum of the irradiated sample, to enable identification of the relative extent of carbonation in each of the formulations. The free water content of the geopolymers is given by the initial peak between 30 – 150 °C; the intensity of this peak shows that the heating of the sample to 50 °C during curing leads to a reduction in the free water content of the geopolymer formulations, which is expected in geopolymer metakaolin cements [98, 170]. The RC MK geopolymers (Figure 7-9) contain more free water than those based on FC MK (Figure 7-10), due to the higher water content of these systems (Table 7-1). Therefore, more water is available to be hydrolysed during irradiation of the RC MK geopolymers. This explains why a greater reduction in the water content is seen for the RC MK system when compared to the FC MK formulation after exposure to gamma irradiation.

Increasing the water content of the mix shows, as expected, a greater free water content at temperatures below 100 °C for the room temperature controls. The total water content is reduced upon heating, specifically seen in the TG data at temperatures below 100 °C, but somewhat more strongly bound water is now present in these samples, shown by a shoulder between 100 – 150 °C. Irradiation reduces this water content further, consistent with the observations presented by

Mobasher et al. [270] on blended Portland cement systems and also the work by El-Nabarawy et al. [281] on the thermal properties of irradiated Na-Y zeolites
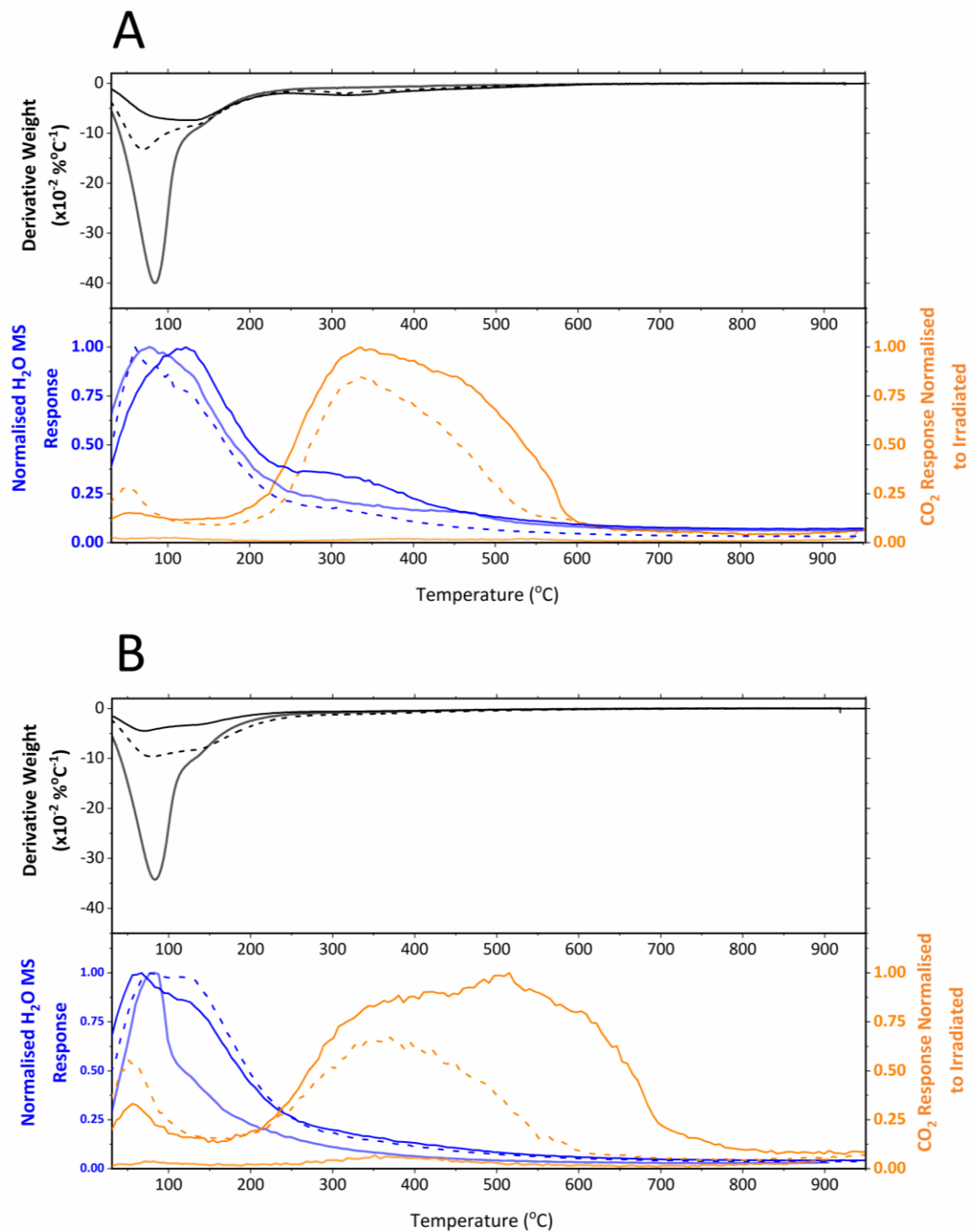
Figure 7-9 – Differential thermogravimetric analysis (dTG) coupled with normalised mass spectrometry (MS) data for the RC MK geopolymer formulations with H_2O/K_2O = 13 (A) and 11 (B). The data for 20 °C formulations are shown as dot-dash lines, the 50 °C heated samples as dashed lines, and the 3 MGy irradiated samples as solid lines. The MS data are shown in blue for H_2O and orange for CO_2. The H_2O data are normalised to the maximum of each trace, and the CO_2 data are normalised to the maximum of the trace for the irradiated sample

The normalised water loss mass spectrometry curves show differences in the temperatures at which the most water is released from each formulation. The irradiated $H_2O/K_2O = 11$ (Figure 7-9B and Figure 7-10B) has a maximum at 60 °C and a small shoulder at 150 °C, while the opposite trend is shown in the samples with $H_2O/K_2O = 13$ (Figure 7-9A and Figure 7-10A), and the irradiated sample does not lose much of the bound water compared to the free water. This is where the similarities between the RC and FC MK geopolymers have changed. The RC MK formulations presented in Figure 7-9 shows that the difference between the irradiated and heated samples is significant. The total water content seen at the shoulder, centred around 150 °C remains unchanged. This shoulder is related to the bound gel structure water which is held within the K-A-S-H [82, 83]. This is an indication that the gel structure does not change upon irradiation and further studies will be shown in section 7.3.2.3, via nuclear magnetic resonance.

The free water which is centred at approx. 60 °C shows significant differences. This water is physically bound within the pores and is removed with ageing and/or thermal treatment of MK based geopolymers [249]. The removal of this pore water using gamma irradiation has been shown [172] and it is expected to cause changes to the pore structure and also cause cracking within the systems [172, 272], which will be examined in section 7.3.2.4.. As an interesting side note, heating of all the formulations (RC and FC MK) appears to lead to an increase in the amount of bound water present in all formulations, and therefore curing at higher temperatures appears to produce a more stable geopolymer product. This is likely due to the higher temperature leading to a greater extent of reaction. A faster reaction has been shown at 40 °C compared to 20 °C in the isothermal calorimetry data shown in Figure 4-7. As these samples are cured at 50 °C, it is expected that the rate of reaction will be similar if not slightly faster.

The FC MK system does appear to show a significant resistance to gamma irradiation when compared to the RC MK, in specific respect to the free and bound (gel phase) water. The $H_2O/K_2O = 11$ (Figure 7-10B) does lose a small amount of the free water present when compared to the $H_2O/K_2O = 13$ (Figure 7-10A). This higher water content system loses more free water that the lower system upon heating, and therefore upon irradiation no more free water is lost. It is likely to that heating to 50 °C has removed the majority of the free water and all that remains are the bound/gel phase water. The mass spectrometry data for the water does show a larger area of response when comparing the heated to the irradiated samples and therefore, this likely shows that there is still a small quantity of free water that is available for radiolysis but this is not in the same quantities as the RC MK formulations.
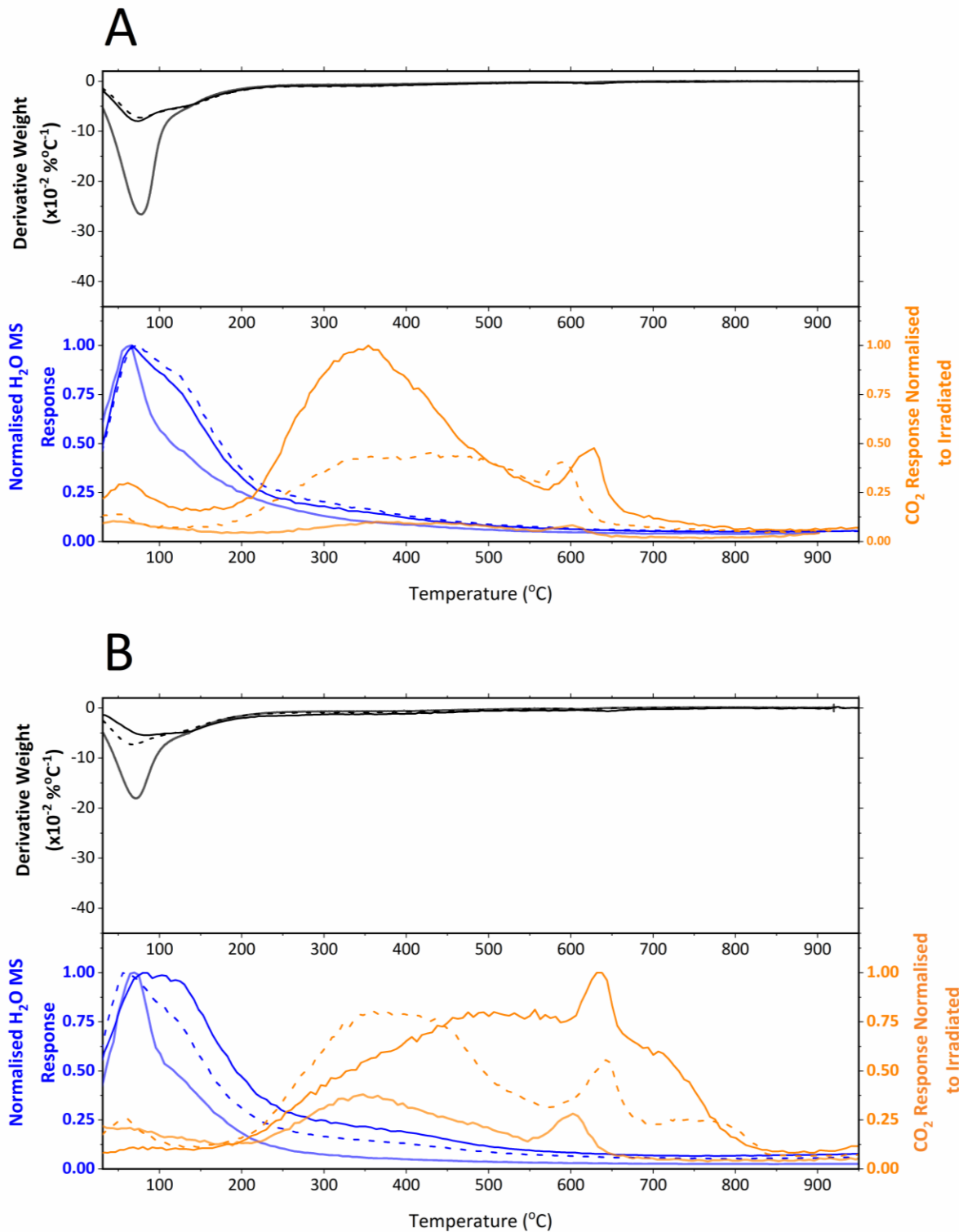
Figure 7-10 – dTG-MS data for the FC MK geopolymer formulations with H_2O/K_2O = 13 (A) and 11 (B). The data for 20 °C formulations are shown as dot-dash lines, the 50 °C heated samples as dashed lines, and the 3 MGy irradiated samples as solid lines. The MS data are shown in blue for H_2O and orange for CO_2. The H_2O data are normalised to the maximum of each trace, and the CO_2 data are normalised to the maximum of the trace for the irradiated sample.

7.3.2.1.2. The effect of carbonation

The w/b ratio of the RC MK formulations is greater than that of the FC MK formulations, which lead to the differences in the peak intensity between 50 – 200 °C in Figure 7-9 and Figure 7-10. However, when comparing the dTG traces for the H_2O/K_2O = 13 and 11 geopolymers based on FC MK (Figure 7-10A and B), similar effects are seen to those shown in Figure 7-9, particularly related to the water content. A reduction in the free water content is seen upon heating and more bound water is formed. However, upon irradiation the geopolymers based on FC MK appears to follow different trends from those of geopolymers based on the RC MK. The H_2O/K_2O = 13 sample (Figure 2A) shows a reduction in the free water but not in the structural/bound water upon irradiation when compared to the heated and room temperature controls; this reduction in free water is much smaller than that of the equivalent RC MK formulation. The H_2O/K_2O = 11 sample (Figure 7-10B) does not appear to be affected by irradiation; the water content does not change upon irradiation when compared to the heated formulation. Therefore, for this system the lower water content formulation (Figure 7-10B) appears to be more resistant to gamma irradiation.
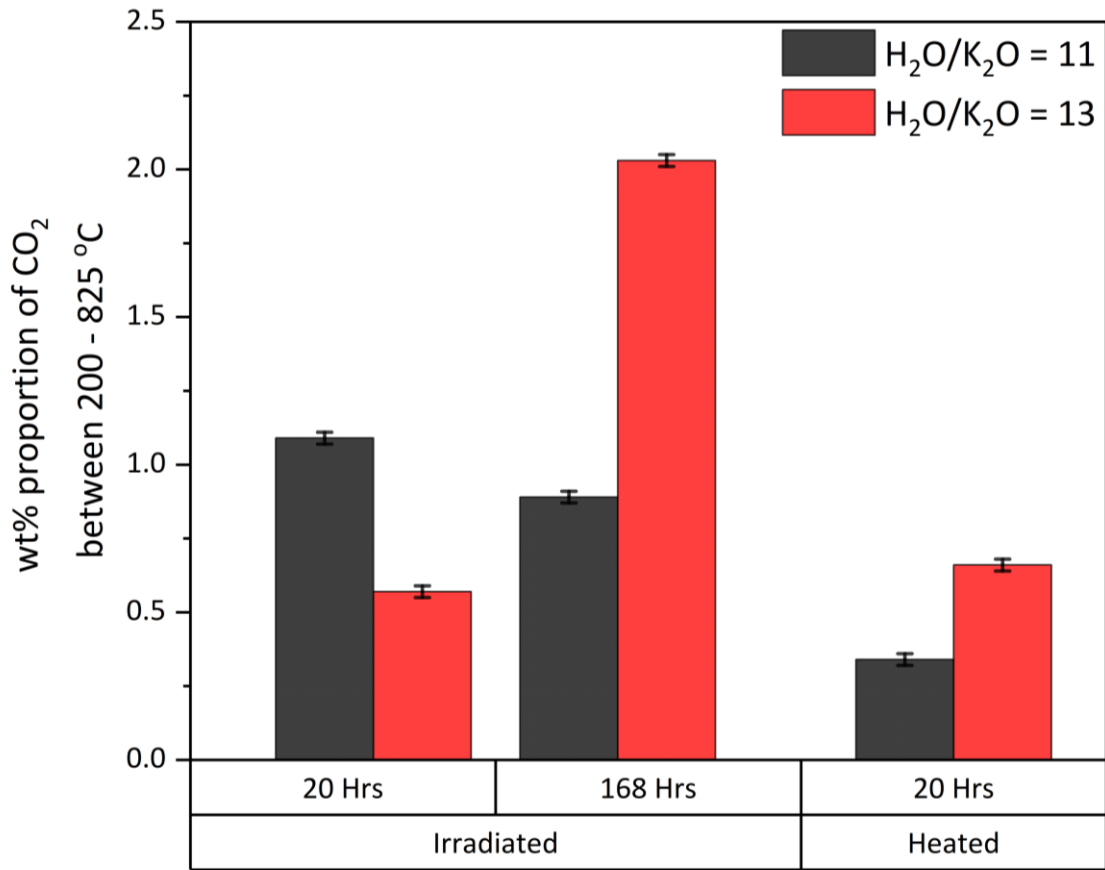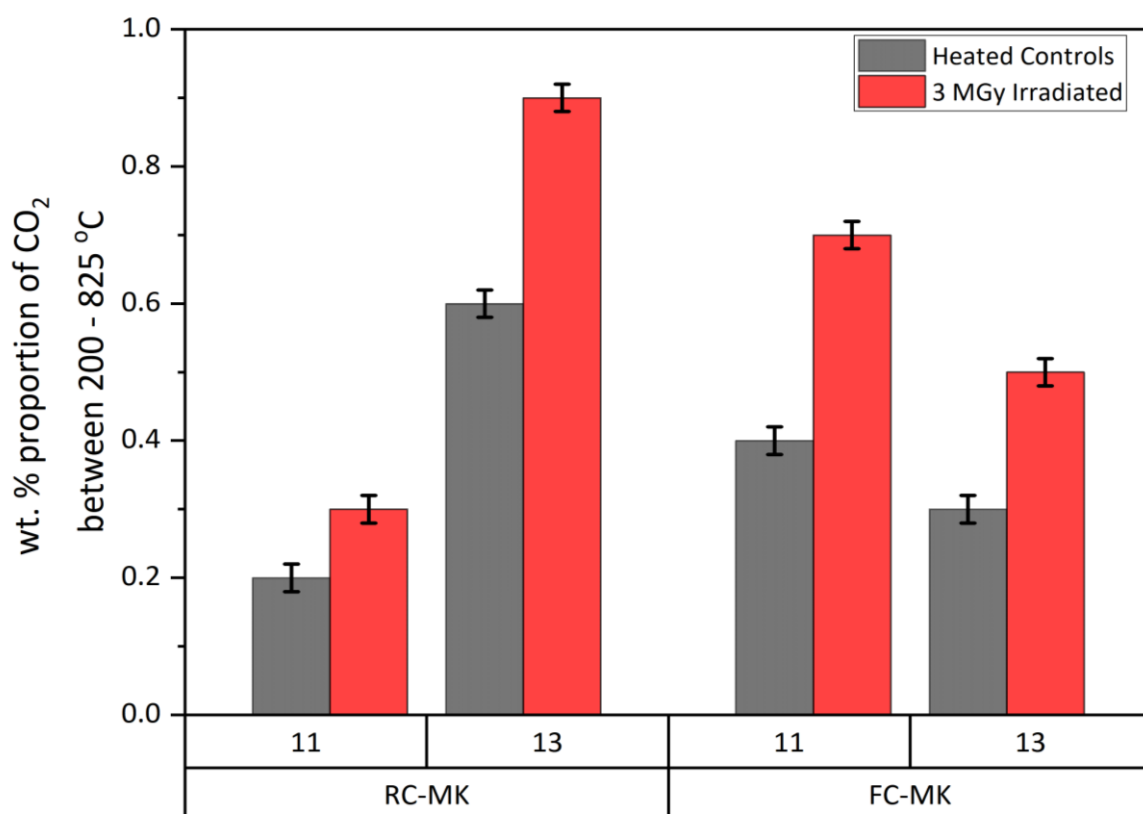

Figure 7-11 – Integrated mass spectrometry data showing the wt.% proportion of CO_2 that is present in the heated controls and the 3 MGy irradiated samples.

Carbonation has occurred within all the irradiated and heated formulations, although to different degrees. Carbonation has however been seen only to a very small level in the FC-MK, due to a small impurity in the clay, and is non-existent in the RC-MK formulations. In order to compare the carbonation within these formulations, the raw MS data for the H_2O and CO_2 responses has been integrated to find the contribution that they are giving to the change in sample mass between 200 – 825 °C. The assumption has been made that no other elements have been released over this range and that the change in wt.% over the range 200 – 825 °C is solely related to the H_2O and CO_2 that is released. The wt.% proportion of CO_2 for each formulation is seen in Figure 7-11. The proportions of carbonation within these formulations is strongly dependent on the clay type and also the water content of the activator. Over all the formulations, the CO_2 content has increased upon irradiation and also water content, compared to that of the heated control. This show that irradiation does make the geopolymers more prone to suffer carbonation, similar to what has been shown by Vodak et al. [272, 273] for conventional Portland cement. Carbonation in conventional Portland cement leads to the formation of $CaCO_3$, which is not present in these formulations, and it is expected that potassium carbonate/bicarbonate salts are likely to form [282], if similar mechanisms as what occur in sodium activated systems are followed [88, 280]. X-ray diffraction (Figure 7-12) has been used to try and decipher the crystal products formed during the carbonation. However, no crystalline products have been observed in the diffractogram. This is likely due to the incredibly low level of carbonation that has been shown in the integration of the dTG-MS data as shown in Figure 7-11.

The FC-MK follows the opposite trend to what would be expected, as the degree of carbonation decreases as water content increases. However, with the results shown in section 7.3.2.1.1 demonstrating the lack of removal of water under irradiation then the pores are likely to still be filled, at least in part, with water. The level of carbonation within these formulations, sits between the H_2O/K_2O = 11 and 13 for the RC MK product. The highest level of CO_2 released by any of the formulations tested is 0.9 wt.%. This can be compared to the study by Pouhet and Cyr on MK-based geopolymers using the same FC-MK used within this study [280], which shows that 97 % of the pore solution within these samples is carbonated within 14 days of exposure to CO_2. These samples have been irradiated for a total of 10 days and have not been exposed to CO_2 at levels equal to or less than 400 ppm (level of CO_2 in air) [283], but the level of carbonation within the bulk has reduced from this value by approx. 100 fold. This shows that the level of carbonation within these samples is very small.

7.3.2.2. X-ray Diffraction
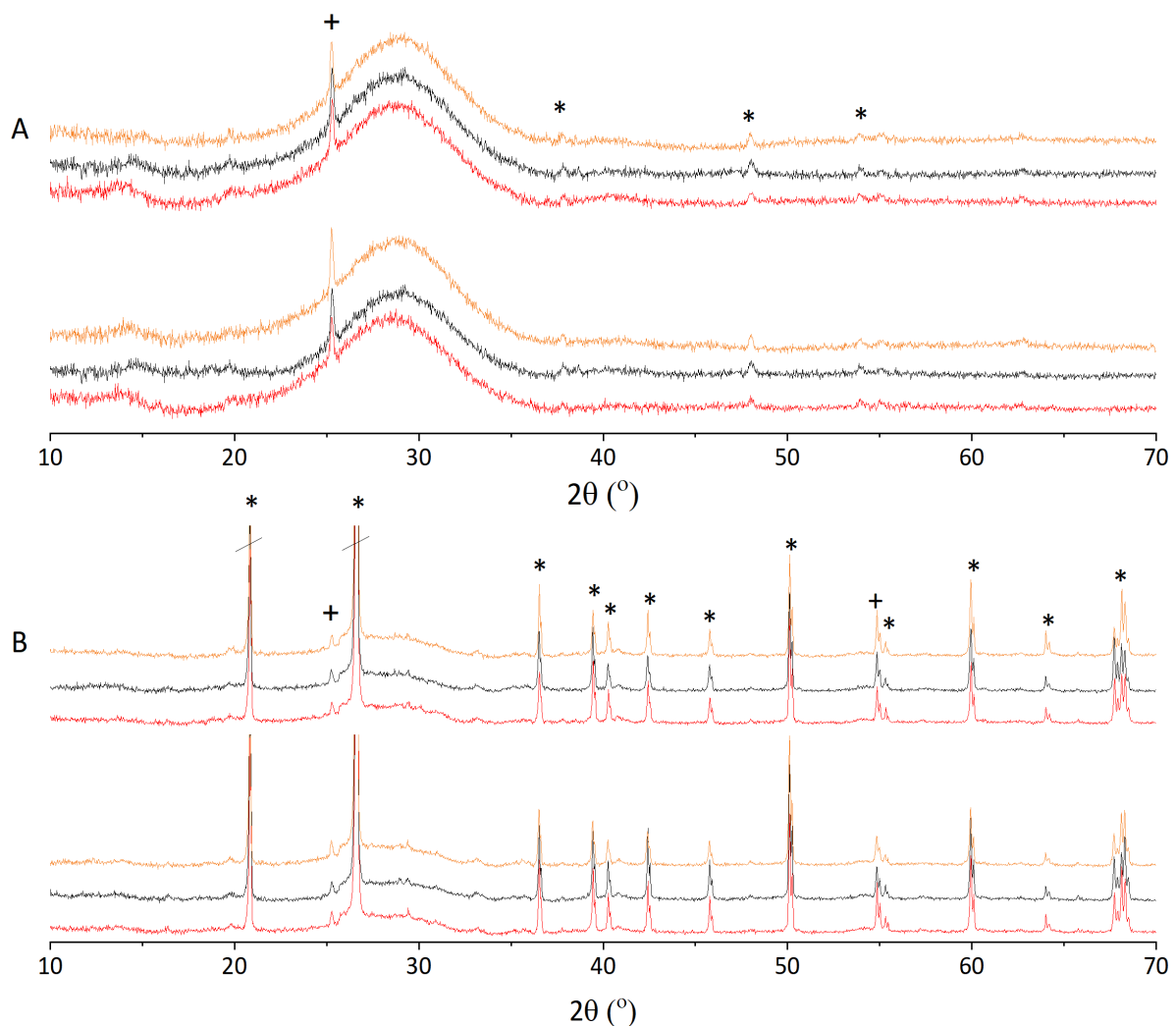
Figure 7-12 – X-ray diffractograms for the irradiated (red), heated control (black) and room temperature control (orange) geopolymers. The top set of diffractograms corresponds to the H_2O/K_2O = 13 and the bottom set to H_2O/K_2O = 11. A represents the RC MK and B represents the FC MK. Peaks due to anatase (TiO_2, powder diffraction file (PDF) # 01-071-1166) are marked +, and those due to quartz (SiO_2, PDF# 01-078-1252) are marked *.

X-ray diffraction data for the irradiated samples are shown in Figure 7-12. X-ray diffraction of geopolymer samples is widely used but cannot always be the most useful technique for demonstrating the stability of these materials due to the X-ray amorphous characteristics of the material. Irradiation has been shown in the literature to not affect or cause a slight increase in the crystallinity of Portland cement blends, with the formation of $Ca(OH)_2$ and $CaCO_3$ [273] which is attributed to the increase in porosity from irradiation. However, when Portland cement with high proportions of slag has been analysed, no changes in crystallinity has been observed [270]. As the samples evaluated here do not

content any calcium, the effect of gamma irradiation will be significantly different. It has been stated that geopolymers probably contain nanocrystalline phases and changing the reaction conditions b by increasing the temperature of curing could lead to the propagation of much larger crystals [117].

The FC MK contains a large proportion (approx. 45 %, batch dependent [154]) of crystalline quartz. This quartz is considered to be unreactive in geopolymerisation, and therefore remains present in the X-ray diffractograms of all samples containing the FC MK. In contrast to this, the RC MK contains a negligible quantity of quartz. A small level of anatase is shown to be present within each MK, and is similarly unreactive. When comparing all the diffractograms and accounting for the changes in MK type, no additional crystalline phases have been detected to form due to irradiation, and no changes can be seen in the intensity or positioning of the signal due to the disordered aluminosilicate geopolymer gel, that is shown by the broad diffuse scattering feature between 20 – 35 ° 2θ.

7.3.2.3. Nuclear Magnetic Resonance

The structure of the geopolymer gel after irradiation has been assessed using [27]Al magic angle spinning nuclear magnetic resonance (MAS-NMR), shown in Figure 7-13. Tetrahedrally coordinated Al(IV) is shown by the resonance peak with a maximum in intensity between 60.1 and 60.4 ppm [198]. The small difference in the chemical shift values for this resonance is due to small differences in the Al chemistry of the two MK precursors, potentially related to some degree of Fe substitution which will distort and broaden [27]Al resonances [284]. However, the ability to systematically detect this small difference between the RC and FC MKs shows that the instrument resolution will allow for the identification of small-scale changes in the gel structure of the geopolymer if any are induced by irradiation.

The spectrum of the geopolymers based on FC MK does contain a secondary small intensity at 4.1 ppm, which is associated with the octahedral Al(IV) coordination, and present in small quantities in this MK. The structure of the gel network appears to remain unchanged before and after irradiation according to this analysis, as any change to the aluminosilicate gel backbone or the charge balancing potassium species would be expected to be visible as a minor difference in the Al spectra. As is expected, changes in the water content have not shown any changes in the coordination of Al within these materials. The ^{27}Al MAS-NMR spectra do not show an effect of irradiation on the carbonation of these materials.
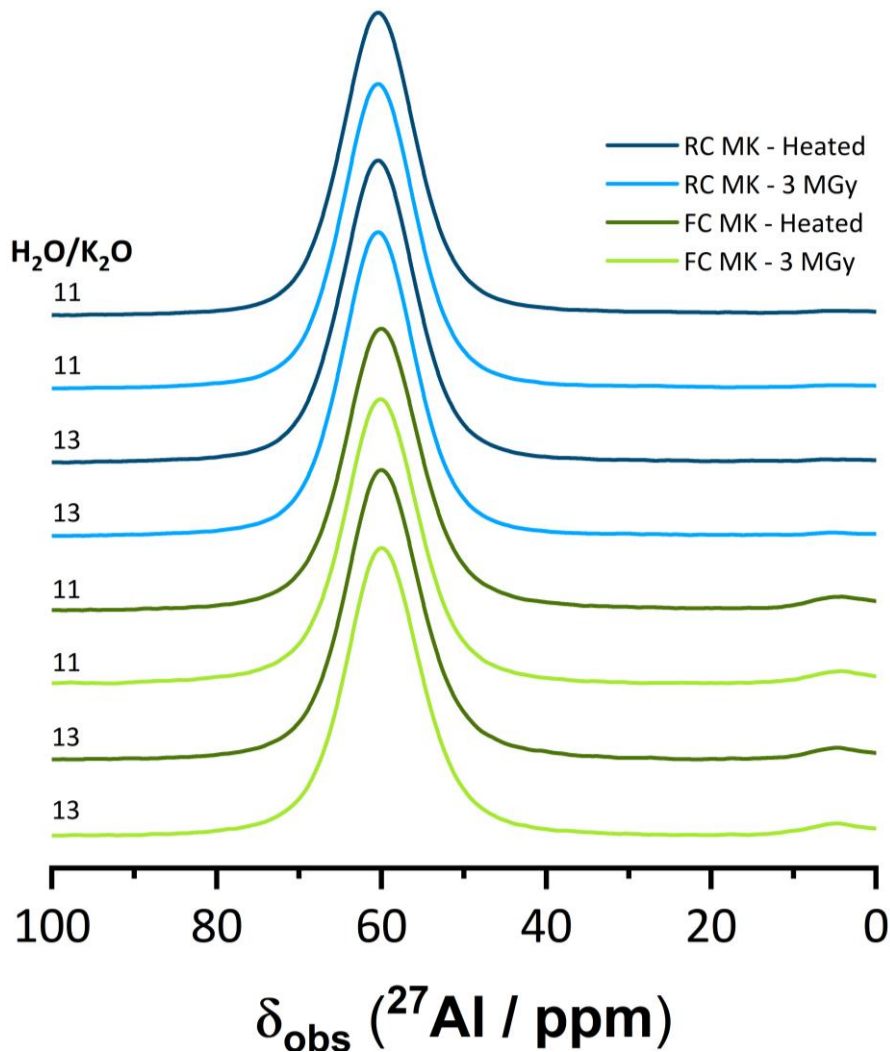
Figure 7-13 – ^{27}Al MAS NMR data for the irradiated and heated geopolymer samples. The blue data corresponds to the RC MK and the green data sets are the FC MK.

7.3.2.4. Imaging of the irradiated samples

Upon visual observation the samples have remained solid and not disintegrated due to the exposure to radiation and/or the heating, and therefore, the drying that has been shown in Figure 7-9 and Figure 7-10 does not appear to have drastically affected the structural stability of these materials. This rapid drying can lead to the formation of drying cracks and therefore, lead to the disintegration of the samples [98]. In order to analyse the cracking of these samples they are analysed by scanning electron microscopy (SEM). However, the conventional process of SEM preparation and image collection involves a range of techniques which can lead to cracking within the samples, including the polishing stages and the use of high vacuum in the SEM imaging chamber.
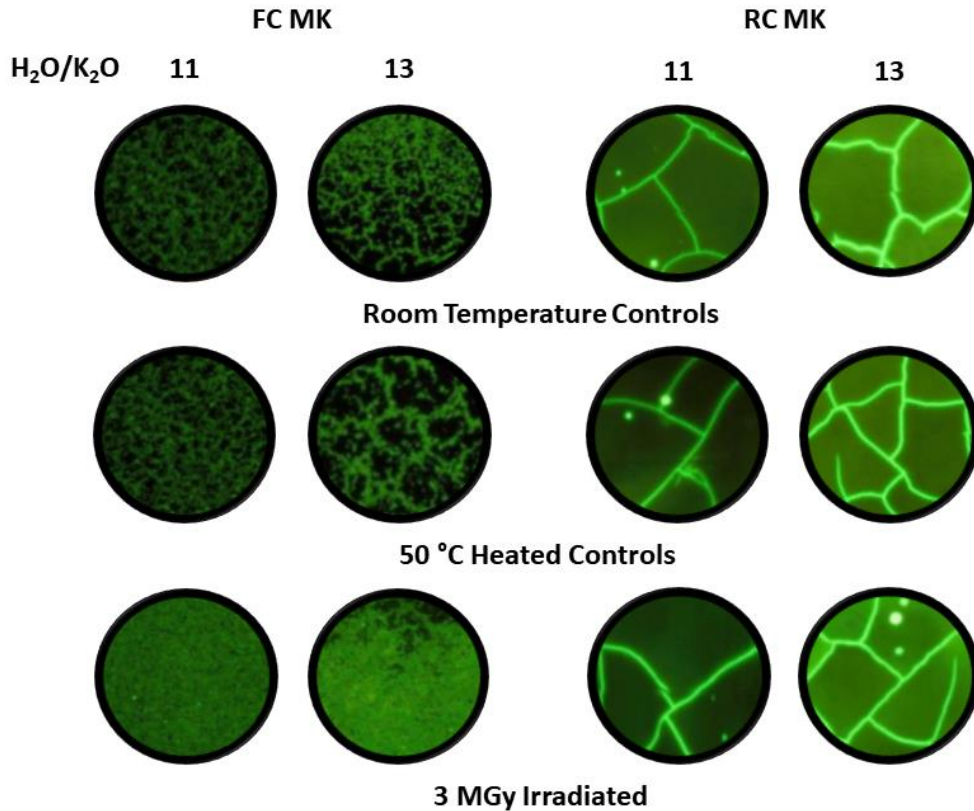
Figure 7-14 - Fluorescent optical microscopy images of the room temperature and heated controls compared to the irradiates formulations. The diameter of the circle framing each image is 6 mm.

Therefore, to distinguish between the cracks that have been created from the irradiation and those that have been created during sample preparation, epoxy resin has been impregnated into the cracks and pores prior to sample sectioning and polishing. The use of UV light for optical imaging of the samples (Figure 7-14) shows that the fluorescent dye has been impregnated into the cracks and pores that have been created from the different curing and irradiation conditions. The conditions of curing have played a significant role in the cracks that have been formed in these materials. The work of Perera et al. [285] has shown that the rapid drying of these materials in low humidity environments can lead to the formation of significant surface cracks. As gamma irradiation leads to the radiolysis of water, and allows for the production of H_2 gas, then the humidity of the irradiator will be much lower than surrounding areas. This was combated in the control samples by sealing within air tight containers during storage. However, the relative humidity of storage for these samples was not identical and therefore this could have lead to some of the extra cracks seen upon irradiation. This cracking is particularly pronounced on the FC MK samples, and therefore these differences are greater than the effects of small differences in relative humidity. Interestingly it has been seen that the

addition of sand to MK geopolymers has increased the structural stability of these materials under changes to humidity and temperature [286]. Therefore, the FC MK material, which includes a significant quartz impurity, is likely to be more stable to changes in curing conditions. This would further the discussion that the obviously increased damage to these materials, which can be seen from more fluorescent dye impregnation, is due to the gamma irradiation process. For the RC MK samples, the cracking appears to be very uniform and not change drastically based around irradiation when compared to the FC MK product.
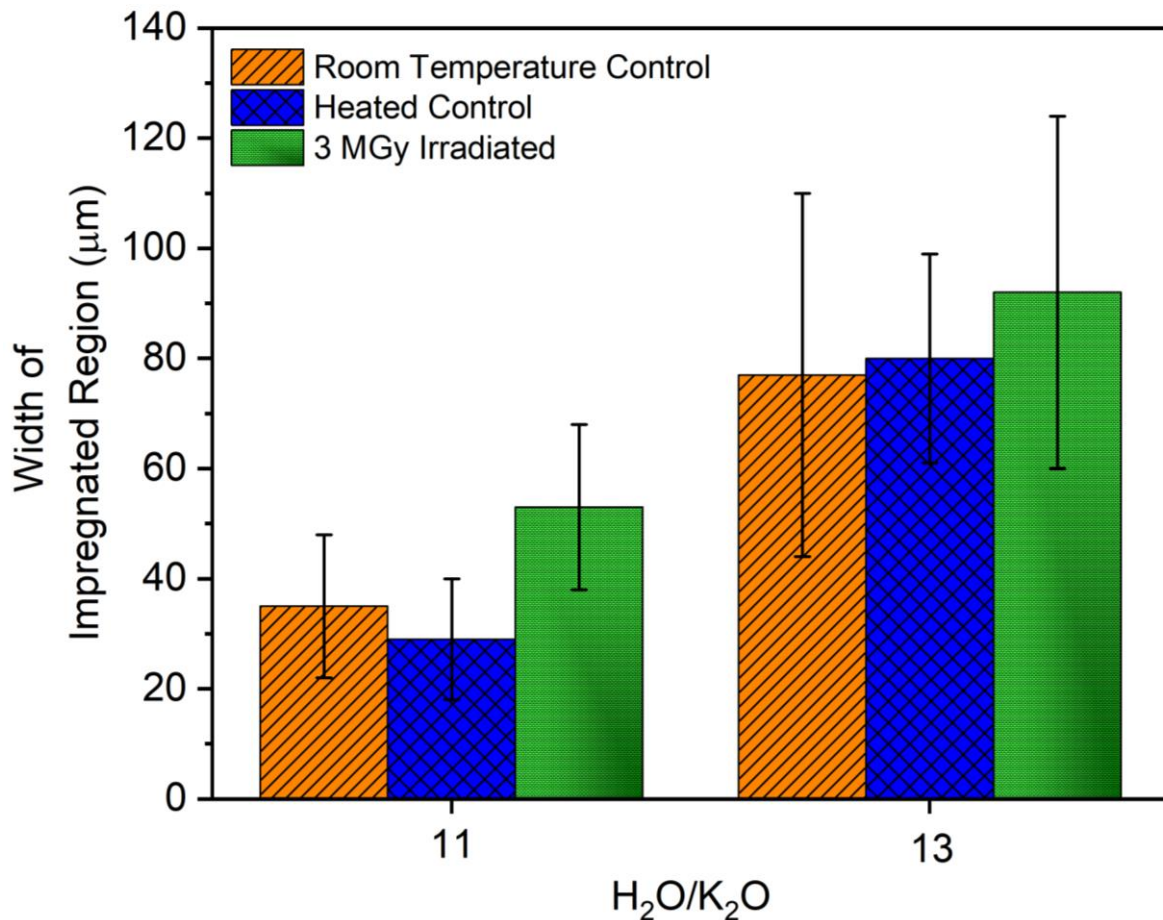
Figure 7-15 – Crack width analysis of the RC MK geopolymers, by analysing the width of the impregnated band. The error bars represent the standard deviation over 50 measurements.

An explanation of the variation in crack widths and therefore the potential cracking of the RC MK formulation is presented in Figure 7-15. The formation of interconnected cracks within the RC MK materials has been of a significant interest, further examination using SEM imaging has been undertaken in Figure 7-16. Irradiation has affected the physical structure of the RC MK and the FC MK formulations differently and the cracking that can be seen within these systems has been shown within literature related to the drying of MK-based geopolymers to be a common occurrence [98].

Kuenzel et al. [98] has shown that the cracking of MK based geopolymers is interconnected and are very similar to those shown in Figure 7-14 for the "dried" samples that have undergone irradiation. This work has however demonstrated that the cracking of K based systems is less than that of Na activated systems.
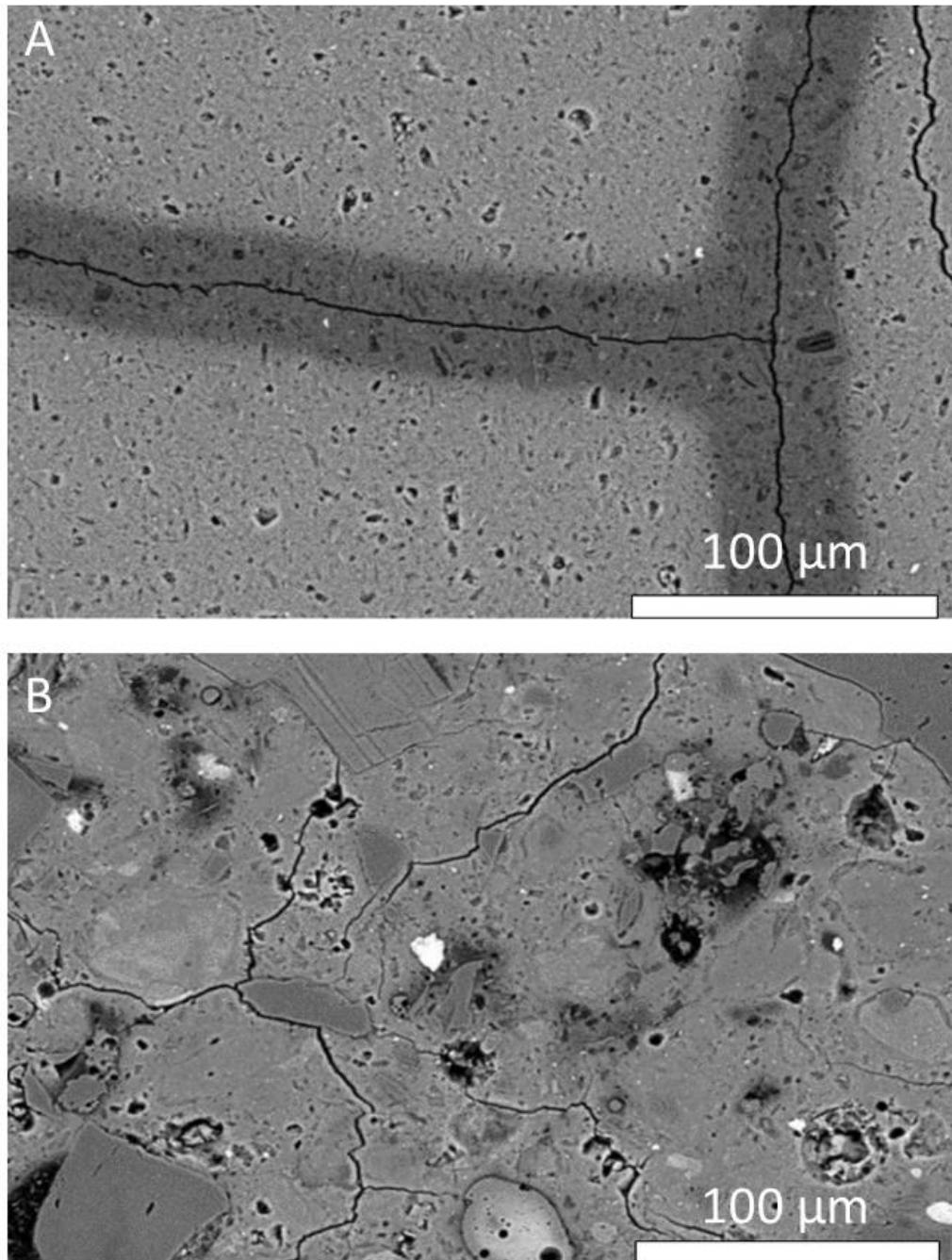
Figure 7-16 – Backscattered scanning electron microscope (SEM) images of the room temperature control formulations, at H_2O/K_2O = 13. A represents the RC MK formulation and B represents the FC MK formulation.

When SEM images of the different MKs are analysed (Figure 7-16), the epoxy impregnation method has worked well on the both formulations. Epoxy resin, when shown under SEM, appears as a dark shaded region, that is darker than other cementitious phases [287]. Cracks that have been formed prior to irradiation and are therefore a result of the storing conditions of these formulations appear as a darker crack with grey shading. This darker shading does not appear in cracks that have been produced from the evaporative drying process within the SEM or during the sample preparation stages. Which for the first time, has led to conclusions being drawn on the effects of irradiation solely on the cracking of these products. This process has been performed on the RC MK products and the results are shown in Figure 7-15. Detailed analysis has been performed on the cracks with the widths of the dark shaded cracks on the epoxy impregnated RC MK samples has been performed on 50 individual measurements per formulation. An example of these images in given in Figure 7-17. The cracking has increased due to both the irradiation and also the heating conditions, but this is a fairly small change by comparison to the observation that the water content being increased from 11 to 13 has caused the crack width to double, in the room temperature control samples. This has shown the applicability of this technique, as the work of Perera et al. [285] has shown that increasing the water content of an MK geopolymer will lead to an increase in the cracking.

The release of free water that has been seen in the TG-MS data shown in Figure 7-9, can be an explanation for the slight difference in the crack width when comparing the heated and irradiated samples [98]. Carbonation products forming within the pore solution of these systems, has the potential to have caused cracking. The work by Zhang et al. [264] shows that the carbonation of fly ash based geopolymers can lead to subflorescence within these materials. It has been shown in Figure 7-11 that the level of carbonation is very small however the carbonation could lead to the small differences between the room temperature samples and the ones that have been heated and irradiated. For the FC MK geopolymers, the presence of the additional quartz phases and the changes to the structure, size and shape/distribution of the pores has meant the effects of irradiation on the cracking of these products have been shielded on the SEM images.
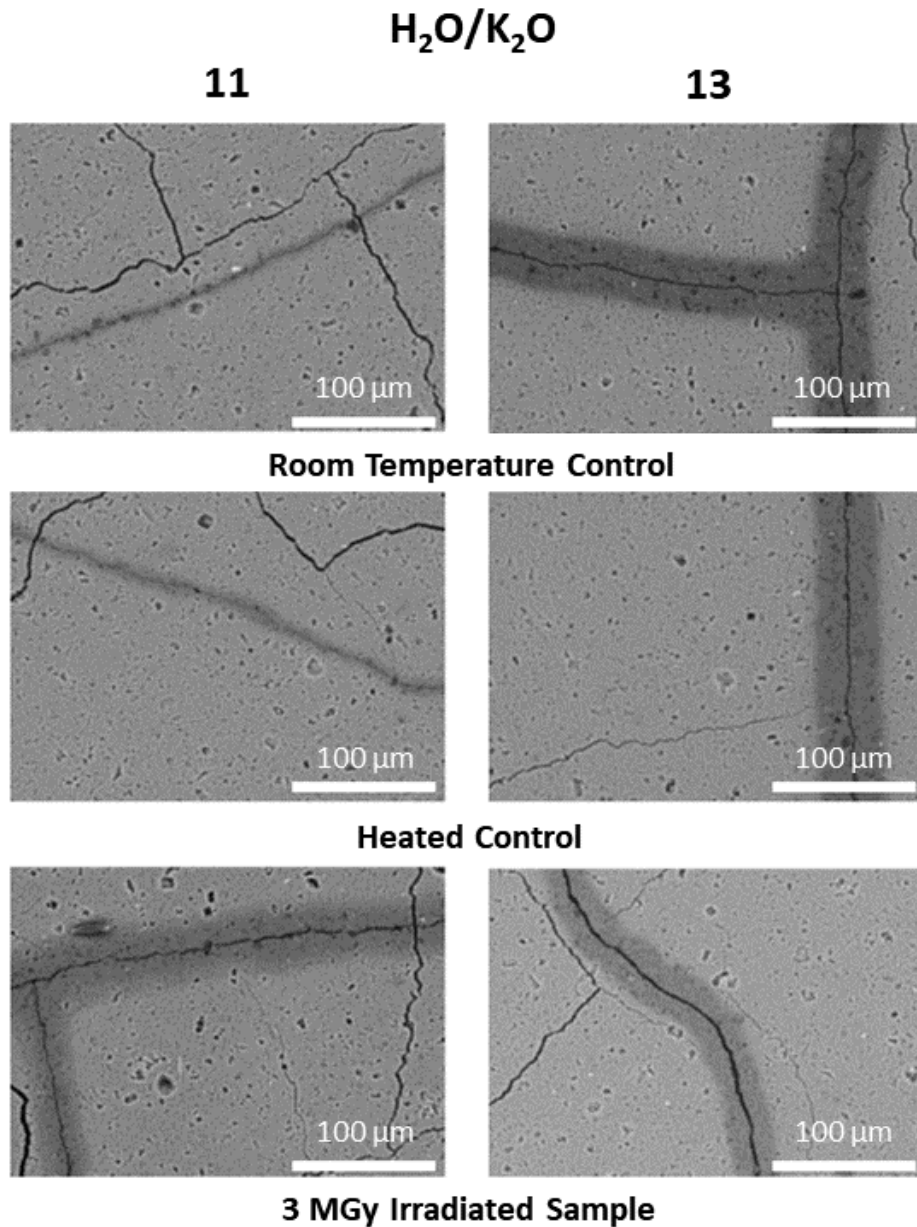
Figure 7-17 – Backscattered SEM images of the room temperature control formulations, at H_2O/K_2O = 11 and 13 for the RC MK precursor.

Further investigation of the porosity of these materials needs to be undertaken and is not presented here. This will allow a full understanding of the effect of irradiation on the porosity of these materials, which will allow for the development of the safety case of these materials. microCT imaging is a potential technique that will allow the development of the understanding of the porosity of these materials. Leay et al. [175] has shown that for fly ash activated systems that the porosity, which will include the pores and also any induced cracks does not change upon irradiation. The work presented

in this chapter has postulated that some changes are occurring and therefore, further analysis into the adaptation of the pore structure is needed.

7.4. Conclusions and Future Work

The irradiation resistance of geopolymer cements is an important characteristic when trying to develop these materials for use within the nuclear industry. The work that has been presented above has taken a step forward in analysing the potential of MK-based geopolymers for this use. Comparisons have been drawn throughout for the FC and RC MK geopolymer formulations with a H_2O/K_2O = 11 and 13. It has been presented in this chapter that the precuring before irradiation is an important factor that should be studied. Analysis has shown that large volumes of free water are removed from formulations that have been precured for 20 hours and samples that have been pre-cured for 168 hours prior to irradiation. Analysis of the degree of carbonation has shown that the 168-hour formulation has carbonated significantly less. Therefore, in order to provide realistic analysis as waste containers that have been used to encapsulate radioactive waste will be dosed from hour one; a pre-curing time of 48 hours has been selected for future study. Analysis of the RC and FC MK formulations has shown that the RC MK system is resistant to irradiation and the free water content of the H_2O/K_2O = 13 system shows very minimal reduction in free and bound water when compared to the heated control. Structural changes can be seen in the FC MK samples that have been impregnated with epoxy resin, further studies of this need to be undertaken. It has been shown throughout this chapter that the micro/nanostructural stability of these MK-based geopolymers remains chemically unchanged when exposed to 3 MGy of gamma irradiation. It has however been shown that carbonation can be induced through the process of irradiation, which has the potential to lead to an increase in cracking. A combination of this carbonation induced cracking and the hydrolysis of free water is hypothesised to be responsible for the changes in crack width and connectivity that are experienced.

Further work can be undertaken within this section to understand the cracking within the FC MK geopolymers and also the adaptation of the porosity within all of the samples tested. Analysis can be performed using microCT imaging. ^{29}Si NMR will also be able to show the potential changes in the chemical structure that may have been missed by [27]Al spectroscopy. This will allow for a detailed understanding of the effects of irradiation on geopolymer cements. Analysis of samples that are dosed at a much slower rate than that of the samples presented here will offer an understanding of the dose rate effects that have been suggested as to be problematic for very high dose rates.

Chapter 8: Understanding the interactions of simulated oil-based waste on the physiochemical properties of MK-geopolymers

The irradiation stability of these geopolymer formulations has been presented at the RILEM Spring Convention, Rovinj, Croatia, 18 – 22 March 2019 in the paper entitled "Irradiation Resistance of MK Geopolymers Encapsulating Oily Wastes", by D. A. Geddes, S. A. Bernal, M. Hayes and J. L. Provis.

8.1. Introduction

The processing of oil and/or organic based nuclear waste can be a real problem when considering the options for the safe radioactive disposal of these materials. When these materials are introduced to cementitious systems, they cause an emulsion layer to form around standard cement particles which prevents hydration [14]. Therefore, waste loadings are incredibly low when trying to immobilise oils within Portland cement systems.

It has been shown that geopolymer cements can offer an alternative encapsulation system for oil based systems with waste loadings in excess of 20 vol. % [15]. The encapsulation of oil within geopolymer systems has been explained in detail in section 2.2.4.4.4 of the literature review. The UK Radioactive Waste Inventory for 2019, has shown that the majority of the oils that are currently held by the nuclear estate are pump oils and greases [1]. These type of oils tend to take the form of silicone oils. The stability of oils within geopolymer systems has been proven to be successful. However, studies regarding the irradiation of oil encapsulated systems have only been presented by the authors [288].

8.2. Results and Discussion

8.2.1. Fresh State Properties

8.2.1.1. Formulation Selection

In order to assess the compatibility of the MK-based geopolymer matrix for the incorporation of different oils, at 20 wt.%, then a complete sample matrix would need to be assessed. The main parameter to be examined upon mixing for acceptance is the ability to set, as this is a good marker of stability and the extent of the reaction. A complete study was conducted, using three different types of oils: 45 V 350 silicone oil, 60000 cSt silicone oil, and petroleum jelly. These oils cover a range of viscosities with the 45 V 350 cSt silicone oil being thin (kinematic viscosity 350 cSt), the 60000 cSt

silicone oil being thick but still remaining liquid and requiring significant energy to cause movement within the paste, and petroleum jelly which is a solid lubricating grease. These have been incorporated into 8 geopolymer formulations that have been studied in detail throughout this thesis. The overall notable properties, including information about the setting time, for each combination is shown in Table 8-1, and conclusions and discussion will be drawn based on the findings presented here.

Table 8-1 – Formulation design table showing the effects of oil on the setting and notable properties of the cementitious matrix.

Oil Type	MK Type	H_2O/K_2O	SiO_2/K_2O	Setting		Remarks
				24 hrs	48 hrs	
Silicone Oil 45 V 350 cSt	Argicem	11	0.5	Y	-	*The sample has set at 24 hours but was visibly weak. It had hardened at 48 hours.*
			1.0	Y	-	*Unremarkable sample that set.*
			1.5	Y	-	*The sample has set at 24 hours but was visibly weak. It had hardened at 48 hours.*
		13	1.0	Y	-	*Unremarkable sample that set.*
	MetaMax	11	0.5	N	Y	*Set with gel on the surface*
			1.0	Y	-	*Unremarkable sample that set with a small oily bleed at 72 hrs.*
			1.5	Y	-	*Set but lacks structural integrity that leads to chipping.*
		13	1.0	Y	-	*Unremarkable sample that set.*
60000 cSt Silicone Oil	Argicem	11	0.5	N	N	*The sample appeared to become more solid with time but did not completely set.*
			1.0	Y	-	*Oily bleed with a small oil layer has appeared on the surface.*
			1.5	Y	-	*The surface of the sample contains a small amount of oily bleed.*
		13	1.0	-	Y	*A small amount of oil is seen on the surface and appears to leach out.*
	MetaMax	11	0.5	Y	-	*This sample was incredibly thick to mix.*

Oil Type	MK Type	H_2O/K_2O	SiO_2/K_2O	Setting		Remarks
				24 hrs	48 hrs	
			1.0	Y	-	*This sample was incredibly thick to mix but set unremarkably.*
			1.5	Y	-	*Very weak sample that cracks and chips*
		13	1.0	Y	-	*Unremarkable sample that set*
Petroleum Jelly	Argicem	11	0.5	N	N	*Separation occurred between the cement and the waste*
			1.0	Y	-	*Unremarkable sample that set*
			1.5	Y	-	*The sample set but bleeding has been seen at 48 hrs plus.*
		13	1.0	Y	-	*Unremarkable sample that set*
	MetaMax	11	0.5	Y	-	*The sample lacks structural integrity and lead to chipping.*
			1.0	N	Y	*The sample lacked structural integrity and leading to large amounts of chipping.*
			1.5	N	N	*Separation occurred between the cement and the waste*
		13	1.0	Y	-	*This sample set at 24 hours, the distribution of the oil within the sample is uneven*

The structural stability of MK based geopolymers with the incorporation of 20 wt.% oil has shown high overall stability, compared to other cementitious systems [14], that has led to many of the formulations tested being postulated for potential use within nuclear waste disposal. Over all the formulations tested, the H_2O/K_2O 11 and 13 geopolymers with SiO_2/K_2O = 1.0 have been shown to be most resilient to the changes in oil type, over both MK types. MK type was expected to cause a significant difference due to the interactions of the oil with the MK particles. Oil has been shown to successfully adhere to kaolinite particles [289], although this was studied at low pH. The contact angle of the oil to the kaolinite particles was found to be 88° at pH 4; this was conducted using organic oils but the coating of the particles is expected to follow a similar mechanism. It has also been shown that for higher ionic strength solutions, such as the pore solution of an MK-based geopolymer [290], then there is a reduction in the coating of the particles. When the MK is mixed with the activating solution and also the oil then an emulsion is created between the oil and the silicate activating solution, this can be visually observed when mixing these solutions together [186, 291]. This emulsion templating

has the potential to be used to produce foam cements, in a non-nuclear application of these materials [292]. Further literature has shown that emulsions formed from sodium silicate and silicone oil can be stable at a pH below 12.5 [293]. Stabilisation of silicone oil and water emulsions using quartz is also a possibility [294]. This stabilisation is in the form of a Pickering emulsion; which is where a colloid, surfactant or particle is used to stabilise and prevent the bursting of the emulsion droplets [295]. Further research is needed to understand the emulsions formed during the initial mixing and to potentially stabilise these emulsions using the cementitious matrix. Stabilisation before encapsulation of this waste will allow for the oils to be successfully incorporated within the cementitious matrix, whilst leading to a potential reduction in leaching due to the stability of the emulsion formed [16]. The work that has been produced by Davy et al. [16, 186], has shown the successful inclusion of oil within geopolymer formulations is possible. This work has predominantly focused on sodium activation and the work here has demonstrated the formation of the same emulsions within potassium activated systems.

When the alkalinity of the activating solution was increased (SiO$_2$/K$_2$O = 0.5) this tended to cause segregation or lack of structural integrity within the final geopolymer. Some of the mixes did appear to be stable, however overall this composition did not allow for the setting of all the formulations trialled. The formulation is not very robust to changes in oil types and is therefore, will probably not offer a viable formulation for the stabilisation of oils. Increasing the silica content of the activating solution (SiO$_2$/K$_2$O = 1.5) also leads to the formation of products that show large amounts of bleed, have large structural instabilities and some simply do not set. This shows that the reaction of oil with the geopolymer matrix is driven by the composition of the activating solution. This is likely due to the different viscosities of the activating solutions, the ionic composition of the activating solution, and also the variation in pH across the solutions.

Interestingly, the formulations that have been used for the encapsulation of petroleum jelly have shown potential to work for some formulations but have generally been unsuccessful in the encapsulation of oil based waste. This is likely due to the highly viscous nature of this oil, which does not combine with the activating solution prior to the addition of MK but sits as a large mass of material that is then directly encapsulated. More work on the dispersion of greases and more near-solid oils like this within the geopolymer matrix needs to be studied in greater detail. Therefore, the remainder of this study will focus on changing water contents (H$_2$O/K$_2$O) between 11 and 13, whilst keeping the SiO$_2$/K$_2$O ratio constant. The petroleum jelly will no longer be tested, and rheology will be investigated for mixes containing the two silicone oils.

8.2.1.2. Rheological Analysis

A detailed understanding of the rheological parameters of these basic geopolymer formulations without added oil was presented in section 4.2.2.1. The addition of oil to these raw geopolymer pastes has, as expected, vastly changed the rheological properties of the pastes. The flow curves, with the mathematically calculated power or linear models given by the orange and black curves, respectively, are shown in Figure 8-1 and Figure 8-2 for the Argicem and MetaMax MK geopolymers respectively. The descriptions of the rheological models are provided in

Table 8-2.

For the geopolymers based on the FC MK (Figure 8-1), the viscosity of the oil has played a large role in causing the changes in the overall shear stress (τ) of these pastes at 100 s^{-1}. The thicker, 60000 cSt oil has caused the pastes to become incredibly viscous and difficult to mix (as has been indicated in Table 8-1). However, the fact that this oil has caused a dramatic increase in the overall viscosity of the paste is not unexpected. A kinematic viscosity of 60000 centistokes (cSt) is an incredibly large kinematic viscosity, that exceeds that of high viscosity asphalt by 20-fold (at 60 °C) [296], and this oil is greater than 1000-fold more viscous than olive oil (at 37.7 °C) [297]. When this is compared to the lower viscosity silicone oil chosen, with a kinematic viscosity of 350 cSt, then it is clear that the overall viscosities of the oils that have been encapsulated have contributed to the increase in viscosity of these cementitious systems.
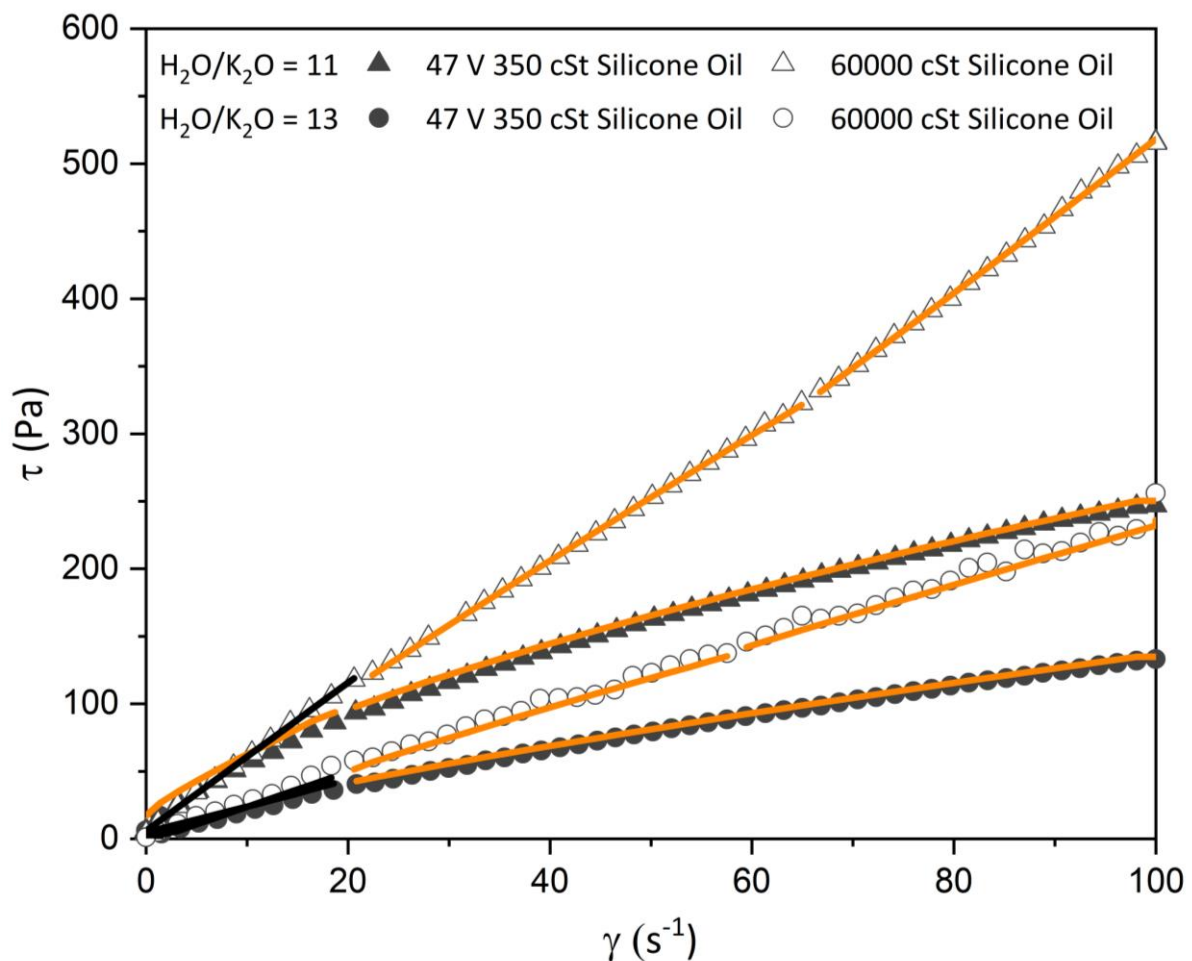
Figure 8-1 - Flow curves of the Argicem MK-geopolymer formulations mixed with thin and thick silicone oils, shown by the filled and hollow symbols, respectively. H$_2$O/K$_2$O values of 11 and 13 are

shown by the triangles and circles, respectively. The orange lines denote a power law fit and the black lines represent a linear fit.

The inclusion of the more viscous oil within the Argicem $H_2O/K_2O = 13$ system has caused small fluctuations in the shear stress points on the curve in Figure 8-1. These fluctuations or steps are caused by the jamming of the vane blade [298], which leads to a gradual increase in the shear stress upon decreasing shear rates of the flow curve, once the energy is significantly low then the jamming is reduced and a larger reduction in apparent viscosity is seen. The rheological model applied to this system is not a very close fit to the data, but the overall rheology appears to change between a Bingham and then two shear thinning regimes with increasing shear stress at a low yield stress. This is different from what has been shown in section 4.2.2.1.1 for this formulation without oil, which shows a low yield stress fluid that is described by a Bingham model followed by a shear thickening model with a reduced yield stress. Reducing the H_2O/K_2O ratio to 11 causes a dramatic increase in the viscosity but the jamming is no longer seen. The paste does, however, now fluctuate between a Bingham, shear thinning and then a final Bingham region. This has significantly altered the behaviour from the previously measured Bingham fluid. The low viscosity silicone oil has increased the viscosity of these pastes, while also producing a paste that is shear thinning in nature. Both of these formulations show low yield stresses, as is expected for these formulations. However, the degree of shear thinning (n = 0.63) is increased for the $H_2O/K_2O = 11$, low viscosity oil curve that is shown in Figure 8-1. This shows a significant degree of shear thinning, which can be helpful when developing a robust processing envelope for these materials.
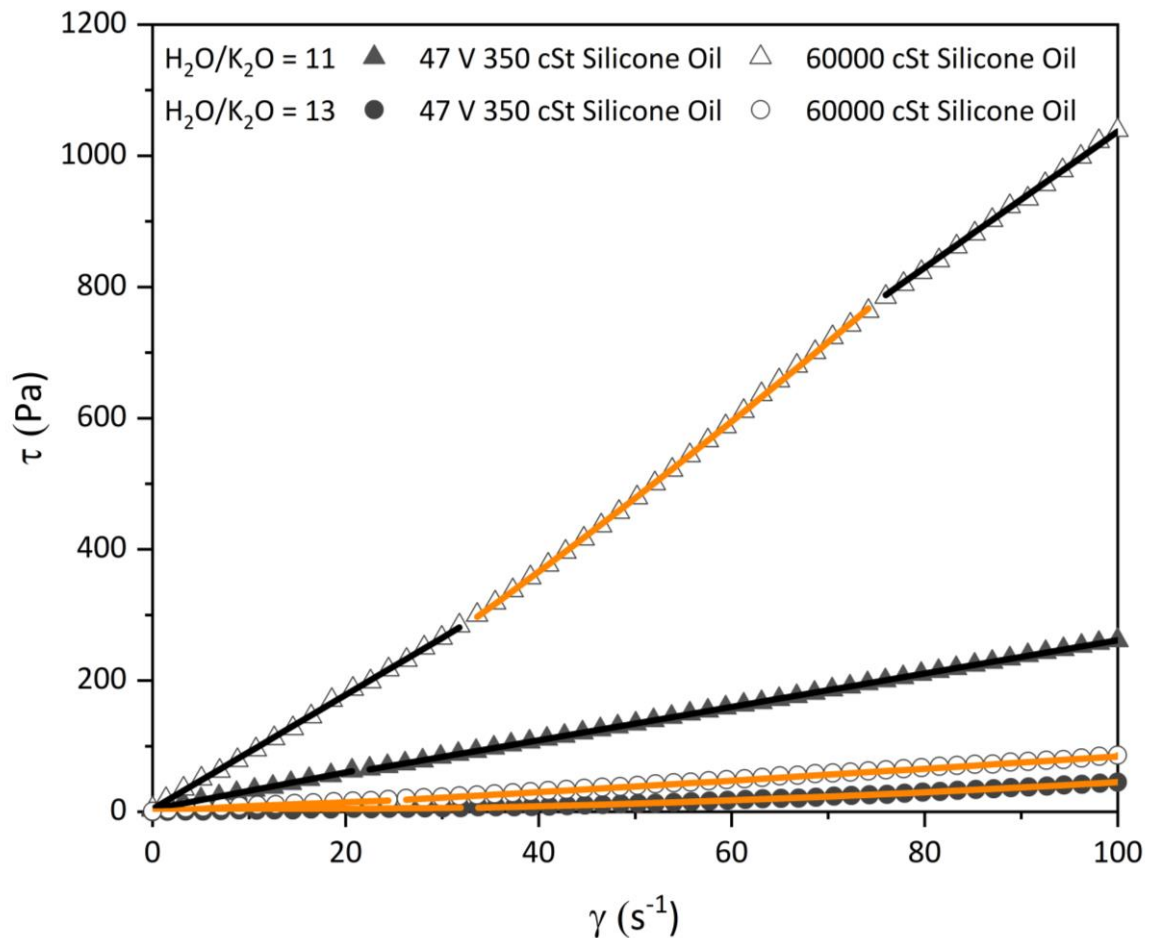
Figure 8-2 - Flow curves of the MetaMax MK-geopolymer formulations mixed with a thin and thick silicone oil, shown by the filled and hollow symbols, respectively. H_2O/K_2O values of 11 and 13 are shown by the triangles and circles, respectively. The orange lines denote a power law fit and the black lines represent a linear fit.

In Figure 8-2, for the MetaMax geopolymers, the interaction with the 60000 cSt silicone oil has produced a highly viscous geopolymer paste, as has also been seen for the Argicem product. However, when comparing the rheological models that have been used for the raw and oil-containing pastes, then similar trends can be seen but overall vastly different rheological properties are present within these pastes. Both the raw pastes that are formulated with a $H_2O/K_2O = 11$ and 13 show Bingham characteristics at low shear, followed by shear thickening at higher shear rate, whilst having a low yield stress. This has slightly changed with the incorporation of both oil types within the matrix but similar trends are shown. For both formulations when $H_2O/K_2O = 11$, then a Bingham law model is applied from 0 to 20 s^{-1}. A yield stress of approx. 4 Pa is found for both formulations, which therefore shows that the oil does not affect the yield stress of the MetaMax based geopolymers.

Increasing the H_2O/K_2O to 13 for the MetaMax based geopolymers and then combining with oil does cause a change in the rheological properties, following a shear thinning model (n < 0.85) followed by a shear thickening model with n > 1.15. This occurs with a near zero yield stress over both rheological models, which has also been shown for the raw pastes in Table 4-1. The change between shear thinning and shear thickening has occurred at $25 - 35$ s^{-1} depending on the formulation. The transition for the higher viscosity oil system happens at a lower shear rate than the lower viscosity system; this shows that the lower viscosity oil has a greater range in which shear stress can be consistent and is therefore safer to control, the pastes do remain shear thickening after 35 s^{-1} but this is only to a small degree.

When comparing the overall rheological parameters of the Argicem and MetaMax geopolymers, the low water content (H_2O/K_2O = 11) and high viscosity oil/MetaMax formulation has a viscosity that is twice that of the corresponding formulation for the Argicem MK. This shows that the MetaMax formulations are not ideal for the disposal of high viscosity oils. However, when comparing the results for low viscosity oils to that of the Argicem product, the viscosities at 100 s^{-1} remain much more consistent with those studied in 4.2.2.1.2. Therefore, the irradiation studies that are performed in section 8.2.2 will use the H_2O/K_2O = 13 formulations for the low viscosity oil that has produced the smallest overall shear stress of any of the formulations analysed.

Table 8-2 – The rheological constants associated with the model fits that are presented in Figure 8-1 and Figure 8-2.

Oil Type	Clay Type	H_2O/K_2O	Rheological Properties											
			Model 1				Model 2				Model 3			
			n	τ_0 (Pa)	K (Pa s^n)	r^2	n	τ_0 (Pa)	K (Pa s^n)	r^2	n	τ_0 (Pa)	K (Pa s^n)	r^2
47 V 350 Silicone Oil	Argicem	11	0.79	6.63	7.92	0.999	0.63	0.00	13.67	0.999	-	-	-	-
		13	1.00	1.39	1.90	0.998	0.77	0.00	3.84	0.999	-	-	-	-
	MetaMax	11	1.00	3.96	2.80	0.998	1.00	7.27	2.54	0.999	-	-	-	-
		13	0.81	0.00	0.37	0.969	1.91	0.64	0.007	1.00	-	-	-	-
60000 cSt Silicone Oil	Argicem	11	1.00	5.98	5.48	0.999	0.90	0.09	6.99	0.997	1.15	13.6	2.56	0.995
		13	1.00	2.64	2.57	0.998	0.87	0.18	4.05	0.997	0.90	0.00	3.41	0.971
	MetaMax	11	1.00	4.20	8.70	0.999	1.20	0.00	4.37	1.00	1.00	0.00	10.4	1.00
		13	0.71	0.49	1.81	0.994	1.10	0.00	0.55	1.00	-	-	-	-

Studies regarding the leaching of these samples were set up to follow the ANSI/ANS 16.1 standard [299] on leaching. Samples were produced for 1 hr, 1 day, 3 days and 7 days but no longer term duration tests were collected due to the COVID-19 pandemic. Analysis of this pre-existing leaching data was halted and therefore only a small amount of pH measurements has been undertaken. These were omitted from this thesis and will be examined at a later date.

8.2.2. Irradiation Stability

The samples that have been analysed within this section have been irradiated to a total dose of 1 MGy; this is less than what has been shown in Chapter 7, but will offer a good understanding of the overall stability of these materials under irradiation. The same conditions that have been explained in sections 3.2.2 and 7.2, with regards to dose rates and sample curing conditions, have been used. Due to limitations in access to the irradiation facility and also in order to develop an in-depth understanding of the effect of oil on the MK-based geopolymers, then this section will focus solely on the RC MK precursor with an activating solution with a $H_2O/K_2O = 13$. This precursor has also shown to be stable under the application of different oils and is relatively stable under irradiation, as shown in Chapter 7. Therefore, introducing the condition of irradiation to one formulation will allow for the understanding of the overall structural stability of these materials.

8.2.2.1. Thermogravimetric Analysis

Comparison of the thermogravimetric results for non-oil-encapsulated geopolymer grouts has been presented in Chapter 7. This has shown that the heating of the samples to 50 °C causes a reduction in the water loss. The data shown in Figure 8-3 for heated and irradiated oil-containing samples show that exposure of this grout to 50 °C for the heated control causes a reduction in the weight loss below 150 °C, which corresponds to free water present in the sample, and also the bound water present within the geopolymeric gel. A higher reduction in the weight loss in this range of temperature is observed in irradiated samples, demonstrating that irradiation is inducing further removal of water from the geopolymer gel. When these oil-containing samples are heated to between 150-225 °C, the control and heated samples show that a distinct and new peak is formed, as this peak does not fall near the original mass loss temperature measured for the silicone oil (400 – 550 °C).

Literature has shown that in basic solutions, silicone based polymers can be hydrolysed to form dimethylsilanediol and its dimer tetramethyl-1,3-disiloxanediol [300]. The TG data presented in Figure 8-3 show two peaks that centre around 100 °C and 170 °C. The boiling points of dimethylsilanediol and tetramethyl-1,3-disiloxanediol are 122 °C and 167.4 °C [301], respectively. Therefore, some of the

oil products may be disguised in the water loss peak that centres around 100 °C but the majority of the hydrolysed oil phases, formed within the 28 days of curing prior to testing, can be seen within the peak that centres around 170 °C. This reaction of the oil with the activating solution is interesting and does show that these materials are not as stable as has been suggested by Cantarel et al. [15] in alkali silicate (waterglass) solutions. Upon exposure to gamma irradiation, this peak due to hydrolysis products has significantly reduced, and has become blended into the water peak. When exposed to irradiation then it is expected that the water attached to the hydrolysed dimers of the silicone oil will undergo radiolysis, form radicals of the hydrogen and oxygen species, and then partly re-undergo a polymerisation mechanism [302]. This mechanism including the generation of an efficient initiating radical species has been described for silane materials that have undergone photolysis [303]. Although the gamma irradiation of silicone polymeric species remains unstudied in the literature, vinyl-substituted silanes have been examined, and consumption of monomers and the driving of a polymerisation reaction (upon initiation) has been proven to be possible [304]. This denotes a mechanism for the potential chemical changes that have been elucidated using the TG data presented in Figure 8-3. A full understanding of the above mechanism would require structural analysis of the silicone oil in simulated pore solution that is exposed to varying doses of gamma irradiation and heat, this would then be examined using FTIR.
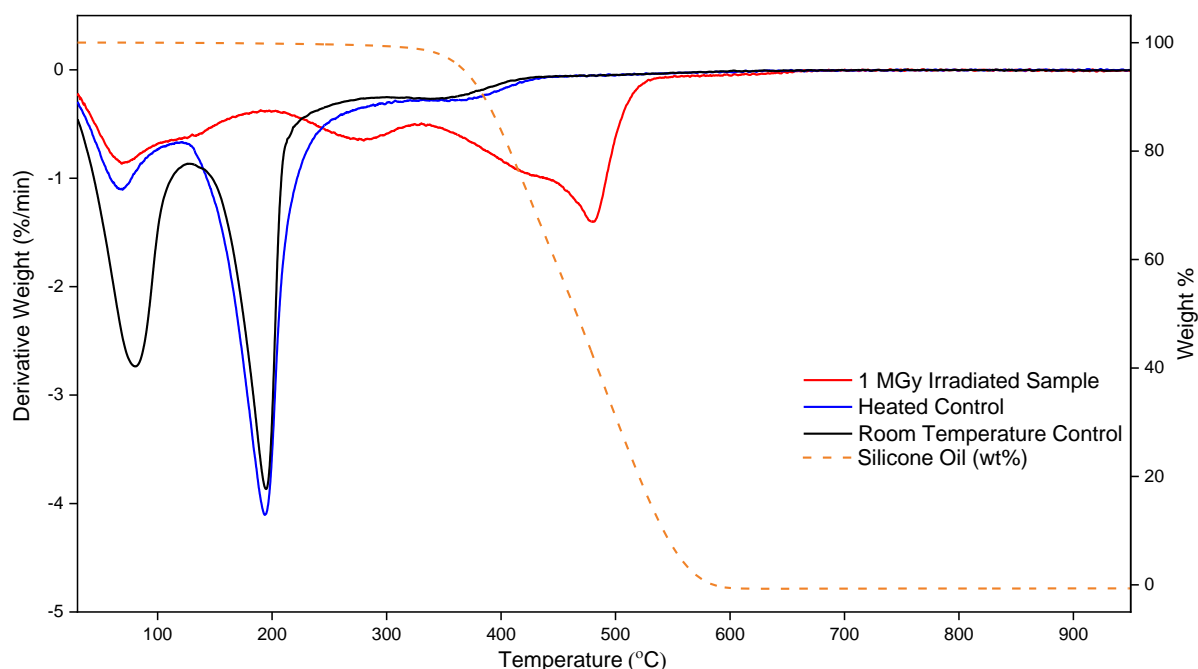
Figure 8-3 - Derivative thermogravimetric analysis of the room temperature control, heated controls, and irradiated samples, that all contain 20 wt.% 47 V 350 silicone oil. This will be produced using the RC MK with a H_2O/K_2O = 13. The thermogravimetric data for the silicone oil is shown with the orange dashed line.

Even though a mechanism of hydrolysis followed by re-polymerisation under irradiation has been proposed, the increase in temperature at which the oil is removed does show that these samples are potentially more stable following irradiation. The study of the mass spectrometry data presented in the comparison of heated and irradiated encapsulated samples, shown in Figure 8-4, does not show much difference to the heated and irradiated formulations that do not contain oil. When this is compared with the mass spectrometry shown in Figure 7-5, no difference can be seen. It is therefore expected that the silicone oil has changed within the geopolymer matrix, and is responsible for the differences between the silicone oil encapsulated and non-encapsulated system. The composition of the silicone oil cannot be examined using the mass spectrometer that has been used here, due to the high molecular weight of the polymeric structure.

Figure 8-4 shows that effectively the mass loss below 200 °C corresponds to release of H_2O from the samples, and is less in the irradiated samples. This is to be expected and has already been discussed in detail in section 7.3.2.1. The MS traces show an increase in the release of CO_2 and N_2/CO between 200 – 700 °C, and show small changes around the points that are associated with the oil release, which could be attributed to the release of small quantity of carbon based species from the silicone oil. However, the carbonation mechanism of these cements has not been fully understood and therefore, these could also be related to in situ carbonation during the irradiation experiments (as shown in section 7.3.1.2.2). The resolution of the instrument used does not allow for discrimination between nitrogen and carbon monoxide gases, which both have a molecular weight of 28 g mol^{-1}. However, the N_2 is flowing at a constant flow rate from the gas supply, therefore any variations from a horizontal line can be associated with the release of CO or release of N_2 from within the pore structure of the powder as it begins to sinter.
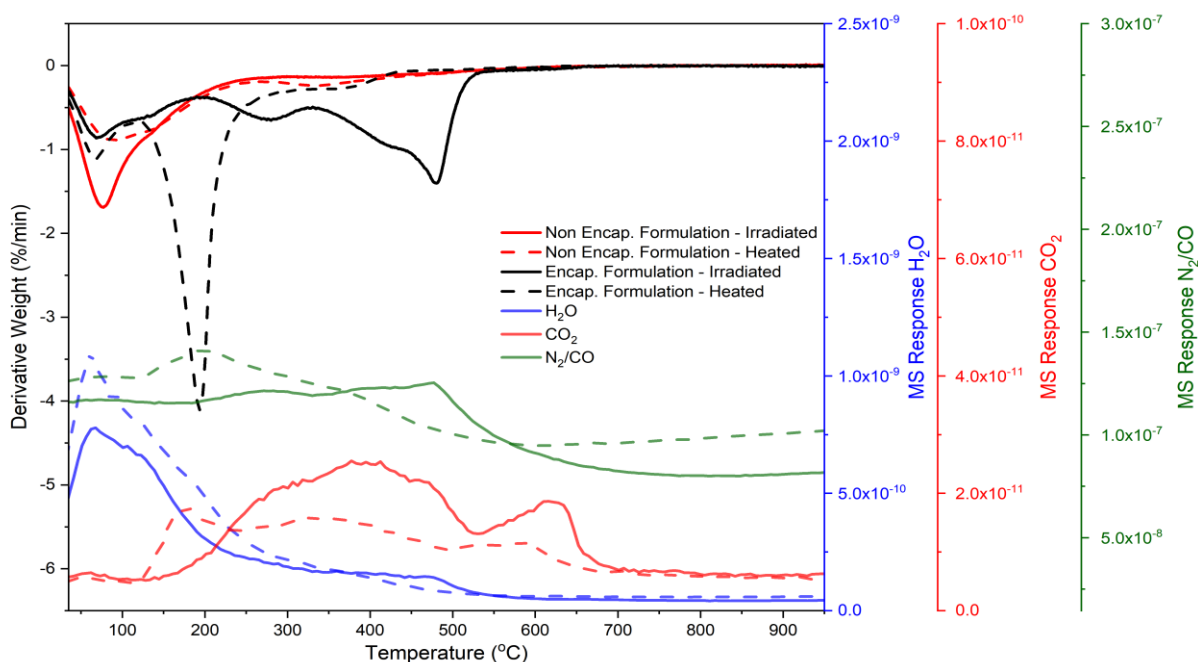
Figure 8-4 - dTG-MS data comparing oil encapsulated (black) and non-oil encapsulated (red) formulations. The solid lines represent the irradiated samples and the dashed lines represent heated controls. The mass spectrometry traces are given for the oil encapsulated formulations, and relate to the right-hand vertical axes.

8.2.2.2. X-ray diffraction

In order to determine any differences in the mineralogy and phase assemblage of the irradiated sample, XRD (shown in Figure 8-5) was used. Irradiation to 1 MGy induced minimal changes in the diffractograms compared with the room temperature control, both with and without oil, and also the heated samples. There is a slight increase in intensity of a broad reflection between 10-15° 2θ (noted as A_{m1} in the diffractogram), that could potentially be related to additional short range order that has been generated within the hydrolysed and then re-polymerised oils. The standard amorphous hump between 23 – 35° 2θ is denoted by A_{m2}, and is the trademark characteristic of the short range order of a geopolymer matrix (shown in detail in 6.2.1). Anatase is the only crystalline phase identified in these samples, and is an impurity present in the MK used to produce the geopolymer grouts, as shown in Figure 3-1. Overall the XRD data for these systems is unremarkable and shows that these systems, even when they have incorporated 20 wt.% silicone oil, still undergo a reaction, form a geopolymer gel network and allow for the successful incorporation of the waste oil.
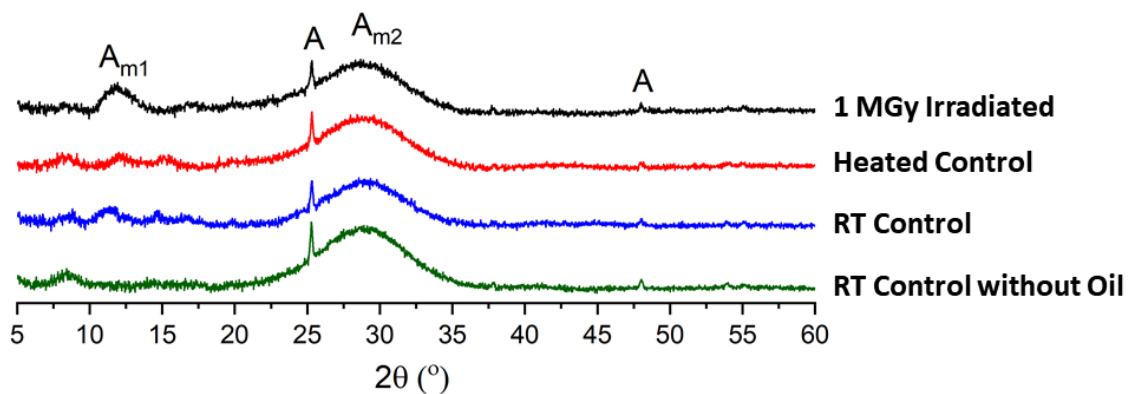
Figure 8-5 - XRD patterns of the oil-encapsulating and oil-free AAM formulations. $A_{m1/2}$ represent different amorphous phases and A represents anatase (PDF - 01-071-1166).

8.3. Conclusions and Future Work

The encapsulation of oil based wastes within a Portland cement system is problematic and significant waste loadings are unable to be achieved. Geopolymer cements based around silicate activated MK have previously shown promise in the encapsulation of lubricating oils, such as engine oil. However, as most pump oils tend to be based around silicone oil, this needed to also be tested. This study presents the stability of geopolymer systems that have been used to encapsulate silicone oil of 2 viscosities and also a petroleum jelly type oil. The encapsulation of petroleum jelly was problematic however a more focused methodology may find an alternative encapsulation matrix based around MK-based geopolymers. The incorporation of silicone oil was successful at both a high and low viscosity oil. Analysis of the rheological properties has shown that the oil alters the rheological properties of the paste compared to those demonstrated in section 4.2.2.1. The incorporation of a highly viscous oil at 20 wt.% loading has caused a significant increase in the viscosity of the paste. Irradiation stability of the RC MK based geopolymer that contains the low viscosity silicone oil has been studied and it has been shown that hydrolysis of the oil occurs upon mixing with the activating solution, which is then reversed using radiolysis. This will cause a breakdown in the oil and lead to chemical changes that need to be studied in greater detail. However, the radiation does appear to increase the stability of these materials. Further work will be undertaken in order to analyse the effect of gamma irradiation on the porosity of these materials which are already macroporous (visually noticeable). A chemical analysis of the oil components that remain in these cements will allow for a thorough understanding of the effect of irradiation on the oil within these materials. Oil stability within these materials will be an important parameter when looking at the potential long term stability of these materials for the UK nuclear industry. In-depth leach testing will also help with the development of this long term stability.

Chapter 9: Conclusions and Future Work

9.1. Conclusions

The work that is presented in this thesis has shown a comprehensive analysis of the physiochemical properties of metakaolin based geopolymers, that have been activated using potassium silicate solutions. This is not the common method of activation, due to the expense of potassium silicate not being viable for construction applications. Therefore, a thorough and comprehensive study of the baseline parameters of this system was needed.

In-depth analysis of the fresh state properties has been analysed within Chapter 4 for metakaolin based geopolymers produced from both rotary and flash calcined metakaolin. When flash calcined metakaolin is included with secondary mineral phases, such as quartz, this reduces the reactivity of the activated metakaolin solution and by this method, it lowers the apparent viscosity. Comparisons of the rotary and flash calcined metakaolin (with secondary mineral phases), show that the rotary calcined metakaolin has a lower apparent viscosity than that of the flash calcined metakaolin. However, the inclusion of the secondary mineral phases within the flash calcined metakaolin has allowed for a much more controlled and more linear rheological properties. It undergoes much less shear thickening than the rotary calcined formulations. For the first time within cementitious systems, changes in rheological properties occur along a flow curve between 0 and 100 s^{-1}. These changes manifest as steps within the curves, and it has been shown along all curves that changes between the degree of a specific non-Newtonian rheological property or alterations of the rheological property are dependent on the shear imparted. These steps appear to be finite and dependent on the metakaolin used, however further study is needed in order to prove this explicitly. It is common amongst these pastes to see a change in properties that represents shear thinning-Bingham-shear thickening, or similar, over the shear range above. The rotary calcined metakaolin has been shown to be much more reactive than the conventional flash calcined metakaolin, which is the reason for the slower setting times of the flash calcined metakaolin, which also includes secondary mineral phases. The alternative, highly reactive flash calcined metakaolin has not been selected as appropriate for nuclear applications and is therefore not used throughout the rest of this study.

Studies have been produced to show the effects of shear on the overall viscosity of the geopolymers produced from rotary and flash calcined metakaolins, where careful analysis of the data sets shows that steps appear. Therefore, in order to understand these steps and to also provide a detailed explanation as to the shear dependency of these pastes, shear rates of 650, 1300 and 2000 RPM were examined at mixing times of 10 and 20 mins. This has been performed for the high water content

activating solutions, and showed that the flash calcined MK geopolymer is strongly shear dependent. When the shear rate is increased at 10 mins of shear, then the apparent viscosity decreases as shear is applied. It is also shown that the rheological model changes, as is shown in Chapter 4. This however is dependent on the shear speed that is applied to the paste. Therefore, when the shear rate goes past the step at 16 s^{-1} (which correlates as closely as possible to 1300 RPM) then the model changes at this point from a Bingham model to a shear thinning-Bingham-shear thickening model. This then moves back to a Bingham model at 2000 RPM. It has been shown that the mixing can affect the cumulative heat output of geopolymers. However, the effects of shear-induced heating, and also variations in the room temperature adaptations need to be considered.

With a thorough understanding of the fresh state properties being shown in Chapter 4 and Chapter 5, then it is fitting to follow this with a study of the hardened state properties, up to 1 year of curing. This was presented in Chapter 6. It has been shown that overall the chemical analysis of these materials does not change for either formulation. There is a small deviation in the amount of bound water when comparing 7 and 360 day cured samples, with more bound water being present at longer ages. This is to be expected. Interesting studies have shown that the strength of these formulations tends to decrease at curing times of 360 days, this has been shown previously in the literature [260]. Studies at later ages will allow for an understanding as to the reasons behind this strength decrease. The porosity is found to be dependent on the water content, which again is to be expected but is useful for the explanations presented in Chapter 7 with regards to the irradiation resistance of these materials. Due to the production of salt crystals, it has been shown that using environmental SEM has some disadvantages for the analysis of potassium based geopolymers.

As mentioned above, Chapter 7 has discussed the irradiation stability of these materials. These materials can be generally classified as being stable under gamma irradiation. This has been shown by a lack of reduction in the bound water and a minimal reduction in the free water when compared to samples that have been heated to 50 °C, the same internal temperature as the irradiator. This has shown the need to develop effective controls when performing irradiation studies on cementitious systems. While discussing the experimental parameters of these tests, it was clear that pre-curing regimes are dependent on the institution running the tests. Therefore, a study has been presented on this precuring time, and through analysis of the water content and the degree of carbonation, it was found that a precuring time of 48 hours was appropriate for these materials. It has been shown for the first time, that gamma irradiation of geopolymer cements can lead to the production of carbonate phases within the cementitious system. It is believed that this is due to the release of water via radiolysis, which can lead to an increase in cracking, which has been demonstrated, and therefore increases the size of the pore/crack network which will allow for the ingress of atmospheric CO_2. This

has led to the small degree of carbonation seen within these samples. Irradiation has been shown to increase the cracks within these samples, however they still remain structurally integral following these tests. This is a good demonstration of the overall stability of these materials when exposed to high doses (at high dose rates) of gamma radiation.

The incorporation of oil within geopolymer systems has been proposed in the literature [12, 15, 186], and this has been successful for systems that have a $SiO_2/K_2O = 1.0$. Silicone oils at 2 different viscosities (350 and 60000 cSt) have been tested, compared and total waste loadings of 20 wt.% have been achieved. It has been shown that the increasing viscosity of the oil does increase the apparent viscosity of all formulations. However, when the high viscosity oil is incorporated into a system with a high water content ($H_2O/K_2O = 13$) then the overall viscosity is already below the criterion of a shear stress of 400 Pa at $100s^{-1}$ shear rate; this is still met for the rotary and flash calcined metakaolins. Studies of the irradiation stability of these materials shows that when the 350 cSt, low viscosity, silicone oil is incorporated within the metakaolin based geopolymer then hydrolysis of the oil occurs initially. This is then reversed via radiolysis and it is hypothesised that a more stable product is formed. It has been shown that the irradiated samples have remained chemically stable and upon visual inspection, all samples remained physically stable.

It has been shown throughout this thesis that metakaolin based geopolymers, activated with potassium silicate, offer a viable alternative for the encapsulation of problematic nuclear wastes. Further studies need to be performed and will be explained in the following section.

9.2. Future Work

The study presented here has shown a comprehensive analysis of the fresh and solid state properties of geopolymer cements for nuclear applications, including the stability to gamma irradiation and the incorporation of wastes. However, there are a number of experiments that could be run to enhance the understanding of these materials for their potential use within the nuclear industry and beyond:

- Develop and understand the incorporation of oil within the geopolymer matrix. This will include the development of a leaching test, based around the ANSI 16.1 [299] test procedure. If samples that have been irradiated are leach tested, a measure of how the chemical changes induced by radiation can be understood and changes can be made to the formulation to influence the overall stability of these materials.

- Irradiation has been performed using gamma radiation. However, ILW is likely to include also emitters of alpha or beta radiation. Therefore, a study of the alpha radiation stability of metakaolin based geopolymers will be an important further study.

- The work of Davy et al. [186] has shown that microCT imaging can be an effective technique for examination of oil encapsulated geopolymers. It should be possible to analyse the porosity of these geopolymers. This will allow for an understanding of the irradiation stability and also the effect of activating solution on the porosity of these materials. Comparing the use of mercury intrusion porosimetry to microCT will also show the benefits of this technique.

- Implementation of solid state nuclear magnetic resonance, probing the ^{29}Si nuclei, will allow for an understanding of the overall gel structure of the irradiated and unirradiated samples. This will show if the irradiation has caused any of the silicon nuclei to become dislocated.

- Further studies of the rheological properties, including thixotropy measurements, will allow for a detailed understanding of the overall rheological properties of these materials. The use of alternative rheological measurements can conclusively prove the steps in the flow curves that have been demonstrated here.

- Analysis of the hardened state properties at longer curing times will allow for an understanding of the long term stability of these materials.

Chapter 10: References

[1]   N. D. Authority, "2019 UK Radioactive Waste Inventory," Department for Business, Energy & Industrial Strategy, December 2019 2019. [Online]. Available: https://ukinventory.nda.gov.uk/wp-content/uploads/2020/01/2019-Waste-Report-Final.pdf

[2]   J. L. Provis and J. S. J. van Deventer, *Alkali Activated Materials - State of the Art Report, RILEM TC 224-AAM*. Dordrecht: Springer/RILEM, 2014, p. 388.

[3]   J. L. Provis, "Geopolymers and other alkali activated materials: why, how, and what?," *Materials and Structures,* journal article vol. 47, no. 1, pp. 11-25, 2014, doi: 10.1617/s11527-013-0211-5.

[4]   C. Reeb, C. Pierlot, C. Davy, and D. Lambertin, "Incorporation of organic liquids into geopolymer materials - A review of processing, properties and applications," *Ceramics International,* vol. 47, no. 6, pp. 7369-7385, 2021/03/15/ 2021, doi: https://doi.org/10.1016/j.ceramint.2020.11.239.

[5]   E. R. Vance, D. S. Perera, and Z. Aly, "Feasibility of Immobilizing Tank Wastes in Geopolymers," in *Environmental Issues and Waste Management Technologies in the Ceramic and Nuclear Industries XI*, 2006, pp. 75-80.

[6]   M. I. Ojovan and W. E. Lee, *An introduction to nuclear waste immobilisation*. Oxford: Newnes, 2013.

[7]   "Radioactive Waste Detailed Data," Department for Business, Energy & Industrial Strategy, 2019.

[8]   "UK Strategy for the Management of Solid Low Level Waste from the Nuclear Industry," Department of Energy and Climate Change, February 2016 2016. [Online]. Available: https://assets.publishing.service.gov.uk/government/uploads/system/uploads/attachment_data/file/497114/NI_LLW_Strategy_Final.pdf

[9]   (2015). *Basic principles of radioactive waste management: An introduction to the management of higher activity radioactive waste on nuclear licensed sites*. [Online] Available: http://www.onr.org.uk/wastemanage/basic-principles.pdf

[10]   "Geological Disposal RWM HAW Innovation and Delivery: A Review of Cement Powders Securityof Supply, Specifications and Disposability Issues," Radioactive Waste Management, NDA/RWM/144, May 2016 2016.

[11]   H. C. Mark Cowper, Holly Cresswell, "Problematic Waste IPT - 2017 Problematic Waste Inventory Summary," Radioactive Waste Management, NWP/REP/196, May 2018 2018. [Online]. Available: https://assets.publishing.service.gov.uk/government/uploads/system/uploads/attachment_data/file/733944/Problematic_Waste_Inventory_Summary_-_May_2018.pdf

[12]   M. French and I. Tanase, "Management of Contaminated Oils - Feasibility Study," LLW Respository Ltd, March 2015 2015.

[13]   S. K. Chopra *et al.*, "Predisposal Management of Organic Radioactive Waste," IAEA, 2004. [Online]. Available: https://www-pub.iaea.org/MTCD/publications/PDF/TRS427_web.pdf

[14]   S. Trussell and R. D. Spence, "A review of solidification/stabilization interferences," *Waste Management,* vol. 14, no. 6, pp. 507-519, 1994/01/01/ 1994, doi: https://doi.org/10.1016/0956-053X(94)90134-1.

[15]   V. Cantarel, F. Nouaille, A. Rooses, D. Lambertin, A. Poulesquen, and F. Frizon, "Solidification/stabilisation of liquid oil waste in metakaolin-based geopolymer," *Journal of Nuclear Materials,* vol. 464, pp. 16-19, 2015, doi: 10.1016/j.jnucmat.2015.04.036.

[16]   B. Planel *et al.*, "Water permeability of geopolymers emulsified with oil," *Cement and Concrete Research,* vol. 135, pp. 106-108, 2020/09/01/ 2020, doi: https://doi.org/10.1016/j.cemconres.2020.106108.

[17]   J. Zhang and G. W. Scherer, "Comparison of methods for arresting hydration of cement," *Cement and Concrete Research,* vol. 41, no. 10, pp. 1024-1036, 2011/10/01/ 2011, doi: https://doi.org/10.1016/j.cemconres.2011.06.003.

[18]   R. Snellings *et al.*, "RILEM TC-238 SCM recommendation on hydration stoppage by solvent exchange for the study of hydrate assemblages," *Materials and Structures,* vol. 51, no. 6, p. 172, 2018/12/13 2018, doi: 10.1617/s11527-018-1298-5.

[19]   "Solvent Wastes in the Laboratory – Disposal and/or Recycling." [Online]. Available: https://www.oc-praktikum.de/nop/en/articles/pdf/SolventRecyclingDisposal_en.pdf

[20]   G. A. Fairhall and J. D. Palmer, "The encapsulation of Magnox Swarf in cement in the United Kingdom," *Cement and Concrete Research,* vol. 22, no. 2, pp. 293-298, 1992/03/01/ 1992, doi: http://dx.doi.org/10.1016/0008-8846(92)90068-7.

[21]   F. P. Glasser, "Progress in the immobilization of radioactive wastes in cement," *Cement and Concrete Research,* vol. 22, no. 2, pp. 201-216, 1992/03/01/ 1992, doi: https://doi.org/10.1016/0008-8846(92)90058-4.

[22]   E. Bernard, B. Lothenbach, C. Cau-Dit-Coumes, C. Chlique, A. Dauzères, and I. Pochard, "Magnesium and calcium silicate hydrates, Part I: Investigation of the possible magnesium incorporation in calcium silicate hydrate (C-S-H) and of the calcium in magnesium silicate hydrate (M-S-H)," *Applied Geochemistry,* vol. 89, pp. 229-242, 2018/02/01/ 2018, doi: https://doi.org/10.1016/j.apgeochem.2017.12.005.

[23]   N. C. Collier and N. B. Milestone, "The encapsulation of Mg(OH)2 sludge in composite cement," *Cement and Concrete Research,* vol. 40, no. 3, pp. 452-459, 2010/03/01/ 2010, doi: https://doi.org/10.1016/j.cemconres.2009.10.007.

[24]   "Sellafield Plan," Nuclear Decomissioning Authority, August 2011 2011, issue 1.

[25]   "The 2017/18 Technology Development and Delivery Summary," Sellafield Ltd, 2018. [Online]. Available: https://assets.publishing.service.gov.uk/government/uploads/system/uploads/attachment_data/file/792030/Technology_Development_and_Delivery_Report18_FINAL_LoRes.pdf

[26]   N. B. Milestone, "Reactions in cement encapsulated nuclear wastes: need for toolbox of different cement types," *Advances in Applied Ceramics,* vol. 105, no. 1, pp. 13-20, 2006/02/01 2006, doi: 10.1179/174367606X81678.

[27]   D. Chartier, J. Sanchez-Canet, L. Bessette, S. Esnouf, and J. P. Renault, "Influence of formulation parameters of cement based materials towards gas production under gamma irradiation," *Journal of Nuclear Materials,* vol. 511, pp. 183-190, 2018/12/01/ 2018, doi: https://doi.org/10.1016/j.jnucmat.2018.09.024.

[28]   A. Rooses, P. Steins, A. Dannoux-Papin, D. Lambertin, A. Poulesquen, and F. Frizon, "Encapsulation of Mg–Zr alloy in metakaolin-based geopolymer," *Applied Clay Science,* vol. 73, pp. 86-92, 2013, doi: Encapsulation of Mg–Zr alloy in metakaolin-based geopolymer.

[29]   D. P. Prentice, B. Walkley, S. A. Bernal, M. Bankhead, M. Hayes, and J. L. Provis, "Thermodynamic modelling of BFS-PC cements under temperature conditions relevant to the geological disposal of nuclear wastes," *Cement and Concrete Research,* vol. 119, pp. 21-35, 2019/05/01/ 2019, doi: https://doi.org/10.1016/j.cemconres.2019.02.005.

[30]   F. P. Glasser, "Mineralogical aspects of cement in radioactive waste disposal," *Mineralogical Magazine,* vol. 65, no. 5, pp. 621-633, 2001, doi: 10.1180/002646101317018442.

[31]   M. Angus, J. Borwick, G. Cann, M. Hayes, B. McLuckie, and J. Jowsey, "The Specification of Cement Powders for Waste Encapsulation Processes at Sellafield site," *Proceedings of Nuwcem 2011, Avignon, France,* pp. 48-58, 2011.

[32]   B.S.I., "Cement: Composition, specifications and conformity criteria for common cements," ed: B.S.I, 2011, p. 50.

[33]   R. A. Sanderson, "Optimising Blends of Blast Furnace Slag for the Immobilisation of Nuclear Waste," Engineering Doctorate, Department of Materials Science and Engineering, University of Sheffield, White Rose Libraries, 2019.

[34]   "Integrated Waste Management Radioactive Waste Stratergy," NDA, July 2018 2018. [Online]. Available: https://assets.publishing.service.gov.uk/government/uploads/system/uploads/attachment_data/file/729845/Radioactive_Waste_Strategy_July_2018.pdf

[35]   F. Winnefeld and B. Lothenbach, "Hydration of calcium sulfoaluminate cements — Experimental findings and thermodynamic modelling," *Cement and Concrete Research,* vol. 40, no. 8, pp. 1239-1247, 2010/08/01/ 2010, doi: https://doi.org/10.1016/j.cemconres.2009.08.014.

[36]   A. Moore and H. F. W. Taylor, "Crystal Structure of Ettringite," *Nature,* vol. 218, no. 5146, pp. 1048-1049, 1968/06/01 1968, doi: 10.1038/2181048a0.

[37]   H. F. W. Taylor, C. Famy, and K. L. Scrivener, "Delayed ettringite formation," *Cement and Concrete Research,* vol. 31, no. 5, pp. 683-693, 2001/05/01/ 2001, doi: https://doi.org/10.1016/S0008-8846(01)00466-5.

[38]   Q. Zhou, N. B. Milestone, and M. Hayes, "An alternative to Portland Cement for waste encapsulation—The calcium sulfoaluminate cement system," *Journal of Hazardous Materials,* vol. 136, no. 1, pp. 120-129, 2006/08/10/ 2006, doi: https://doi.org/10.1016/j.jhazmat.2005.11.038.

[39]   S. Rubert, C. Angulski da Luz, M. V. F. Varela, J. I. Pereira Filho, and R. D. Hooton, "Hydration mechanisms of supersulfated cement," *Journal of Thermal Analysis and Calorimetry,* vol. 134, no. 2, pp. 971-980, 2018/11/01 2018, doi: 10.1007/s10973-018-7243-6.

[40]   N. C. Collier, N. B. Milestone, L. E. Gordon, and S. C. Ko, "The suitability of a supersulfated cement for nuclear waste immobilisation," *Journal of Nuclear Materials,* vol. 452, no. 1, pp. 457-464, 2014/09/01/ 2014, doi: https://doi.org/10.1016/j.jnucmat.2014.05.078.

[41]   H. El-Didamony, A. A. Amer, and M. S. Mohammed, "Hydration and mechanical properties of cement/sludge/anhydrite gypsum system," *Advances in Cement Research,* vol. 26, no. 5, pp. 248-255, 2014/10/01 2014, doi: 10.1680/adcr.13.00049.

[42]   F. Bellmann and J. Stark, "Activation of blast furnace slag by a new method," *Cement and Concrete Research,* vol. 39, no. 8, pp. 644-650, 2009/08/01/ 2009, doi: https://doi.org/10.1016/j.cemconres.2009.05.012.

[43]   K. Piekkari, K. Ohenoja, V. Isteri, P. Tanskanen, and M. Illikainen, "Immobilization of heavy metals, selenate, and sulfate from a hazardous industrial side stream by using calcium sulfoaluminate-belite cement," *Journal of Cleaner Production,* vol. 258, p. 120560, 2020/06/10/ 2020, doi: https://doi.org/10.1016/j.jclepro.2020.120560.

[44]   R. Berardi, R. Cioffi, and L. Santoro, "Matrix stability and leaching behaviour in ettringite-based stabilization systems doped with heavy metals," *Waste Management,* vol. 17, no. 8, pp. 535-540, 1998/01/01/ 1998, doi: https://doi.org/10.1016/S0956-053X(97)10061-7.

[45]   M. L. D. Gougar, B. E. Scheetz, and D. M. Roy, "Ettringite and C · S · H Portland cement phases for waste ion immobilization: A review," *Waste Management,* vol. 16, no. 4, pp. 295-303, 1996/01/01/ 1996, doi: https://doi.org/10.1016/S0956-053X(96)00072-4.

[46]   M. A. Chavda, H. Kinoshita, and J. L. Provis, "Phosphate modification of calcium aluminate cement to enhance stability for immobilisation of metallic wastes," *Advances in Applied Ceramics,* vol. 113, no. 8, pp. 453-459, 2014/11/01 2014, doi: 10.1179/1743676114Y.0000000147.

[47]   S. Rashid, P. Barnes, J. Bensted, and X. Turrillas, "Conversion of calcium aluminate cement hydrates re-examined with synchrotron energy-dispersive diffraction," *Journal of materials science letters,* vol. 13, no. 17, pp. 1232-1234, 1994.

[48]   S. Rashid, P. Barnes, and X. Turrillas, "The rapid conversion of calcium aluminate cement hydrates, as revealed by synchrotron energy-dispersive diffraction," *Advances in Cement Research,* vol. 4, no. 14, pp. 61-67, 1992, doi: 10.1680/adcr.1992.4.14.61.

[49]   S. A. Walling and J. L. Provis, "Magnesia-Based Cements: A Journey of 150 Years, and Cements for the Future?," *Chemical Reviews,* vol. 116, no. 7, pp. 4170-4204, 2016/04/13 2016, doi: 10.1021/acs.chemrev.5b00463.

[50]   A. Wilson, "The chemistry of dental cements," *Chemical Society Reviews,* vol. 7, no. 2, pp. 265-296, 1978.

[51]   X. Lu and B. Chen, "Experimental study of magnesium phosphate cements modified by metakaolin," *Construction and Building Materials,* vol. 123, pp. 719-726, 2016/10/01/ 2016, doi: https://doi.org/10.1016/j.conbuildmat.2016.07.092.

[52]   S. S. Seehra, S. Gupta, and S. Kumar, "Rapid setting magnesium phosphate cement for quick repair of concrete pavements — characterisation and durability aspects," *Cement and Concrete Research,* vol. 23, no. 2, pp. 254-266, 1993/03/01/ 1993, doi: https://doi.org/10.1016/0008-8846(93)90090-V.

[53]   A. S. Wagh, M. D. Maloney, and G. H. Thompson, "Ceramicrete stabilization of U-and Pu-bearing materials," Patent US7294291B2 Patent Appl. US7294291B2, 2007.

[54]   A. S. Wagh *et al.*, "Experimental study on cesium immobilization in struvite structures," *Journal of Hazardous Materials,* vol. 302, pp. 241-249, 2016/01/25/ 2016, doi: https://doi.org/10.1016/j.jhazmat.2015.09.049.

[55]   A. Covill, N. C. Hyatt, J. Hill, and N. C. Collier, "Development of magnesium phosphate cements for encapsulation of radioactive waste," *Advances in Applied Ceramics,* vol. 110, no. 3, pp. 151-156, 2011/04/01 2011, doi: 10.1179/1743676110Y.0000000008.

[56]   D. Chartier *et al.*, "Behaviour of magnesium phosphate cement-based materials under gamma and alpha irradiation," *Journal of Nuclear Materials,* vol. 541, p. 152411, 2020/12/01/ 2020, doi: https://doi.org/10.1016/j.jnucmat.2020.152411.

[57]   W. Montague, "The suitability of magnesium phosphate cement for uranium metal encapsulation," 2014.

[58]   L. J. Gardner, "Assessment of magnesium potassium phosphate cements for radioactive waste encapsulation," Department of Materials Science and Engineering, University of Sheffield, 2016.

[59]   S. A. Walling, H. Kinoshita, S. A. Bernal, N. C. Collier, and J. L. Provis, "Structure and properties of binder gels formed in the system Mg(OH)2–SiO2–H2O for immobilisation of Magnox sludge," *Dalton Transactions,* 10.1039/C5DT00877H vol. 44, no. 17, pp. 8126-8137, 2015, doi: 10.1039/C5DT00877H.

[60]   B. Lothenbach, D. Nied, E. L'Hôpital, G. Achiedo, and A. Dauzères, "Magnesium and calcium silicate hydrates," *Cement and Concrete Research,* vol. 77, pp. 60-68, 2015/11/01/ 2015, doi: https://doi.org/10.1016/j.cemconres.2015.06.007.

[61]   E. Bernard, A. Dauzères, and B. Lothenbach, "Magnesium and calcium silicate hydrates, Part II: Mg-exchange at the interface "low-pH" cement and magnesium environment studied in a C-S-H and M-S-H model system," *Applied Geochemistry,* vol. 89, pp. 210-218, 2018/02/01/ 2018, doi: https://doi.org/10.1016/j.apgeochem.2017.12.006.

[62]   T. Zhang *et al.*, "Immobilization of Radionuclide 133Cs by Magnesium Silicate Hydrate Cement," *Materials,* vol. 13, no. 1, p. 146, 2020.

[63]   T. Zhang, J. Zou, Y. Li, Y. Jia, and C. R. Cheeseman, "Stabilization/Solidification of Strontium Using Magnesium Silicate Hydrate Cement," *Processes,* vol. 8, no. 2, p. 163, 2020.

[64]   T. Zhang, L. J. Vandeperre, and C. R. Cheeseman, "Magnesium-silicate-hydrate cements for encapsulating problematic aluminium containing wastes," *Journal of Sustainable Cement-Based Materials,* vol. 1, no. 1-2, pp. 34-45, 2012/06/01 2012, doi: 10.1080/21650373.2012.727322.

[65]   H. Kinoshita *et al.*, "Corrosion of aluminium metal in OPC- and CAC-based cement matrices," *Cement and Concrete Research,* vol. 50, pp. 11-18, 2013/08/01/ 2013, doi: https://doi.org/10.1016/j.cemconres.2013.03.016.

[66]   E. Bernard, B. Lothenbach, C. Cau-Dit-Coumes, I. Pochard, and D. Rentsch, "Aluminum incorporation into magnesium silicate hydrate (M-S-H)," *Cement and Concrete Research,* vol. 128, p. 105931, 2020/02/01/ 2020, doi: https://doi.org/10.1016/j.cemconres.2019.105931.

[67]   V. Cantarel, T. Motooka, and I. Yamagishi, "Geopolymers and Their Potential Applications in the Nuclear Waste Management Field-A Bibliographical Study," 2017.

[68]   J. Lehne and F. Preston, "Making Concrete Change: Innovation in Low-carbon Cement and Concrete," The Royal Institute for International Affairs, 13 June 2018 2018. [Online]. Available: https://reader.chathamhouse.org/making-concrete-change-innovation-low-carbon-cement-and-concrete#

[69]   "Global Change Institute - Annual Report," Global Change Institute, University of Queensland, 2017. Accessed: 28/5/2019.

[70]   J. Whiting, "Manufacture of Cement," United States Patent 544,706 Patent Appl. 544,706, 1895. [Online]. Available: https://patentimages.storage.googleapis.com/cb/eb/96/03a307e2f2d0a9/US544706.pdf

[71]   H. Kuehl, "Slag cement and process of making the same," US Patent 900939, 1908. [Online]. Available: http://www.google.co.uk/patents/US900939

[72]   A. Purdon, "The action of alkalis on blast-furnace slag," *Journal of the Society of Chemical Industry,* vol. 59, no. 9, pp. 191-202, 1940.

[73]   V. Glukhovsky, "Soil silicates (Gruntosilikaty)," *USSR Kiev: Budivelnik Publisher,* 1959.

[74]   V. Glukhovsky, G. Rostovskaja, and G. Rumyna, "High strength slag-alkaline cements," in *Proceedings of the seventh international congress on the chemistry of cement*, 1980, vol. 3, pp. 164-8.

[75] P. Krivenko, "Why Alkaline Activation – 60 Years of the Theory and Practice of Alkali-Activated Materials," *Journal of Ceramic Science and Technology,* Review vol. 8, no. 3, pp. 323 - 333, 14/8/2017 2017, doi: 10.4416/JCST2017-00042.

[76] C. Shi, D. Roy, and P. Krivenko, *Alkali-activated cements and concretes*. CRC press, 2003.

[77] P. V. Krivenko, "Alkaline cements," in *Proceedings of the 1st International Conference on Alkaline Cements and Concretes, Kiev, Ukraine, 1994*, 1994, vol. 1: Vipol Stock Company, pp. 11-129.

[78] Á. Palomo, S. Alonso, A. Fernandez-Jiménez, I. Sobrados, and J. Sanz, "Alkaline Activation of Fly Ashes: NMR Study of the Reaction Products," *Journal of the American Ceramic Society,* vol. 87, no. 6, pp. 1141-1145, 2004, doi: 10.1111/j.1551-2916.2004.01141.x.

[79] S. Alonso and A. Palomo, "Alkaline activation of metakaolin and calcium hydroxide mixtures: influence of temperature, activator concentration and solids ratio," *Materials Letters,* vol. 47, no. 1, pp. 55-62, 2001/01/01/ 2001, doi: https://doi.org/10.1016/S0167-577X(00)00212-3.

[80] A. Palomo, M. W. Grutzeck, and M. T. Blanco, "Alkali-activated fly ashes: A cement for the future," *Cement and Concrete Research,* vol. 29, no. 8, pp. 1323-1329, 1999/08/01/ 1999, doi: https://doi.org/10.1016/S0008-8846(98)00243-9.

[81] P. Duxson, J. L. Provis, G. C. Lukey, F. Separovic, and J. S. J. van Deventer, "29Si NMR Study of Structural Ordering in Aluminosilicate Geopolymer Gels," *Langmuir,* vol. 21, no. 7, pp. 3028-3036, 2005, doi: 10.1021/la047336x.

[82] P. Duxson, G. C. Lukey, and J. S. van Deventer, "Thermal evolution of metakaolin geopolymers: Part 1–Physical evolution," *Journal of Non-Crystalline Solids,* vol. 352, no. 52, pp. 5541-5555, 2006.

[83] P. Duxson, G. C. Lukey, and J. S. van Deventer, "The thermal evolution of metakaolin geopolymers: Part 2–Phase stability and structural development," *Journal of Non-Crystalline Solids,* vol. 353, no. 22, pp. 2186-2200, 2007.

[84] P. Duxson, S. W. Mallicoat, G. C. Lukey, W. M. Kriven, and J. S. J. van Deventer, "The effect of alkali and Si/Al ratio on the development of mechanical properties of metakaolin-based geopolymers," *Colloids and Surfaces A: Physicochemical and Engineering Aspects,* vol. 292, no. 1, pp. 8-20, 2007, doi: http://dx.doi.org/10.1016/j.colsurfa.2006.05.044.

[85] J. S. J. van Deventer, J. L. Provis, P. Duxson, and D. G. Brice, "Chemical research and climate change as drivers in the commercial adoption of alkali activated materials," *Waste and Biomass Valorization,* vol. 1, no. 1, pp. 145-155, 2010.

[86] J. G. S. van Jaarsveld, J. S. J. van Deventer, and G. C. Lukey, "The characterisation of source materials in fly ash-based geopolymers," *Materials Letters,* vol. 57, no. 7, pp. 1272-1280, 2003, doi: http://dx.doi.org/10.1016/S0167-577X(02)00971-0.

[87] J. G. S. van Jaarsveld, J. S. J. van Deventer, and G. C. Lukey, "The effect of composition and temperature on the properties of fly ash- and kaolinite-based geopolymers," *Chemical Engineering Journal,* vol. 89, no. 1, pp. 63-73, 2002/10/28/ 2002, doi: https://doi.org/10.1016/S1385-8947(02)00025-6.

[88] S. A. Bernal *et al.*, "Gel nanostructure in alkali-activated binders based on slag and fly ash, and effects of accelerated carbonation," *Cement and Concrete Research,* vol. 53, pp. 127-144, 2013, doi: http://dx.doi.org/10.1016/j.cemconres.2013.06.007.

[89] B. Walkley, J. L. Provis, R. San Nicolas, M. A. Sani, and J. S. J. van Deventer, "Stoichiometrically controlled C–(A)–S–H/N–A–S–H gel blends via alkali-activation of synthetic precursors," *Advances in Applied Ceramics,* vol. 114, no. 7, pp. 372-377, 2015/10/03 2015, doi: 10.1179/1743676115Y.0000000057.

[90] B. Walkley, R. San Nicolas, M.-A. Sani, J. D. Gehman, J. S. J. van Deventer, and J. L. Provis, "Phase evolution of Na2O-Al2O3-SiO2-H2O gels in synthetic aluminosilicate binders," *Dalton Transactions,* 10.1039/C5DT04878H vol. 45, no. 13, pp. 5521-5535, 2016, doi: 10.1039/C5DT04878H.

[91] R. J. Myers, S. A. Bernal, R. San Nicolas, and J. L. Provis, "Generalized Structural Description of Calcium–Sodium Aluminosilicate Hydrate Gels: The Cross-Linked Substituted Tobermorite Model," *Langmuir,* vol. 29, no. 17, pp. 5294-5306, 2013/04/30 2013, doi: 10.1021/la4000473.

[92] R. J. Myers, S. A. Bernal, and J. L. Provis, "A thermodynamic model for C-(N-)A-S-H gel: CNASH_ss. Derivation and validation," *Cement and Concrete Research,* vol. 66, pp. 27-47, 12// 2014, doi: 10.1016/j.cemconres.2014.07.005.

[93] R. J. Myers, S. A. Bernal, and J. L. Provis, "Phase diagrams for alkali-activated slag binders," *Cement and Concrete Research,* vol. 95, pp. 30-38, 2017/05/01/ 2017, doi: http://dx.doi.org/10.1016/j.cemconres.2017.02.006.

[94] B. Walkley, "Nanostructure of CaO-(Na₂O)-Al₂O₃-SiO₂-H₂O Gels Revealed by Multinuclear Solid-State Magic Angle Spinning and Multiple Quantum Magic Angle Spinning Nuclear Magnetic Resonance Spectroscopy," *Journal of physical chemistry,* vol. v. 124, no. no. 2, pp. pp. 1681-1694-2019 v.124 no.2, 2019-12-17 2019, doi: 10.1021/acs.jpcc.9b10133.

[95] B. Walkley, A. Kashani, M.-A. Sani, T. D. Ngo, and P. Mendis, "Examination of alkali-activated material nanostructure during thermal treatment," *Journal of Materials Science,* vol. 53, no. 13, pp. 9486-9503, 2018/07/01 2018, doi: 10.1007/s10853-018-2270-z.

[96] S. A. Bernal, V. Rose, and J. L. Provis, "The fate of iron in blast furnace slag particles during alkali-activation," *Materials Chemistry and Physics,* vol. 146, no. 1, pp. 1-5, 2014/07/15/ 2014, doi: https://doi.org/10.1016/j.matchemphys.2014.03.017.

[97] S. Mundra, M. Criado, S. A. Bernal, and J. L. Provis, "Chloride-induced corrosion of steel rebars in simulated pore solutions of alkali-activated concretes," *Cement and Concrete Research,* vol. 100, pp. 385-397, 2017/10/01/ 2017, doi: http://dx.doi.org/10.1016/j.cemconres.2017.08.006.

[98]   C. Kuenzel, L. J. Vandeperre, S. Donatello, A. R. Boccaccini, and C. Cheeseman, "Ambient Temperature Drying Shrinkage and Cracking in Metakaolin‐Based Geopolymers," *Journal of the American Ceramic Society,* vol. 95, no. 10, pp. 3270-3277, 2012, doi: 10.1111/j.1551-2916.2012.05380.x.

[99]   C. Kuenzel, T. P. Neville, S. Donatello, L. Vandeperre, A. R. Boccaccini, and C. R. Cheeseman, "Influence of metakaolin characteristics on the mechanical properties of geopolymers," *Applied Clay Science,* vol. 83–84, pp. 308-314, 2013, doi: 10.1016/j.clay.2013.08.023.

[100]   C. Kuenzel *et al.*, "Encapsulation of aluminium in geopolymers produced from metakaolin," *Journal of Nuclear Materials,* vol. 447, no. 1–3, pp. 208-214, 2014, doi: 10.1016/j.jnucmat.2014.01.015.

[101]   C. Kuenzel *et al.*, "Encapsulation of Cs/Sr contaminated clinoptilolite in geopolymers produced from metakaolin," *Journal of Nuclear Materials,* vol. 466, pp. 94-99, 2015, doi: 10.1016/j.jnucmat.2015.07.034.

[102]   E. Adesanya, K. Ohenoja, T. Luukkonen, P. Kinnunen, and M. Illikainen, "One-part geopolymer cement from slag and pretreated paper sludge," *Journal of Cleaner Production,* vol. 185, pp. 168-175, 2018/06/01/ 2018, doi: https://doi.org/10.1016/j.jclepro.2018.03.007.

[103]   P. N. Lemougna *et al.*, "Thermal stability of one-part metakaolin geopolymer composites containing high volume of spodumene tailings and glass wool," *Cement and Concrete Composites,* vol. 114, p. 103792, 2020/11/01/ 2020, doi: https://doi.org/10.1016/j.cemconcomp.2020.103792.

[104]   J. L. Provis, A. Palomo, and C. Shi, "Advances in understanding alkali-activated materials," *Cement and Concrete Research,* vol. 78, Part A, pp. 110-125, 12// 2015, doi: 10.1016/j.cemconres.2015.04.013.

[105]   M. Criado, A. Fernández-Jiménez, A. Palomo, I. Sobrados, and J. Sanz, "Effect of the SiO2/Na2O ratio on the alkali activation of fly ash. Part II: 29Si MAS-NMR Survey," *Microporous and Mesoporous Materials,* vol. 109, no. 1, pp. 525-534, 2008, doi: http://dx.doi.org/10.1016/j.micromeso.2007.05.062.

[106]   G. Kovalchuk, A. Fernández-Jiménez, and A. Palomo, "Alkali-activated fly ash: Effect of thermal curing conditions on mechanical and microstructural development – Part II," *Fuel,* vol. 86, no. 3, pp. 315-322, 2007, doi: http://dx.doi.org/10.1016/j.fuel.2006.07.010.

[107]   B. Walkley, G. J. Rees, R. San Nicolas, J. S. J. van Deventer, J. V. Hanna, and J. L. Provis, "New Structural Model of Hydrous Sodium Aluminosilicate Gels and the Role of Charge-Balancing Extra-Framework Al," *The Journal of Physical Chemistry C,* vol. 122, no. 10, pp. 5673-5685, 2018/03/15 2018, doi: 10.1021/acs.jpcc.8b00259.

[108]   J. L. Provis, "Alkali-activated materials," *Cement and Concrete Research,* 2017, doi: https://doi.org/10.1016/j.cemconres.2017.02.009.

[109]   J. L. Provis *et al.*, "RILEM TC 247-DTA round robin test: mix design and reproducibility of compressive strength of alkali-activated concretes," *Materials and Structures,* vol. 52, no. 5, p. 99, 2019/09/10 2019, doi: 10.1617/s11527-019-1396-z.

[110]   A. Fernández-Jiménez and A. Palomo, "Mid-infrared spectroscopic studies of alkali-activated fly ash structure," *Microporous and Mesoporous Materials,* vol. 86, no. 1, pp. 207-214, 2005.

[111]   J. L. Provis and S. A. Bernal, "Geopolymers and related alkali-activated materials," *Annual Review of Materials Research,* vol. 44, pp. 299-327, 2014.

[112]   S. A. Bernal and J. L. Provis, "Durability of Alkali-Activated Materials: Progress and Perspectives," *Journal of the American Ceramic Society,* vol. 97, no. 4, pp. 997-1008, 2014, doi: 10.1111/jace.12831.

[113]   J. L. Provis and J. S. J. van Deventer, "Geopolymerisation kinetics. 2. Reaction kinetic modelling," *Chemical Engineering Science,* vol. 62, no. 9, pp. 2318-2329, 2007, doi: http://dx.doi.org/10.1016/j.ces.2007.01.028.

[114]   L. D. Rollmann, E. W. Valyocsik, and R. D. Shannon, "Zeolite Molecular Sieves," in *Inorganic Syntheses*, D. W. M. a. L. V. Interrante Ed. New York: John Wiley & Sons, Inc., 2007, pp. 227-234.

[115]   M. Arbel Haddad *et al.*, "Formation of zeolites in metakaolin-based geopolymers and their potential application for Cs immobilization," *Journal of Nuclear Materials,* vol. 493, pp. 168-179, 2017/09/01 2017, doi: http://dx.doi.org/10.1016/j.jnucmat.2017.05.046.

[116]   E. Ofer-Rozovsky, M. Arbel Haddad, G. Bar Nes, and A. Katz, "The formation of crystalline phases in metakaolin-based geopolymers in the presence of sodium nitrate," *Journal of Materials Science,* vol. 51, no. 10, pp. 4795-4814, 2016/05/01 2016, doi: 10.1007/s10853-016-9767-0.

[117]   J. L. Provis, G. C. Lukey, and J. S. J. van Deventer, "Do Geopolymers Actually Contain Nanocrystalline Zeolites? A Reexamination of Existing Results," *Chemistry of Materials,* vol. 17, no. 12, pp. 3075-3085, 2005, doi: 10.1021/cm050230i.

[118]   J. Davidovits, "Geopolymers," *Journal of Thermal Analysis,* journal article vol. 37, no. 8, pp. 1633-1656, 1991, doi: 10.1007/bf01912193.

[119]   T. Prasomsri, W. Jiao, S. Z. Weng, and J. G. Martinez, "Mesostructured zeolites: bridging the gap between zeolites and MCM-41," *Chemical Communications,* vol. 51, no. 43, pp. 8900-8911, 2015.

[120]   P. Duxson, A. Fernández-Jiménez, J. L. Provis, G. C. Lukey, A. Palomo, and J. S. J. van Deventer, "Geopolymer technology: the current state of the art," *Journal of Materials Science,* journal article vol. 42, no. 9, pp. 2917-2933, 2007, doi: 10.1007/s10853-006-0637-z.

[121]   P. Duxson, J. L. Provis, G. C. Lukey, J. S. J. van Deventer, F. Separovic, and Z. H. Gan, "39K NMR of Free Potassium in Geopolymers," *Industrial & Engineering Chemistry Research,* vol. 45, no. 26, pp. 9208-9210, 2006/12/01 2006, doi: 10.1021/ie060838g.

[122] B. Walkley, X. Ke, O. H. Hussein, S. A. Bernal, and J. L. Provis, "Incorporation of strontium and calcium in geopolymer gels," *Journal of Hazardous Materials,* vol. 382, p. 121015, 2020/01/15/ 2020, doi: https://doi.org/10.1016/j.jhazmat.2019.121015.

[123] H. Rahier, J. Denayer, and B. Van Mele, "Low-temperature synthesized aluminosilicate glasses Part IV Modulated DSC study on the effect of particle size of metakaolinite on the production of inorganic polymer glasses," *Journal of Materials Science,* vol. 38, no. 14, pp. 3131-3136, 2003.

[124] Z. Zhang, H. Wang, J. L. Provis, F. Bullen, A. Reid, and Y. Zhu, "Quantitative kinetic and structural analysis of geopolymers. Part 1. The activation of metakaolin with sodium hydroxide," *Thermochimica Acta,* vol. 539, pp. 23-33, 2012, doi: http://dx.doi.org/10.1016/j.tca.2012.03.021.

[125] J. L. Provis, "Modelling the formation of geopolymers," Ph.D. dissertation, Department of Chemical Engineering, University of Melbourne, Melbourne, 2006. [Online]. Available: http://hdl.handle.net/11343/39075

[126] A. Poulesquen, F. Frizon, and D. Lambertin, "Rheological behavior of alkali-activated metakaolin during geopolymerization," *Journal of Non-Crystalline Solids,* vol. 357, no. 21, pp. 3565-3571, 2011, doi: 10.1016/j.jnoncrysol.2011.07.013.

[127] J. L. Provis and J. S. J. van Deventer, "Geopolymerisation kinetics. 1. In situ energy-dispersive X-ray diffractometry," *Chemical Engineering Science,* vol. 62, no. 9, pp. 2309-2317, 2007, doi: http://dx.doi.org/10.1016/j.ces.2007.01.027.

[128] A. Gualtieri, P. Norby, G. Artioli, and J. Hanson, "Kinetics of formation of zeolite Na-A [LTA] from natural kaolinites," *Physics and Chemistry of Minerals,* journal article vol. 24, no. 3, pp. 191-199, 1997, doi: 10.1007/s002690050032.

[129] J. L. Provis, A. Kilcullen, P. Duxson, D. G. Brice, and J. S. J. van Deventer, "Stabilization of Low-Modulus Sodium Silicate Solutions by Alkali Substitution," *Industrial & Engineering Chemistry Research,* vol. 51, no. 5, pp. 2483-2486, 2012, doi: 10.1021/ie202143j.

[130] T. Luukkonen, Z. Abdollahnejad, J. Yliniemi, P. Kinnunen, and M. Illikainen, "One-part alkali-activated materials: A review," *Cement and Concrete Research,* vol. 103, pp. 21-34, 2018/01/01/ 2018, doi: https://doi.org/10.1016/j.cemconres.2017.10.001.

[131] K.-H. Yang, J.-K. Song, A. F. Ashour, and E.-T. Lee, "Properties of cementless mortars activated by sodium silicate," *Construction and Building Materials,* vol. 22, no. 9, pp. 1981-1989, 2008, doi: http://dx.doi.org/10.1016/j.conbuildmat.2007.07.003.

[132] Z. Zhang, J. L. Provis, H. Wang, F. Bullen, and A. Reid, "Quantitative kinetic and structural analysis of geopolymers. Part 2. Thermodynamics of sodium silicate activation of metakaolin," *Thermochimica Acta,* vol. 565, pp. 163-171, 2013, doi: http://dx.doi.org/10.1016/j.tca.2013.01.040.

[133] M. Król, J. Minkiewicz, and W. Mozgawa, "IR spectroscopy studies of zeolites in geopolymeric materials derived from kaolinite," *Journal of Molecular Structure,* vol. 1126, pp. 200-206, 2016/12/15/ 2016, doi: https://doi.org/10.1016/j.molstruc.2016.02.027.

[134] A. R. Brough, A. Katz, G. K. Sun, L. J. Struble, R. J. Kirkpatrick, and J. F. Young, "Adiabatically cured, alkali-activated cement-based wasteforms containing high levels of fly ash: Formation of zeolites and Al-substituted C-S-H," *Cement and Concrete Research,* vol. 31, no. 10, pp. 1437-1447, 2001/10/01/ 2001, doi: https://doi.org/10.1016/S0008-8846(01)00589-0.

[135] J. G. S. van Jaarsveld and J. S. J. van Deventer, "Effect of the Alkali Metal Activator on the Properties of Fly Ash-Based Geopolymers," *Industrial & Engineering Chemistry Research,* vol. 38, no. 10, pp. 3932-3941, 1999/10/01 1999, doi: 10.1021/ie980804b.

[136] P. Hewlett and M. Liska, *Lea's chemistry of cement and concrete*. Butterworth-Heinemann, 2019.

[137] P. Banfill, "Rheology of fresh cement and concrete," *Rheology Reviews,* pp. 61 - 130, 2006.

[138] A. Favier, J. Hot, G. Habert, N. Roussel, and J.-B. d. E. de Lacaillerie, "Flow properties of MK-based geopolymer pastes. A comparative study with standard Portland cement pastes," *Soft Matter,* vol. 10, no. 8, pp. 1134-1141, 2014.

[139] A. Favier, G. Habert, J. B. d'Espinose de Lacaillerie, and N. Roussel, "Mechanical properties and compositional heterogeneities of fresh geopolymer pastes," *Cement and Concrete Research,* vol. 48, no. Supplement C, pp. 9-16, 2013/06/01/ 2013, doi: https://doi.org/10.1016/j.cemconres.2013.02.001.

[140] A. Favier, J. Hot, G. Habert, J.-B. d. E. de Lacaillerie, and N. Roussel, "Rheology of geopolymer: comparative study between Portland cement and metakaolin based geopolymer," in *1st RILEM International Conference on Rheology and Processing of Construction Materials*, Paris, France, 2013, pp. 49-56.

[141] P. Coussot, "Introduction to the rheology of complex fluids," in *Understanding the rheology of concrete*: Elsevier, 2012, pp. 3-22.

[142] G. Ovarlez, "Introduction to the rheometry of complex suspensions," in *Understanding the Rheology of Concrete*, N. Roussel Ed.: Woodhead Publishing, 2012, ch. 2, pp. 23-62.

[143] D. Han and R. D. Ferron, "Effect of mixing method on microstructure and rheology of cement paste," *Construction and Building Materials,* vol. 93, pp. 278-288, 2015/09/15/ 2015, doi: https://doi.org/10.1016/j.conbuildmat.2015.05.124.

[144] D. A. Williams, A. W. Saak, and H. M. Jennings, "The influence of mixing on the rheology of fresh cement paste," *Cement and Concrete Research,* vol. 29, no. 9, pp. 1491-1496, 1999/09/01/ 1999, doi: https://doi.org/10.1016/S0008-8846(99)00124-6.

[145] M. Khalifeh, A. Saasen, T. Vralstad, and H. Hodne, "Potential utilization of class C fly ash-based geopolymer in oil well cementing operations," *Cement and Concrete Composites,* vol. 53, pp. 10-17, 2014/10/01/ 2014, doi: https://doi.org/10.1016/j.cemconcomp.2014.06.014.

[146] D. A. Geddes, X. Ke, S. A. Bernal, M. Hayes, and J. L. Provis, "Metakaolin-Based Geopolymers for Nuclear Waste Encapsulation," in *International Conference on Calcined Clays for Sustainable Construction*, Havanna, Cuba, 2018: Springer, Netherlands, in Calcined Clays for Sustainable Concrete, pp. 183-188.

[147] Y. Dhandapani *et al.*, "Review of Fresh Properties of Concrete Containing Calcined Clays," 2020.

[148] S. Ferreiro, D. Herfort, and J. S. Damtoft, "Effect of raw clay type, fineness, water-to-cement ratio and fly ash addition on workability and strength performance of calcined clay – Limestone Portland cements," *Cement and Concrete Research,* vol. 101, pp. 1-12, 2017/11/01/ 2017, doi: https://doi.org/10.1016/j.cemconres.2017.08.003.

[149] M. Hayes, M. Angus, and R. Garland, "Current status paper on the potential use of Superplasticisers in a Geological Disposal Facility," National Nuclear Laboratory, 2012.

[150] Amy Shelton, Helen Kendall, and M. Rigby, "Geological Disposal: Guidance on the use of polycarboxylate ether superplasticisers for the packaging of low heat generating wastes," Nuclear Decomissioning AUthority, 30/08/2019 2019.

[151] T. Vehmas *et al.*, "Characterization of Cebama low-pH reference concrete and assessment of its alteration with representative waters in radioactive waste repositories," *Applied Geochemistry,* vol. 121, p. 104703, 2020/10/01/ 2020, doi: https://doi.org/10.1016/j.apgeochem.2020.104703.

[152] M. Sonebi, M. Lachemi, and K. M. A. Hossain, "Optimisation of rheological parameters and mechanical properties of superplasticised cement grouts containing metakaolin and viscosity modifying admixture," *Construction and Building Materials,* vol. 38, pp. 126-138, 2013/01/01/ 2013, doi: https://doi.org/10.1016/j.conbuildmat.2012.07.102.

[153] F. Cassagnabère, P. Diederich, M. Mouret, G. Escadeillas, and M. Lachemi, "Impact of metakaolin characteristics on the rheological properties of mortar in the fresh state," *Cement and Concrete Composites,* vol. 37, pp. 95-107, 2013/03/01/ 2013, doi: https://doi.org/10.1016/j.cemconcomp.2012.12.001.

[154] R. San Nicolas, M. Cyr, and G. Escadeillas, "Characteristics and applications of flash metakaolins," *Applied Clay Science,* vol. 83–84, pp. 253-262, 2013, doi: 10.1016/j.clay.2013.08.036.

[155] R. Siddique and J. Klaus, "Influence of metakaolin on the properties of mortar and concrete: A review," *Applied Clay Science,* vol. 43, no. 3, pp. 392-400, 2009.

[156] J. L. Provis and J. S. van Deventer, *Alkali Activated Materials*. Dordrecht: Springer/RILEM, 2014.

[157] S. Sperinck, P. Raiteri, N. Marks, and K. Wright, "Dehydroxylation of kaolinite to metakaolin—A molecular dynamics study," *Journal of Materials Chemistry,* vol. 21, no. 7, pp. 2118-2125, 2011.

[158] A. Autef *et al.*, "Role of metakaolin dehydroxylation in geopolymer synthesis," *Powder technology,* vol. 250, pp. 33-39, 2013.

[159] M. Cyr, "Contribution to the characterisation of mineral additives and to the comprehension of their effect on the rheological behaviour of cementitious materials," INSA de Toulouse, Université de Sherbrooke, 1999. [Online]. Available: https://tel.archives-ouvertes.fr/tel-00489599

[160] M. Claverie *et al.*, "Structural and chemical changes in kaolinite caused by flash calcination: Formation of spherical particles," *Applied Clay Science,* vol. 114, pp. 247-255, 2015/09/01/ 2015, doi: https://doi.org/10.1016/j.clay.2015.05.031.

[161] R. San Nicolas, M. Cyr, and G. Escadeillas, "Performance-based approach to durability of concrete containing flash-calcined metakaolin as cement replacement," *Construction and Building Materials,* vol. 55, pp. 313-322, 2014/03/31/ 2014, doi: https://doi.org/10.1016/j.conbuildmat.2014.01.063.

[162] A. McIntosh, S. E. M. Lawther, J. Kwasny, M. N. Soutsos, D. Cleland, and S. Nanukuttan, "Selection and characterisation of geological materials for use as geopolymer precursors," *Advances in Applied Ceramics,* vol. 114, no. 7, pp. 378-385, 2015/10/03 2015, doi: 10.1179/1743676115Y.0000000055.

[163] S. Salvador, "Pozzolanic properties of flash-calcined kaolinite: A comparative study with soak-calcined products," *Cement and Concrete Research,* vol. 25, no. 1, pp. 102-112, 1995/01/01/ 1995, doi: https://doi.org/10.1016/0008-8846(94)00118-I.

[164] Z. Zuhua, Y. Xiao, Z. Huajun, and C. Yue, "Role of water in the synthesis of calcined kaolin-based geopolymer," *Applied Clay Science,* vol. 43, no. 2, pp. 218-223, 2009, doi: http://dx.doi.org/10.1016/j.clay.2008.09.003.

[165] M. Król and P. Rożek, "The effect of calcination temperature on metakaolin structure for the synthesis of zeolites," *Clay Minerals,* vol. 53, no. 4, pp. 657-663, 2018, doi: 10.1180/clm.2018.49.

[166] G. S. Barney, "Immobilization of aqueous radioactive cesium wastes by conversion to aluminosilicate minerals," Atlantic Richfield Hanford Co., 1975.

[167] M. Khalil and E. Merz, "Immobilization of intermediate-level wastes in geopolymers," *Journal of Nuclear Materials,* vol. 211, no. 2, pp. 141-148, 1994.

[168] J. Davidovits, "Properties of geopolymer cements," in *First international conference on alkaline cements and concretes*, 1994, vol. 1, pp. 131-149.

[169] D. Lambertin, F. Frizon, and F. Bart, "Mg–Zr alloy behavior in basic solutions and immobilization in Portland cement and Na-geopolymer with sodium fluoride inhibitor," *Surface and Coatings Technology,* vol. 206, no. 22, pp. 4567-4573, 2012/06/25/ 2012, doi: https://doi.org/10.1016/j.surfcoat.2012.05.008.

[170] F. Chupin, A. Dannoux-Papin, Y. Ngono Ravache, and J.-B. d'Espinose de Lacaillerie, "Water content and porosity effect on hydrogen radiolytic yields of geopolymers," *Journal of Nuclear Materials,* vol. 494, pp. 138-146, 2017/10/01/ 2017, doi: https://doi.org/10.1016/j.jnucmat.2017.07.005.

[171] W.-H. Lee, T.-W. Cheng, Y.-C. Ding, K.-L. Lin, S.-W. Tsao, and C.-P. Huang, "Geopolymer technology for the solidification of simulated ion exchange resins with radionuclides," *Journal of Environmental Management,* vol. 235, pp. 19-27, 2019/04/01/ 2019, doi: https://doi.org/10.1016/j.jenvman.2019.01.027.

[172] D. Lambertin, C. Boher, A. Dannoux-Papin, K. Galliez, A. Rooses, and F. Frizon, "Influence of gamma ray irradiation on metakaolin based sodium geopolymer," *Journal of Nuclear Materials,* vol. 443, no. 1–3, pp. 311-315, 2013, doi: 10.1016/j.jnucmat.2013.06.044.

[173] V. Cantarel, M. Arisaka, and I. Yamagishi, "On the hydrogen production of geopolymer wasteforms under irradiation," *Journal of the American Ceramic Society,* vol. 102, no. 12, pp. 7553-7563, 2019, doi: 10.1111/jace.16642.

[174] N. Deng *et al.*, "Effects of gamma-ray irradiation on leaching of simulated 133Cs+ radionuclides from geopolymer wasteforms," *Journal of Nuclear Materials,* vol. 459, pp. 270-275, 2015/04/01/ 2015, doi: https://doi.org/10.1016/j.jnucmat.2015.01.052.

[175] L. Leay, A. Potts, and T. Donoclift, "Geopolymers from fly ash and their gamma irradiation," *Materials Letters,* vol. 227, pp. 240-242, 2018/09/15/ 2018, doi: https://doi.org/10.1016/j.matlet.2018.05.088.

[176] R. D. Spence and C. Shi, *Stabilization and solidification of hazardous, radioactive, and mixed wastes*. CRC press, 2004.

[177] C. Colella, "Environmental applications of natural zeolitic materials based on their ion exchange properties," in *Natural Microporous Materials in Environmental Technology*: Springer, 1999, pp. 207-224.

[178] S. A. Bernal, J. S. J. van Deventer, and J. L. Provis, "What Happens to 5 Year Old Metakaolin Geopolymers' the Effect of Alkali Cation," in *Calcined Clays for Sustainable Concrete: Proceedings of the 1st International Conference on Calcined Clays for Sustainable Concrete*, Dordrecht, K. Scrivener and A. Favier, Eds., 2015: Springer Netherlands, pp. 315-321, doi: 10.1007/978-94-017-9939-3_39. [Online]. Available: http://dx.doi.org/10.1007/978-94-017-9939-3_39

http://link.springer.com/chapter/10.1007%2F978-94-017-9939-3_39

https://link.springer.com/chapter/10.1007%2F978-94-017-9939-3_39

[179] S. Berger, F. Frizon, and C. Joussot-Dubien, "Formulation of caesium based and caesium containing geopolymers," *Advances in Applied Ceramics,* vol. 108, no. 7, pp. 412-417, 2009, doi: 10.1179/174367609X422072.

[180] J. L. Provis, P. A. Walls, and J. S. J. van Deventer, "Geopolymerisation kinetics. 3. Effects of Cs and Sr salts," *Chemical Engineering Science,* vol. 63, no. 18, pp. 4480-4489, 2008/09/01/ 2008, doi: https://doi.org/10.1016/j.ces.2008.06.008.

[181] J. G. Jang, S. M. Park, and H. K. Lee, "Physical barrier effect of geopolymeric waste form on diffusivity of cesium and strontium," *Journal of Hazardous Materials,* vol. 318, pp. 339-346, 2016/11/15/ 2016, doi: https://doi.org/10.1016/j.jhazmat.2016.07.003.

[182] T. Hanzlicek, M. Steinerova, and P. Straka, "Radioactive Metal Isotopes Stabilized in a Geopolymer Matrix: Determination of a Leaching Extract by a Radiotracer Method," *Journal of the American Ceramic Society,* vol. 89, no. 11, pp. 3541-3543, 2006, doi: 10.1111/j.1551-2916.2006.01024.x.

[183] Q. Li *et al.*, "Immobilization of simulated radionuclide 133Cs+ by fly ash-based geopolymer," *Journal of Hazardous Materials,* vol. 262, pp. 325-331, 2013/11/15/ 2013, doi: https://doi.org/10.1016/j.jhazmat.2013.08.049.

[184] C. Bai, T. Ni, Q. Wang, H. Li, and P. Colombo, "Porosity, mechanical and insulating properties of geopolymer foams using vegetable oil as the stabilizing agent," *Journal of the European Ceramic Society,* vol. 38, no. 2, pp. 799-805, 2018/02/01/ 2018, doi: https://doi.org/10.1016/j.jeurceramsoc.2017.09.021.

[185] A. Barneoud-Chapelier, J. Causse, and A. Poulesquen, "Synthesis of geopolymer emulsions," *Materials Letters,* vol. 276, p. 128188, 2020/10/01/ 2020, doi: https://doi.org/10.1016/j.matlet.2020.128188.

[186] C. A. Davy, G. Hauss, B. Planel, and D. Lambertin, "3D structure of oil droplets in hardened geopolymer emulsions," *Journal of the American Ceramic Society,* vol. 102, no. 3, pp. 949-954, 2019, doi: 10.1111/jace.16142.

[187] *Cement. Composition, specifications and conformity criteria for common cements*, BSI, 30 September 2011 2011.

[188] *Alkali-activated cementatious material and concrete*, B.S.I., 2016 2016.

[189] B. EN, "Methods of testing cement," in *Determination of setting times and soundness* vol. 196-3, ed: British Standards Instiution, 2016, p. 18.

[190] P. Duxson, "The structure and thermal evolution of metakaolin geopolymers," Department of Chemical Engineering, 2006. [Online]. Available: http://hdl.handle.net/11343/39114

[191] L. Leay *et al.*, "Development of irradiation capabilities to address the challenges of the nuclear industry," *Nuclear Instruments and Methods in Physics Research Section B: Beam Interactions with Materials and Atoms,* vol. 343, pp. 62-69, 2015/01/15/ 2015, doi: https://doi.org/10.1016/j.nimb.2014.11.028.

[192] H. A. Barnes and Q. D. Nguyen, "Rotating vane rheometry — a review," *Journal of Non-Newtonian Fluid Mechanics,* vol. 98, no. 1, pp. 1-14, 2001/03/15/ 2001, doi: https://doi.org/10.1016/S0377-0257(01)00095-7.

[193] K. Walters and W. M. Jones, "Measurement of Viscosity," in *Instrumentation Reference Book (Fourth Edition)*, W. Boyes Ed. Boston: Butterworth-Heinemann, 2010, ch. 7, pp. 69-75.

[194] S. A. Bernal, R. M. de Gutierrez, J. L. Provis, and V. Rose, "Effect of silicate modulus and metakaolin incorporation on the carbonation of alkali silicate-activated slags," *Cement and Concrete Research,* vol. 40, no. 6, pp. 898-907, 2010/06/01/ 2010, doi: https://doi.org/10.1016/j.cemconres.2010.02.003.

[195] K. Scrivener, R. Snellings, and B. Lothenbach, *A practical guide to microstructural analysis of cementitious materials.* Crc Press, 2018.

[196] M. A. Longhi, E. D. Rodríguez, B. Walkley, Z. Zhang, and A. P. Kirchheim, "Metakaolin-based geopolymers: Relation between formulation, physicochemical properties and efflorescence formation," *Composites Part B: Engineering,* vol. 182, p. 107671, 2020/02/01/ 2020, doi: https://doi.org/10.1016/j.compositesb.2019.107671.

[197] R. Snellings, A. Salze, and K. L. Scrivener, "Use of X-ray diffraction to quantify amorphous supplementary cementitious materials in anhydrous and hydrated blended cements," *Cement and Concrete Research,* vol. 64, pp. 89-98, 2014/10/01/ 2014, doi: https://doi.org/10.1016/j.cemconres.2014.06.011.

[198] B. Walkley and J. L. Provis, "Solid-state nuclear magnetic resonance spectroscopy of cements," *Materials Today Advances,* vol. 1, p. 100007, 2019/03/01/ 2019, doi: https://doi.org/10.1016/j.mtadv.2019.100007.

[199] J. Skibsted, "High-resolution solid-state nuclear magnetic resonance spectroscopy of portland cement-based systems," in *A Practical Guide to Microstructural Analysis of Cementitious Materials*: CRC Press, 2018, pp. 232-305.

[200] B. C. Smith, *Fundamentals of Fourier transform infrared spectroscopy.* CRC press, 2011.

[201] C. A. Rees, J. L. Provis, G. C. Lukey, and J. S. J. van Deventer, "The mechanism of geopolymer gel formation investigated through seeded nucleation," *Colloids and Surfaces A: Physicochemical and Engineering Aspects,* vol. 318, no. 1, pp. 97-105, 2008/04/01/ 2008, doi: https://doi.org/10.1016/j.colsurfa.2007.12.019.

[202] Z. Zhang, H. Wang, and J. L. Provis, "Quantitative study of the reactivity of fly ash in geopolymerization by FTIR," *Journal of Sustainable Cement-Based Materials,* vol. 1, no. 4, pp. 154-166, 2012/12/01 2012, doi: 10.1080/21650373.2012.752620.

[203] S. Diamond, "Mercury porosimetry: An inappropriate method for the measurement of pore size distributions in cement-based materials," *Cement and Concrete Research,* vol. 30, no. 10, pp. 1517-1525, 2000/10/01/ 2000, doi: https://doi.org/10.1016/S0008-8846(00)00370-7.

[204] H. Ma, "Mercury intrusion porosimetry in concrete technology: tips in measurement, pore structure parameter acquisition and application," *Journal of porous materials,* vol. 21, no. 2, pp. 207-215, 2014.

[205] Q. Zeng, K. Li, T. Fen-Chong, and P. Dangla, "Analysis of pore structure, contact angle and pore entrapment of blended cement pastes from mercury porosimetry data," *Cement and Concrete Composites,* vol. 34, no. 9, pp. 1053-1060, 2012/10/01/ 2012, doi: https://doi.org/10.1016/j.cemconcomp.2012.06.005.

[206] ASTM, "Standard Test Method for Compressive Strength of Hydraulic Cement Mortars (Using 2-in. or [50-mm] Cube Specimens)," ed: ASTM International, 2016.

[207] G. Cann, "A Technical Specification for Portland Cement, Blast Furnace Slag and Fly Ash Powders for Use in the Encapsulation/Immobilisation of Radioactive Waste Materials (9th Revision)," National Nuclear Laboratory, NNL (16) 13324, 28/09/2016 2016, issue 2.

[208] A. Palomo, P. F. G. Banfill, A. Fernández-Jiménez, and D. S. Swift, "Properties of alkali-activated fly ashes determined from rheological measurements," *Advances in Cement Research,* vol. 17, no. 4, pp. 143-151, 2005, doi: 10.1680/adcr.2005.17.4.143.

[209] M. Palacios, P. F. Banfill, and F. Puertas, "Rheology and setting of alkali-activated slag pastes and mortars: effect of organic admixture," *Materials Journal,* vol. 105, no. 2, pp. 140-148, 2008.

[210] F. Puertas, C. Varga, and M. M. Alonso, "Rheology of alkali-activated slag pastes. Effect of the nature and concentration of the activating solution," *Cem. Concr. Compos.,* vol. 53, pp. 279-288, 10// 2014, doi: http://dx.doi.org/10.1016/j.cemconcomp.2014.07.012.

[211] M. Romagnoli, C. Leonelli, E. Kamse, and M. Lassinantti Gualtieri, "Rheology of geopolymer by DOE approach," *Construction and Building Materials,* vol. 36, pp. 251-258, 2012/11/01/ 2012, doi: https://doi.org/10.1016/j.conbuildmat.2012.04.122.

[212] J. L. Provis, P. Duxson, and J. S. J. van Deventer, "The role of particle technology in developing sustainable construction materials," *Advanced Powder Technology,* vol. 21, no. 1, pp. 2-7, 2010/01/01/ 2010, doi: https://doi.org/10.1016/j.apt.2009.10.006.

[213] P. Duxson, J. L. Provis, G. C. Lukey, S. W. Mallicoat, W. M. Kriven, and J. S. J. van Deventer, "Understanding the relationship between geopolymer composition, microstructure and mechanical properties," *Colloids and Surfaces A: Physicochemical and Engineering Aspects,* vol. 269, no. 1, pp. 47-58, 2005/11/01/ 2005, doi: https://doi.org/10.1016/j.colsurfa.2005.06.060.

[214] N. Roussel, "4 - From industrial testing to rheological parameters for concrete," in *Understanding the Rheology of Concrete*, N. Roussel Ed.: Woodhead Publishing, 2012, pp. 83-95.

[215] N. Roussel, A. Lemaître, R. J. Flatt, and P. Coussot, "Steady state flow of cement suspensions: A micromechanical state of the art," *Cement and Concrete Research,* vol. 40, no. 1, pp. 77-84, 2010/01/01/ 2010, doi: https://doi.org/10.1016/j.cemconres.2009.08.026.

[216] T. H. Phan, M. Chaouche, and M. Moranville, "Influence of organic admixtures on the rheological behaviour of cement pastes," *Cement and Concrete Research,* vol. 36, no. 10, pp. 1807-1813, 2006/10/01/ 2006, doi: https://doi.org/10.1016/j.cemconres.2006.05.028.

[217] L. J. Struble and W.-G. Lei, "Rheological changes associated with setting of cement paste," *Advanced Cement Based Materials,* vol. 2, no. 6, pp. 224-230, 1995/11/01/ 1995, doi: https://doi.org/10.1016/1065-7355(95)90041-1.

[218] V. Medri, S. Fabbri, J. Dedecek, Z. Sobalik, Z. Tvaruzkova, and A. Vaccari, "Role of the morphology and the dehydroxylation of metakaolins on geopolymerization," *Applied Clay Science,* vol. 50, no. 4, pp. 538-545, 2010/12/01/ 2010, doi: https://doi.org/10.1016/j.clay.2010.10.010.

[219] F. Avet, R. Snellings, A. Alujas Diaz, M. Ben Haha, and K. Scrivener, "Development of a new rapid, relevant and reliable (R3) test method to evaluate the pozzolanic reactivity of calcined kaolinitic clays," *Cement and Concrete Research,* vol. 85, pp. 1-11, 2016/07/01/ 2016, doi: https://doi.org/10.1016/j.cemconres.2016.02.015.

[220] D. Feys, R. Verhoeven, and G. De Schutter, "Why is fresh self-compacting concrete shear thickening?," *Cem. Concr. Res.,* vol. 39, no. 6, pp. 510-523, 2009/06/01/ 2009, doi: https://doi.org/10.1016/j.cemconres.2009.03.004.

[221] M. Cyr, C. Legrand, and M. Mouret, "Study of the shear thickening effect of superplasticizers on the rheological behaviour of cement pastes containing or not mineral additives," *Cem. Concr. Res.,* vol. 30, no. 9, pp. 1477-1483, 2000/09/01/ 2000, doi: https://doi.org/10.1016/S0008-8846(00)00330-6.

[222] A. Hajimohammadi, J. L. Provis, and J. S. J. van Deventer, "Effect of Alumina Release Rate on the Mechanism of Geopolymer Gel Formation," *Chemistry of Materials,* vol. 22, no. 18, pp. 5199-5208, 2010/09/28 2010, doi: 10.1021/cm101151n.

[223] C. A. Rees, J. L. Provis, G. C. Lukey, and J. S. J. van Deventer, "In Situ ATR-FTIR Study of the Early Stages of Fly Ash Geopolymer Gel Formation," *Langmuir,* vol. 23, no. 17, pp. 9076-9082, 2007/08/01 2007, doi: 10.1021/la701185g.

[224] W. K. W. Lee and J. S. J. van Deventer, "Use of Infrared Spectroscopy to Study Geopolymerization of Heterogeneous Amorphous Aluminosilicates," *Langmuir,* vol. 19, no. 21, pp. 8726-8734, 2003/10/01 2003, doi: 10.1021/la026127e.

[225] D. Zaharaki, K. Komnitsas, and V. Perdikatsis, "Use of analytical techniques for identification of inorganic polymer gel composition," *Journal of Materials Science,* vol. 45, no. 10, pp. 2715-2724, 2010/05/01 2010, doi: 10.1007/s10853-010-4257-2.

[226] M. Criado, A. Fernández-Jiménez, and A. Palomo, "Alkali activation of fly ash: effect of the SiO 2/Na 2 O ratio: Part I: FTIR study," *Microporous and Mesoporous Materials,* vol. 106, no. 1, pp. 180-191, 2007.

[227] O. Henning and V. C. Farmer, "Cements: the Hydrated Silicates and Aluminates," in *The Infrared Spectra of Minerals*, vol. 4: Mineralogical Society of Great Britain and Ireland, 1974, p. 0.

[228] C. A. Rees, "Mechanisms and kinetics of gel formation in geopolymers," Department of Chemical Engineering, University of Melbourne, 2007.

[229] C. A. Rees, J. L. Provis, G. C. Lukey, and J. S. J. van Deventer, "Attenuated Total Reflectance Fourier Transform Infrared Analysis of Fly Ash Geopolymer Gel Aging," *Langmuir,* vol. 23, no. 15, pp. 8170-8179, 2007/07/01 2007, doi: 10.1021/la700713g.

[230] S. A. Bernal, E. D. Rodríguez, R. Mejia de Gutiérrez, J. L. Provis, and S. Delvasto, "Activation of Metakaolin/Slag Blends Using Alkaline Solutions Based on Chemically Modified Silica Fume and Rice Husk Ash," *Waste and Biomass Valorization,* vol. 3, no. 1, pp. 99-108, 2012/03/01 2012, doi: 10.1007/s12649-011-9093-3.

[231] Y. F. Houst and F. H. Wittmann, "Influence of porosity and water content on the diffusivity of CO2 and O2 through hydrated cement paste," *Cement and Concrete Research,* vol. 24, no. 6, pp. 1165-1176, 1994/01/01/ 1994, doi: https://doi.org/10.1016/0008-8846(94)90040-X.

[232] B. S. Lartiges, J. Y. Bottero, L. S. Derrendinger, B. Humbert, P. Tekely, and H. Suty, "Flocculation of Colloidal Silica with Hydrolyzed Aluminum: An 27Al Solid State NMR Investigation," *Langmuir,* vol. 13, no. 2, pp. 147-152, 1997/01/01 1997, doi: 10.1021/la951029x.

[233] S. Slomkowski *et al.*, "Terminology of polymers and polymerization processes in dispersed systems (IUPAC Recommendations 2011)," (in English), *Pure and Applied Chemistry,* vol. 83, no. 12, p. 2229, 10 Sep. 2011 2011, doi: https://doi.org/10.1351/PAC-REC-10-06-03.

[234] J. C. Chang, F. F. Lange, and D. S. Pearson, "Viscosity and Yield Stress of Alumina Slurries Containing Large Concentrations of Electrolyte," *Journal of the American Ceramic Society,* vol. 77, no. 1, pp. 19-26, 1994, doi: 10.1111/j.1151-2916.1994.tb06952.x.

[235] A. E. James and D. J. A. Williams, "Flocculation and rheology of kaolinite/quartz suspensions," *Rheologica Acta,* vol. 21, no. 2, pp. 176-183, 1982/03/01 1982, doi: 10.1007/BF01736416.

[236] T. Kumaresan and J. B. Joshi, "Effect of impeller design on the flow pattern and mixing in stirred tanks," *Chemical Engineering Journal,* vol. 115, no. 3, pp. 173-193, 2006/01/15/ 2006, doi: https://doi.org/10.1016/j.cej.2005.10.002.

[237] P. T. Spicer, W. Keller, and S. E. Pratsinis, "The Effect of Impeller Type on Floc Size and Structure during Shear-Induced Flocculation," *Journal of Colloid and Interface Science,* vol. 184, no. 1, pp. 112-122, 1996/12/01/ 1996, doi: https://doi.org/10.1006/jcis.1996.0601.

[238] A. M. Ley-Hernández, D. Feys, and A. Kumar, "How do different testing procedures affect the rheological properties of cement paste?," *Cement and Concrete Research,* vol. 137, p. 106189, 2020/11/01/ 2020, doi: https://doi.org/10.1016/j.cemconres.2020.106189.

[239] H. J. Yim, J. H. Kim, and S. P. Shah, "Cement particle flocculation and breakage monitoring under Couette flow," *Cement and Concrete Research,* vol. 53, pp. 36-43, 2013/11/01/ 2013, doi: https://doi.org/10.1016/j.cemconres.2013.05.018.

[240] S. Jogun and C. F. Zukoski, "Rheology of dense suspensions of platelike particles," *Journal of Rheology,* vol. 40, no. 6, pp. 1211-1232, 1996, doi: 10.1122/1.550798.

[241] D. Lootens, P. Jousset, L. Martinie, N. Roussel, and R. J. Flatt, "Yield stress during setting of cement pastes from penetration tests," *Cement and Concrete Research,* vol. 39, no. 5, pp. 401-408, 2009/05/01/ 2009, doi: https://doi.org/10.1016/j.cemconres.2009.01.012.

[242] P. D. Silva, K. Sagoe-Crenstil, and V. Sirivivatnanon, "Kinetics of geopolymerization: Role of Al2O3 and SiO2," *Cement and Concrete Research,* vol. 37, no. 4, pp. 512-518, 2007/04/01/ 2007, doi: https://doi.org/10.1016/j.cemconres.2007.01.003.

[243] M. Choi, K. Park, and T. Oh, "Viscoelastic Properties of Fresh Cement Paste to Study the Flow Behavior," *International Journal of Concrete Structures and Materials,* vol. 10, no. 3, pp. 65-74, 2016/09/01 2016, doi: 10.1007/s40069-016-0158-3.

[244] P. Shankar, J. Teo, Y.-K. Leong, A. Fourie, and M. Fahey, "Adsorbed phosphate additives for interrogating the nature of interparticles forces in kaolin clay slurries via rheological yield stress," *Advanced Powder Technology,* vol. 21, no. 4, pp. 380-385, 2010/07/01/ 2010, doi: https://doi.org/10.1016/j.apt.2010.02.013.

[245] M. Kosmulski and P. Dahlsten, "High ionic strength electrokinetics of clay minerals," *Colloids and Surfaces A: Physicochemical and Engineering Aspects,* vol. 291, no. 1, pp. 212-218, 2006/12/15/ 2006, doi: https://doi.org/10.1016/j.colsurfa.2006.06.037.

[246] H. H. Murray and J. E. Kogel, "Engineered clay products for the paper industry," *Applied Clay Science,* vol. 29, no. 3, pp. 199-206, 2005/06/01/ 2005, doi: https://doi.org/10.1016/j.clay.2004.12.005.

[247] M. Ben Haha, G. Le Saout, F. Winnefeld, and B. Lothenbach, "Influence of activator type on hydration kinetics, hydrate assemblage and microstructural development of alkali activated blast-furnace slags," *Cement and Concrete Research,* vol. 41, no. 3, pp. 301-310, 2011/03/01/ 2011, doi: http://dx.doi.org/10.1016/j.cemconres.2010.11.016.

[248] X. Chen, A. Sutrisno, L. Zhu, and L. J. Struble, "Setting and nanostructural evolution of metakaolin geopolymer," *Journal of the American Ceramic Society,* vol. 100, no. 5, pp. 2285-2295, 2017, doi: 10.1111/jace.14641.

[249] M. Lizcano, A. Gonzalez, S. Basu, K. Lozano, and M. Radovic, "Effects of Water Content and Chemical Composition on Structural Properties of Alkaline Activated Metakaolin-Based Geopolymers," *Journal of the American Ceramic Society,* vol. 95, no. 7, pp. 2169-2177, 2012, doi: 10.1111/j.1551-2916.2012.05184.x.

[250] M. Sufian Badar, K. Kupwade-Patil, S. A. Bernal, J. L. Provis, and E. N. Allouche, "Corrosion of steel bars induced by accelerated carbonation in low and high calcium fly ash geopolymer concretes," *Construction and Building Materials,* vol. 61, pp. 79-89, 2014/06/30/ 2014, doi: https://doi.org/10.1016/j.conbuildmat.2014.03.015.

[251] V. Balek and M. Murat, "The emanation thermal analysis of kaolinite clay minerals," *Thermochimica Acta,* vol. 282-283, pp. 385-397, 1996/07/10/ 1996, doi: https://doi.org/10.1016/0040-6031(96)02886-9.

[252] "Principles of X-ray Diffraction," in *Thin Film Analysis by X‑Ray Scattering*, 2005, pp. 1-40.

[253] J. L. Provis and J. S. J. Van Deventer, *Geopolymers: structures, processing, properties and industrial applications*. Elsevier, 2009.

[254] Q. Wan *et al.*, "Geopolymerization reaction, microstructure and simulation of metakaolin-based geopolymers at extended Si/Al ratios," *Cement and Concrete Composites,* vol. 79, pp. 45-52, 2017/05/01/ 2017, doi: http://dx.doi.org/10.1016/j.cemconcomp.2017.01.014.

[255] S. A. Bernal, J. L. Provis, V. Rose, and R. Mejía de Gutierrez, "Evolution of binder structure in sodium silicate-activated slag-metakaolin blends," *Cement and Concrete Composites,* vol. 33, no. 1, pp. 46-54, 2011/01/01/ 2011, doi: https://doi.org/10.1016/j.cemconcomp.2010.09.004.

[256] N. Y. Mostafa, S. A. S. El-Hemaly, E. I. Al-Wakeel, S. A. El-Korashy, and P. W. Brown, "Characterization and evaluation of the pozzolanic activity of Egyptian industrial by-products: I: Silica fume and dealuminated kaolin," *Cement and Concrete Research,* vol. 31, no. 3, pp. 467-474, 2001/03/01/ 2001, doi: https://doi.org/10.1016/S0008-8846(00)00485-3.

[257] V. C. Farmer, *The Infrared Spectra of Minerals*. Mineralogical Society of Great Britain and Ireland, 1974.

[258] C. Martin, I. Martin, V. Rives, B. Grzybowska, and I. Gressel, "A FTIR spectroscopy study of isopropanol reactivity on alkali-metal-doped MoO3/TiO2 catalysts," *Spectrochimica Acta Part A: Molecular and Biomolecular Spectroscopy,* vol. 52, no. 7, pp. 733-740, 1996/07/15/ 1996, doi: https://doi.org/10.1016/0584-8539(96)01665-0.

[259] M. Soutsos, A. P. Boyle, R. Vinai, A. Hadjierakleous, and S. J. Barnett, "Factors influencing the compressive strength of fly ash based geopolymers," *Construction and Building Materials,* vol. 110, pp. 355-368, 2016/05/01/ 2016, doi: https://doi.org/10.1016/j.conbuildmat.2015.11.045.

[260] R. R. Lloyd, "8 - Accelerated ageing of geopolymers," in *Geopolymers*, J. L. Provis and J. S. J. van Deventer Eds.: Woodhead Publishing, 2009, pp. 139-166.

[261] M. Hartman, K. Svoboda, B. Čech, M. Pohořelý, and M. Šyc, "Decomposition of Potassium Hydrogen Carbonate: Thermochemistry, Kinetics, and Textural Changes in Solids," *Industrial & Engineering Chemistry Research,* vol. 58, no. 8, pp. 2868-2881, 2019/02/27 2019, doi: 10.1021/acs.iecr.8b06151.

[262] P. C. Fonseca and H. M. Jennings, "The effect of drying on early-age morphology of C–S–H as observed in environmental SEM," *Cement and Concrete Research,* vol. 40, no. 12, pp. 1673-1680, 2010/12/01/ 2010, doi: https://doi.org/10.1016/j.cemconres.2010.08.007.

[263] J. Duchesne, L. Duong, T. Bostrom, and R. Frost, "Microstructure study of early in situ reaction of fly ash geopolymer observed by environmental scanning electron microscopy (ESEM)," *Waste and Biomass Valorization,* vol. 1, no. 3, pp. 367-377, 2010.

[264]   Z. Zhang, J. L. Provis, X. Ma, A. Reid, and H. Wang, "Efflorescence and subflorescence induced microstructural and mechanical evolution in fly ash-based geopolymers," *Cement and Concrete Composites,* vol. 92, pp. 165-177, 2018/09/01/ 2018, doi: https://doi.org/10.1016/j.cemconcomp.2018.06.010.

[265]   Z. Wu, H. S. Wong, C. Chen, and N. R. Buenfeld, "Anomalous water absorption in cement-based materials caused by drying shrinkage induced microcracks," *Cement and Concrete Research,* vol. 115, pp. 90-104, 2019/01/01/ 2019, doi: https://doi.org/10.1016/j.cemconres.2018.10.006.

[266]   H. S. Wong, K. Matter, and N. R. Buenfeld, "Estimating the original cement content and water–cement ratio of Portland cement concrete and mortar using backscattered electron microscopy," *Magazine of Concrete Research,* vol. 65, no. 11, pp. 693-706, 2013, doi: 10.1680/macr.12.00201.

[267]   Z. Wu, H. S. Wong, and N. R. Buenfeld, "Influence of drying-induced microcracking and related size effects on mass transport properties of concrete," *Cement and Concrete Research,* vol. 68, pp. 35-48, 2015/02/01/ 2015, doi: https://doi.org/10.1016/j.cemconres.2014.10.018.

[268]   C. Künzel, "Metakaolin based geopolymers to encapsulate nuclear waste," Ph.D. dissertation, Department of Civil and Environmental Engineering, Imperial College London, London, 2013.

[269]   C. Künzel, A. Boccaccini, and C. Cheeseman, "Influence of water content on the properties of geopolymers for nuclear waste encapsulation," in *Decommissioning, Immobilisation and Management of Nuclear Waste for Disposal DIAMOND 2009 Conference*, 2009.

[270]   N. Mobasher, S. A. Bernal, H. Kinoshita, C. A. Sharrad, and J. L. Provis, "Gamma irradiation resistance of an early age slag-blended cement matrix for nuclear waste encapsulation," *Journal of Materials Research,* vol. 30, no. 9, pp. 1563-1571, 2015, doi: 10.1557/jmr.2014.404.

[271]   "Geological Disposal: Waste Package Evolution status report," Radioactive Waste Management, DSSC/451/01, 2016. [Online]. Available: https://rwm.nda.gov.uk/publication/geological-disposal-waste-package-evolution-status-report/

[272]   F. Vodák, K. Trtík, V. Sopko, O. Kapičková, and P. Demo, "Effect of γ-irradiation on strength of concrete for nuclear-safety structures," *Cement and Concrete Research,* vol. 35, no. 7, pp. 1447-1451, 2005/07/01/ 2005, doi: https://doi.org/10.1016/j.cemconres.2004.10.016.

[273]   F. Vodák, V. Vydra, K. Trtík, and O. Kapičková, "Effect of gamma irradiation on properties of hardened cement paste," *Materials and Structures,* journal article vol. 44, no. 1, pp. 101-107, January 01 2011, doi: 10.1617/s11527-010-9612-x.

[274]   G. Bar-Nes, A. Katz, Y. Peled, and Y. Zeiri, "The combined effect of radiation and carbonation on the immobilization of Sr and Cs ions in cementitious pastes," *Materials and Structures,* journal article vol. 41, no. 9, pp. 1563-1570, November 01 2008, doi: 10.1617/s11527-007-9348-4.

[275]   I. Maruyama *et al.*, "Impact of gamma-ray irradiation on hardened white Portland cement pastes exposed to atmosphere," *Cement and Concrete Research,* vol. 108, pp. 59-71, 2018/06/01/ 2018, doi: https://doi.org/10.1016/j.cemconres.2018.03.005.

[276]   "Waste package specification and guidance documentation, WPS/800: wasteform specification for 500 litre drum waste package: explanatory material and design guidelines," NDA, 2008.

[277]   M. S. Muñiz-Villarreal *et al.*, "The effect of temperature on the geopolymerization process of a metakaolin-based geopolymer," *Materials Letters,* vol. 65, no. 6, pp. 995-998, 2011/03/31/ 2011, doi: https://doi.org/10.1016/j.matlet.2010.12.049.

[278]   M. Lizcano, H. S. Kim, S. Basu, and M. Radovic, "Mechanical properties of sodium and potassium activated metakaolin-based geopolymers," *Journal of Materials Science,* journal article vol. 47, no. 6, pp. 2607-2616, 2012, doi: 10.1007/s10853-011-6085-4.

[279]   S. von Greve-Dierfeld *et al.*, "Understanding the carbonation of concrete with supplementary cementitious materials-a critical review by RILEM TC 281-CCC," *Materials And Structures,* 2020.

[280]   R. Pouhet and M. Cyr, "Carbonation in the pore solution of metakaolin-based geopolymer," *Cement and Concrete Research,* vol. 88, pp. 227-235, 2016/10/01/ 2016, doi: https://doi.org/10.1016/j.cemconres.2016.05.008.

[281]   T. El-Nabarawy, G. A. El-Shobaky, and A. M. Dessouki, "Effects of γ-irradiation on thermal and textural properties of Na-Y zeolites," *Thermochimica Acta,* vol. 111, pp. 249-255, 1987/02/15/ 1987, doi: https://doi.org/10.1016/0040-6031(87)88051-6.

[282]   K. Pasupathy, M. Berndt, A. Castel, J. Sanjayan, and R. Pathmanathan, "Carbonation of a blended slag-fly ash geopolymer concrete in field conditions after 8years," *Construction and Building Materials,* vol. 125, pp. 661-669, 2016/10/30/ 2016, doi: https://doi.org/10.1016/j.conbuildmat.2016.08.078.

[283]   W. Lu, J. P. Sculley, D. Yuan, R. Krishna, and H.-C. Zhou, "Carbon Dioxide Capture from Air Using Amine-Grafted Porous Polymer Networks," *The Journal of Physical Chemistry C,* vol. 117, no. 8, pp. 4057-4061, 2013/02/28 2013, doi: 10.1021/jp311512q.

[284]   P. A. Schroeder, R. J. Pruett, and V. J. Hurst, "Effects of Secondary Iron Phases on Kaolinite 27Al MAS NMR Spectra," *Clays and Clay Minerals,* vol. 46, no. 4, pp. 429-435, 1998/08/01 1998, doi: 10.1346/CCMN.1998.0460407.

[285]   D. S. Perera, O. Uchida, E. R. Vance, and K. S. Finnie, "Influence of curing schedule on the integrity of geopolymers," *Journal of Materials Science,* vol. 42, no. 9, pp. 3099-3106, 2007/05/01 2007, doi: 10.1007/s10853-006-0533-6.

[286]   C. Kuenzel, L. Li, L. Vandeperre, A. R. Boccaccini, and C. R. Cheeseman, "Influence of sand on the mechanical properties of metakaolin geopolymers," *Construction and Building Materials,* vol. 66, pp. 442-446, 2014/09/15/ 2014, doi: https://doi.org/10.1016/j.conbuildmat.2014.05.058.

[287]   L. Struble and P. Stutzman, "Epoxy impregnation of hardened cement for microstructural characterization," *Journal of Materials Science Letters,* vol. 8, no. 6, pp. 632-634, 1989/06/01 1989, doi: 10.1007/BF01730426.

[288]   D. A. Geddes, S. A. Bernal, M. Hayes, and J. L. Provis, "Irradiation Resistance of MK-Geopolymers Encapsulating Oily Wastes," in *RILEM Spring Convention amd Sustainable Materials, Systems and Structures 2019*, Rovinj, Croatia, 18 - 22 March 2019 2019: Springer, Netherlands.

[289]   E. V. Lebedeva and A. Fogden, "Adhesion of Oil to Kaolinite in Water," *Environmental Science & Technology,* vol. 44, no. 24, pp. 9470-9475, 2010/12/15 2010, doi: 10.1021/es102041b.

[290]   J. L. Provis, P. Duxson, G. C. Lukey, F. Separovic, W. M. Kriven, and J. S. J. van Deventer, "Modeling Speciation in Highly Concentrated Alkaline Silicate Solutions," *Industrial & Engineering Chemistry Research,* vol. 44, no. 23, pp. 8899-8908, 2005/11/01 2005, doi: 10.1021/ie050700i.

[291]   V. Cantarel, D. Lambertin, A. Poulesquen, F. Leroux, G. Renaudin, and F. Frizon, "Geopolymer assembly by emulsion templating: Emulsion stability and hardening mechanisms," *Ceramics International,* vol. 44, no. 9, pp. 10558-10568, 2018/06/15/ 2018, doi: https://doi.org/10.1016/j.ceramint.2018.03.079.

[292]   D. Medpelli, J.-M. Seo, and D.-K. Seo, "Geopolymer with Hierarchically Meso-/Macroporous Structures from Reactive Emulsion Templating," *Journal of the American Ceramic Society,* vol. 97, no. 1, pp. 70-73, 2014, doi: 10.1111/jace.12724.

[293]   J. C. Saam, "Silicone emulsion which provides an elastomeric product and methods for preparation," Patent US4244849A Patent Appl. US4244849A, 1981.

[294]   B. P. Binks and C. P. Whitby, "Silica particle-stabilized emulsions of silicone oil and water: aspects of emulsification," *Langmuir,* vol. 20, no. 4, pp. 1130-1137, 2004.

[295]   S. U. Pickering, "CXCVI.—Emulsions," *Journal of the Chemical Society, Transactions,* 10.1039/CT9079102001 vol. 91, no. 0, pp. 2001-2021, 1907, doi: 10.1039/CT9079102001.

[296]   H. E. S. Lw Corbett, W. Gunderman, Ed. *Viscosity Characterization of Asphalt Cement: Viscosity Testing of Asphalt and Experience with Viscosity Graded Specifications*. West Conshohocken, PA: ASTM International, 1973, pp. 51-1973.

[297]   A. Rescorla and F. Carnahan, "ANIMAL AND VEGETABLE OILS Viscosity-Temperature Characteristics," *Industrial & Engineering Chemistry,* vol. 28, no. 10, pp. 1212-1213, 1936.

[298]   D. Bonn, M. M. Denn, L. Berthier, T. Divoux, and S. Manneville, "Yield stress materials in soft condensed matter," *Reviews of Modern Physics,* vol. 89, no. 3, p. 035005, 08/21/ 2017, doi: 10.1103/RevModPhys.89.035005.

[299]   *Measurement of the leachability of solidified low-level radioactive wastes by a short-term test procedure*, ANSI/ANS 16.1-1986, ANSI, 1986.

[300]   R. J. Hamilton, "Hydrolysis of silicone polymers in aqueous systems," Department of Chemistry, Lakehead University, 2001.

[301]   W. M. Haynes, *CRC handbook of chemistry and physics*. CRC press, 2014.

[302]   M. M. Ghobashy, "Ionizing radiation-induced polymerization," *Ionizing Radiation Effects and Applications,* p. 113, 2018.

[303]   J. Lalevée, A. Dirani, M. El-Roz, X. Allonas, and J. P. Fouassier, "Silanes as New Highly Efficient Co-initiators for Radical Polymerization in Aerated Media," *Macromolecules,* vol. 41, no. 6, pp. 2003-2010, 2008/03/01 2008, doi: 10.1021/ma702301x.

[304]   K. Hayakawa, K. Kawase, H. Yamakita, and S. Inagaki, "γ-Ray-induced polymerization of some vinyl-substituted silanes," *Journal of Polymer Science Part B: Polymer Letters,* vol. 5, no. 12, pp. 1077-1081, 1967, doi: 10.1002/pol.1967.110051207.